UNIVERSITÉ DE TOURS

ÉCOLE DOCTORALE :

SSBCV

EA 6295 NanoMédicaments et NanoSondes (NMNS)

THÈSE présentée par :

Alaa MAKKI

soutenue le : **16 Novembre 2020**

pour obtenir le grade de : **Docteur de l'université de Tours**

Discipline/ Spécialité : Chimie Analytique

Analyse de solutions thérapeutiques pour le traitement du Cancer par spectroscopie vibrationnelle

THÈSE dirigée par :

Mr BONNIER Franck	Maître de conférences-HDR, université de Tours
Mr MOHAMMED AHMED Elhadi	Professeur, Université de Gezira

RAPPORTEURS :

Mme GAUDIN Karen	Professeur, Université de Bordeaux
Mr HUMBERT Bernard	Professeur, Université de Nantes

JURY :

Mme BLASCO Hélène	PU-PH Université de Tours - CHU Tours
Mr BONNIER Franck	Maître de conférences-HDR, Université de Tours
Mr CHOURPA Igor	Professeur, Université de Tours
Mme GAUDIN Karen	Professeur, Université de Bordeaux
Mr HUMBERT Bernard	Professeur, Université de Nantes
Mr MOHAMMED AHMED Elhadi	Professeur, Université de Gezira
Mr ABDELRAHMAN Mohammed	Maître de conférences, Université de Gezira

Table of contents

ACKNOWELDGMENT **4**
RÉSUMÉ **6**
ABSTRACT : **7**
LIST OF FIGURES: **8**
LIST OF TABLES: **10**
LIST OF ABBREVIATIONS: **11**
1. INTRODUCTION **13**
1.1 Context 13
1.2 Literature review: 16
1.2.1 Analytical quality control (AQC) 18
2. MATERIAL AND METHODS **24**
2.1 Principle of vibrational spectroscopy 24
2.1.1 Electromagnetic radiation (EMR) 24
2.1.2 Molecular motion and modes of vibrations 27
2.2 Absorption Infrared Spectroscopy 32
2.2.1 Principle 32
2.2.2 Instrumentation 35
2.2.2.1 Michelson interferometers 36
2.2.2.2 Attenuated total reflectance (ATR) 37
2.3 Raman Spectroscopy 39
2.3.1 Principle 39
2.3.2 Instrumentation 40
2.3.3 Confocal Raman spectroscopy 41
2.3.4 Macro sampling in quartz cuvettes 43
2.3.5 Miniaturisation of confocal Raman spectroscopy 43
2.4 Complementarity of Raman and IR spectroscopy: 45
2.4.1 Selection rules of vibrations 45
2.4.2 Bands positions 47
2.4.3 Analysis of solutions 48
2.4.5 Fluorescence 50
2.5 Data mining: pre-processing and Multivariate analysis: 51
2.5.1 Pre-processing methods: 51
2.5.2 Principal Component Analysis (PCA) 52

2.5.3 Partial Least Square – Discriminant Analysis (PLS-DA) 53
2.5.4 Partial Least Square Regression (PLSR) 55
2.5.5 Cross validation 56
3. COMPARISON OF INFRARED AND RAMAN SPECTROSCOPY FOR ANALYTICAL QUALITY CONTROL OF CHEMOTHERAPEUTIC SOLUTIONS **58**
3.1 Context and motivation: 58
PUBLICATION 1: Qualitative and quantitative analysis of therapeutic solutions using Raman and infrared spectroscopy 59
PUBLICATION 2: Vibrational spectroscopy for discrimination and quantification of clinical chemotherapeutic preparations 72
3.2 Discussion and perspectives 102
4. UNDERSTANDING THE DISCRIMINATION AND QUANTIFICATION OF MONOCLONAL ANTIBODIES PREPARATIONS USING VIBRATIONAL SPECTROSCOPY **106**
4.1 Context and motivation: 106
4.2 Ultrafiltration approach 107
4.3 PUBLICATION 3: Understanding the Discrimination and Quantification of Monoclonal Antibodies preparations using Raman Spectroscopy 110
4.4 Evaluating Silicon Internal Reflection Element (Si IRE) disposable ATR slides for quantification and discrimination of mAbs compared to standard ATR-FTIR 119
4.4.1 Context and motivation 119
4.4.2 Materials and Methods 120
4.4.3 Results 121
4.4.4 Discussion and perspectives 129
4.4.5 Conclusion 130
5. DIRECT CONFOCAL RAMAN ANALYSIS IN INFUSION BAGS FOR INCREASED SAFETY OF PERSONNEL **131**
5.1 Context and motivation 131
5.2 PUBLICATION 4: In situ Analytical Quality Control of chemotherapeutic solutions in infusion bags by Raman spectroscopy 136
5.2.1 Discussion on experimental conditions 160
5.2.2 Perspectives and future work with CRM 165
6. PERSPECTIVES AND FUTURE WORK **168**
7. REFERENCES: **169**

ACKNOWELDGMENT

First of all, I would like to thank Mr. Franck Bonnier (Maître de conférences-HDR, EA6296 NMNS- université de Tours) and Mr. Igor Chourpa (Professor and director of EA6296 NMNS laboratory) for accepting me and giving me opportunity to do my PhD in this laboratory.

No word can express my thanks to the main director of thesis Mr. Franck Bonnier for his continuous help, advice, guidance and patience during all the time of thesis work.

I thank the co-director of thesis Mr. Elhadi Mohammed Mohammed Ahmed, a professor at faculty of pharmacy- university of Gezira for his agreement to be the co-director of my thesis as the Sudanese part of France-Sudan co-tuttelled program. I would like to thank Mr. Mohammed Abdelrahman for his kind help and support to be enrolled in this program.

This thesis work can't be accomplished without collaboration with the UBCO (Unité de Biopharmacie Clinique Oncologique, Tours, France), thanks for Mr. Renaud Respaud and Mr. Victor Massot for their kind help and continuous support of chemotherapeutic drugs and information needed about the real practice at the hospital for quality control.

I would like to thank Mr. Dominique Bertrand (Data-Frame, Nantes-France) for his kind help on providing some scripts for MATLAB analysis performed on this thesis.

Great thank for Mr. Igor Chourpa for his help, advice and discussion on nanoparticles synthesis and work of surface enhanced Raman spectroscopy. I would like to thank Mr. Franck Bonnier and Mme. Suha Elderderi for their help on doing some experiments on thesis I couldn't finish on my last stay in the laboratory. Also, I thank Mr. Yoaan Misericordia for help on transferring some sample under PSM (poste de sécurité microbiologique).

I thank Mr. Martin Souce for discussion on some aspects concerning chromatography and analysis of monoclonal antibodies.

Thanks for Mr. Hicham Kichou, Mrs. Kamilia Kemel and Mr. Yuri Danick for their appreciation to my time frame, collaboration and arranging the booking time with me for the work with confocal Raman microscope.

I thank Mr. Hugh J. Byrne a professor and director of FOCAS Research Institute at Technological University Dublin for his kind help in corrections of the papers that have been written for thesis work.

I would like to thank all the jury members who agreed to give me honour as referees for my PhD thesis.

I thank all the permeants in EA 6296 Nanomedicine and Nanoprobes and special thanks to Mrs. Emilie Munnier for her kind talk and motivation during thesis work.

I will never forget to thank the nice group of internship/PhD/post doc/researchers: Lynda Miloudi, Sanaa BenDjemaa, Sahar Eljack, Sandra Henry, Almar Alasaad, Suha Elderderi, Loiuse van Gheluwe, Christophe Eklouch-Molinier, Vinh Nguyen, Iveta Vilimovia, Lucia Lombardi, Dilshad Hussein, Hicham Kichou, Ravil Rashitovich Petrov and Yuri Danick for their support and good moments of enjoyment we had outside the lab.

Special thanks to my close friends: Sarra Bashier, Sahar Ahmed, Hyam Omer and Sumia Elshiekh for giving me part of their time to talk, continuous support and kindness during my hard times.

Any success in my life is meaningless and not achievable without the presence, endless support and encouragement of my family since childhood- all thanks for them.

RÉSUMÉ

L'amélioration de la qualité et de la sécurité dans la délivrance des préparations de chimiothérapie est assurée par des protocoles de contrôle qualité. Le contrôle analytique en postproduction a pour vocation de réaliser un dosage quantitatif (mesure de la concentration) et une analyse qualitative (identification de la molécule) afin d'assurer que la solution libérée corresponde à la prescription médicale (dose injectée conforme). Bien que les techniques chromatographiques soient bien établies, la cadence dans les unités centralisées de préparation impose d'explorer des approches analytiques alternatives plus rapides et moins couteuses. Les spectroscopies d'absorption infrarouge et de spectroscopie Raman (SR) sont des méthodes optiques de caractérisation chimique. Il est démontré que les signatures spectrales sont de véritables empreintes moléculaires qui permettent une identification spécifique des agents anticancéreux en solutions mais également leur quantification. Notamment, la SR pourrait aussi s'appliquer directement sur les poches sont nécessité de réaliser des prélèvements, donc de limiter les risque d'exposition pour les personnels hospitaliers.

Mots clés: Spectroscopie vibrationnelle, contrôle qualité, solutions thérapeutiques, anticancéreux, chimiométrie

ABSTRACT :

Improvement in the quality and safety in the delivery of chemotherapy preparations is ensured by quality control protocols. The purpose of postproduction analytical control is to perform a qualitative analysis (identification of the molecule) and a quantitative assay (measurement of the concentration) and in order to ensure that the solution released corresponds to the medical prescription (conformity of dose injected). Although chromatographic techniques are well established, the workload in centralised preparation units requires exploring faster and less expensive alternative analytical approaches. Infrared absorption spectroscopy and Raman spectroscopy (RS) are optical methods of chemical characterization. It has been demonstrated that the spectral signatures are molecular fingerprints that allow a specific identification of anticancer agents in solutions but also their quantification. In particular, RS could also be applied directly to infusion bags without requirement to withdraw sample, thus limiting the risk of exposure for hospital staff.

Keywords: Vibrational spectroscopy, quality control, therapeutic solutions, anticancer, chemometrics

LIST OF FIGURES:

Figure 1. Amplitude of the electric vector of electromagnetic radiation as a function of time. The wavelength (λ) is the distance between two crests [83] 24
Figure 2. Energy units for various regions of the electromagnetic radiation [83]. 26
Figure 3. Stretching and bending vibrational modes of -CH_2 [86] 28
Figure 4. vibrational mode observed for H_2O molecule [88] 29
Figure 5. Vibrational modes of CO_2 [83] 29
Figure 6. Harmonic oscillator of diatomic molecule 30
Figure 7. Relationship between the atomic masses, force constant and the hybridization to the frequency of vibration [86] 31
Figure 8. Absorption process in IR region 33
Figure 9. IR absorption according to Beer Lambert's law 34
Figure 10. Typical components of a FT-IR instrument 35
Figure 11. Michelson interferometer [26] 36
Figure 12. Fourier transform infrared Frontier (Perkin Elmer, France) equipped with: A) mono-reflection and B) multireflection ATR diamond accessary 37
Figure 13. Basic principle of ATR [95] 38
Figure 14. Light diffusion phenomenon [97] 39
Figure 15. Instrumental parts of Raman microscope 40
Figure 16. Principle of confocality of microscope 42
Figure 17. Cuvette holder attachment to Raman micro-spectroscopy (https://www.technospex.com/resources/cuvette-holder-attachment-uraman-micro-spectroscopy-liquid-sample-measurements/) 43
Figure 18. Portable Raman spectrometer from Metrohm, France 44
Figure 19. Handheld Raman spectrometer from Metrohm, France(https://www.metrohm.com/en/products/spectroscopy/mira-handheld-raman-spectrometers/). 45
Figure 20. Raman (a) and IR (b) spectra of DOX (2 $g{\cdot}L^{-1}$) 46
Figure 21. Jablonski diagram of absorption IR and Raman scattering 48
Figure 22. Mean ATR-FTIR spectra of: a) MTX 21 $g{\cdot}L^{-1}$ from air dried drop and b) from solution. Spectra are offset for clarity 49
Figure 23. Mean Raman spectra of: a) MTX 21 $g{\cdot}L^{-1}$ solution and b) water. Spectra are offset for clarity 50
Figure 24. PCA performed on ATR-FTIR Raw spectra. A: scatter plot of PC scores 1 and 2. B: loading for PC1 53
Figure 25. PLS 2 based predictive model for PLS-DA 54
Figure 26. Data arrangement before PLSR 55
Figure 27. Mean ATR-FTIR spectra of: a) DOX (1.2 $g{\cdot}L^{-1}$), b) EPI (0.65 $g{\cdot}L^{-1}$) and c) DAU (2 $g{\cdot}L^{-1}$) in 5% glucose. Spectra are offset for clarity. 103
Figure 28. Mean Raman spectra of: a) DOX (1.2 $g{\cdot}L^{-1}$), b) EPI (0.65 $g{\cdot}L^{-1}$) and c) DAU (2 $g{\cdot}L^{-1}$) in 5% glucose. Spectra are offset for clarity. 104
Figure 29. Mean Raman spectra of: a) CYA (7.75 $g{\cdot}L^{-1}$) and b) IFA (17.75 $g{\cdot}L^{-1}$) in 5% glucose solution. Spectra are offset for clarity. 105
Figure 30. A) Ultra-filtration device Amicon® and B) ultrafiltration protocol 108
Figure 31. ATR-FTIR spectra recorded form concentrate (A) and filtrate (B) for ONTRUZANT® during ultrafiltration cycles. Spectra are organised from the top to the bottom from cycle 1 to cycle 10. Spectra are offset for clarity 109

Figure 32. ATR-FTIR spectra recorded from the concentrate after cycle 10 of commercial stock solutions of: ERBITUX® (a), TRUXIMA® (b), ONTRUZANT® (c) and AVASTIN® (d). Spectra are offset for clarity 110
Figure 33. Silicon internal reflection element (Si IRE) are sandwiched between a 3D printed plastic holder and a medical grade labelled sticker [129]. 119
Figure 34. Mean ATR-FTIR spectra recorded from commercial stock solutions of: ERBITUX® 5 $g{\cdot}L^{-1}$ (a), TRUXIMA® 10 $g{\cdot}L^{-1}$ (b), ONTRUZANT® 21 $g{\cdot}L^{-1}$ (c) and AVASTIN® 25 $g{\cdot}L^{-1}$ (d). Spectra are offset for clarity 122
Figure 35. Mean ATR-FTIR spectra obtained by Si IRE recorded from solutions prepared in 0.9% NaCl solution: ERBITUX® 4 $g{\cdot}L^{-1}$ (a), TRUXIMA® 4 $g{\cdot}L^{-1}$ (b), ONTRUZANT® 4 $g{\cdot}L^{-1}$ (c) and AVASTIN® 15 $g{\cdot}L^{-1}$ (d). Spectra are offset for clarity 123
Figure 36. Mean IR spectra in the fingerprint region of ONTRUZANT® in 0.9% NaCl following serial dilution using: A) ATR-FTIR and B) Si IRE-ATR. Spectra ordered from top to the bottom corresponding to 4 $g{\cdot}L^{-1}$, 3 $g{\cdot}L^{-1}$, 2 $g{\cdot}L^{-1}$, 1 $g{\cdot}L^{-1}$ and 0.5 $g{\cdot}L^{-1}$ 124
Figure 37. PLSR analysis performed on ATR-FTIR spectra collected from ONTRUZANT® in 0.9% NaCl using standard multireflection diamond crystal (I) and Si IRE (II). A) RMSECV and B) Regression plot 125
Figure 38. Regression coefficients of PLSR of ATR-FTIR (I) and (II) Si IRE-ATR for: a) ERBITUX®, b) TRUXIMA®, c) ONTRUZANT® and d) AVASTIN®. Spectra are offset for clarity 126
Figure 39. Regression coefficients of the PLSDA. A) the first regression coefficient obtained by a) standard diamond ATR and b) Si IRE-ATR. B) the second regression coefficient obtained by a) standard diamond ATR and b) Si IRE-ATR. Spectra are offset for clarity 129
Figure 40. Chemical structures of: A) MTX, B) 5-FU and C) GEM 132
Figure 41. Absorbance spectra for: A) MTX, B) 5-FU and C) GEM 133
Figure 42. Calibration curve of MTX on the concentration range 133
Figure 43. Illustrates the protocol used for preparation of chemotherapeutic drugs inside the bag and analysis by UV/vis spectrometry and CRM 134
Figure 44. Mean Raman spectra of MTX in 5% glucose bag following at 900 µm for respective concentrations of: a) 20.1 $g{\cdot}L^{-1}$, b) 14.3 $g{\cdot}L^{-1}$, c) 9.5 $g{\cdot}L^{-1}$, d) 4.98 $g{\cdot}L^{-1}$, e) 3.8 $g{\cdot}L^{-1}$ and f) 3.2 $g{\cdot}L^{-1}$ 161
Figure 45. Mean Raman spectra of 5-FU 40 $g{\cdot}L^{-1}$ in 5% glucose bag using 633 nm laser at: a) -300 µm, b) -500 µm, c) -700 µm and d) -900 µm compared to a spectrum of the commercial solution 5-FU (50 $g{\cdot}L^{-1}$) recorded using a quartz cuvette. Spectra are offset for clarity 162
Figure 46. Mean Raman spectra of 5-FU in 5% glucose bag using 633 nm laser at 900 µm. Concentrations are arranged from the top to the bottom according to decrease in intensity. a) 40 $g{\cdot}L^{-1}$, b) 30.6 $g{\cdot}L^{-1}$, c) 20.7 $g{\cdot}L^{-1}$, d) 10.9 $g{\cdot}L^{-1}$, e) 5.4 $g{\cdot}L^{-1}$ and f) 1.3 $g{\cdot}L^{-1}$ 163
Figure 47. Regression coefficients of PLSR at -900 µm for 5-FU by 633 nm laser 164
Figure 48. Regression coefficients of PLSDA; a) the first, b) the second and c) the third. Spectra are offset for clarity 165
Figure 49. PCA performed for MTX, GEM and 5-FU presenting the scatter plot of: A), MTX B), GEM and C) 5-FU. D plot presents the loading spectrum of a) MTX, b) GEM and c) 5-FU. Spectra are offset for clarity 167

LIST OF TABLES:

Table 1. Publications reporting AQC of chemotherapeutic solutions 23
Table 2. Spectral regions and their origins [83] 27
Table 3. Vibrational modes of selected functional groups on IR and Raman 32
Table 4. PLSR results obtained for the 4 mAbs formulations by ATR-FTIR and Si IRE-ATR 127
Table 5. Specificity and sensitivity % obtained by PLSDA for IR data pre-processed with EMSC, Lieber correction and vector normalization 128
Table 6. Summary of PLSR results at depth 900 µm using 532 nm laser for full range spectra 161
Table 7. Summary of PLSR results of data recorded using 633 nm laser at 900µm using 4 LVs 163
Table 8. Specificity and sensitivity% obtained by PLSDA at 900 µm by 633 nm laser 164

LIST OF ABBREVIATIONS:

Acronym	Definition
ACIs	Active Cosmetic Ingredients
APIs	Active Pharmaceutical Ingredients
ATR	Attenuated Total Reflection
AQC	Analytical Quality Control
CCD	Charge Coupled Device
CRM	Confocal Raman Microscopy
CV	Cross Validation
CYA	Cyclophosphamide
CZE	Capillary Zone Electrophoresis
DAU	Daunorubicin
DOX	Doxorubicin
EPI	Epirubicin
EMR	Electromagnetic Radiation
EMSC	Extended Multiplicative Signal Correction
EPGR	Epidermal Growth Factor Receptor
ER	Oestrogen Receptor
ES	Electromagnetic Spectrum
ESR	Electron Spin Resonance
FIA	Flaw Injection Analysis
FTIR	Fourier Transform Infrared spectroscopy
5-FU	5-Fluorouracil
GEM	Gemcitabine
HER2	Human Epidermal Receptor 2
HPLC	High Performance Liquid Chromatography
HPTLC	High Performance Thin Layer Chromatography
IFA	Ifosfamide
LKOCV	Leave K out Cross Validation
LOD	Limit Of Detection
LOOCV	Leave One Out Cross Validation
LSPR	Localised Surface Plasmon Resonance
LVs	Latent Variables
mAbs	Monoclonal Antibodies
MS	Mass spectrometry
MTX	Methotrexate
NMR	Nuclear Magnetic Resonance
ORS	Orbital Raster Scan
PAT	Process Analytical Tool
PCA	Principal Component Analysis
PLSDA	Partial Least Square Discriminant Analysis
PLSR	Partial Least Square Regression
PR	Progesterone Receptors
QC	Quality Control
R^2	Regression
RIC	Raman Illumination Chamber

Acronym	Definition
R_f	Rate of flow
RMSECV	Root Square Error of Cross Validation
Si IRE	Silicon Internal Reflection Element
SNV	Standard Normal Variate
TDM	Therapeutic Drug Monitoring
TO	Therapeutic Object
UBCO	Unité de Biopharmacie Clinique Oncologique
UV/vis	UV/vis absorption spectroscopy
VS	Vibrational Spectroscopy

1. INTRODUCTION

1.1 Context

The potential of vibrational spectroscopy (VS) techniques namely, absorption infrared (IR) and Raman scattering, are being widely investigated for applications in forensic science, biomedical, pharmaceutical and cosmetic analysis. The enthusiasm for these techniques arose from the non-invasive, non-destructive and label free analysis delivered. Moreover, spectral signatures collected encompass specific information about chemical composition of samples and are commonly referred as a molecular fingerprint.

Nowadays, there is an extended range of commercially available instruments for VS techniques with different setups ranging from Confocal Raman microscope used for hyperspectral imaging of biological samples (cells, tissues) or material (for example packaging), to portable/transportable instruments (benchtop apparatus often equipped with remote probes) and, more recently, handheld Raman devices (field analysis). For many years, use of VS for analysis of evidences in forensic science has been reported for analysis of explosives, gunshot residues, illicit drugs, textiles or fibres found in the crime place which can help identifying victim, suspect and other information [1–3].

The label free nature of VS methods has extended its application in the biomedical field for cytology and histology studies. While the biochemical information collected can help to better understand normal physiological state of cell division and maturation, it is also a promising screening tool for early diagnosis of diseases through identification of abnormal cell growth and division (tumours) and it could give further insights in prediction of treatment response and recovery [4,5]. Cell and tissue imaging by VS have helped for detection and monitoring of cell interaction with exogenous agents including toxic agents [6–10], analysis of active pharmaceutical ingredients (APIs) inside cells as part of pharmacokinetic studies [11–14] and evaluation of penetration of cosmetic molecules through skin [15]. Sensitivity and specificity of VS enables quantitative and qualitative analysis of complex liquid matrices such as body fluids. There is increasing number of referenced publications in the literature about quantification of blood serum content of endogenous (enzymes, blood coagulation factors, proteins, lipids, amino acids and carbohydrates) and exogenous agents such as drugs to track their concentration in bioavailability studies [16–18].

VS instrumentation has also implemented in a wide range of applications in industry. They have emerged as tools for large-scale analysis in pharmaceutical and biopharmaceutical industries as

a Process Analytical Tool (PAT) for studying APIs at different production steps [19]. VS is being implemented in drug discovery and development at different stages including chemical identification of the raw material, pre-formulation based pharmacological and toxicological studies, solid dosage form analysis, analysis of formulations in late phases of drug development and quality control of the finished products [20,21]. They have been specifically used to study the polymorphism and crystallisation and their impact on the therapeutic activity as small change in the molecular structure can be detected in their spectral signature [21–24]. VS are often considered as cost effective and alternative to other spectroscopic methods (nuclear magnetic resonance) and chromatographic methods for quantification of APIs to assess contents during and after manufacturing process, in solid, semi-solid and liquid dosage forms [25–27]. Furthermore, their application is extended for field identification of counterfeited drugs [25,28–30]. VS could also be applied to the cosmetic industry for characterisation of active cosmetic ingredients (ACIs) in complex formulations. Notably, it has been recently reported a case study about quantification of ACI encapsulated in nanocarriers without requirement for fastidious extraction protocols [31]. This study demonstrates how VS could be implemented in industry for online analysis of products.

VS analysis generally generates large datasets of spectra hence the data analysis becomes rapidly a fastidious task. Advancement in chemometric methods for data mining, especially multivariate methods, has significantly helped to promote applicability of VS to a wide range of applications thanks to standardisation of mathematical protocols. Simplified representations of results using different models has also contributed to increase the accessibility hence the popularity of techniques among non-specialists (pharmacists, clinicians) which could support faster transfer into biomedical and pharmaceutical fields. Multivariate methods can improve sensitivity and selectivity of identification by extracting the information hidden in complex spectra [32] by applying different pre-processing algorithms to remove spectral interference and/or background that might exist in the collected data [33]. Unsupervised discrimination model such as principal components analysis (PCA), is mainly used for exploratory purposes, to identify similarities and differences between samples, by reducing the dimensionality of the data and/or extracting dominant information in complex matrices [34]. However, more elaborated data mining protocols can be necessary to further strengthen the relevancy of results. Supervised methods for classification, e.g. partial least square discriminant analysis (PLSDA), or for quantification, e.g. partial least square regression (PLSR) are two of most used approaches to analyse spectral data [35–37]. The main risk with the supervised statistical models is the overfitting of the results delivering overoptimistic

outcomes. Therefore, several strategies should be put into consideration when planning to collect data with VS. The experimental design should be constructed to contain enough data sets and large numbers of samples to ensure reliability of the predicted models (quantitative or discriminant analysis). Moreover, cross validation should be used in data analysis protocols to avoid adding any biased interpretation of results [38]. Ideally, the data are organised as calibration, validation and training sets, all independent, but experimentally the main limitation encountered for VS is the lack of fully automated instruments, increasing the acquisition time and as a consequence often resulting in a limited number of samples included in studies.

The ongoing development of new user-friendly technologies (handheld, benchtop systems) coupled to build in software for data mining have significantly participated to recognition of the techniques in the pharmaceutical industry particularly in research and development. In comparison, the transfer of VS into clinics is not achieved yet despite a strong community of specialists promoting their potential for diagnosis and patient care. While many publications report that spectral signatures enable to identify specific biomarkers, biological systems are complex mixtures with inter-patients and numerous cofounding parameters making the data mining difficult. It is however surprising that application for clinical pharmacy is not more investigated. VS could be a valuable tool for daily duties and support the workflow in hospitals while strengthening the safety of patients and staff members.

This thesis will therefore report the application of VS techniques for analytical quality control (AQC) of chemotherapeutic preparations. The work has been conducted in collaboration with the UBCO (Unité de Biopharmacie Clinique Oncologique, Tours, France). UBCO is a centralised unit dealing with the preparation of individualised chemotherapeutic solutions at the university hospital of Tours (CHU Tours, France). The methodological and experimental aspects have been particularly investigated for a better understanding of the origin of the signals collected by IR and Raman, to compare their complementarity and performance but also to optimise methods for data mining using multivariate analysis. The two key criteria were the reliability of quantitative analysis (precision, accuracy) and discrimination rate between different drugs in solutions. Ultimately, the aim was to provide a clear evaluation of VS for AQC of chemotherapeutic solutions and unambiguously highlight their potential for use in centralised units.

The main highlights of the thesis are:

1) Comparative studies of IR and Raman spectroscopy for analysis of small molecules in injectable chemotherapeutic solution (**Section 3**).

2) Evaluation of applicability of VS spectroscopy for AQC of monoclonal antibodies (mAbs) (**Section 4**).

3) Direct analysis of chemotherapeutic preparations through plastic bags using confocal Raman microscopy (CRM) (**Section 5**).

Perspectives and future applications will be discussed in **Section 6**.

1.2 Literature review:

Cancer is considered the second disease leading cause of death after cardiovascular diseases [39]. The disease is characterized by rapidly uncontrolled cell growth and division that invade other cells and tissues [40,41]. Cancer treatment regimens are surgery, chemotherapy, immunotherapy and radiotherapy [42,43]. The selection of treatment protocol depends on the stage of the disease, at early stages surgery is preferred while in metastatic stage systemic therapies (intravenous injection) are used which enable reaching all cancer sites via blood circulation [44,45]. Chemotherapeutics are used with the aim of systemic treatment rather than localised treatment such as radiotherapy and surgery [46]. It the most commonly used regimen in cancer treatment either as a monotherapy or combination therapy [47].

The selection of chemotherapeutic treatment regimen for cancer depends on the histology of the disease, organ of the origin and biomarkers expressed in different organs, which are responsible for growth and division of cancer cells. For example human epidermal growth factor receptor 2 (HER2), oestrogen receptor (ER) and progesterone receptor (PR) are being expressed in breast cancer while epidermal growth factor receptor (EGFR) in lung adenocarcinomas [48,49]. Thereby, selection of chemotherapeutic drug with selective mechanism of action can enhance patient prognosis and survival rate. Systemic anticancer drugs include small molecules drugs and monoclonal antibodies (mAbs).

- Small molecules chemotherapeutic drugs have been classified according to their mechanism of action into alkylating agents, antimetabolite, anti-tumour antibiotics, topoisomerase inhibitors and tubulin binding drugs [50–53]. They lead to cell death by inhibiting tumour cell division and proliferation. Most of side effects caused by

chemotherapeutics affect the normal cells and mainly have a greater effect on cells with high turnover rates such as bone marrow, hair follicles, mucosal cells lining of gastrointestinal tract [54]. They have non targeted toxic effects to tumours as well as to normal cells thereby they are named cytotoxic drugs [55].

- Monoclonal antibodies (mAbs) are biopharmaceuticals with an increasing use in treatment of several types of cancer and some chronic inflammatory diseases. They are classified as targeted therapeutic because of their highest specificity to the tumour sites and hence less adverse effects compared to small chemotherapeutic molecules [56].

With the massive increase in cancer disease, individualised systemic chemotherapeutic preparations have been implemented in centralised preparation units for treatment protocols, where dose is calculated according to the body weight and surface area and prepared by reconstitution of chemotherapeutic formulation in 0.9% normal saline or 5% glucose solutions. Anticancer drugs are considered as high alert medications due to their narrow therapeutic index and iatrogenic toxicity as the threshold between the therapeutic response and the toxicity is very small. High risk is associated with those molecules from the early steps of production to the administration. Hence, following good preparation practices protocols and control of chemotherapeutic preparations in the centralised preparation units can enhance the security of their preparation and reduce medication errors. Medical staff members including physicians, pharmacists and nurses are involved in the control process from prescription to the administration step [57,58].

Quality control (QC) of chemotherapeutic preparations involve non-analytical and analytical methods. Non-analytical methods are widely used methods such as visual control and video assisted control as well as gravimetric control (weight of the prepared sample is compared to the expected weight) [59]. The main drawbacks of non-analytical methods can be summarised in that; the visual control is highly subjective and dependent on the human factor while gravimetric control suffer from the lack of specificity and in some cases is expensive, moreover visual and video control do not enable quantitative analysis [57]. Although, the analytical control is still non-mandatory for chemotherapeutic preparations, most of preparation units have implemented protocols to verify the chemical composition of final anti-cancer drug solutions to ensure safety to patients from iatrogenic toxicity.

1.2.1 Analytical quality control (AQC)

The main purpose of AQC is to assess the identity, purity and the nominal concentration of APIs (for instance anti-cancer drugs) in the prepared solutions. More specifically, the AQC should allow the analytical certification of therapeutic object (TO) prior to the administration to patient. In terms of hospital organization in the day care units, the AQC should be fast, reliable and fully integrated into the preparation process and treatment. Several analytical techniques have been implemented for AQC of TOs, although the choice is different from one centre to another depending on the cost and needs in each clinical setting. High performance liquid chromatography (HPLC) coupled with UV/vis detectors or flow injection analysis (FIA)/UV-vis is a powerful gold standard technique for AQC of chemotherapeutic preparations [59–64].

For example, HPLC and high-performance thin layer chromatography (HPTLC) combined with fluorescence detection have been used at Institute of Gustave Roussy (France) for AQC of camptothecin derivatives, namely irinotecan and topotecan which are used for treatment of colorectal, ovarian and small- cell lung cancers. HPLTLC was applied on the range 100-500 $g{\cdot}L^{-1}$ and for HPLC the range was adapted to 0.1-1 $mg{\cdot}L^{-1}$. The fluorescence excitation wavelength was set at 355 nm and the detection performed at 515 nm. Irinotecan and topotecan, respectively, have been identified by their rate of flow (R_f), 0.10 and 0.35, or their retention time (t_R), 2 and 7 min [65].

Although, chromatographic techniques provide high sensitivity, specificity, accuracy and precision, the major limitations is time required for analysis of large samples cohorts [57,66].

For AQC alternative fast, simple and reliable methods are sought for real time control of chemotherapeutic preparation without delaying the transfer to patient bedroom for administration. In literature, many studies have been published for VS techniques applied in cancer research but very few studies report investigation for AQC of chemotherapeutic solutions.

However, a dedicated instrument coupling UV/vis spectrometry to IR (Multispec® analysers, Microdom, Taverny, France) was commercialised. This commercial instrument has been implemented in the hospital for AQC of chemotherapeutic preparations. The identification principle by Multispec® rely on comparing IR spectra collected to the software library which contains spectra for each drug in 0.9% normal saline and 5% glucose while quantification is based mainly on UV/vis using the calibration curve constructed at single wavelength for each drug either in 0.9% normal saline or 5% glucose [58]. However, in the literature; two studies

have been conducted at the hospital setting using Multispec® analysers for quantitative and qualitative analysis of a considerable number of chemotherapeutic preparations. The first one has been performed by Dziopa et al. in 2013 [58] at Hospital of Edouard Herriot, France. The study included 14 chemotherapeutic drugs (5-fluorouracil, amsacrine, carboplatin, cisplatin, cytarabine, daunorubicin, fludarabine, gemcitabine, irinotecan, oxaliplatin, paclitaxel, bevacizumab, cetuximab and rituximab). The matching factor has been set at 96%; there were some mismatches in term of specifically identifying paclitaxel and docetaxel but also the technique was able to differentiate between structurally related molecules (taxanes, platines and monoclonal antibodies). The second study has been published by Bazin et al. in 2014 [67], which has been conducted on routine control of a centralised unit of chemotherapies in a university hospital over 24 months on the mostly prepared drugs in the unit: amsacrine, bendamustine, asparaginase, busulfan, carboplatin, cisplatin, cyclophosphamide, cytarabine, daunorubicin, dexrazoxane, docetaxel, doxorubicin pegylated lyposomal, epirubicin, etoposide phosphate, 5-fluorouarcil, fotemustine, gemcitabine, ifosfamide, idarubicin, irinotecan, melphalan, methotrexate, oxaliplatin, paclitaxel, streptozocine, temsirolimus, thiotepa, vinblastine, vincristine, vinorelbine, cetuximab, rituximab, trastuzumab and bevacizumab. The outcomes were promising; 97% and 99.9% identification of solvents and molecules has been obtained. However, difficulties have been encountered is discrimination between structurally related molecules like anthracyclines (doxorubicin, epirubicin and daunorubicin), oxazophosphorines (cyclophosphamide and ifosfamide) and monoclonal antibodies (cetuximab, rituximab, trastuzumab and bevacizumab).

In the last decade, Raman spectroscopy has gained interest in AQC of chemotherapeutic solutions [68,69]. A study published by Lê et al. 2018 [70] using Raman micro-spectroscopy (Horiba Jobin Yvon, Lille, France) for AQC of five chemotherapeutic solutions through glass vials: 5-fluorouracil (1 - 50 $g{\cdot}L^{-1}$), gemcitabine (1 - 40 $g{\cdot}L^{-1}$), cyclophosphamide (0.5 - 20 $g{\cdot}L^{-1}$), ifosfamide (1 - 40 $g{\cdot}L^{-1}$) and doxorubicin (0.01 - 2 $g{\cdot}L^{-1}$). Hierarchical PLS-DA model has been used for discrimination while leave one out cross validation (LOOCV) used for quantification. 99% of samples and solvents were correctly identified and classified, misclassification has been observed only for cyclophosphamide. More Recently a study also using Raman micro-spectrometer (Horiba Jobin Yvon, Lille, France) was reported by Lê et al. 2018 [71] for the discrimination between solutions prepared from four mAbs (infliximab, bevacizumab, rituximab and ramucirumab). The discrimination between these molecules poses difficulties due to their high spectral similarities, therefore advanced machine learning approach based on cross-validation bootstrap aggregation has been used to achieve discrimination. A

study reported by Kiehntopf et al. [72] using Raman RXN1^{TM} from Kaiser Optical Systems, Inc. (Ann Arbor, MI, USA) for quality control of 5-fluorouracil aqueous solution prepared in NaCl infusion bags at the range 0 - 5.357 $g{\cdot}L^{-1}$. It has resulted in good quantification (R^2> 0.99487) and identification of 5-fluorouarcil spectral features at 750 – 800 cm^{-1}.

A new generation of dedicated instrument combining UV/vis and Raman analysis (QCPrep®, BWTec, USA) has been developed and commercialised. Notably, it overcomes the main limitation of IR, which is the strong water absorption, thereby making it suitable for analysis of solutions. Despite the interesting set up and the potential enhanced performances achieved through synergic use of UV and Raman detection, only three studies can be found in the literature. The first study using this system has been published by Chouquet et al. [73] for QC of low volume (less than 50 mL) chemotherapeutic preparations for paediatrics. The paper reports good identification and quantification of asparaginase, cyclophosphamide, cytarabine, daunorubicin, doxorubicin, etoposide (base and phosphate), ifosfamide, methotrexate, vinblastine and vincristine. Anthracyclines and oxazophosphorines has been discriminated by Raman while vinca alkaloids were discriminated with the UV\vis detection within the range 255-332 nm. This study has been followed by another one by the same author [74] using more chemotherapeutic preparations (amsacrine, bendamustine, bevacizumab, bleomycin, brentuximab, busulfan, dacarbazine, docetaxel, liposomal daunorubicin, fludarabine and gemcitabine, cisplatin, decitabine, epirubicin, etoposide phosphate, methotrexate, vindesine, vinblastine, vincristine and vinorelbine) over 18 months. The listed drugs have been tested for conformity and non-conformity of preparation in low volume paediatric preparations (20 – 50 mL). The aim was to develop a method for quality control of those preparations to allow this population to benefit from quality control in the same level as adults. The overall conformity rate has been found 94.4% and 5.6% non-conformity. The non-conformity rates have been explained by the difficulty of homogenising small volumes and this have been confirmed by a second re-sampling and 92% of non-conformed (cisplatin, decitabine, epirubicin, etoposide phosphate, methotrexate and vindesine, vinblastine, vincristine and vinorelbine) results were confirmed. A third study has been conducted by Nardella et al. [75] who used QCPrep+® for quality control of 14 molecule-solvent combinations over 18 months of the daily used preparations (ifosfamide, cyclophosphamide, doxorubicin, carboplatin, cisplatin, dacarbazine, docetaxel, etoposide, gemcitabine, oxaliplatin, paclitaxel, pemetrexed, vinorelbine). The acceptance criteria have been set at ±15%; much of preparations matched ±10% and more than 99% dugs and solvents have been identified. Repeated errors concerning cyclophosphamide and pemetrexed has been observed and the reason behind this has been justified by Delmas et

al. [60] who described that the preparation error often increases upon analysis of powder presented drugs in comparison to solution ready for use. The main downside in recent publications with the QCPrep+® is the lack of spectral data provided and the absence of correlation between either the UV/Vis or Raman spectrum and the quantification and identification achieved. It is therefore to clearly evaluate the real contribution of the Raman detection during the AQC. Although, Multispec® and QCPrep+® analysers enable fast analysis, the main limitation remains the invasive nature of analysis (withdrawal from containers) and the large volume (~ 1 mL) which can have an impact on the final dose administered to patient, especially for paediatric preparations.

Non-invasive AQC of chemotherapeutic preparations, i.e. direct analysis into the containers, can help to maintain the integrity of the prepared dose as well as protecting the health care worker and the working environment from the risk of toxicity.

Pioneer work has been conducted by Bourget et al. with comparative studies between HPLC, UV\vis-FTIR Multispec® (as invasive methods) versus Raman spectroscopy (non-invasive analysis using fibre optic as probe) for AQC of chemotherapeutic solution prior to administration. The first one [76] was a comparison between HPLC system and Raman spectroscopy (using fibre optic as a probe and 785 nm laser) have been performed for AQC of 5-fluorouracil prepared in a complex medical device (elastomeric infusion pump). Both of the used methods have shown good results that matched the validation criteria (trueness, precision and accuracy) in the range 7.5 - 50 $g{\cdot}L^{-1}$ in either 0.9% normal saline or 5% dextrose. The Spearman and Kendall correlation tests and statistical methods have been used to compare between the two methods confirmed a strong correlation between the obtained results under applied experimental conditions, p-value $< 1 \times 10^{-15}$. In Raman spectroscopy, the spectral region 700 and 1400 cm^{-1} has been selected for both the characterization and quantification. The second study [68] included three classes of chemotherapeutic drugs have been selected which present the mostly prescribed on oncology preparation units: oxazophosphorines (cyclophosphamide and ifosfamide) packaged in flexible polyolefin bags, anthracyclines (epirubicin and adriamycin) packaged in polyethylene syringes and 5-fluorouracil prepared in elastomeric infusion pump. The comparison between the three methods has been performed by using non-parametric correlation rank tests. The comparison criteria for AQC here was based on analytical mode, analytical target, operator safety, cost and environmental preservation. In all parameters Raman was superior in that degradation is discarded, the capability of quantitative and qualitative analysis was augmented even in the presence of degradation products and the technique preserved the operator safety due to non-invasive analysis. Also, the

operational cost of analysis with Raman was the lowest one since no sample preparation and consumable needed, followed by UV\vis-FTIR and HPLC. Raman spectroscopy has met specification for daily AQC work. Furthermore, another comparison has been performed using HPLC and Raman spectroscopy for analysis of ganciclovir (an antiviral drug). Raman recording were however performed in glass vials using 532 nm laser of DXR SmartRaman® spectrometer (Thermo Fisher Scientific, Courtaboeuf, France). Analytical validation criteria have been performed in the range 0.8 - 10 $g{\cdot}L^{-1}$; the results obtained from both techniques were comparable [77].

Despite the promising results for direct analysis with Raman spectroscopy, the literature did not significantly expanded on the topic. Considering the wide range of molecules used for cancer treatment, validation of Raman spectroscopy for AQC directly in containers (infusion bags, syringes or elastomeric pumps) remain not fully addressed until extended investigation are proposed.

In recent years, development in Raman spectroscopy instrumentation has led to miniaturisation with the introduction of handheld Raman devices. These instruments could also represent a new generation of tools for AQC of chemotherapeutic solutions due the simplicity of use and application for non-invasive analysis through different containers (glass or plastic). The potential of handheld Raman analysis has been highlighted by Lê et al. with a Metrohm Instant Handheld Raman Analyzer (MIRA, Metrohm, France) equipped with 785 nm laser excitation source. A first study has been published in 2014, for analysis of doxorubicin (0.1 - 2 $g{\cdot}L^{-1}$) and epirubicin (0.08 - 2 $g{\cdot}L^{-1}$) in glass vials. [78]. A second follow up study was published in 2018 for the analysis of taxanes antineoplastic drugs [79]: cabazitaxel (0.05 - 0.25 $g{\cdot}L^{-1}$), docetaxel (0.2 - 0.75 $g{\cdot}L^{-1}$), paclitaxel (0.24 - 1.2 $g{\cdot}L^{-1}$). Although in these studies Raman spectroscopy has demonstrated very good discrimination using PLS-DA. Handheld Raman spectroscopy showed limited sensitivity for quantification of low concentrations in the therapeutic range. Moreover, the analysis performed in glass vials somehow limit the relevancy of the application. Nevertheless, later in 2018, Lê et al. have reported a study for direct AQC of gemcitabine (1-20 $g{\cdot}L^{-1}$) directly through plastic infusion bags using the handheld Raman technology [80]. Results presented are promising but more development in terms of multivariate analysis for better understanding the impact of spectral contribution from containers on the discrimination and/or quantification are needed.

Table 1 summarise the publications from the literature reporting application of VS for AQC of chemotherapeutic solutions.

Table 1. Publications reporting AQC of chemotherapeutic solutions

Author	Year	System	Set up	Citation
Dziopa et al.	2013	Multispec® analyser	FIA	[58]
Bazin et al.	2014	Multispec® analyser	FIA	[81]
Kiehntopf et al.	2012	Raman DXN1	Plastic infusion bag	[72]
Lê et al.	2018	Raman microscopy	Glass vials (sample holder)	[70]
Lê et al.	2018	Raman microscopy	Glass vials (sample holder)	[71]
Chouquet et al.	2016	QC-Prep® analyser	FIA	[73]
Chouquet et al.	2017	QC-Prep® analyser	FIA	[74]
Nardella et al.	2016	QC-Prep® analyser	FIA	[75]
Lê et al.	2014	Handheld Raman	Glass vials	[78]
Lê et al.	2018	Handheld Raman	Glass vials	[79]
Lê et al.	2018	Handheld Raman	Plastic infusion bags	[80]
Bourget et al.	2014	Multispec® analyser, RXN1 Raman using fibre optic and HPLC	Elastomeric infusion pump	[76]
Amin et al.	2014	DXR SmartRaman® and HPLC	Glass vials	[77]
Bourget et al.	2014	Multispec® analyser HPLC RXN1 Raman using fibre optic	FIA Polyolefin bags, polyethylene syringes and elastomeric infusion pump	[68]

2. MATERIAL AND METHODS

Spectroscopy relies on the interaction of light and matter and the analysis of signals resulting from phenomenon like absorption, emission, fluorescence and/or scattering [82]. The present work focuses on vibrational spectroscopy, namely absorption infrared spectroscopy (IR) and Raman scattering spectroscopy.

IR and Raman spectroscopy deliver spectra composed of bands (or peaks) assigned to vibrational modes. Positions and intensities of spectral features are specific to the chemical structures analysed and therefore it is well accepted that techniques provide molecular fingerprint of samples. Used together IR and Raman enable to elucidate the chemical structure based on the interpretation of the complex spectral signatures collected.

Although IR and Raman are considered complementary techniques, they rely on different physical phenomenon hence greatly differ in their instrumental set ups, the information collected and their applicability depending on the type of sample.

This chapter provides insight in their fundamental principles and their technical aspects.

2.1 Principle of vibrational spectroscopy

2.1.1 Electromagnetic radiation (EMR)

The EMR can be described by the continuous sinusoidal wave motion of the electric and magnetic radiation. Figure 1 illustrates the amplitude of electric field as a function of time.

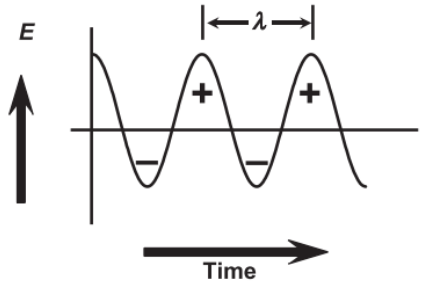


Figure 1. Amplitude of the electric vector of electromagnetic radiation as a function of time. The wavelength (λ) is the distance between two crests [83]

The parameters of the electric field are combined in Equation 1 below [83]:

$$\bar{\upsilon} = \frac{\nu}{\left(\frac{c}{n}\right)} = \frac{1}{\lambda} \quad (\textit{Equation 1})$$

where $\bar{\upsilon}$ is the wavenumbers, c is the speed of light, ν is the frequency, n is the refractive index of the medium that the light is passing through, λ is the wavelength.

A number of techniques have been developed over time based on different sections of the electromagnetic spectrum (EMR) (Figure 2). γ-ray are found in the region of the highest frequency (shortest wavelength) which can lead to bond breaking in the molecule. In the opposite, nuclear magnetic resonance (NMR) and electron spin resonance (ESR) correspond to the longest wavelength (lowest energy) of the EMR. IR and Raman spectroscopy lie approximately in the middle of the spectrum in the infrared and visible regions.

IR radiation interval starts from the end of the visible region (780 nm) and ends at the beginning of microwave (1 mm). The IR range include three regions: near IR (780 nm – 2.5 µm), mid-IR (2.5 µm – 25 µm) and far-IR (25 µm – 1000 µm) [6]. IR spectroscopy is performed in the Mid IR region which contains the predominant features of the molecular vibrations. These vibrations are characteristic of the functional groups present in the molecule, thereby will help for its structure elucidation [84]. Raman spectroscopy corresponds to region extending from visible and near infrared depending on the laser source used, most common excitation wavelengths are comprised between 488 nm and 830 nm.

IR and Raman are associated with rotation and vibration in the molecule without bond breaking.

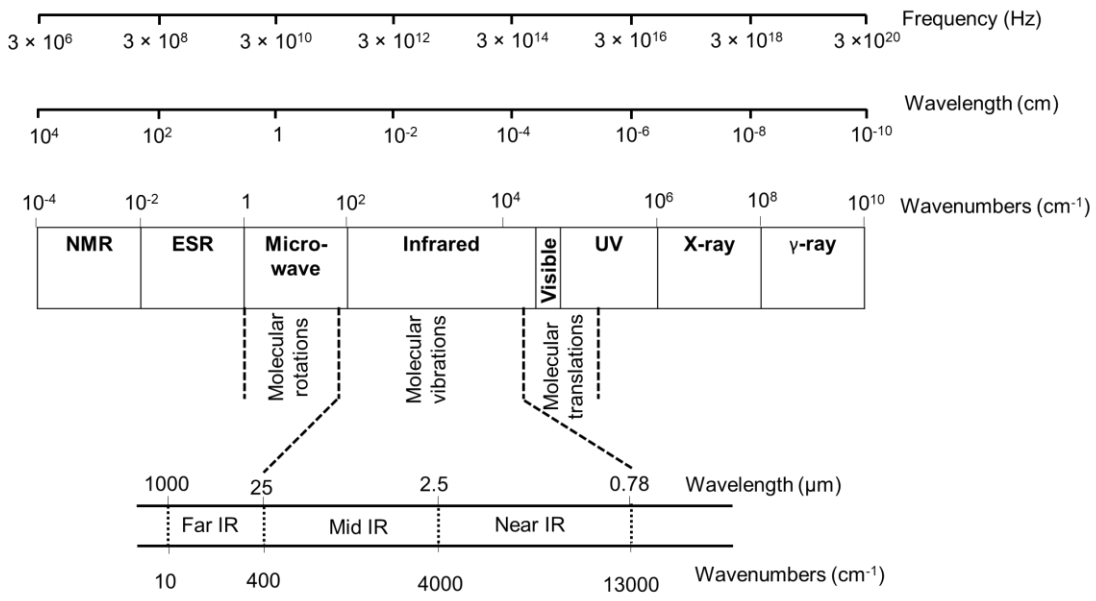


Figure 2. Energy units for various regions of the electromagnetic radiation [83].

Table 2 summarises the transitions in each region of the EMR. Each region in the EMR is presenting a separate analytical technique/discipline that has its specific application in science. Absorption in UV/vis spectroscopy (200-700 nm) leads to transition of the electrons in the bonds to higher quantum state and absorb some of the radiation passing through the sample. It has numerous applications in the pharmaceutical fields; quantification of drugs in formulations, determination of drugs solubility, the dissolution rate and the degradation kinetics, pk_a values of drugs as well as for identification [85].

In NMR (either proton or carbon), radiation in the radiofrequency region is used to excite atoms, thereby their spinning will be switched according to the applied electromagnetic field. The spinning and splitting pattern are characteristic of the chemical structure of the molecules. NMR is commonly used for characterisation of the raw, intermediate and finished products as well as determination of impurities, and non-destructive quantification of drugs in formulation [86].

Table 2. Spectral regions and their origins [83]

Spectroscopy	Range (λ, cm)	Origin
γ -rays	10^{-10} – 10^{-8}	Rearrangement of elementary particles in the nucleus
X- rays	10^{-8} - 10^{-6}	Transitions between energy levels of inner electrons of atoms and molecules
UV-Visible	10^{-6} - 10^{-4}	Transitions between energy levels of valence electrons of atoms and molecules
Raman and Infrared	10^{-4} - 10^{-2}	Transitions between vibrational levels (change of configuration)
Microwaves	10^{-2} - 1	Transitions between rotational levels (change of orientation)
Electron spin resonance (ESR)	1 - 10^{2}	Transitions between electron spin levels in magnetic field
Nuclear magnetic resonance (NMR)	10^{2} - 10^{4}	Transitions between nuclear spin levels in magnetic fields

Spectra for IR and Raman are displayed as intensity as function of wavenumbers (cm^{-1}), thereby in VS; wavenumbers (cm^{-1}) are usually used to express bands positions rather than the wavelength. The mid IR spectra are usually collected over the spectral window 4000 - 400 cm^{-1}.

2.1.2 Molecular motion and modes of vibrations

a) Vibrational modes

Theoretically, vibrational modes of a molecule depend on the number of atoms, their types and their geometry. The major types of molecular vibrations are stretching and bending as illustrated in Figure 3 with stretching and bending vibrations of -CH_2 group.

- ***Stretching modes:*** In the stretching mode; the length of the bond is only changed without change in the bond angle which can either be symmetric (υ_s) or asymmetric (υ_{as}).

- ***Bending modes:*** Bending (deformation) modes are characterised by the change in the bond angle without change in the bong length. They are subdivided into in-plane (rocking (γ_r) and scissoring (γ_s)) and out of plane (twisting (γ_t), wagging (γ_w)) [6].

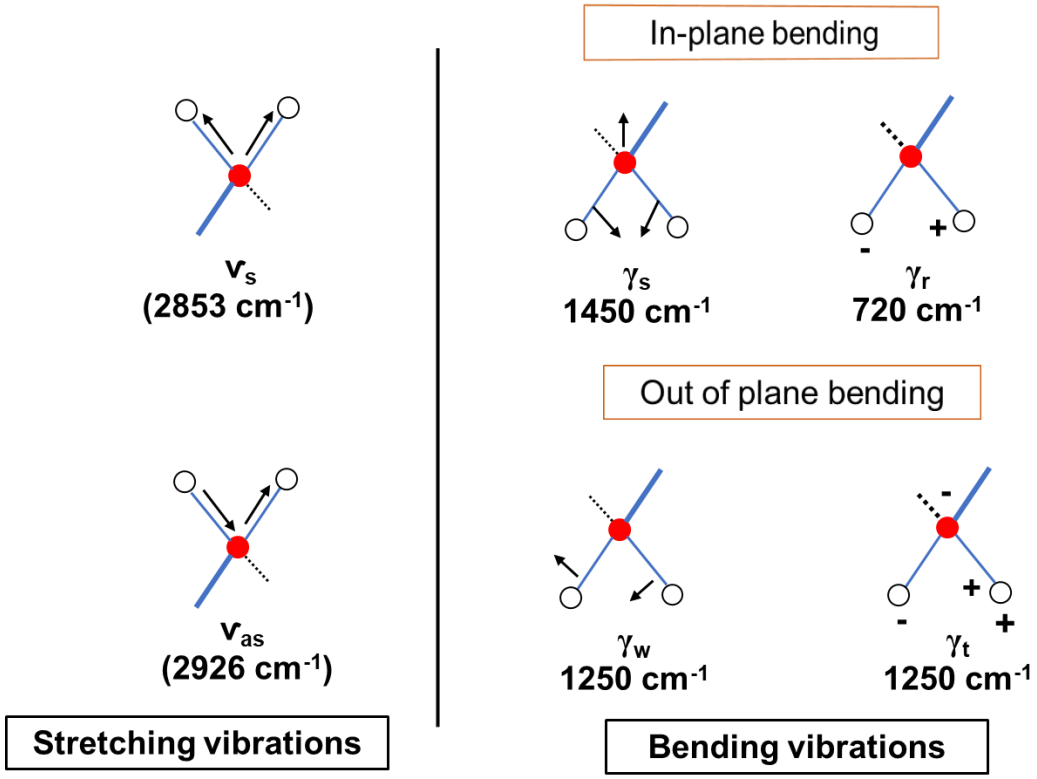


Figure 3. Stretching and bending vibrational modes of -CH_2 [86]

Degrees of freedom are used to describe the molecular motion that results from molecular vibrations according to thumb rule. A non-linear molecule containing n atoms will have 3 degrees of the translation in space and 3 for rotational, thus there are 3n-6 the number of vibrations possible. For the linear molecule only 2 types of rotations are possible hence the number of vibration becomes to 3n-5 [87].

For H_2O, there are 3×3-6 = 3 degrees of freedom, corresponding to asymmetric stretching (3490 cm^{-1}), symmetric stretching (3280 cm^{-1}) and bending vibrations (1654 cm^{-1}) as seen in Figure 4.

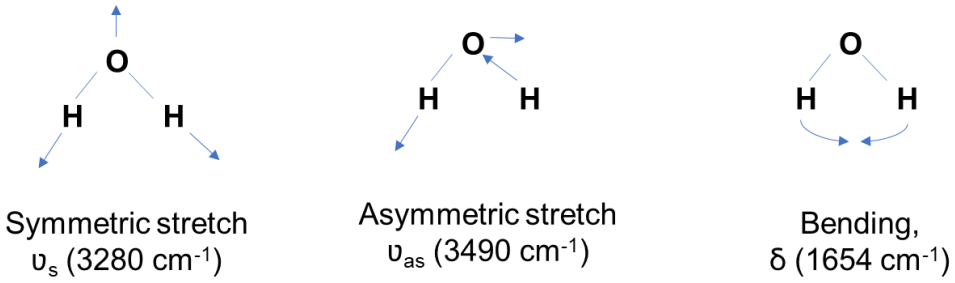


Figure 4. vibrational mode observed for H_2O molecule [88]

For CO_2 , 4 vibrations (3×3-5) are possible which are symmetric stretching at 1340 cm^{-1}, asymmetric stretching at 2350 cm^{-1} and 2 bending vibrations at 667 cm^{-1} [83,89] as shown in Figure 5.

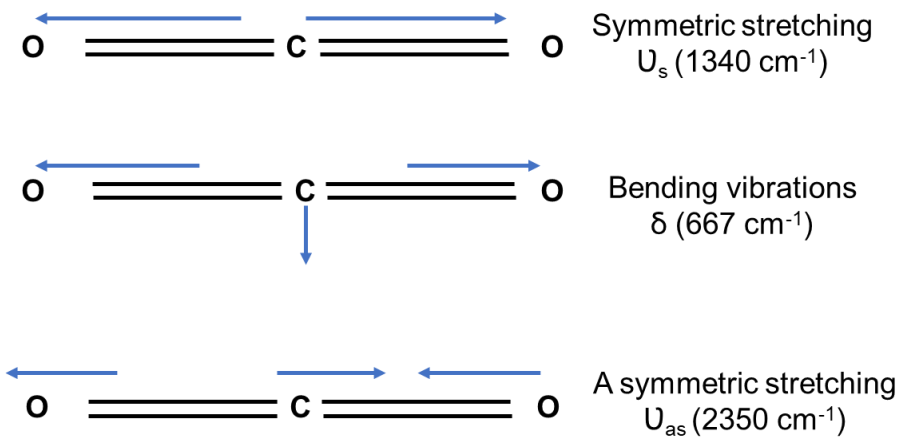


Figure 5. Vibrational modes of CO_2 [83]

b) Spectral interpretation

Spectral interpretation of IR and Raman spectra helps identifying the different functional groups present in the molecules and thereby can help for its identification.

i) Vibrational frequency of diatomic molecule:

A simple illustration of the molecular vibration is considering the diatomic molecule two vibrating masses connected by a spring. The bond distance continually changes, but still an

equilibrium or average bond distance can be defined. The potential energy of the system increases when the spring is continuing to stretch or compress beyond the equilibrium distance. Figure 6 presents the harmonic oscillator, when a bond vibrates, its energy of vibration is continually and periodically changing from kinetic to potential energy and back again [86].

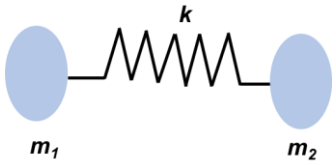


Figure 6. Harmonic oscillator of diatomic molecule

The molecular vibrations observed in Raman and IR spectra are calculated from frequency of a simple diatomic oscillator in terms of force constant (K) and μ reduced masses of the 2 atoms involved (Equation 2) [83].

$$\bar{\upsilon} = \frac{1}{2\pi}\sqrt{\frac{K}{\mu}} \quad \textit{(Equation 2)}$$

The force constant (K) is derived from Hooke's rule of the reduced masses of the system.

$$\mu = \frac{m1 \times m2}{m1 + m2} \quad \textit{(Equation 3)}$$

Where, m_1 is the mass of the first atom and m_2 is the mass of the second atom.

In spectra, the bands (peaks) positions depends on the type of the atoms present in the molecule as well as the type of the bonds. Figure 7, illustrates that the lower frequency vibrations are associated with the heavier atoms (Equation 3) while the increase in the bond strength is linked to higher frequencies as shown before in Equation 2, where the atomic force constant k (millidynes/Angstroms) with the order triple bonds > double bonds > single bonds. Hybridization affects the force constant K, also. Bonds are stronger in the order $sp > sp^2 > sp^3$.

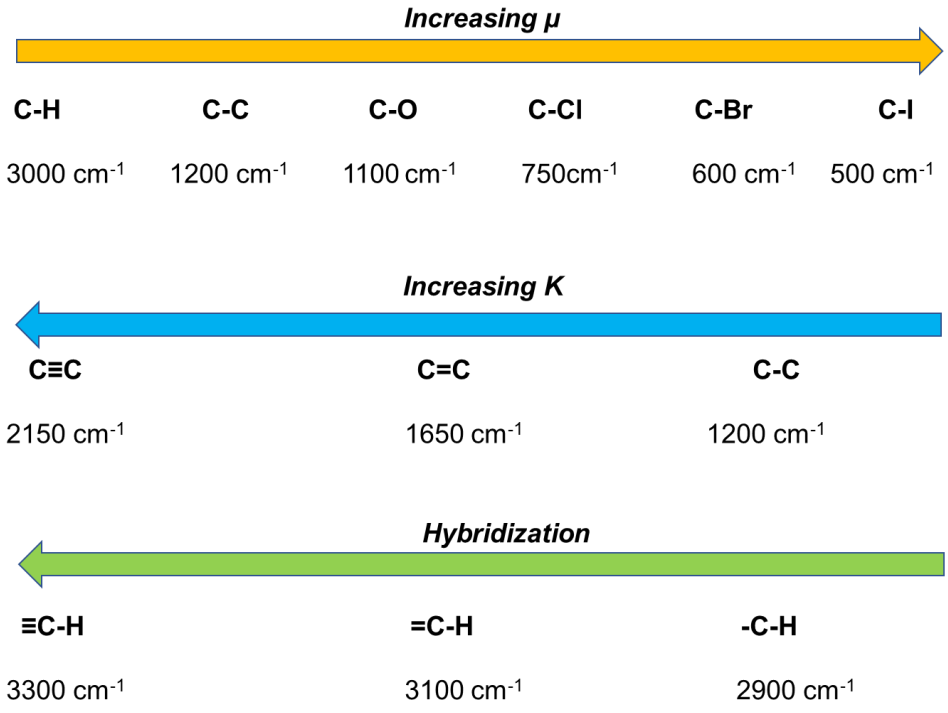


Figure 7. Relationship between the atomic masses, force constant and the hybridization to the frequency of vibration [86]

ii) Vibrational frequency of group vibrations:

For complex polyatomic molecules, the simplified models based on pairs of atoms do not reflect the reality. The notion of group vibration describes the role of the chemical environment on the frequency of vibrations hence the positions of spectral features. Although the vibrational frequency of specific functional group is not always presented as its own characteristic frequency, rather it is being affected by neighbouring environment [86].

For example; in ethers (R-O-R') the vibrational frequency of C-O is depending on the type of neighbouring functional groups attached to the carbon atom, so this group exhibit a frequency in the range (1000 – 1300 cm^{-1}). Asymmetric stretching of C-O-C of di-alkyl eithers give a single strong band at 1120 cm^{-1} while aryl alkyl ethers give two strong bands around 1250 cm^{-1} and 1040 cm^{-1} due to asymmetric and symmetric stretching of C-O-C. Vinyl alkyl ethers result in two bands; one is strong at 1220 cm^{-1} due to asymmetric stretching and another weak band at 850 cm^{-1} due to symmetric stretching [86].

Another example is for the vibrational frequency of C-H group which depends also on the environment in which it presents; aliphatic (alkane, alkene, alkyne), aromatic, etc. Table 3

presents typical vibrational modes observed in IR and Raman spectrum of selected functional group.

Table 3. Vibrational modes of selected functional groups on IR and Raman

Functional group/vibration	Region (cm^{-1})	IR	Raman
υ_s(C-O-C)	800 - 970	weak	medium
υ_{asy}(C-O-C)	1060 - 1150	strong	weak
υ(C−H)	2800 - 3000	strong	strong
υ(=(C-H))	3000 - 3100	medium	strong
υ(≡(C-H))	3300	strong	weak
υ(C=O)	1680 - 1820	strong	medium
δ(H_2O)	~1640	strong	weak broad
υ(O-H)	3100 - 3650	strong	weak

2.2 Absorption Infrared Spectroscopy

2.2.1 Principle

2.2.1.1 Physical aspects of absorption IR

IR region has been discovered since 1800 by William Herschel [90]. The molecule absorbs in IR when the frequency of the incident radiation matches that of its vibration, then the molecule promotes from the ground state to the vibrational excited state as shown in Figure 8 [87]. The absorbed energy causes an increase in the amplitude of the vibrational motions of the bonds within a molecule.

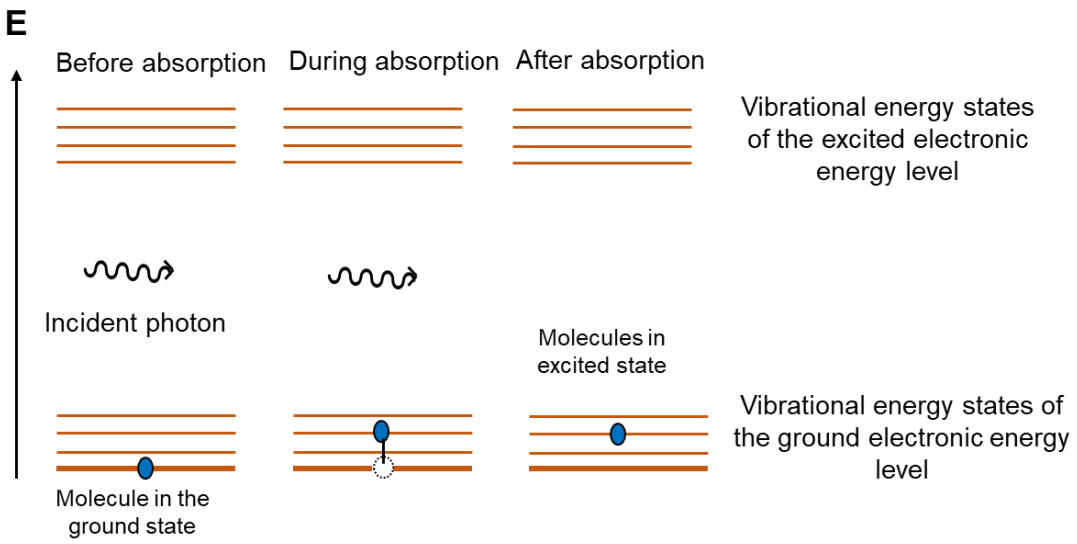


Figure 8. Absorption process in IR region

Electric radiation is emitted as photons hence the photon energy is governed by:

$$Ep = h\,\nu \quad (Equation\ 4)$$

Ep is the energy of the photon, *h* is Planck's constant (= 6.6256×10^{-27} erg·sec), ν is the frequency. Energy transfer from the electromagnetic field to the molecule can happen only when Bohr's equation is satisfied [83].

$$\Delta E = hc\bar{\upsilon} \quad (Equation\ 5)$$

Where, ΔE is the difference in energy of the quantised molecule and *c* is the velocity of light.

2.2.1.2 Experimental considerations

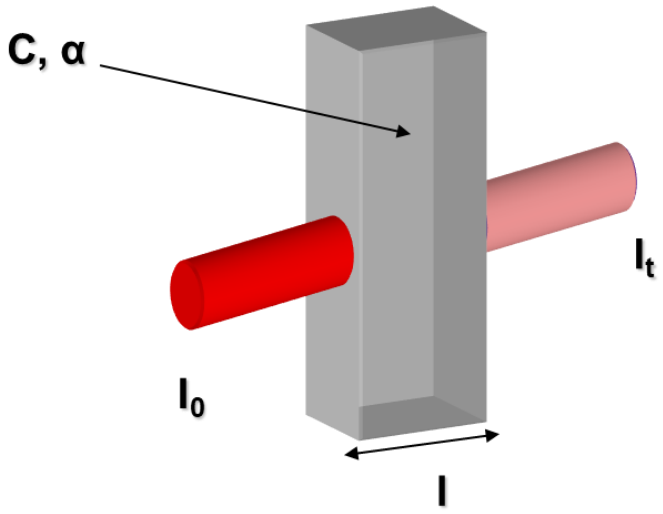


Figure 9. IR absorption according to Beer Lambert's law

Absorbance is obtained by measuring the decrease of intensity of a radiation beam passing through the sample (Figure 9). Firstly, the %T transmittance is obtained from the ratio between the intensity of the transmitted radiation (I) and the incident radiation (I_0) expressed as percentage (Equation 6).

$$\%T = \left(\frac{I}{I_0}\right) \times 100 \text{ (}equation\ 6\text{)}$$

Secondly, the absorbance is calculated using the negative decadic logarithm of the transmittance (Equation 7) [84]:

$$A = -\log_{10}(T) \quad (Equation\ 7)$$

Similarly to UV-Vis spectroscopy, IR spectroscopy is also dictated by Beer Lambert's law (Equation 8) [84]:

$$A = \varepsilon l c \quad (Equation\ 8)$$

Where; ε is the absorption coefficient, l is the path length in cm (inside the sample) and c is the concentration (Figure 9). The absorptivity can be expressed as the molar attenuation coefficient

($L \cdot mol^{-1} \cdot cm^{-1}$) or the mass attenuation coefficient ($mL \cdot g^{-1} \cdot cm^{-1}$) depending on units used for the concentration. IR remain known as a semi-quantitative technique due to interferences from refractive index of the sample, temperature or thickness of the sample hence sometimes limiting the applicability of Beer Lambert's law. However, with optimised experimental set up coupled to multivariate data mining absolute quantification can be achieved. Recently, the literature has seen increasing studies developing IR quantitative analysis [91,92].

2.2.2 Instrumentation

A simple representation of on FT-IR (Fourier transform infrared) instrument is shown in Figure 10.

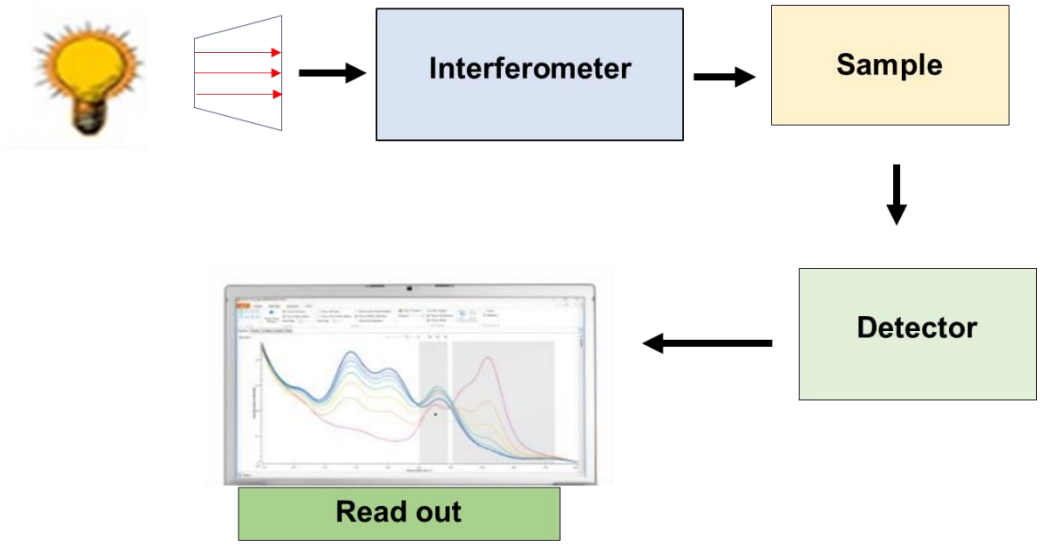


Figure 10. Typical components of a FT-IR instrument

During the PhD, a Frontier (Perkin Elmer, France) was used for data collection. The main components are: 1) A polychromatic light source, 2) Michelson interferometer which is the main component in FTIR system, 3) sample compartment and 4) the detector (temperature-stabilized DTGS - deuterated triglycine sulfate).

2.2.2.1 Michelson interferometers

Figure 11 illustrates the principle of the Michelson interferometer. It consists of moving mirror, fixed mirrors and semi-reflective lens or beam splitter which generate destructive and constructive interferences between the light and the matter. In brief, a radiation from the broadband IR source is collimated and passed to the interferometer, then hit the beam splitter. At the beam splitter, half the IR beam is transmitted to the fixed mirror and the remaining half is reflected to the moving mirror. After the divided beams are reflected from the two mirrors, they are recombined at the beam splitter [26] and then going to the detector and recorded as interferogram. The interferogram is considered as a sum of all cosine waves from the light source, then the interferogram is converted into a full spectrum by the mathematical function of Fourier transform [86].

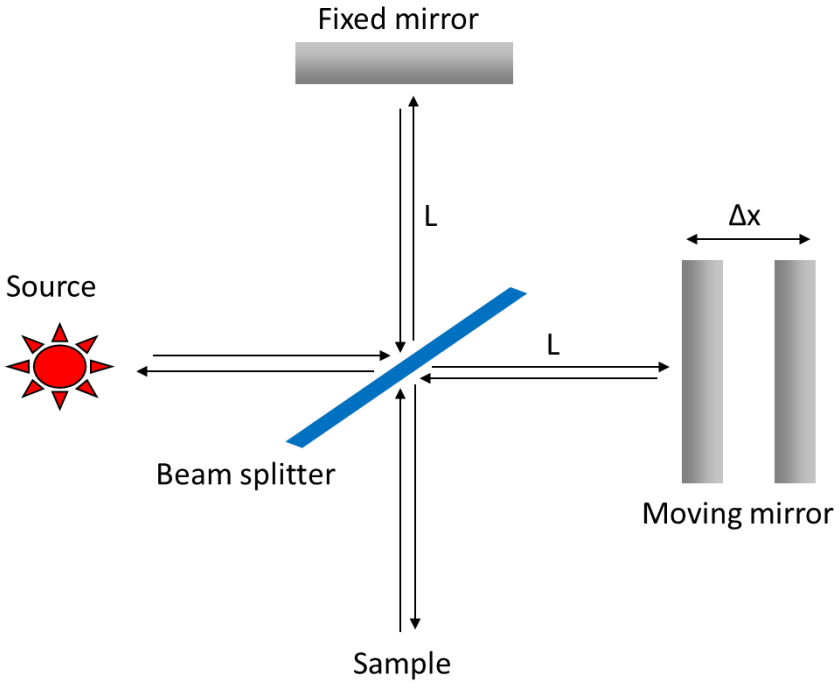


Figure 11. Michelson interferometer [26]

2.2.2.2 Attenuated total reflectance (ATR)

ATR technique has been developed between 1950 – 1960. ATR-FTIR is the most widely implemented IR sampling technique that provide high reproducible analysis through measuring the change of an internally reflected beam in contact to the sample via crystal surface made of zinc selenide, germanium or diamond [90,93]. ATR accessories are available and enable analysis of solid, paste, liquids and gaseous samples [84]. It requires no or a little sample preparation and a very small sample volume. For this work 2 accessories were used to perform the analysis with a mono-reflection or a multireflection diamond ATR crystal (Figure 12). An evanescent wave is formed at the interface between the ATR crystal and the sample enabling to measure an absorbance.

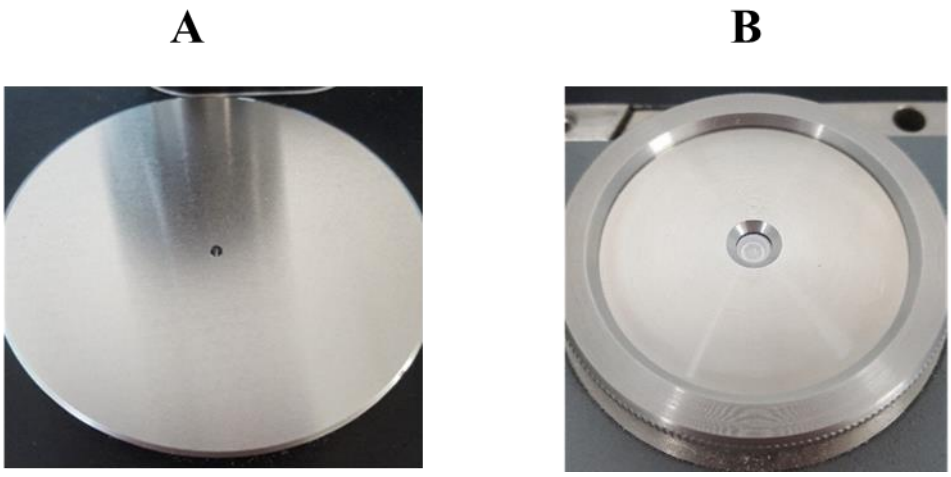


Figure 12. Fourier transform infrared Frontier (Perkin Elmer, France) equipped with: A) mono-reflection and B) multireflection ATR diamond accessary

ATR occurs when a beam of radiation enters from a higher refractive index (more-dense) into with a lower refractive index (less dense) medium. The reflected fraction of the incident beam increases with the increase of incidence beam angle. When the angle of incidence is greater than the critical angle, the incident radiation is being completely reflected at the interface. The incident beam can penetrate a very short distance beyond the interface as well as into the less dense medium before the complete reflection occurs. This penetration is called the evanescent

wave and typically is at a depth of a few micrometers (µm). Its intensity is reduced (attenuated) by the sample in regions of the IR spectrum where the sample absorbs [94]. Intensity of ATR absorption depends on the refractive indices of the sample and the crystal, the angle of the incidence for the incoming radiation and the wavelength of the radiation [26]. Figure 13 illustrates the basic ATR principle.

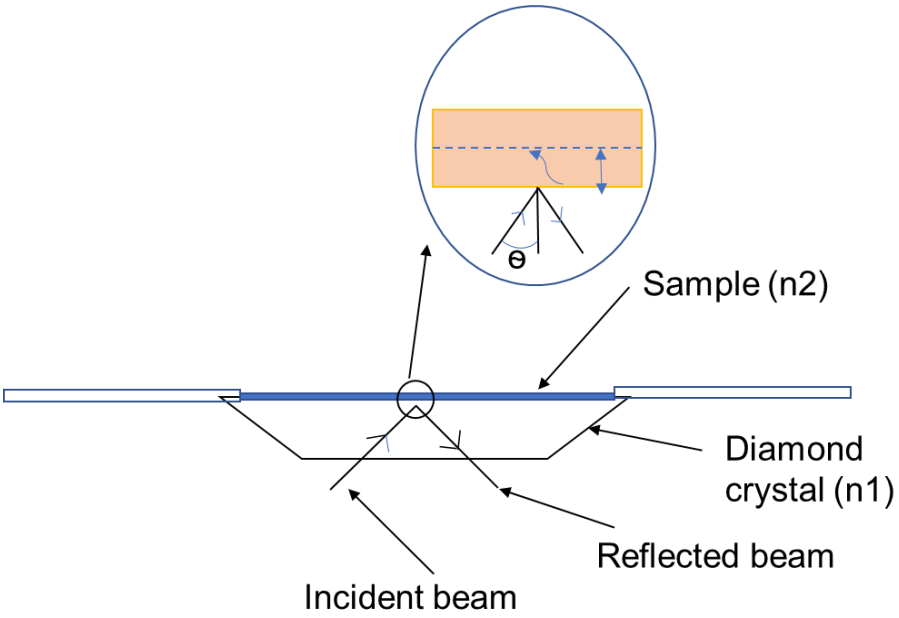


Figure 13. Basic principle of ATR [95]

The penetration depth (d_p) of the evanescent wave can be explained as the distance required for the electric field amplitude to fall into its 1/e of its value at the interface and given by Equation 9 [95]:

$$d_p = \frac{\lambda_i}{2\pi n_1 \left(\sin^2\theta - n_{21}^2\right)^{1/2}} \qquad \textit{(Equation 9)}$$

Where λ is the wavelength, *n1* and *n2*, the refractive indices of the ATR crystal and the sample. *Θ* is the angle of incidence. As seen in Equation 9, the penetration depth of the beam depends on the wavelength [26]. For a polymeric sample with n2=1.6 on the surface of the ATR crystal (Diamond) of n1=2.417 with a 45^0 angle of incidence, the penetration depth will in the range 2.8 - 1.4 µm for the spectral range 1000 - 2000 cm^{-1} [26].

2.3 Raman Spectroscopy

2.3.1 Principle

The concept of inelastic scattering of light was initially predicted in 1923 by Adolf Smekal but only observed later in 1928 [96]. The technique was named after the Indian scientist C. V. Raman who was awarded a Nobel prize in 1930 [90]. The Raman effect describes the probability to observe a change in the frequency of scattered photons compared to the incident photons [87] (Figure 14).

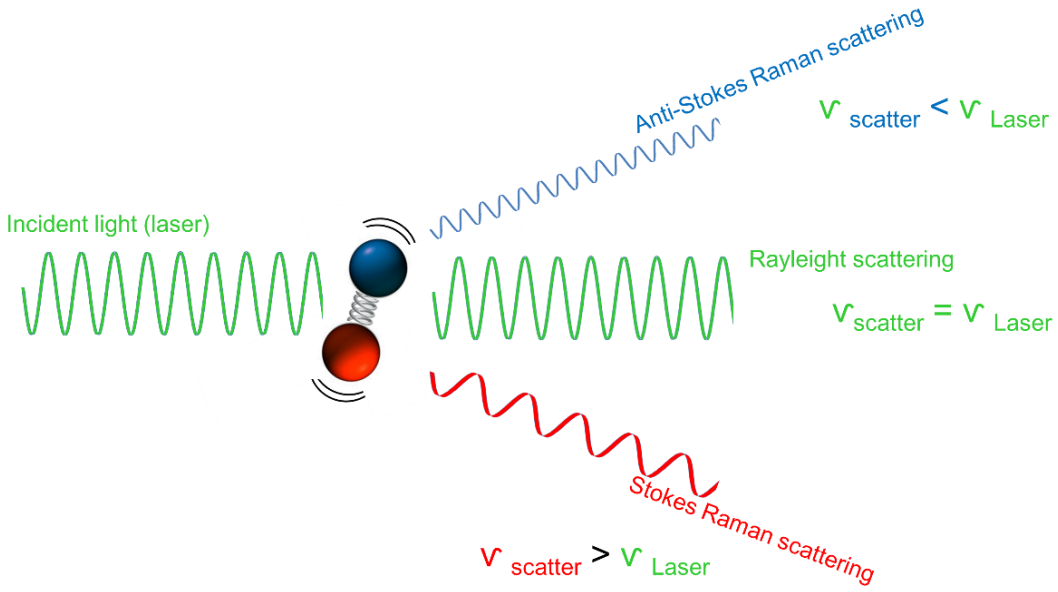


Figure 14. Light diffusion phenomenon [97]

When performing Raman analysis and irradiating the sample with a monochromatic laser source, it will be dispersed in all directions either due to elastic or inelastic scattering. In case of elastic scattering, which is the strongest, there is no difference in frequency (υ_0) in scattered photons, it is the Rayleigh scattering (Figure 14). There is also a probability that the molecules excited to a virtual state do not return to the same fundamental energy level, resulting in emission of photons with a shift in their wavelength. Two possibilities are described, Stockes scattering: when the frequency of the incident radiation is greater than the frequency of scattered radiation, (υ_0 - ν). Or anti-Stockes: the frequency of the incident radiation is less than that of the scattered radiation anti-Stockes lines appear (υ_0 + ν) [82,98]. The probability for inelastic

scattering and occurrence of Raman effect is 1 out of 10^8 compared to Rayleigh scattering. Experimentally, Raman spectroscopy analysis is usually based on the recording of Stokes scattering which has a higher probability to occur (hence stronger signal) compared to the anti-Stockes scattering [97,99].

2.3.2 Instrumentation

During the initial work of the thesis a LabRAM spectrometer (Horiba Jobin-Yvon, France) has been used. The main parts of the micro-spectrometer are: 1) laser source, 2) a confocal microscope, 2) monochromator and 3) the detector.

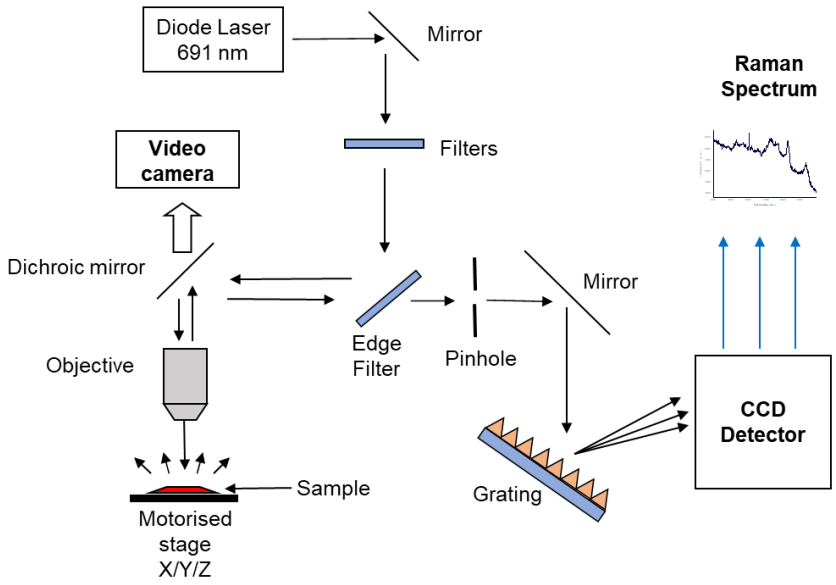


Figure 15. Instrumental parts of Raman microscope

A simplified representation of the Raman system is presented in Figure 15. The light sources used for Raman spectroscopy monochromatic lasers delivering high power through the system. Raman microscope can be used for mapping small sample area with a lateral resolution of roughly 1µm [82] depending on the wavelength used and the objective lenses selected. Raman microscopes also enable confocal analysis i.e. collection of the scattered light from a short focal volume, excluding the out off-focus or off-axis photons (pinhole). Finally, the back-scattered

light is dispersed onto the charge coupled device (CCD) camera to produce a Raman spectrum [96,100].

Detectors: CCD detector is used which is a highly sensitive photon detector which is containing large number of light-sensitive small areas (either in one dimension or two) known as pixels [96]. A CCD is a silicon-based multi-channel array detector of UV, visible and NIR light, making these detectors suitable for analysis of the inherently weak Raman signal. In a typical Raman spectrometer, the back-scattered light is dispersed using a diffraction grating. This dispersed light is projected onto the long axis of the CCD array. The first element will detect light from the lowest cm^{-1} edge of the spectrum. The second element will detect light from the next spectral position, and so on until the last element will detect light from the higher cm^{-1} edge of the spectral range selected.

Dispersive element: The grating disperses the signal into CCD detector by deflection of each wavelength at different angle. Grating is determined by the number of grooves/mm or lines/mm on the surface which can be in the range 300 – 3600 lines/mm according to the diffraction ability and angular dispersion of the grating. Spectral resolution depends on the grating used; 300 lines/mm grating provides low resolution while grating of 1800 line/mm can provide higher resolution by dispersion of signal override a wide number of CCD pixels. Spectral resolution also depends on the laser wavelength and the spectrometer focal length.

Filters: Holographic notch and dielectric edge filters are most used as Rayleigh filters which must be selected according to the laser wavelength. Holographic notch filters can filter only the laser wavelength and allowing measurement of Stokes and anti-Stokes lines while edge filters can only transmit light wavelengths above that of the laser in use [99].

2.3.3 Confocal Raman spectroscopy

Confocal Raman spectroscopy reduces the unwanted signals and at the same time increase the axial resolution of the recorded Raman spectra. In the setup, the pinhole is designed to exclude signal from the out-of-focus region, thereby only the signal from one focal plane is collected (optical slice) corresponding to one volumetric pixel (voxel) as shown in Figure 16 [9,101].

To focus the light onto the sample and collect the backscattered light, a high numerical aperture (NA) objective is used in order to achieve small focal volumes and to collect as much of the back-scattered light as possible. Taking the advantage of flexible movement of the sample positioner in 3 directions (X, Y, Z) will allow measurement of different positions. The depth of focus (axial resolution) can be calculated according to Berek formula, it depends on the NA and the magnification of objective lenses as seen in Equation 10:

$$depth\ of\ focus = \frac{350}{NA+M} + \frac{0.275}{NA^2} \quad (Equation\ 10)$$

M is the total magnification which = objective lens magnification × eyepiece magnification.

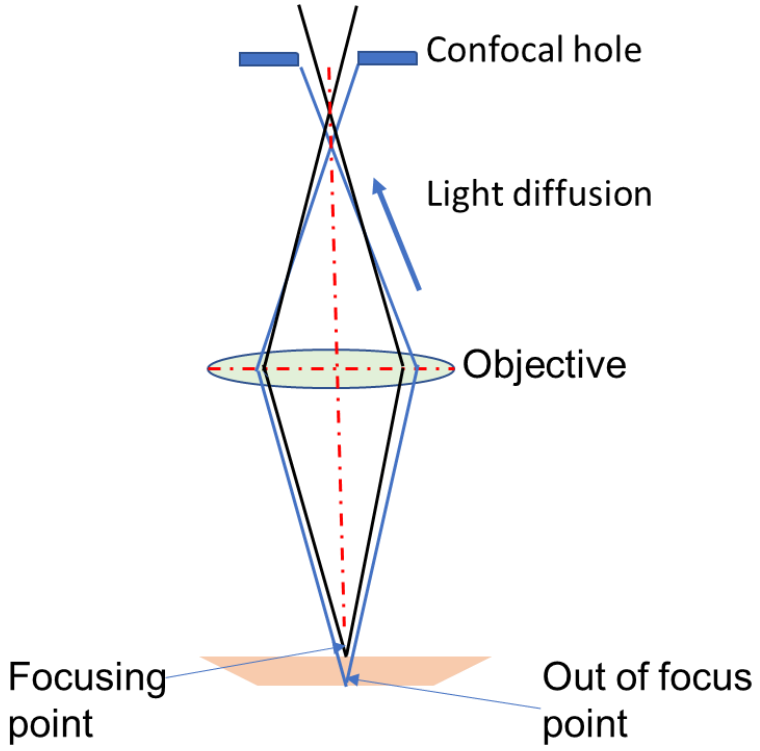


Figure 16. Principle of confocality of microscope

2.3.4 Macro sampling in quartz cuvettes

In case of macro- analysis, a cuvette holder (Figure 17) is fixed on the turret of the microscope. In that case the laser in not focus but directed trough the sample thanks to a mirror at 45^0. A second mirror is positioned behind the cuvette, reflecting the laser through the sample a second time to increase the intensity of the spectra collected.

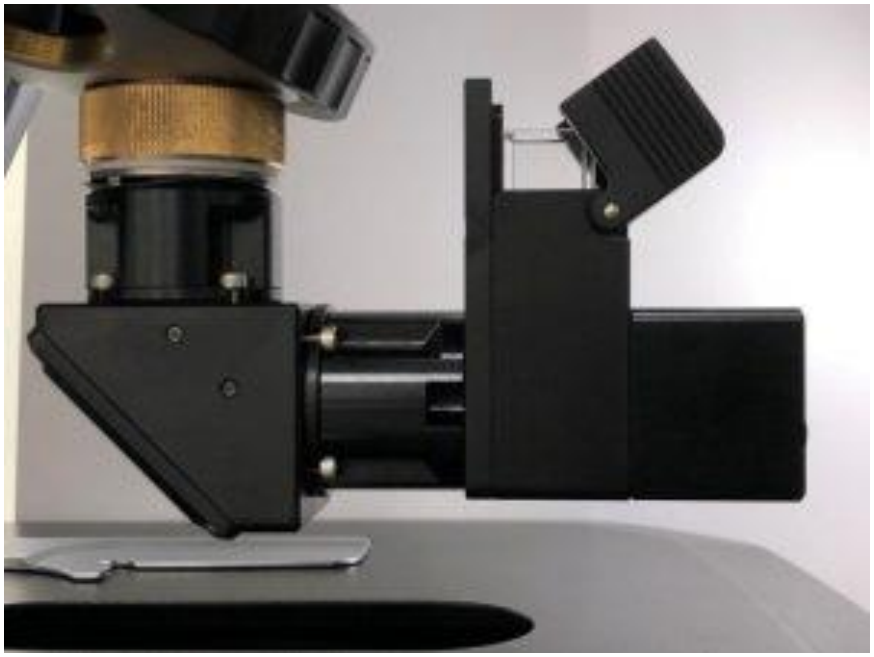


Figure 17. Cuvette holder attachment to Raman micro-spectroscopy (https://www.technospex.com/resources/cuvette-holder-attachment-uraman-micro-spectroscopy-liquid-sample-measurements/)

2.3.5 Miniaturisation of confocal Raman spectroscopy

Miniaturisation of Raman spectrometers has resulted in commercialisation of two types of compact confocal apparatus that can be categorised as (trans) portable (benchtop) and handheld Raman system. Portable Raman system (Figure 18) equipped with fiber-optic remote probe in which filters and lenses are directly positioned on the end of the optical fiber [102] which are

either made of glass or fused silica. Several lasers are available on the commercial instruments, 532 nm , 785 nm and 1064 nm.



Figure 18. Portable Raman spectrometer from Metrohm, France (https://www.metrohm.com/en-sg/products/spectroscopy/bw-tek-spectroscopy/bw-tek-portable-raman/BWT-840000880)

The development of Handheld Raman spectrometers (Figure 19) has resulted in a good implementation for quality control in pharmaceutical industries especially for raw material identification. The systems are portable and flexible for use, no need for large space. Furthermore, its software doesn't need specific experience for routine use neither specific sample preparation in the production environment. Handheld Raman spectrometers enable analysis through glass, transparent packing material and plastic using 785 nm or 532 nm. However, devices with 830 nm and 1064 nm lasers are also available for specific applications. More advanced handheld systems use orbital raster scan (ORS) technology which has a good impact on the accuracy, repeatability and reliability of analysis [79].



Figure 19. Handheld Raman spectrometer from Metrohm, France(https://www.metrohm.com/en/products/spectroscopy/mira-handheld-raman-spectrometers/)

2.4 Complementarity of Raman and IR spectroscopy:

2.4.1 Selection rules of vibrations

IR and Raman spectroscopy are usually described as complementary techniques which is explained by the differences in the molecular information encompassed in the spectra. Selection rules relate the strength of spectral features observed in infrared and Raman spectra. It is described that while some vibrational modes are active in both infrared and Raman, others would be only active for IR or Raman spectroscopy. The comparison of IR and Raman spectra collected from doxorubicin (DOX) unambiguously highlights that the 2 signatures significantly differ (Figure 20).

The band at 762 cm^{-1} and 789 cm^{-1} (=C-H (aromatic) bending vibrations), 817 cm^{-1} (N-H out of plane bending) and 1700 cm^{-1} (C=O stretching) are observed in IR but not Raman. Experimentally the selection rules don't necessary lead to complete desperation/apparition of spectral bands but has an influence on their intensities. For instance, bands at 1210 cm^{-1} (C-O-H vibrations) and 1445 cm^{-1} (aromatic ring stretching) are stronger in Raman whereas bands at 987 cm^{-1} (C=O bending vibrations), 1079 cm^{-1} (C-O bending vibrations), 1286 cm^{-1} (H-bonding

vibrations of O-H--O coupled to ring vibrations) and 1576 cm^{-1} (N-H bending vibrations) appear stronger for IR. It is also important to keep in mind that the spectral signature is strongly influenced by the instrumental set up, the optics, acquisition parameters, detector response therefore direct comparison of IR and Raman spectra can be difficult.

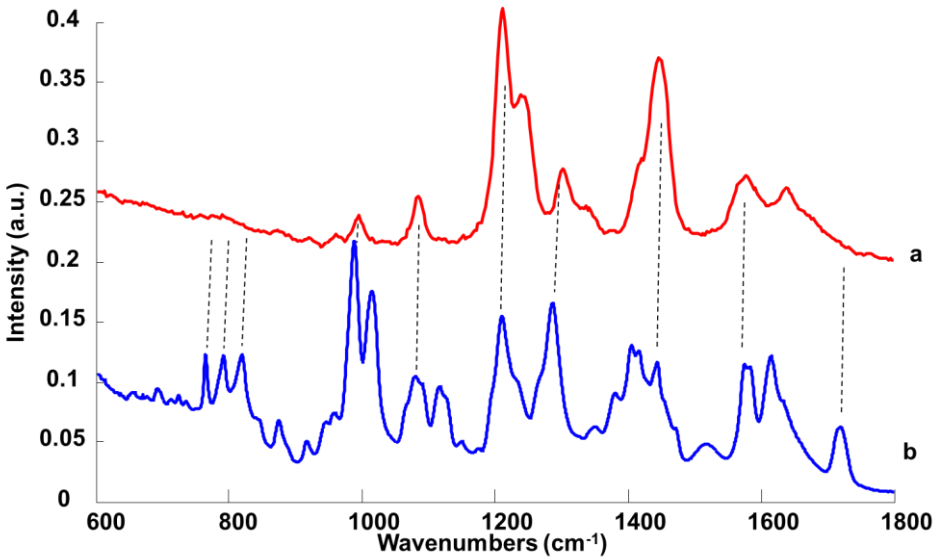


Figure 20. Raman (a) and IR (b) spectra of DOX (2 $g{\cdot}L^{-1}$)

Interaction between electromagnetic radiation and a molecule causes change in its charged particles and hence causes an induced dipole moment (Equation 11) [89]

$$\mu = \alpha E \quad (Equation\ 11)$$

Where, μ is the induced dipole, α is the polarizability of the molecule and E is the incident electric field. The main rules that govern the vibrations with IR and Raman spectroscopy can be illustrated as following [89]:

a) The dipole moment (μ) for a molecule is a function of the magnitude of the atomic charges (e_i) and their positions (r_i)

$$\mu = \sum e_i r_i \ (Equation\ 12)$$

In terms of quantum mechanics, the IR absorption is considered as an electric dipole operator mediated transition where the change in the dipole moment of the molecule, μ, with respect to the change in the vibrational amplitude, Q, is greater than zero (Equation 13):

$$\frac{\partial \mu}{\partial Q} \neq 0 \quad \textit{(Equation 13)}$$

A molecule will absorb in IR if there is a change in the dipole moment which will result in a change in the vibrational energy level. Consequently, the polar groups (e.g., C=O, N-H) are strongly IR active and associated with active asymmetric modes of vibrations.

b) The induced dipole moment occurs as a result of the molecular polarizability α, where the polarizability can be described as the deformation of the electron cloud around the molecule by an external electric field. Thereby, the change in the polarizability with respect to a change in the vibrational amplitude, Q, is greater than zero (Equation 14).

$$\frac{\partial \alpha}{\partial Q} \neq 0 \quad \textit{(Equation 14)}$$

Symmetric modes and homopolar bonds (e.g. C=C or S-S) are Raman active [103].

A general selection rule specified that molecules with a centre of symmetry follows a mutual exclusion effect. This is the case of homonuclear diatomic molecules (X_2) such as H_2, Cl_2, O_2, N_2 that are IR inactive but Raman active. In centrosymmetric molecules; the symmetric vibrations can't give rise to IR absorption because there is no change in the dipole moment, instead the change in polarizability give Raman spectra. Diatomic molecules such as O_2 there will be only one vibration (O-O stretching) which is centrosymmetric [87].

2.4.2 Bands positions

According to Jablonski diagram (Figure 21) the energy difference between vibrational fundamental levels in absorption IR and the energy of photons emitted during the inelastical scattering for Raman spectroscopy are equal. Therefore, a vibrational mode active in both techniques has the same position and spectra can be superimposed. Experimentally this is

verified because the axis Raman spectra is expressed as "Raman shift" in cm^{-1} and is calculated as according to Equation 15:

$$Raman\ shift\ (cm^{-1}) = 10^7/(\lambda_{ex}\ (nm)\ ) - 10^7/\lambda(nm) \qquad \textit{(Equation 15)}$$

It is the energy difference between the incidence radiation and the scattered radiation.

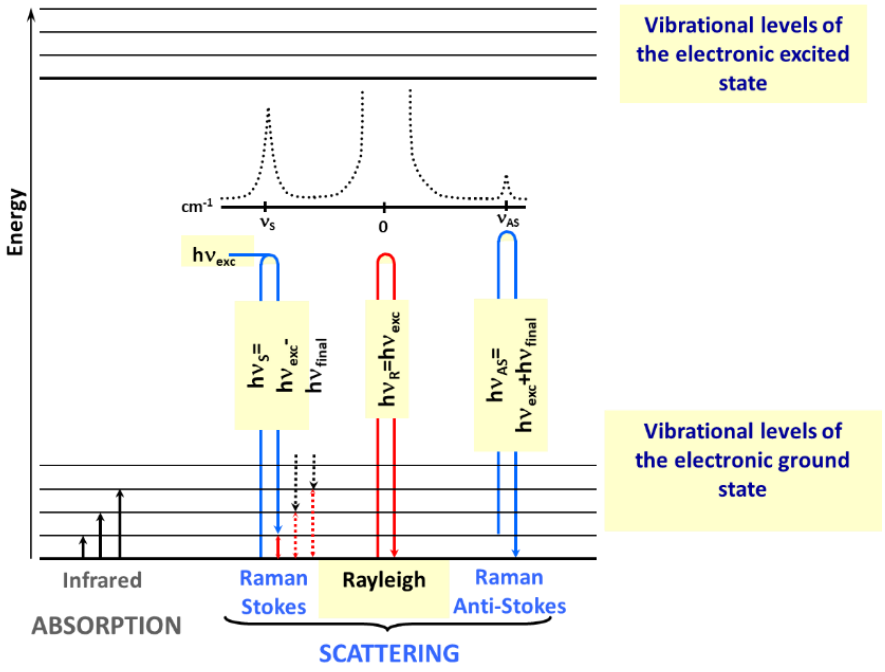


Figure 21. Jablonski diagram of absorption IR and Raman scattering

2.4.3 Analysis of solutions

H_2O molecule presents strong absorbance in the IR while it is a weak Raman scatterer. IR Analysis of aqueous solutions is difficult due to the bands at 1640 cm^{-1} and 3650 cm^{-1} corresponding to bending and stretching vibrations. The features from analyte in solutions are often overlaid with those of water making detection and quantification impossible.

Therefore, IR analysis in this thesis are performed from air dried drops where water contribution is removed. Figure 22 presents IR spectra of methotrexate (MTX) 21 $g{\cdot}L^{-1}$ recorded from air dried drop (Figure 22a) and from solution (Figure 22b).

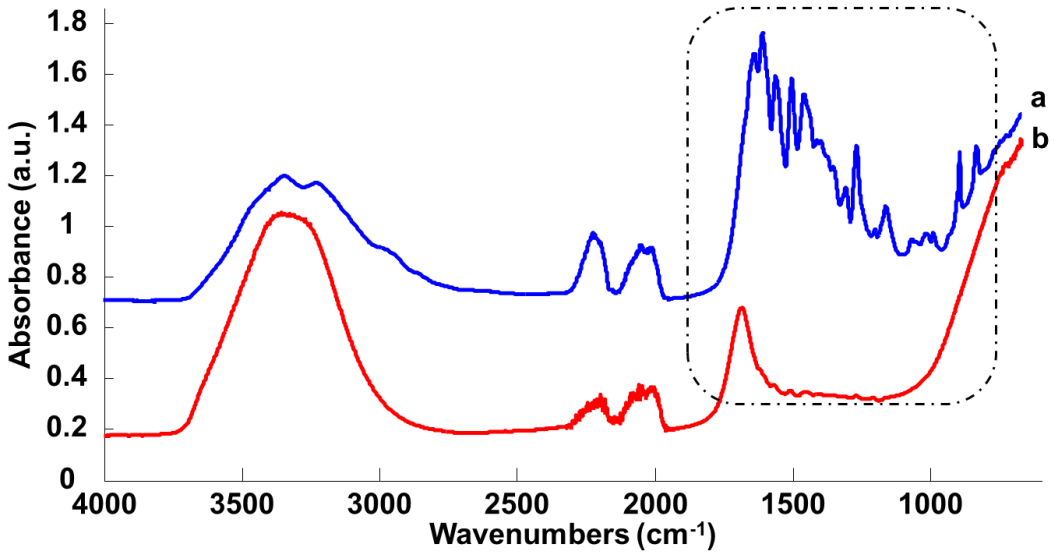


Figure 22. Mean ATR-FTIR spectra of: a) MTX 21 $g{\cdot}L^{-1}$ from air dried drop and b) from solution. Spectra are offset for clarity

On contrary, Raman analysis of solutions is less affected by the weak contribution for H_2O bands. Figure 23a presents a spectrum of MTX at 21 $g{\cdot}L^{-1}$ compared to the spectrum of water. Notably, the band at 1640 cm^{-1} doesn't interfere with interpretation of MTX bands in the fingerprint region.

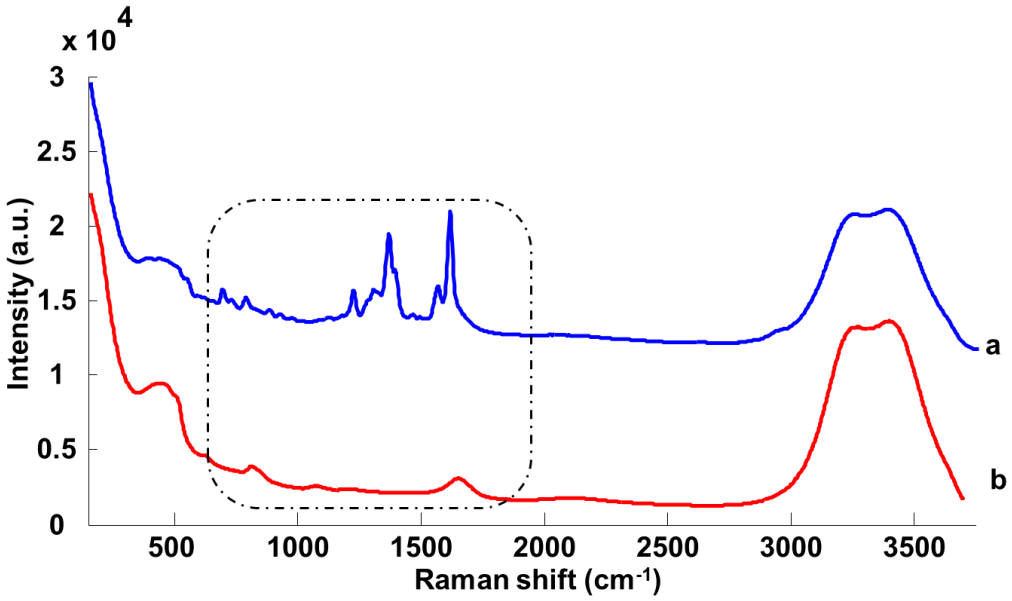


Figure 23. Mean Raman spectra of: a) MTX 21 $g \cdot L^{-1}$ solution and b) water. Spectra are offset for clarity

2.4.5 Fluorescence

Fluorescence can interfere with Raman analysis. Fluorescence depends on the chemical structure of the molecule, more specifically the presence of a fluorophore. For example, anticancer drugs camptothecins have strong native fluorescence due to the quinoline ring in their chemical structure. Fluorescence emission also corresponds to a Stokes shift in the emitted photons therefore the spectral range for both modes can overlap. Notably, anthracyclines class are fluorescent molecules due to the aromatic anthraquinone moiety, including doxorubicin, daunorubicin and mitoxantrone [104]. However, Raman systems are equipped with multiple wavelength enable to customise the experimental set up to reduce fluorescence interferences. For instance, during the thesis red lasers (633 nm, 691 nm) were used to collect data from chemotherapeutic solutions with witnessing fluorescence. In comparison, IR spectroscopy is not affecting by such effect and the intrinsic fluorescence of molecules isn't a concern.

2.5 Data mining: pre-processing and Multivariate analysis:

2.5.1 Pre-processing methods:

IR and Raman spectra are usually containing a huge and complex spectral information which could be extracted by applying many chemometric methods which comprise mathematical and statistical methods to enable prediction and classification. Pre-processing of spectral data could remove spectral background noise, interference and hence improve the quality of spectra and thereby extracting all relevant information. For example, background effect is a substrate related in both IR and Raman which is difficult to remove experimentally, thereby correction methods extended from polynomial line subtraction to extended multiplicative signal correction (EMSC) are applied [105,106]. EMSC is the one of the major model-based framework for pre-processing of VS data with a particular application for IR to correct for water vapour, carbon dioxide, salt concentration and temperature [107]. EMSC can correct for additive effects such as baseline effects, multiplicative scaling effects, Mie scattering and interference effect [108]. In absorption IR; the multiplicative effect is related to the effective optical path length [109] while in Raman scattering it is related to the variability in the sample volume, intensity of the laser and the focusing or sample positioning [107]. The algorithm of EMSC takes the reference spectrum and attempts to recreate the raw spectrum to be corrected by adding an offset, a slope and amplifying the reference by multiplication [33].
The basic MSC model is usually expressed as Equation 16 [106]:

$$A(\bar{\upsilon}) = \alpha + \chi(\bar{\upsilon}).b + e(\bar{\upsilon}) \quad (\textit{Equation 16})$$

$A(\bar{\upsilon})$ is the absorbance at wavenumber $\bar{\upsilon}$, α is additive baseline constant, and b is a multiplicative constant, $\chi(\bar{\upsilon})$ is the average spectrum, $e(\bar{\upsilon})$ is the residual vector which contains the chemical difference between the samples.

$A(\bar{\upsilon})$ is estimated by weighted least square regression, then the spectra will be corrected after estimation α and b parameters by Equation 17 [106]:

$$A_{corr}(\bar{\upsilon}) = (A(\bar{\upsilon}) - \alpha)/ b \quad (\textit{Equation 17})$$

Iterative polynomial fitting methods are used for baseline correction of them Lieber and Mahadevan Jansen algorithm is implemented [110], standard normal variate (SNV) and Savitzky-Golay filtering. SNV enables removal the slope variation and additive baseline signals whereas Savitzky-Golay filtering with the first and second polynomial filters enable to smooth the spectra by resolution of overlapping peaks and remove baseline variations [110]. After pre-processing different multivariate methods can be used to extract qualitative and quantitative information from IR and Raman spectra.

2.5.2 Principal Component Analysis (PCA)

PCA is the most widely used model for data analysis in research area and considered the basis for other methods [111,112]. It is used to describe the maximum variance in the data set, in doing that it reduces the data dimensionality by creating new variables known as principle components (PCs) which are also as known loadings or eigenvectors. PC1 describes the maximum variance in the information contained in the data set followed by the PC2 for the next most variance, and so on [105]. PCs scores gives coordinate information of the original spectra in the loading system. PCA can be used to describe the major spectral variabilities that can be observed between groups [113].

The result of PCA is a bilinear model of T scores and P loadings which can expressed as in Equation 18 [32].

$$X = TP^T + E = t_1p_1T + t_2p_2T \pm \cdots + t_Ap_AT + E \quad (\textit{Equation 18})$$

Where, X is M × N matrix, consisting of M samples (rows) with N measured variable, A is the number of calculated PCs. T and P, respectively, consist of orthogonal and orthonormal vectors. E is an M × N matrix containing the residuals, that is, variance not explained by the PCs.

Figure 24 presents an example of PCA applied to discriminated between doxorubicin and daunorubicin. Figure 24A is the resulted scatter plot which presents percentage of explained variance observed by PC1 and PC2 while Figure 24B illustrates spectral features used in loading plot.

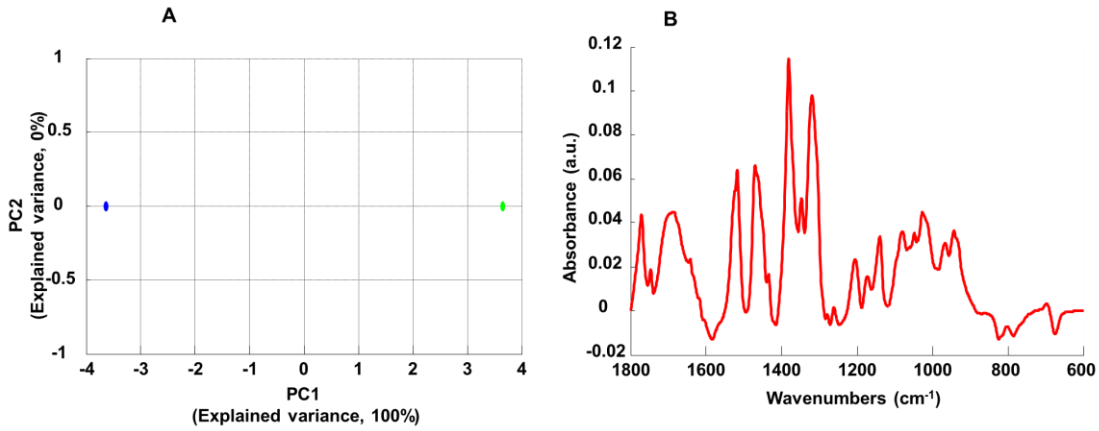


Figure 24. PCA performed on ATR-FTIR Raw spectra. A: scatter plot of PC scores 1 and 2. B: loading for PC1

Another application of PCA model for discriminant analysis is performed by coupling to factorial discriminant analysis (FDA) which is considered an advanced modelling of PCA. The notion FDA used to assess a synthetic variable called discriminant factor. PCA-FDA Converts the data into their PCs thereby allowing better separation of data around the centre of the considered group.

2.5.3 Partial Least Square – Discriminant Analysis (PLS-DA)

Partial least squares (PLS) algorithm has been first developed for regression task and then developed into a classification/discrimination method known as PLS-discriminant analysis (PLS-DA). PLS-DA algorithm is well implemented for predictive and descriptive modelling, as well as discriminative variable selection . Theoretically, PLS-DA combines dimensionality reduction and discriminant analysis into one algorithm. PLS-DA predictive model includes two main procedures; construction of PLS component (i.e. dimension reduction) and construction of the predictive model for discriminant analysis [36]. It reduces the number of variables and on the same time maintains the original spectral characteristics that is responsible for the variance [78]. PLS-DA predictive models can be either constructed using PLS1 or PLS2 algorithms. Figure 25 presents PLS-DA model constructed using PLS 2 algorithm which can operate more than one class at the same time. In PLS-DA modelling the first step is recoding of the categorical variables (ordinal or nominal) into continuous variables (numerical) [36].

The out-put of PLS-DA is presented in a form of confusion matrix; then mathematical calculation can be performed to have percentage expression of sensitivity and specificity of analysis. In this context, sensitivity can be defined as the proportions or percentages that are truly identified by the classifier whereas specificity is the measure of the accuracy of the test against false positive (Equation 19 and 20) [114,115].

$$Sensitivity = \ TP/((TP + TN)\ ) \quad (equation\ 19)$$

$$Specificity = \ TN/((TN + FP)\ ) \quad (equation\ 20)$$

Where, TP is the true positive, TN is the true negative and FP is the false positive.

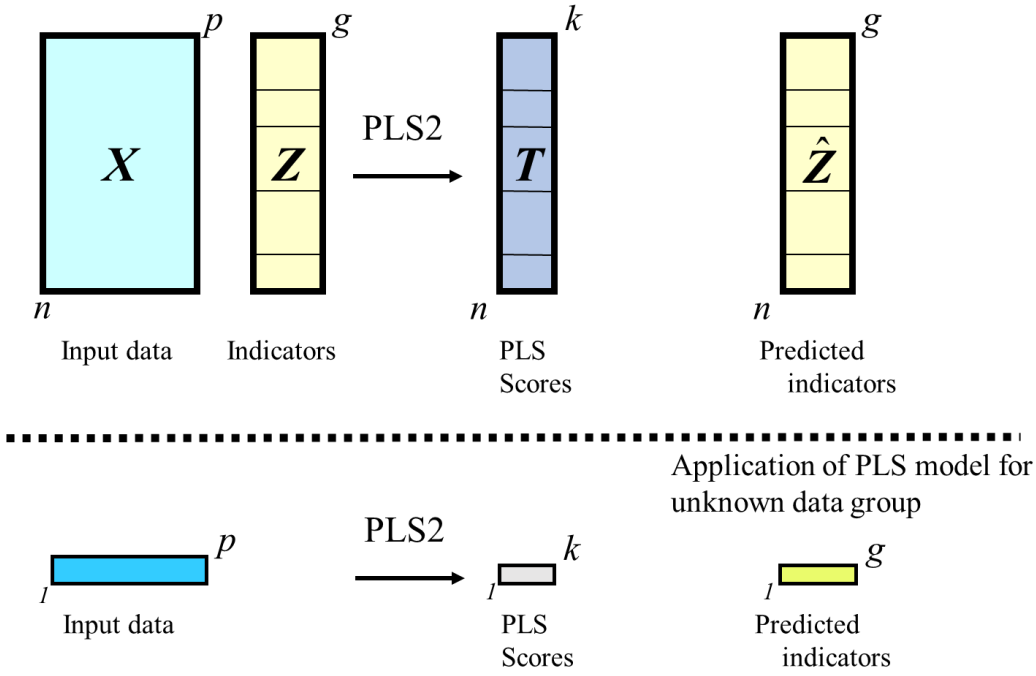


Figure 25. PLS 2 based predictive model for PLS-DA

2.5.4 Partial Least Square Regression (PLSR)

Regression methods such as partial least square root (PLSR) has been developed as a generalisation of multi-linear regression (MLR) for quantitative analysis. In basic MLR method, regression coefficient (*a*) is used to find the correlation relationship between two variables; Y (dependent variable, e.g. intensity) and X (predictor or independent variable, e.g. concentration) as seen in Equation 21.

$$Y = aX + b \quad (Equation\ 21)$$

MLR is of limited use in analysis of VS data due to data's complexity as it contains a large number of strongly related Y variables and X variables which can limit determination of regression coefficient. Therefore, PLSR method applying multivariate analysis can be used to analyse strongly related co-linear, noisy variables in realistic way [116]. PLSR maximizes the covariance between the spectral information and the concentration [116,117].

In linear PLSR model, data of a PLSR can be arranged as two tables, matrices, X and Y and the data will logarithmically transformed and being centred and scaled before analysis and decomposed into factorial coordinates T and U, respectively as seen in Figure 26 [116]. Before PLSR, X matrix is arranged into X-loading vectors (P') and X-weight matrix (W') containing number of objects (N) and number of components (A). While Y is arranged into Y-weight matrix (C').

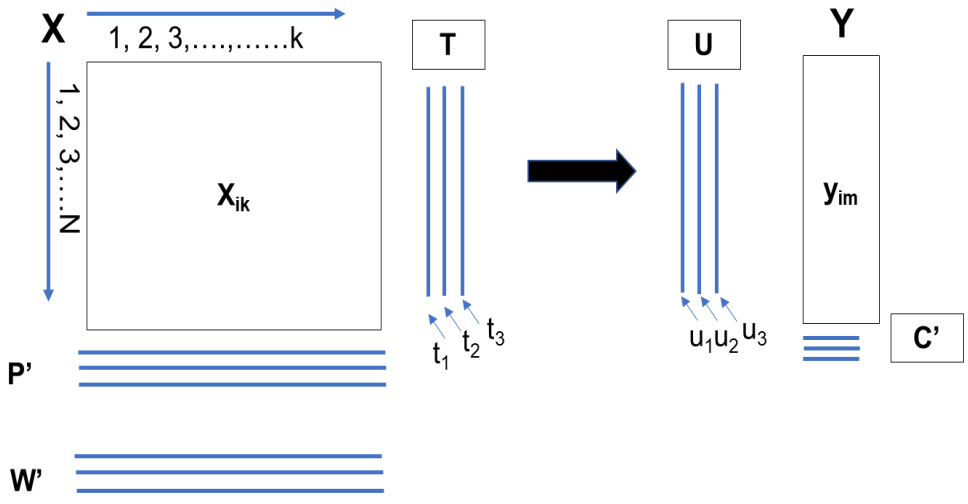


Figure 26. Data arrangement before PLSR

Where T= (N×A) in which columns are ta (X scores) while U= (N×A) in which columns are u (Y scores).

The measure of the specificity of PLSR is resides in the weighting vector or regression co-efficient which presents the wavenumbers (variables) used for quantification. The weighting vector of PLS can be calculated according to variance between y response and X data matrix, Equation 22 [32]:

$$W^{T}_{PLS,1} = y^{T}X/\|y^{T}X\| \quad (Equation\ 22)$$

Where, X is the data matrix, y is the response and T is an orthogonal vector.

2.5.5 Cross validation

Cross validation (CV) methods is applied in PCA and PLS methods to enable optimal selection of variables for prediction [110]. In real practical condition, building optimal predictive model containing independent data sets (training, validation and test sets) is somehow time consuming to produce enough data set. Within data set, manual selection of validation set and the training set can be biased and can give overoptimistic results. Therefore, CV become a routine method for evaluation of model with a limited data [38,118].

Different types of CV algorithms are existing for different purposes, of them Leave K Out Cross Validation (LKOCV) and Leave One Out CV (LOOCV). LKOCV works by random splitting the data set into equal sized subsamples/segments or fold called K where $K \leq n$ (number of samples). Each fold will be kept aside once and considered as validation set which will be predicted by the remaining *K-1* segments [110]. LOOCV simply works by excluding one object each iteration and be validated in the training set [119].

LKOCV and LOOCV give strength for PLS and PCA models by avoiding overfitting and overestimation. In PLSR, the best quantitative model is that delivers the lowest and the highest regression value, Although, care should be taken when selection number of latent variables (LVs) to not overestimate the model. A robust and accurate model can be constructed when the optimal number LVs is selected during the process of cross validation from error root mean square error of cross validation (RMSECV). The selection of LVs should be in region where

no further statistical difference could be observed and the rest of LVs contain no more than spectral noise [117].

RMSECV can be calculated according to Equation 23 [120]:

$$RMSECV = \sqrt{\sum_{i=0}^{m} \frac{(c_i - \hat{c}_i)^2}{m}} \quad (Equation\ 23)$$

Where, c_i is the actual concentration of the analyte in the *i*th sample, $\hat{c}_i$ is the predicted concentration of the analyte in the *i*th sample, and *m* is the number of samples in the set.

3. COMPARISON OF INFRARED AND RAMAN SPECTROSCOPY FOR ANALYTICAL QUALITY CONTROL OF CHEMOTHERAPEUTIC SOLUTIONS

3.1 Context and motivation:

AQC implemented to prevent medication errors. Chemotherapeutic preparations are individualised therefore specific doses are prescribed for intravenous injection for each patient. Their Safety relies on the administration of the correct drug at a specific concentration, thus performing qualitative and quantitative analysis have become the final step of AQC before release of solutions from centralised units. Without a doubt HPLC can deliver the results with high specificity and sensitivity, however the dense workload due to the high number of solutions prepared each day requires to propose fast analytical alternatives. Moreover, chromatography are time consuming and demanding consumables wise (e.g. solvents). To reduce the analysis time UV-Vis flow injection analysers (FIA) have been developed for AQC. However, the absorbance spectrum sometime lack of specificity to discriminate chemically close anticancer drugs. To address this concern, coupling of FIA with vibrational spectroscopy has been explored. Although commercial systems are available, there is vagueness around the role played by IR and Raman spectroscopy in the analysis and the final outcome.
This chapter is focused on applicability of IR and Raman spectroscopy for identification and quantification of small chemotherapeutic molecules within the clinical concentration range.

Publication 1: Qualitative and quantitative analysis of therapeutic solutions using Raman and infrared spectroscopy (*accepted in Spectro Chemical Acta Part I: Molecular and Biomolecular Spectroscopy in March 17th, 2020*):

The study includes three structurally related anticancer drugs commercial formulations belong to anthracyclines: TEVA®, MYLAN® and CERUBIDINE® (doxorubicin, epirubicin and daunorubicin). The preparation of the clinical range is performed using Milli Q deionised water. Anthracyclines are group of antibiotic antitumor drugs that are being produced by *streptomyces* species, their mechanism of action is by inhibiting topoisomerase II, intercalating to DNA and

via production of free radical causing protein damage, thereby inhibit nucleic acid synthesis and lead to cell death [121,122]. While doxorubicin and epirubicin are positional isomers, epirubicin differs in the orientation of hydroxyl group around the daunosamine sugar moiety whereas daunorubicin is structurally different from doxorubicin in that the hydroxyl group of alkyl moiety is being replaced with methyl group in daunorubicin. The potential of IR and Raman spectroscopy has been explored to deliver quantitative analysis but also discriminate the isomeric forms. The investigation considered the spectral basis of discrimination between those drugs and potential role of excipients.

Publication 2: Vibrational spectroscopy for discrimination and quantification of clinical chemotherapeutic preparations (*Submitted to Vibrational Spectroscopy in December 1th, 2020*)

This follow up study was performed on 4 commercial formulations: DOXORUBICIN TEVA®, CERUBIDINE®, HOLOXAN® and METHOTREXATE MYLAN® containing respectively the anticancer drugs doxorubicin, daunorubicin, ifosfamide and methotrexate. As part of investigation, the motivation was to analyse samples mirroring the AQC conditions. For instance, at the CHU Tours chemotherapeutic solutions are prepared in either 0.9% NaCl or 5% glucose solution not solely deionised water like it was done for the first publication. The main scope of the study was to investigate the spectral effect of the matrix/solvent on the discrimination and quantification of selected molecules. While, NaCl is not expected to significantly contribute during analysis, glucose at 5% could display spectral features. Especially for IR analysis, the samples are dried onto the ATR crystal hence the intensity of glucose bands can be further enhanced.

PUBLICATION 1: Qualitative and quantitative analysis of therapeutic solutions using Raman and infrared spectroscopy

Spectrochimica Acta Part A: Molecular and Biomolecular Spectroscopy 218 (2019) 97–108

Contents lists available at ScienceDirect

Spectrochimica Acta Part A: Molecular and Biomolecular Spectroscopy

journal homepage: www.elsevier.com/locate/saa

Qualitative and quantitative analysis of therapeutic solutions using Raman and infrared spectroscopy

Alaa A. Makki [a,g], Franck Bonnier [a,*], Renaud Respaud [b], Fatma Chtara [a], Ali Tfayli [c], Clovis Tauber [d], Dominique Bertrand [e], Hugh J. Byrne [f], Elhadi Mohammed [g], Igor Chourpa [a]

[a] Université François-Rabelais de Tours, EA 6295 Nanomédicaments et Nanosondes, 31 avenue Monge, 37200 Tours, France
[b] Université François-Rabelais de Tours, UMR 1100, CHRU de Tours, Service de Pharmacie, F-37032 Tours, France
[c] U-Psud, University of Paris-Saclay, Lip (Sys)2, EA7357, UFR-Pharmacy, Châtenay-Malabry, France
[d] UMR U1253 iBrain, Université de Tours, Inserm, 37032 Tours, France
[e] Data_Frame, 25 rue Stendhal, 44300 Nantes, France
[f] FOCAS Research Institute, Technological University Dublin, Kevin Street, Dublin 8, Ireland
[g] Department of Pharmacognosy, Faculty of Pharmacy, University of Gezira, Sudan

ARTICLE INFO

Article history:
Received 11 October 2018
Received in revised form 6 February 2019
Accepted 17 March 2019
Available online 24 March 2019

Keywords:
Infrared spectroscopy
Raman spectroscopy
Quantitative analysis
Discriminative analysis
Anthracyclines

ABSTRACT

Anticancer drugs are prescribed and administrated to an increasing number of patients on a daily basis. As a consequence, a number of concerns have been raised about the patient health and safety in the case that the drugs administered are not at the required concentration or even worse not the correct ones. Quality control of therapeutic solutions has therefore been extensively implemented in hospital environments, in order to avoid any failure in the intense workflow faced by administering pharmacists. In the present study, infrared (IR) and Raman spectroscopy have been employed for the analysis of 3 commercially available therapeutic solutions TEVA®, MYLAN®, CERUBIDINE®, respectively containing doxorubicin, epirubicin and daunorubicin. They perfectly illustrate the analytical difficulties encountered, as these 3 chemotherapeutic drugs are isomers, hardly distinguishable with conventional approaches such as UV/VIS spectrometry. Any analytical failure to identify these molecules can lead to delays in patient treatment. While Partial Least Squares Regression analysis demonstrates that both Raman and IR can deliver satisfactory quantitative analysis in the clinical range, with respective Root Mean Square Error of Cross Validation (RMSECV) between 0.0127 – 0.0220 $g \cdot L^{-1}$ and 0.0573 – 0.0759 $g \cdot L^{-1}$, the identification rate between the 2 techniques differs substantially. Indeed, Principal Component Analysis – Factorial Discriminant Analysis (PCA-FDA) highlights that, depending on the data preprocessing applied to Raman spectra, the discrimination between the 3 drugs is decreased, with in some cases specificity and sensitivity below 50%. However, IR analysis displays encouraging results with an overall specificity and sensitivity between 99 and 100%, suggesting that reliable validation of the therapeutic solution for administration to patients can be achieved. IR and Raman spectroscopy could assist and support quality control of chemotherapeutic solutions prepared in personalised concentrations for each patient. The effective and reliable characterisation of therapeutic solutions could have a lot to offer to improve current practices in a near future.

© 2019 Published by Elsevier B.V.

1. Introduction

Evolutions of clinical procedures and protocols in recent years are motivated by improvement of patient safety. Anticancer drugs are extensively used on a daily basis, the number of patients treated still increasing annually. Errors in medications are the main risk leading to therapeutic failure, which, considering the hazardous nature of most anti-cancers drugs, can have disastrous repercussion for a patient's health. As a result, numerous hospitals have implemented internal regulations to standardise their own procedures and minimise the risk of erroneous treatment of a patient. High performance liquid chromatography (HPLC) remains the gold standard for quantitative analysis of organic compounds as part of daily quality control and is therefore one of most commonly found methods in clinical analytical laboratories attached to preparation facilities. Mass spectrometry is also a powerful technique for drug screening and analysis, extensively employed in the development of new pharmaceutical compounds or patient monitoring through detection and quantification in body fluids such as serum, urine or saliva [1,2]. However, it is not currently an option for therapeutic screening applications, due to time constraints of the clinical workflow, requirements for sample preparation, and simply the cost involved. However, some limitations such as high operating costs,

* Corresponding author at: EA 6295 NMNS "Nanomédicaments et Nanosondes", UFR Sciences Pharmaceutiques, 31, avenue Monge, 37200 Tours, France.
E-mail address: franck.bonner@univ-tours.fr (F. Bonnier).

https://doi.org/10.1016/j.saa.2019.03.056
1386-1425/© 2019 Published by Elsevier B.V.

relatively low output and the requirement of specialised skills make it less than ideal for routine analysis of chemotherapy preparations [3,4]. Flow-injection analysis (FIA) spectroscopic based methods are the most commonly implemented, with Ultraviolet-coupled to Fourier-transform infrared spectrometry (UV/vis-FTIR) probably the most widespread [5,6]. Recent evolutions have seen the infrared detection replaced by Raman technologies to overcome some of the limitations, but implementation in clinics still requires an aliquot to be taken for injection into the analytical device [7,8]. Moreover, investigations are ongoing about the possibility to use Raman spectroscopy as a non-invasive tool to overcome some current limitation such as large volume required for FIA, but mostly to avoid any risk in relation to exposure of staff to hazardous solutions [9].

Vibrational spectroscopic techniques, both infrared (IR) absorption and Raman scattering, deliver specific molecular fingerprinting signatures of samples. They have been extensively studied for biomedical applications [10,11] thus can be used and exploited as novel and accurate methods for histopathology [12], cytology [13], biopsy characterisation [14], surgical guidance [15], treatment monitoring [16] and drug studies [17]. The rapid, cost effective, label free and non-destructive advantages are indeed often pointed out to highlight the benefits of those techniques, but it is the analytical capabilities in terms of both qualitative and quantitative performances are also most relevant for a wide range of clinically oriented applications [18,19]. IR and Raman spectroscopy are powerful analytical tools widely used for characterisation of organic molecules such as, for example, therapeutic drugs [20]. Although primarily used in industry and research laboratories as screening tools to monitor whether a synthesis process has been successful [21], coupling the molecular specificity of the spectra collected with optimised quantitative approaches strongly promotes the techniques for therapeutic solution screening in the clinical environment [22]. In previous studies, although encouraging results are documented for monitoring a number of molecules such as ganciclovir [23] or 5FU [24], directly in the infusion bag, the material used for the packaging, often polystyrene like, also has strong contributions to the spectra that can limit the usable analytical range and lead to difficulties in quantifying and/or identifying the chemotherapeutic drugs accurately [25]. Therefore, such developments remain only at the research level and no translation into the clinic has been achieved as yet, suggesting that the present workflow, entailing analysis of aliquots from the therapeutic solutions is still the most realistic approach.

In the present study, three commercial formulations, TEVA® (Doxorubicin), MYLAN® (epirubicin) and CERUBIDINE® (daunorubicin) have been used to evaluate the potential of Raman and infrared spectroscopy for the analysis of therapeutic solutions in such a workflow. The chemotherapeutic agents are chemically similar, and thus present difficulties in terms of their identification and/or quantification with UV absorbance spectroscopy. Consequently, a comparative study has been conducted as a demonstration of the potential of vibrational spectroscopy as quality control tools for clinical use. A two-step approach to this demonstration has been implemented, firstly evaluating the discriminative capabilities of both techniques, irrespective of concentrations, by means of Principal Component Analysis (PCA) coupled to Factorial Discriminant Analysis (PCA-FDA); and secondly determination of the precision of the quantitative analysis of the approaches using the Partial Least Squares Analysis (PLSR).

2. Materials and methods

2.1. Anticancer drugs selected and sample preparation

The study includes three commercial anthracycline forms, TEVA® (doxorubicin, injectable solution, 2 $g \cdot L^{-1}$), MYLAN® (epirubicin injectable solution, 2 $g \cdot L^{-1}$) and CERUBIDINE® (daunorubicin, lyophilised powder, 20 mg) which were provided through a collaboration established with the University Hospital of Tours. While TEVA® and MYLAN® contain small amounts of HCl and NaOH (<1%), CERUBIDINE® has mannitol added to the formulation, in concentrations as high as 100 mg per 20 mg daunorubicin. Mannitol is a commonly found excipient in commercialized daunorubicin-based chemotherapeutics approved for clinical use. The UCBO unit (Unité de Biopharmacie Clinique Oncologique, Tours, France) deals with the preparation of anticancer drug formulations directly on site for rapid administration to patients. Based on recent clinical protocols, a set of 8 aqueous solutions, with drug concentrations of 2 $g \cdot L^{-1}$, 1.5 $g \cdot L^{-1}$, 1 $g \cdot L^{-1}$, 0.5 $g \cdot L^{-1}$, 0.25 $g \cdot L^{-1}$, 0.125 $g \cdot L^{-1}$, 0.0625 $g \cdot L^{-1}$ to 0.03125 $g \cdot L^{-1}$, corresponding to clinically relevant concentrations, have been prepared for each chemotherapeutic drug. The samples were prepared from the stock solution using serial dilutions, which were analysed directly with Raman and infrared spectroscopy. The procedure has been repeated 5 times in order to obtain 5 independent sets of spectra. All quoted concentrations refer to the amount of drug present in the solution without taking into account excipients. All samples were prepared freshly on the day of analysis and stored at 4 °C in a dark room to avoid photo-damage prior to spectral analysis. ATR-IR spectra have also been recorded for mannitol 10 $g \cdot L^{-1}$ and 0.15625 $g \cdot L^{-1}$ which correspond to the concentrations of mannitol found in CERUBIDINE® 2 $g \cdot L^{-1}$ and 0.03125 $g \cdot L^{-1}$, respectively.

2.2. Data collection

The current work flow in place at the UCBO unit (Unité de Biopharmacie Clinique Oncologique, Tours, France) is based on a Multipsec® analyser (MICRODOM, France). The pharmacists receive between 100 and 150 anticancer drug solutions on a daily basis which require analysis and clearance before they are administered to patients. For each individual sample, 1.5 mL is extracted to an aliquot and injected in the analyser with a syringe. The protocols employed in this study for Raman and Infrared analysis have been derived from the current procedures and designed to improve on the analytical performance.

2.2.1. Raman spectroscopy analysis

Raman spectra were collected using a Labram spectrometer (Horiba Jobin-Yvon, France) equipped with a 690 nm laser source delivering ~10 mW at the sample. 500 μL of the solution were placed in a quartz cuvette and the data was collected by illumining the sample through the wall of the cuvette. In order to ensure maximum reproducibility between measurements, a macro sampling holder, consisting of a cuvette holder attached to the turret of the microscope was employed. Basically, the laser coming out of the turret is reflected by a 45° mirror and directed through the quartz cuvette. Although the set up requires larger volumes to perform the analysis, the laser is not tightly focused and thus the risk of any photothermal damage is minimised. The spectral range was set between 150 and 3700 cm^{-1}, resulting in a spectral resolution of about 2.5 cm^{-1}, achieved using a 300 lines/mm grating. Two accumulations of 20 s were taken for each spectrum. 5 independent sets of dilutions have been prepared for each formulation and analysed on different days to capture possible instrumental variability in measurements. Additionally, 5 spectra have been measured for each concentration tested. In total, 200 spectra were recorded over the range of concentrations for each anticancer drug included in this study.

2.2.2. Infrared spectroscopy analysis

Infrared spectra were recorded with a Frontier spectrometer (Perkin Elmer, France) equipped with a multi-reflection ($n = 10$) Attenuated Total Reflectance (ATR) accessory (Eurolabo, France). The IR spectra collected result from 4 scans performed over the range 600–4000 cm^{-1} with a spectral resolution of 4 cm^{-1}. A background was acquired (4 scans) and ratioed with the sample spectra by the software. 2 μL drops were deposited directly on the diamond crystal and allowed to air dry prior to analysis. 5 independent replicates have been measured for

each concentration tested, 5 spectra recorded each time. In total, 200 spectra were recorded over the range of concentrations for each anticancer drug included in this study. The time required to record spectra from one drop is about 5 min, including drying time and data collection, which is comparable to protocols currently employed at the Hospital of Tours.

2.2.3. Data handling

The Raman and IR data sets have been pre-processed and analysed using MATLAB (Mathworks, USA). For the purpose of the study, although the preprocessing and data analysis steps have been broken down as individual procedures subsequently applied to data, one should keep in mind that the optimised data processing and analysis protocols are easily incorporated in instrumental software and implemented as automated functions. Once the protocol has been established, total computational time to apply quantitative and discriminative analysis is <1 min

a) Discriminative analysis: Raman spectra have been cut in order to focus on the fingerprint region (300–1800 cm^{-1}) in which the most relevant spectral features are observed. Pre-processing of Raman spectra included baseline correction, using Lieber or Extended Multiplicative Scattering Correction (EMSC), followed by vector normalisation. While the Lieber algorithm estimates the background by a polynomial function and by an iterative method based on least squares [26], the EMSC is more advanced approach allowing to correct for additive baseline effects, multiplicative scaling effects, and interference effects [27]. For instance, spectra of deionised water were provided to neutralise its contribution to the Raman spectra collected from the different solutions. For consistency, infrared spectra have also been reduced to the fingerprint region (600–1800 cm^{-1}) prior to being subjected to baseline correction (rubber band) and a vector normalisation. The lower limit of the spectral range for ATR-IR is defined by the crystal material to be at 600 cm^{-1}. In contrast, Raman spectroscopy allows analysing the finger print region down to tens of cm^{-1}, 200 in this study. Once pre-processing was completed, both Raman and IR spectra were analysed by PCA [28] and PCA-FDA (PCA-Factorial-Discrimination-Analysis) [29]. Although PCA is a well-established method for rapid evaluation of the data, highlighting the spectral variability present in data sets, more advanced approaches such as PCA-FDA are required to deliver information about the discriminative performance of the techniques. PCA-FDA includes a 100 fold cross validation through a leave K-out cross validation routine. This approach ensures no replicate of a given sample can be found in both the calibration and validation sets and avoids over optimistic outcome of the quantitative analysis [30]. 1/3 of the data is selected as a test set, while the 2/3 of the remaining samples were used as calibration and validation sets. The test set is kept constant and at each iteration, different combinations of randomly selected calibration/validations sets are tested. Ultimately, the results are presented in the form of confusion matrices, allowing calculation of the specificity and sensitivity of the discrimination analysis performed.
b) Quantitative analysis: Normalisation procedures should be avoided to preserve the intensity to concentration relationship in the data. Therefore, only an offset correction has been applied for the spectra pre-processing. PLSR remains the most relevant analysis to evaluate the possibility of performing quantitative analysis of systematically varying vibrational spectra [31,32]. It is a supervised multivariate technique that is highly specific for quantitative methods, and is usually performed via two steps: calibration and validation. Therefore, similarly to the PCA-FDA a 100 fold leave K-out cross validation was implemented. The output of PLSR provides performance criteria defined under the linearity (R^2) and precision, also called Root Mean Square Error for Cross Validation (RMSECV). Additionally, the lower Limit Of Detection – lower (LOD) has been estimated based on the work published by Allegrini et al. [33].

3. Results and discussion

3.1. UV characterisation of anthracycline formulation

Anthracyclines are a group of cytotoxic compounds used as treatment of a wide variety of cancers, from leukemia, thyroid, lung and other neoplasia, ovarian, breast, lung and gastric cancer [34] leading to a large number of solutions being prepared on a daily basis for patients under chemotherapeutic treatment. Doxorubicin, epirubicin and daunorubicn are composed of tetracycline aromatic moiety attached to a sugar moiety of daunsamine via a glyosidic bond. As displayed in Fig. 1, these 3 anthracyclines have the same aromatic chromophore and the difference between them concerns the side chains. Notably, epirubicin is a stereoisomer of doxorubicin, and differs from it only in the orientation of the hydroxyl group of the hexapyranosyl sugar [34]. Daunorubicin differs from doxorubicin only in the shorter side chain terminated with a methyl group instead of a primary alcohol group. As a direct consequence, those molecules cannot be discriminated using UV spectrophotometry. The absorbance spectra were collected for the 3 molecules in their commercial forms (doxorubicin from TEVA®, epirubicin from MYLAN® and daunorubicin from CERUBIDINE®). These spectra have the same profile, with the two main maxima located at ca. 480 and 500 nm. NaOH, HCl and mannitol (a sugar) present in the commercial forms do not have direct contribution to the UV/Vis spectra in this range, and thus the absorbance is solely derived from the drugs. While quantitative analysis is expected to be achievable with UV absorbance spectroscopy, difficulties to perform specific identification of the chemotherapeutic drugs are understandable. As they contain information of all the moieties of the molecule, rather than just the chromophoric π-conjugated structures, vibrational spectra are richer in specific molecular structural information than UV–vis absorption spectra. This study aims to demonstrate this and optimise protocols to implement the analysis in a clinical workflow.

3.2. Quantitative and discriminant analysis using Raman spectroscopy

3.2.1. Raman characterisation of anthracycline formulations

Fig. 2 presents mean Raman spectra collected from the commercial forms of the three chemotherapeutic drugs, TEVA® (spectrum a), MYLAN® (spectrum b) and CERUBIDINE® (spectrum c) diluted to concentrations of 2 $g \cdot L^{-1}$ in deionised water. As expected, due to their similar chromophores, spectral signatures display strong similarities, all major peaks being found in all 3 formulations. To further represent the vibrational modes observed, Table 1 provides a direct comparison of their positions with corresponding assignments. The differences observed are relatively minor, especially for TEVA® (spectrum a) vs MYLAN® (spectrum b), which show only a 2 cm^{-1} shift between 1089 cm^{-1} vs 1091 cm^{-1}. With the exception of the band at 886 cm^{-1} observed in the case of CERUBIDINE®, all other features appear consistent for the 3 molecules, as seen in Fig. 2. Moreover, the recording of Raman spectra from liquid samples can lead to some underlying contribution from water. Although the Raman bands observed have strong intensities, the profile of the signal and the band around 1600–1650 cm^{-1} (Fig. 2) suggest that H_2O (spectrum d) also contributes to the spectra of the drug solutions. The features observed around 450 cm^{-1} and 1300 cm^{-1} in the water spectrum are respectively assigned to the quartz cuvette and the glass of the focusing lens of the macro adapter used. In comparison to the short side chains, the intensity of the peaks associated to the conjugated chromophores is dominant, due to their high Raman activity. Consequently, no major spectral differences can be observed between the 3 formulations.

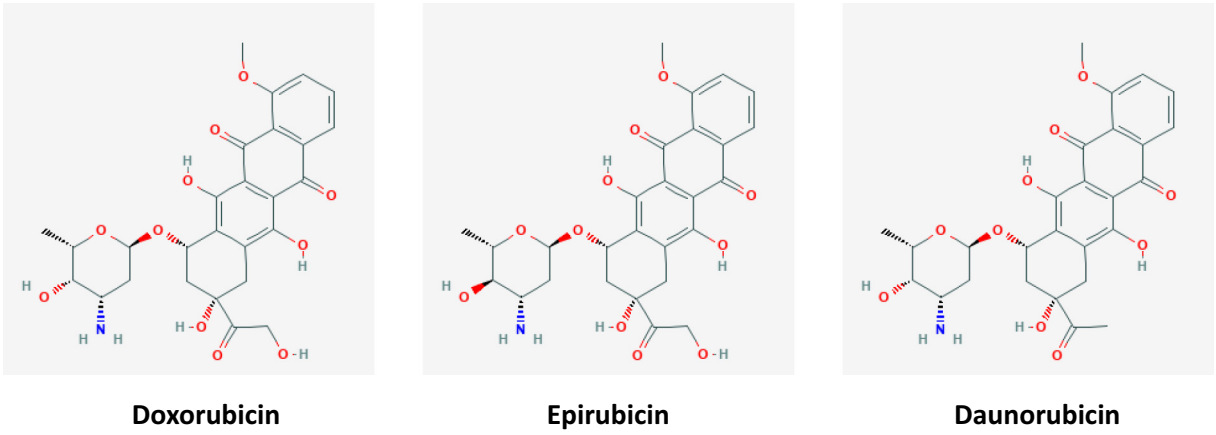


Fig. 1. Chemical structures of the 3 anticancer drugs of interest.

Moreover, in contrast, molecules such as NaOH and HCl do not have any significant contribution to the spectra. In the solution of 2 g·L^{-1} CERUBIDINE®, mannitol is found at 10 g·L^{-1}. Despite the relatively high concentration, the Raman spectrum collected from the mannitol aqueous solution does not exhibit strong features, and the only difference with the water spectrum is at 886 cm^{-1}, where a weak peak arises from the broad background (spectrum 2e).

3.2.2. Discriminant analysis using PCA-FDA

Discriminant and quantitative analysis are two aspects of the data mining process not necessarily achieved through similar approaches, although they remain strongly connected. One could consider that any measurements of concentrations performed cannot be validated without identifying the molecule in solution being analysed. Therefore, it appears to be more relevant to first identify the drug and then aim for the quantification. While the quantitative analysis can establish a correlation between the intensity of the signal and the concentrations measured, when it comes to discriminating data sets based on the molecular information of the spectra, the overall intensity should be disregarded in favour of band positions, number and intensity ratios. Consequently, in the present study, it has been considered more relevant to subject the spectra to both baseline correction and vector normalisation prior to PCA-FDA. Thus, the concentration parameter has been removed from the analysis, focusing solely on the variations described above. Moreover, two methods for baseline correction have been evaluated, the Lieber correction [39] and EMSC [40].

PCA is a well-established unsupervised approach for rapid evaluation of spectral variability in complex data sets. Intensively used for analysis of IR and Raman spectra collected from biological samples, it readily allows visualisation of possible discrimination of samples using scatter plots [41,42]. Fig. 3A displays the scatter plot obtained for Raman spectra collected from 2 g·L^{-1} TEVA®, MYLAN® and CERUBIDINE® subjected to Lieber baseline correction followed by vector normalisation. Although spectral differences are not conspicuous after preprocessing, the scatter plot presents three well separated groups, corresponding to each formulation. It can be seen that, according to Principal Component 1 (PC1), spectra collected from CERUBIDINE® are well separated from the others (Fig. 3A red cluster), while TEVA® and MYLAN® data are only discriminated according to Principal Component 2 (PC2) (Fig. 3A blue and green clusters).

The loadings corresponding to each PC are displayed in Fig. 3B, highlighting the spectral features leading to the distribution of the data points in the scatter plot. Dominant features in the loading of PC1 observed at 447 cm^{-1}, 891 cm^{-1}, 1096 cm^{-1}, 1221 cm^{-1}, 1263 cm^{-1} and 1301 cm^{-1}, 1411 cm^{-1}, 1472 cm^{-1} and 1641 cm^{-1} correspond to dominant peaks previously identified in the mean spectra (Table 1). Loading 2, only accounting for 4.4% of the explained variance discriminating TEVA® (*blue*) and MYLAN® (*green*), displays a lower number of strong features.

(357 cm^{-1}, 475 cm^{-1}, 1210 cm^{-1}, 1306 cm^{-1}, and 1448 cm^{-1}). These 2 forms are really similar with only NaOH and HCl as excipients which have no contribution to the spectral signatures recorded. The features of the loading of PC2 are common to the Raman spectra of both compounds, as shown in Fig. 2, but the differentiating features suggest that small shifts can result from the different stereo-chemistry of the molecules.

Although PCA performed using a single concentration (i.e. 2 g·L^{-1}) exhibits clear separation of the three clusters and thus possible

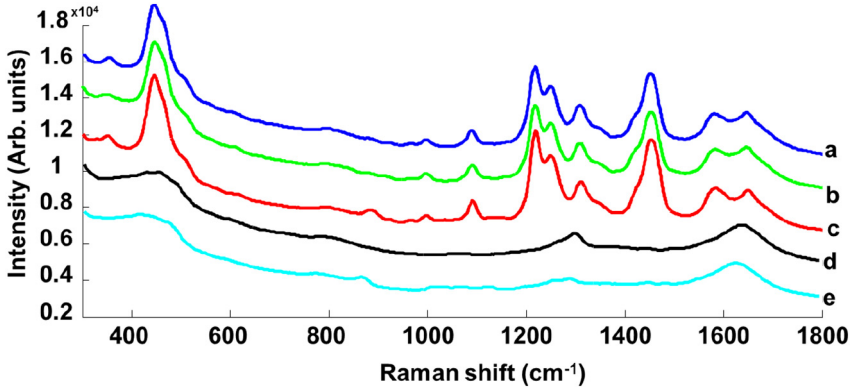


Fig. 2. Mean macro-Raman spectra recorded from TEVA® (a), MYLAN® (b) and CERUBIDINE® (c) commercial forms diluted to drug concentrations of 2 g·L^{-1} in deionised water; deionised water (d) and manitol solution at 10 g·L^{-1} in deionised water (e). Spectra are offset for clarity.

Table 1
Bands assignments of main features observed in the finger print region of TEVA®, MYLAN® and CERUBIDINE® Raman spectra collected from 2 g·L^{-1} solutions in deionised water [34–38].

TEVA® (cm^{-1})	MYLAN® (cm^{-1})	CERUBIDINE® (cm^{-1})	Assignments
355	350	351	–
446	446	447	C—C—O vibrations, C═O in plane deformation
–	–	886	–
1000	1000	998	C—C stretching of alicyclic ring
1089	1091	1091	Ring breathing and aromatic C—H bending vibrations, methoxy C—O stretching and C—C aliphatic chain vibrations
1219	1219	1219	C—O—H vibrations and in plane bending of O—H
1250	1250	1251	C—O vibrations
1309	1309	1311	C—O—H vibrations
1445	1445	1453	Aromatic ring stretching modes
1582	1582	1586	Aromatic ring stretching
1647	1647	1650	Hydrogen bonded stretching vibrations of C═O

identification of the different chemotherapeutic forms, it is also important to address the need to perform discriminant analysis as an overall classifier, including all concentrations. The spectra in Fig. 2 illustrate how similar the Raman spectra of the three formulations are, and the PCA in Fig. 3 indicates that any variations between them are minor differences in peaks positions and intensities. Applying PCA to the range of possible combinations of concentrations would require considerable effort, and thus other multivariate approaches such as PCA-FDA need to be implemented. All the different concentrations and drug types have been considered as distinct groups to classify ($n = 24$). The approach is supervised and implementation of a cross validation procedure is necessary to ensure the robustness of discrimination observed. Specifically, 1/3 of the data was used as a validation set and for each iteration of the 100-fold leave K-out cross validation, calibration and validation sets were constituted from the 2/3 of the remaining spectra. To better appreciate the specificity and sensitivity of the discrimination, at each iteration of the cross validation, results obtained with a model based on 4 principal components are reported in a confusion matrix (Table 3). This step of the analysis aims purely to discriminate the different anticancer drugs without any significance given to their concentrations. Therefore, successful classification was judged solely on the ability to identify the correct drug corresponding to the test spectra, irrespective of the concentration assignment. Although the overall specificity and sensitivity obtained are above 90%, the results are concentration and molecule dependent, and in some cases exhibit rather low values, as for example the TEVA® S7 (specificity = 85%), MYLAN® S1 (specificity = 75%) or CERUBIDINE® S1 (sensitivity 50%) (Table 3).

Although the results are encouraging, observation made in Fig. 2 of minimal spectral differences between TEVA® and MYLAN® formulations, the specificity of the classification achieved is somehow surprising. Raman spectroscopy is a technique particularly sensitive to changes of the light scattering when performing analysis on liquid samples. While the dynamic range of concentrations tested could lead to inconsistencies in the measurements, solutions of commercial formulations also contain excipients which possibly contribute to the spectra collected, not necessarily in terms of spectral features considering the concentrations, but rather affecting the baseline (or background) through scattering [43]. For this reason, more advanced baseline correction, taking into account the water spectrum has been performed by means of EMSC coupled to vector normalisation prior to PCA (Fig. 3C and D). While the scatter plot from the PCA still displays clear separation between data groups according to formulation (Fig. 3C), the corresponding loadings of PC1 and PC2 are strongly affected, and retain only residual features at 895 cm^{-1},

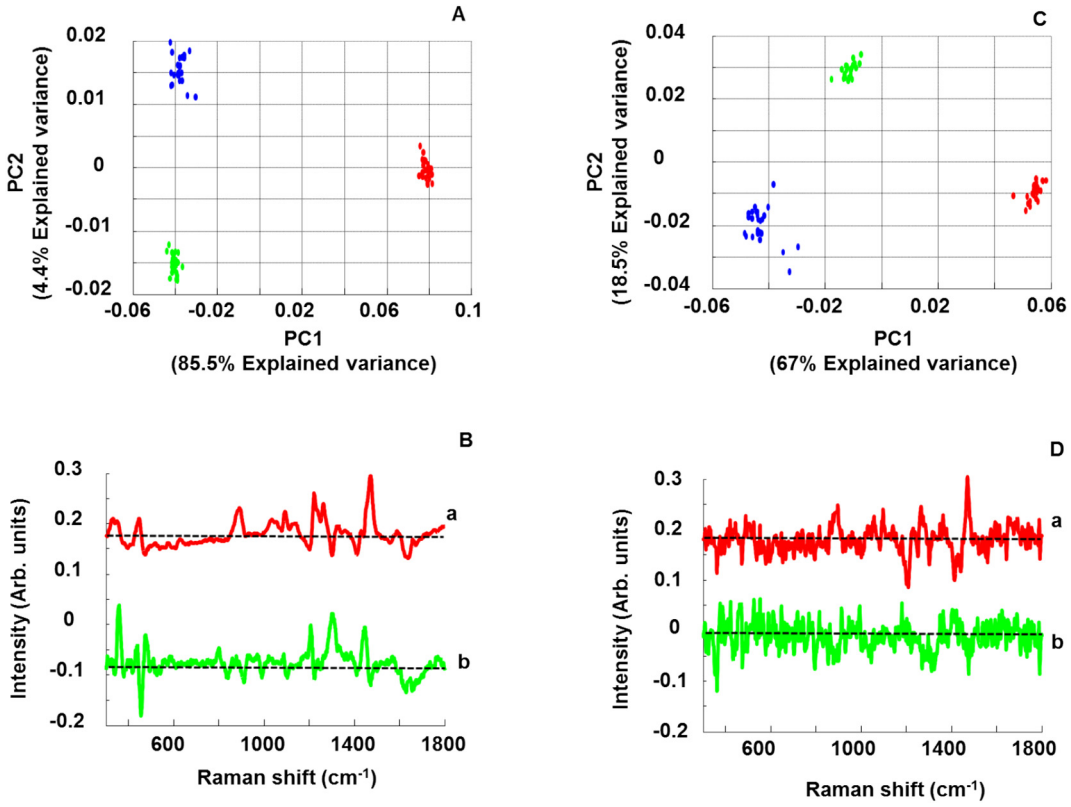


Fig. 3. PCA of Raman data collected from TEVA® (blue), MYLAN® (green) and CERUBIDINE® (red) 2 g·L^{-1} solutions in deionised water. A and B: scatter plot of PC1 and PC2 with corresponding loadings 1 and 2 obtained from data subjected to Lieber baseline correction and vector normalisation; C and D: scatter plot of PC1 and PC2 with corresponding loadings 1 and 2 obtained from data subjected to EMSC correction and vector normalisation. Loading are offset for clarity.

Table 3
Specificity and sensitivity % of PCA_FDA for Raman data processed without EMSC.

Sample concentration ($g \cdot L^{-1}$)	TEVA®		MYLAN®		CERUBIDINE®	
	Specificity %	Sensitivity %	Specificity %	Sensitivity %	Specificity %	Sensitivity %
S1 (0.03125)	93.3	100	75	90	100	50
S2 (0.0625)	100	100	80	100	100	60
S3 (0.125)	88.8	100	90	80	100	80
S4 (0.25)	100	100	100	100	100	100
S5 (0.5)	100	100	100	100	100	100
S6 (1)	100	100	100	100	100	100
S7 (1.5)	85	100	100	70	100	100
S8 (2)	100	100	100	100	100	100
Overall	95.9	100	93.2	92.5	100	86.6

918 cm^{-1}, 993 cm^{-1}, 1096 cm^{-1}, 1180 cm^{-1}, 1265 cm^{-1}, 1471 cm^{-1}. Clearly, a standard baseline correction does not take into account the changes in band ratios induced by underlying background in the spectra possibly leading to misinterpretation of results. Following EMSC, both the residual water and background are removed and relative band intensities are more accurately corrected. Consequently, when performing the PCA-FDA, the outcome is also affected and the overall specificity and sensitivity are now found to respectively be between 64.4%–72.5% and 53.3%–59.2% with the classification model constructed using 3 principal components (Table 4). A number of concentrations exhibit values below 50%, which indicates that a non-negligible number of mis-classifications have occurred, thus raising some serious concerns about the choice of data preprocessing having high impact on the analysis outcome and consequently the robustness of Raman spectroscopy measurements for drug identification can be questioned. In some cases, such as TEVA® S3 and CERUBIDINE® S4, there is obviously a reduced reliability in the drug identification, which for high concentrations can generate higher risks of dose intoxication of patients. Moreover, at lower concentrations, the accuracy is also not suitable for accurate classification, suggesting the specificity of Raman is not sufficient. EMSC is an advanced correction method able to remove instrumental and/or experimental interferences. However, despite applying such correction, the outcome of the PCA-FDA remains quite disappointing, suggesting that the sensitivity and specificity observed are directly linked to the ability of the technique to discriminate the 3 therapeutic solutions rather than the underlying source of variability.

3.2.3. Quantitative analysis using PLSR

While examination of spectra allows identification of the anti-cancer drug with a reasonably high degree of accuracy, the linear relationship existing between the intensity of the peaks and the concentrations prepared can be examined and used as a quantitative prediction model using PLSR. Due to the experimental macro set up used in this study, the reproducibility achieved during the measurements enables unambiguous monitoring of the decrease of the peak intensities according to the dilutions performed, as illustrated for the example of TEVA® in Fig. 4. PLSR is a reliable method to evaluate the quantitative information contained in the data sets collected. However, in order to ensure maximum statistical relevancy, cross validation procedures are generally implemented [30], in order to demonstrate that the analysis is not biased, but also to test the robustness of the predictive model used. Considering the size of the number of spectra available for each concentration, a 100-fold leave K out cross validation with 2/3 of spectra used as calibration and the remaining 1/3 as validation has been preferred for this study. The calibration and validation are therefore completely independent and selected randomly at each iteration of the cross validation, enabling testing of numerous data combinations. The first graph generated during the analysis represents the Root Mean Square Error of Calibration (RMSEC) according to the number of dimensions used to regress the data (Fig. 5A). As a supervised method, and aiming to deliver the lowest RMSEC and thus the best precision, a gradual decrease towards 0 is expected as the number of dimensions employed in the model increases. Once the model has been established using the calibration set, it is then evaluated with the validation spectra. The Fig. 5B exhibits first a steep decrease in the RMSECV (validation) before slightly increasing a stabilizing around 0.015 $g \cdot L^{-1}$. All dimensions calculated from the calibration set are not relevant to the quantification, and according to Fig. 5B, above 3 dimensions over fitting of the data could actually affect the precision of the predictive model. Consequently, the regression plot has been implemented using three dimensions, and is presented in Fig. 5C. The correlation between observed concentration (true concentrations) and predicted concentrations (experimental concentrations) delivers a linear trend characterised by R^2 value of 0.9997 (Table 5). The error bars illustrate the standard deviation calculated from the 100 fold cross validation and further support the high reproducibility of the measurements. The overall RMSECV reached was found to be 0.0127 $g \cdot L^{-1}$ for TEVA® (Table 5). The numbers of dimensions used to construct the PLSR predictive models, respectively 3, 5 and 5 for TEVA®, MYLAN® and DNR, are also indicated in Table 5. Fig. 5D shows the weighting vector corresponding to the PLSR analysis performed on TEVA® solutions. It represents the wavenumbers used to construct the predictive models, confirming the molecular specificity of the analysis has been preserved. The features with major contribution in the PLSR model can be found at 354 cm^{-1}, 445 cm^{-1}, 1000 cm^{-1}, 1090 cm^{-1}, 1219 cm^{-1}, 1249 cm^{-1}, 1309 cm^{-1}, 1453 cm^{-1}, 1581 cm^{-1},

Table 4
Specificity and sensitivity % of PCA_FDA for Raman data processed with EMSC.

Sample concentration ($g \cdot L^{-1}$)	TEVA®		MYLAN®		CERUBIDINE®	
	Specificity %	Sensitivity %	Specificity %	Sensitivity %	Specificity %	Sensitivity %
S1 (0.03125)	50	26.7	33.3	53.3	57.1	13.3
S2 (0.0625)	40.1	46.7	40	53.3	78.9	6.7
S3 (0.125)	93.8	0	31.8	53.3	36.4	46.7
S4 (0.25)	36.8	40	80	6.7	29.1	0.4
S5 (0.5)	58.8	13.3	58.8	13.3	17.4	53.3
S6 (1)	100	100	100	100	100	100
S7 (1.5)	100	100	100	93.3	96.7	100
S8 (2)	100	100	100	100	100	100
Overall	72.5	53.3	72.3	59.2	64.4	57.5

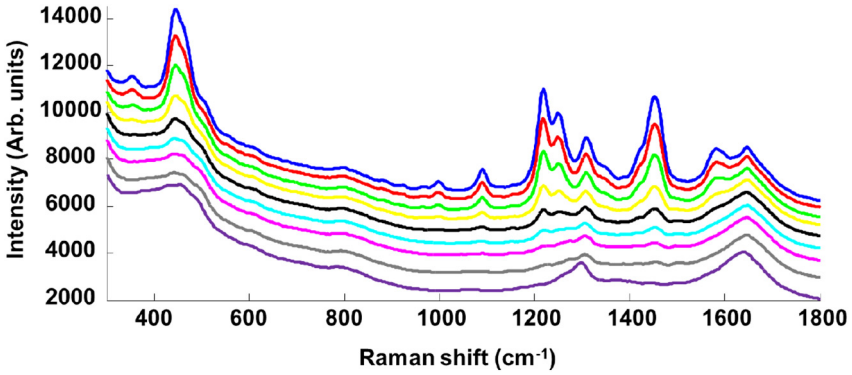


Fig. 4. Mean Raman spectra of the finger print regions collected from TEVA® following serial dilutions. Corresponding drug concentrations are 2 g·L^{-1} (blue), 1.5 g·L^{-1} (red), 1 g·L^{-1} (green), 0.5 g·L^{-1} (yellow), 0.25 g·L^{-1}(black), 0.125 g·L^{-1} (cyan), 0.0625 g·L^{-1} (magenta), 0.03125 g·L^{-1} (grey), water (purple). Spectra are offset for clarity.

1647 cm^{-1} which are the major spectral features previously observed in Fig. 3 and Table 1. Finally, a similar approach has been employed for MYLAN® and CERUBIDINE® formulations, yielding respective RMSECV of 0.0173 g·L^{-1} and 0.0220 g·L^{-1}, as summarised in Table 5. Although inconsistent between patients and hospital, the lowest administered concentration for doxorubicin is roughly 0.15 g·L^{-1}, and therefore the corresponding RMSECV found of 0.0127 g·L^{-1} suggest overall imprecision of about 8.5%. Similarly for MYLAN® and CERUBIDINE®, the RMSECV respectively account for 5.8% and 2.35% compared to the lowest doses typically prescribed (0.3 g·L^{-1} and 1.2 g·L^{-1}). The lower limit of detection (LOD) calculated from the PLSR analysis indicates that Raman spectroscopy can pick up concentrations as low as 0.0290 g·L^{-1}, 0.0383 g·L^{-1} and 0.0778 g·L^{-1} respectively for TEVA®, MYLAN® and CERUBIDINE®, values which are all >10 times below the lowest dose administered to patients.

3.3. Discriminant and quantitative analysis using ATR-IR spectroscopy

3.3.1. ATR-IR characterisation of anthracycline formulations

Although recent work has supported the feasibility to perform IR quantitative analysis with ATR-IR from liquid samples [32,44], in the present study the anti-cancer drug concentrations involved are not sufficient to overcome the strong contribution of the water bands, which completely swamp the features of interest (data not shown). Consequently, air drying of samples following deposition onto the ATR crystal is required to collect exploitable data. Fig. 6 displays the fingerprint region of mean spectra collected from the 3 different formulations. TEVA® and MYLAN® (Fig. 6a and b) deliver spectral signatures with high degree of similarity, but comparison of the peaks positions would suggest some variations in the range 700–1200 cm^{-1} can be observed (Table 6). Interestingly, the major difference compared to Raman spectroscopy is the weaker contribution of conjugated chromophores in the signatures collected. Consequently, other contributions from side chains and excipients can be somehow enhanced and more easily detected. For instance, the CERUBIDINE® mean spectrum differs from the other two without any possible ambiguity. This can be explained by the presence of a high amount of mannitol in the formulation, obviously delivering strong features in the IR signature (Fig. 6d). Summarised in Table 6, the most intense mannitol features at 1454 cm^{-1}, 1085 cm^{-1}, 1023 cm^{-1}, 875 cm^{-1}, 932 cm^{-1} and 890 cm^{-1} clearly dominate in the spectrum. However, a comparison between the IR spectrum collected from CERUBIDINE® (Fig. 6c) and the pure spectrum of mannitol highlights that, despite the lower band intensities, specific contributions from daunorubicin can be identified at 1712 cm^{-1}, 1617 cm^{-1},

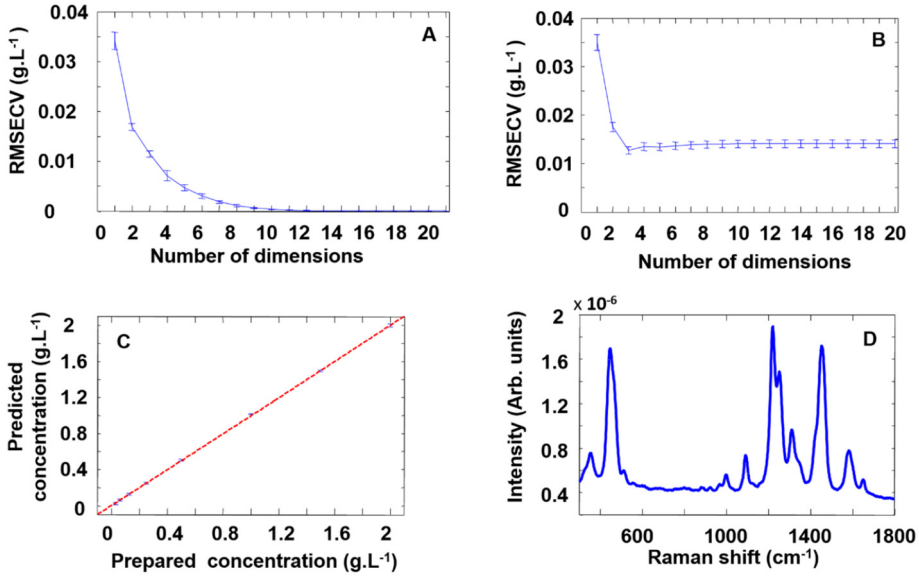


Fig. 5. PLSR analysis performed on TEVA®. A: Standard deviation error of calibration; B: Standard deviation error of validation; C: Regression fitting and D: Weighting vector. Error bars represent the standard deviation.

Table 5
PLSR results obtained from the 3 chemotherapeutic drug solutions tested.

Commercialized formulation	Active drug	R^2	RMSECV ($g \cdot L^{-1}$)	Dimensions
TEVA®	DOX	0.9996	0.0127	3
MYLAN®	EPI	0.9993	0.0173	5
CERUBIDINE®	DAU	0.9990	0.0220	5

1582 cm^{-1}, 1411 cm^{-1}, 1202 cm^{-1}, 1110 cm^{-1}, 996 cm^{-1} and 984 cm^{-1}.

3.3.2. Discriminant analysis using PCA-FDA

Similar to Raman spectra, observations based on PCA enable a rapid visualisation of the spectral variability contained in the data set collected by ATR-IR. While Raman spectra from liquid samples can to some extent be affected by underlying background, the collection of infrared spectra using the ATR set up coupled to air dried drops drastically reduces any distortion of the baseline. Although recording of IR spectra from biological material such as cell or tissues in transmission can lead to Mie or resonant Mie scattering effects [45], direct deposition of the solution on the ATR crystal minimises such phenomena. Consequently, only some offset in the data collected is observed according to the concentrations analysed, but such effects are easily compensated by implementation of a simple straight baseline subtraction such as the rubber band employed here. A rubber band correction with only 2 nodes at 1800 cm^{-1} and 600 cm^{-1} has the effect of bringing the spectral baseline down to 0 across the spectral range. Prior to performing the discriminant analysis, the concentration parameters have been removed using a vector normalisation to rescale all spectra.

The PCA scatter plot displays strong separation of the three formulations according to PC1 and PC2, accounting respectively for 98.7% and 0.82% of the explained variance (Fig. 7A). Similarly to Raman spectra, PC1 unambiguously differentiates TEVA® (Fig. 7A blue) and MYLAN® (Fig. 7A green) formulations from CERUBIDINE® (Fig. 7A red). The corresponding loading suggests that PC1 is basically the spectral signature of mannitol, which is expected due to the strong features observed in the spectra of CERUBIDINE®. Notably, the bands at 1454 cm^{-1}, 1085 cm^{-1}, 1022 cm^{-1}, 931 cm^{-1} and 717 cm^{-1} support this statement. PC2 discriminates TEVA® (Fig. 7A blue) from MYLAN® (Fig. 7A green). The PCA tends to maximise the explained variance expressed by the first principal components. As a consequence of the strong contribution from the features assigned to mannitol, PC2 only accounts for 0.82%. This observation supports the presence of small variations in band positions, as previously witnessed and reported in Table 6. The features of loading 2 confirm that the discrimination is based on the differing spectroscopic profiles of the compounds but, due to the scatter of CERUBIDINE® data points over the 2 other clusters in that dimension, the exact determination of the origin of the features of the loading of PC2 is not trivial. Pairwise PCA is the most direct and unambiguous analysis to highlight the presence of discriminative wavenumbers between 2 datasets [28]. Fig. 7C and D display respectively the scatter plot and loading 1 for the PCA applied to TEVA® and MYLAN®. In the absence of the CERUBIDINE® and associated strong mannitol bands, the scatter plot displays a clear separation of TEVA® and MYLAN® along PC1 with an explained variance of 91.8%. The loading 1 corresponding to PC1 exhibits a quite large number of features but interestingly some of the most intense, located at 767 cm^{-1}, 1014 cm^{-1}, 1060 cm^{-1}, 1123 cm^{-1}, 1212 cm^{-1}, 1576 cm^{-1}, 1615 cm^{-1} and 1719 cm^{-1} either match or are closely related to features found in TEVA® and MYLAN® as listed in Table 6. Although pairwise PCA is a relevant approach to investigate inter and intra data sets variability, it becomes relatively difficult to evaluate all combinations of data and estimate the discrimination

Table 6
Bands positions and assignments in ATR_IR spectra collected from TEVA®, MYLAN® and CERUBIDINE®.

TEVA® (cm^{-1})	*MYLAN®* (cm^{-1})	*CERUBIDINE®* (cm^{-1})	Mannitol (cm^{-1})	Assignments
–	–	–	712	–
762	767	–		=C–H (aromatic) bending
789	791	783	–	vibrations
817	814	–	875	–N–H out of plane bending vibrations, =C–H (aromatic) bending vibrations
884	882	883	890	=C–H (aromatic) bending vibrations
–	–	931	932	–
987	989	984	–	C=O, C–O–H bending vibrations
–	–	996	–	
1014	1019	1019	1023	C–O (alcoholic) bending
1079	1063	1082	1085	vibrations
1117	1122	1110	–	Ring breathing coupled with C–C=O bending vibrations, C–O (alcoholic) bending vibrations
1210	1211	1202	–	C–O (alcoholic) bending vibrations
1286	1286	–	–	H-bonding vibrations of O–H…O coupled with ring vibrations
1407	1407	1411	–	$-CH_3$ bending vibrations
–	–	–	1454	
1578	1578	1582	–	–N–H bending vibrations, Ring
1616	1616	1617	–	vibrations
				–N–H bending vibrations
1709	1709	1712	–	C=O stretching vibrations
1722	1722	–		

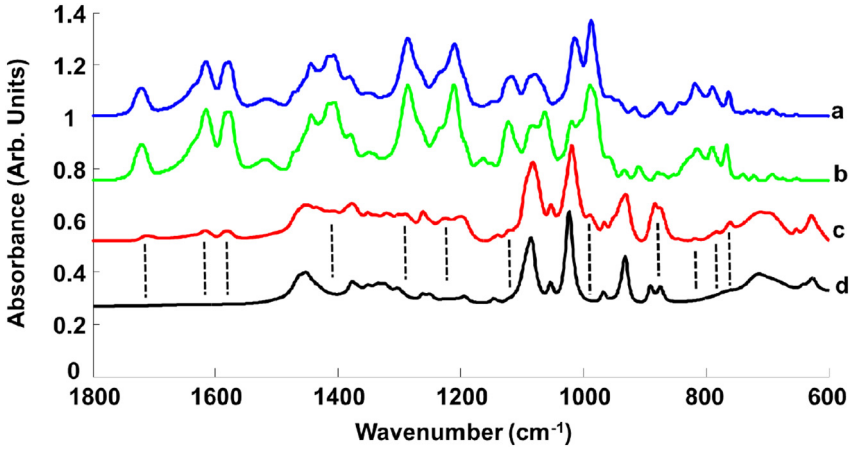


Fig. 6. Mean ATR-IR spectra recorded from TEVA® (A), MYLAN® (B), CERUBIDINE® (C) formulations and Mannitol (D). All spectra were recorded from solutions with final concentration of anticancer drugs at 2 $g \cdot L^{-1}$. Spectra are offset for clarity.

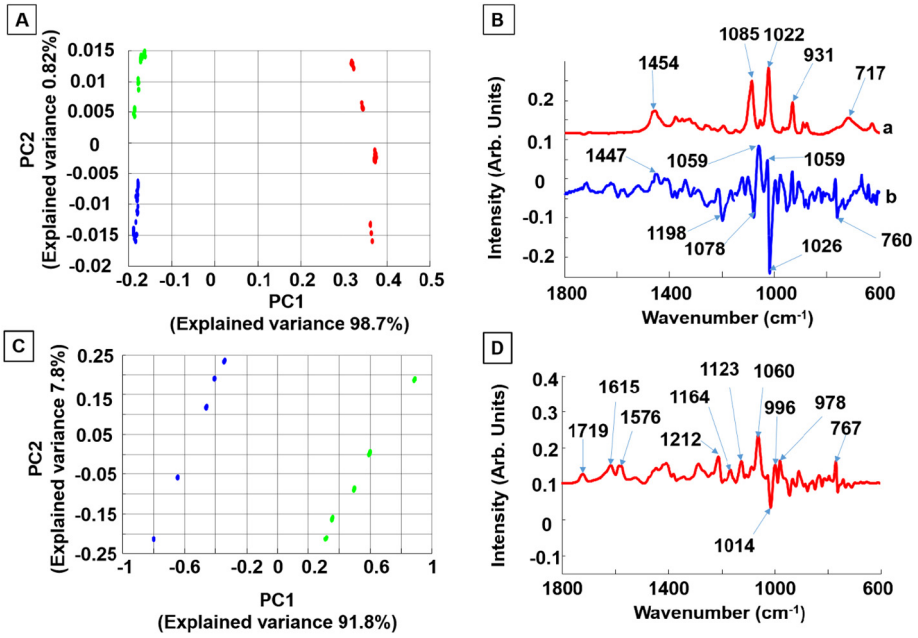


Fig. 7. PCA of ATR_FTIR data collected from chemotherapeutic solutions at 2 g·L^{-1}. A: Scatter plot of PC1 and PC 2 with TEVA® (blue), MYLAN® (green) and CERUBIDINE® (red). B: Loading corresponding to PC1 (a) and PC2 (b). C: Pairwise PCA of ATR_FTIR from TEVA® (blue) and MYLAN® (green) and D: Loading corresponding to loading PC1.

rate when the number of samples is increasing. Therefore, more advanced methods such as PCA-FDA can be used.

The outcome of the PCA-FDA obtained using 3 principal components is presented in Table 7, whereby, once again, the specificity and sensitivity has been calculated for each concentration analysed and for each drug. Using the ATR-IR spectra for discriminative analysis leads to high rates of correct classification with overall values equal or above 99.4%. A more detailed breakdown of the results shows that only the lowest concentrations tested, corresponding to 0.03125 g·L^{-1}, do not deliver 100% specificity and sensitivity for all 3 formulations. However, with 90% as the lowest outcome, the results remain quite satisfactory for accurate and reliable identification of formulations tested in respective formulations.

The main concern of the study is to investigate the discrimination of clinical formulations of the anticancer drugs, rather than their simple solutions. Considering the strong sugar features in the IR spectra collected from CERUBIDINE®, it is obvious that mannitol plays a major role in the discrimination. One could question the specificity of differentiating the therapeutic solution containing CERUBIDINE® from pure solution of mannitol. This can be demonstrated thanks to a pair wise PCA performed from CERUBIDINE® solution at 0.03125 g·L^{-1}, the lowest concentration presently tested, and mannitol solution at 0.15625 g·L^{-1}. The concentration of mannitol has been adjusted accordingly to the dilution factor of the stock solution of CERUBIDINE®. The scatter plot displayed in Fig. 8A exhibits a clear separation of the data along PC1 with 85.4% of the explained variance. Naturally, in a pair wise PCA, PC2, with 6.5% represents the intragroup variability. Loading 1 compared to the pure spectrum of mannitol highlights that numerous spectral features are contributed by other molecules such as daunorubicin in the solutions. Therefore, the discrimination of CERUBIDINE® observed in the PCA-FDA is a combined contribution of both mannitol and other ingredients including the anticancer drug. Similar observations are made with all concentrations included in this study (data not shown) which is perfectly understandable as the mannitol/daunorubicin ratio remains identical for all samples due to the same dilution factor applied during the preparation.

3.3.3. Quantitative analysis using PLSR

Observation of the ATR-IR spectra collected from a set of TEVA® solutions highlights that the intensity of the absorbance tends to decrease according to concentration (Fig. 9). It has been demonstrated that, while ATR-IR measurements can be used for quantitative analysis, the approach has a limited range of concentrations over which the Beer- Lambert law can be directly applied, whereby high concentration samples lead to a plateau effect with a loss of the linear relationship [44]. As the concentration increases, the thickness of the deposited residue film increases, to the extent that is comparable to the spatial extent of the evanescent field of the ATR. This can be accounted for by additional dilution of the higher concentrations. However, in the present study, it appears the dynamic range of concentrations is within the range of

Table 7
Specificity and sensitivity % of PCA_FDA for ATR_FTIR.

Sample concentration (g·L^{-1})	*TEVA®*		*MYLAN®*		*CERUBIDINE®*	
	Specificity %	Sensitivity %	Specificity %	Sensitivity %	Specificity %	Sensitivity %
S1 (0.03125)	95	100	100	90	100	100
S2 (0.0625)	100	100	100	100	100	100
S3 (0.125)	100	100	100	100	100	100
S4 (0.25)	100	100	100	100	100	100
S5 (0.5)	100	100	100	100	100	100
S6 (1)	100	100	100	100	100	100
S7 (1.5)	100	100	100	100	100	100
S8 (2)	100	100	100	100	100	100
Overall	99.4	100	100	98.75	100	100

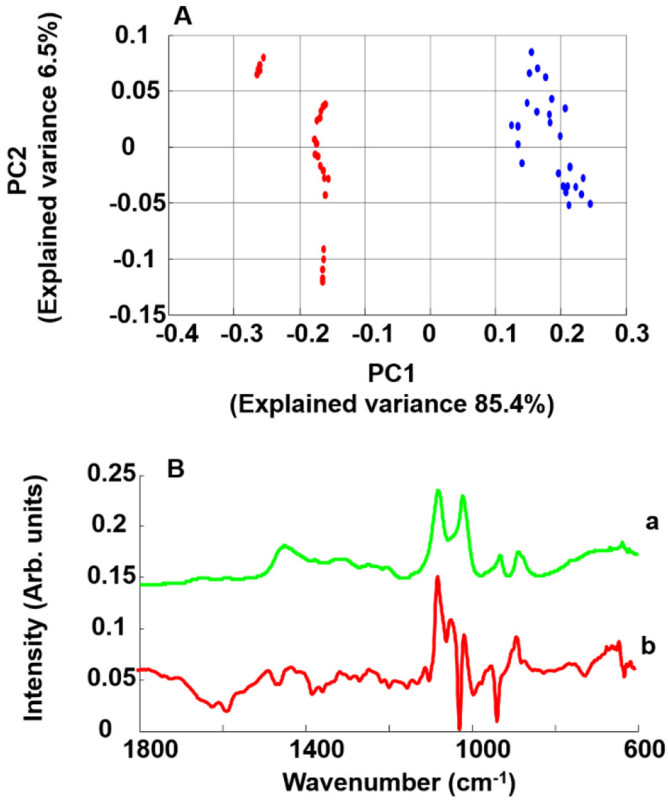


Fig. 8. PCA of ATR_FTIR data collected from CERUBIDINE® 0.03125 g·L^{-1} and Mannitol 0.15625 g·L^{-1}. A: Scatter plot of PC1 and PC 2 with CERUBIDINE® (red) and Mannitol (blue). B: Reference spectrum of mannitol (a) and loading corresponding to PC1 (b). Spectra offset for clarity.

linearity of absorbance response. Similar to the case for Raman, the ATR-IR spectra have been subjected to PLSR analysis in order to evaluate how well correlated the spectral variations are with the concentration of the anticancer formulations. Fig. 10 presents the different steps performed on the TEVA® form, as described previously in Section 3.2.3. As observed with the Raman, the weighting vector extracted from the PLSR analysis is almost an identical copy of the mean spectra presented in Fig. 10D, once more illustrating the molecular specificity of the analysis performed. However, the behaviour of the RMSECV as function of the dimensions number strongly differs in IR from that in Raman analysis. It tends to gradually decrease, with no clearly defined optimal number of dimensions which would ensure no overfitting of the model. Examination of the latent variables suggests that only the first 3 ones exhibit strong relevant features, while subsequent ones become increasingly dominated by noise and random bands. Therefore, considering the limited volume of data in this investigation, it was deemed preferable to limit the number of dimensions to 3, in order to not deliver over optimistic results for the ATR-IR analysis. Ultimately, the outcome of the PLSR analysis delivers RMSECV higher than those observed with Raman spectroscopy, respectively 0.0558 g·L^{-1}, 0.0573 g·L^{-1} and 0.0759 g·L^{-1} for TEVA®, MYLAN® and CERUBIDINE® formulations (Table 8). Nevertheless, with R^2 values all above 0.99, the high degree of linearity in the PLSR model constructed with the IR data is demonstrated.

However, although a multi-reflection crystal has been used, compared to the macro set up for the Raman experiments, the repeatability in the IR analysis remains lower, leading to loss of precision. In order to avoid over fitting of the results, the number of dimensions has been limited to 3 for the 3 drugs. Ultimately the results demonstrate the limited quantitative capabilities of the approach when applied to anticancer formulations. For instance, the LOD calculated from the PLSR analysis are considerably higher than for Raman analysis. LOD of 0.5802 g·L^{-1} (TEVA®), 0.4043 g·L^{-1} (MYLAN®) and 0.3514 g·L^{-1} (CERUBIDINE®) are calculated which are in same order of the lowest administered doses (respectively 0.15 g·L^{-1}, 0.3 g·L^{-1}, 1.2 g·L^{-1}). It appears uncertainties in determination of low concentrations raises questions regarding the reliability of ATR-IR for accurate quantification. The Beer Lambert law is commonly employed to describe the linear relationship between concentration of an analyte in solution and its absorbance, facilitating quantitative analysis. When performing analysis of liquid samples, it is easy to comply with the basic requirements of uniform optical path length of the samples and sample homogeneity, to produce reliable results. As most of other protocols of sample preparation for IR analysis, air drying the samples onto the ATR crystal also raises questions about the uniformity and repeatability of the sample layer thickness and area [45]. In recent years, concerns over the so-called "coffee ring effect" have been raised, in relation to ATR FTIR analysis of dried droplets. The effect refers to the tendency of molecular species to accumulate at the edge of the drop during the drying process [43,44]. Depending on the sample concentration, the coffee ring effect can also lead to complete loss of the signal simply because the sample accumulates outside the area of measurement of the ATR crystal [41]. Different types of crystals are commercially available, defined by the material of the crystal (for example diamond or germanium) but also the number of internal reflections. Since a single reflection accessory delivered no signal from the dried droplets, due to the coffee ring effect (data not shown), we used in the present study the multi-reflection diamond crystal enabling the 2 μL to be completely comprised within the recording area. Nevertheless, the heterogeneity of the dried hand-made deposits remained significant.

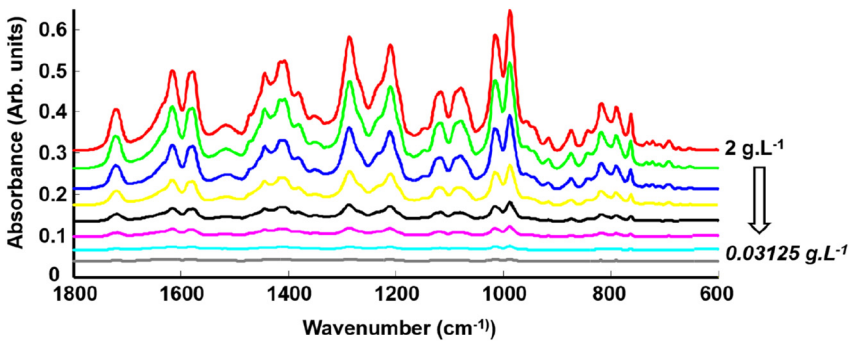


Fig. 9. Mean Raman spectra of fingerprint regions of TEVA® following serial dilutions. Spectra are organised as decreasing concentrations from the top to bottom, respectively corresponding to doxorubicin concentrations of 2 g·L^{-1} (red), 1.5 g·L^{-1} (green), 1 g·L^{-1} (blue), 0.5 g·L^{-1} (yellow), 0.25 g·L^{-1} (black), 0.125 g·L^{-1} (magenta), 0.0625 g·L^{-1} (cyan), and 0.03125 g·L^{-1} (grey). Spectra are offset for clarity.

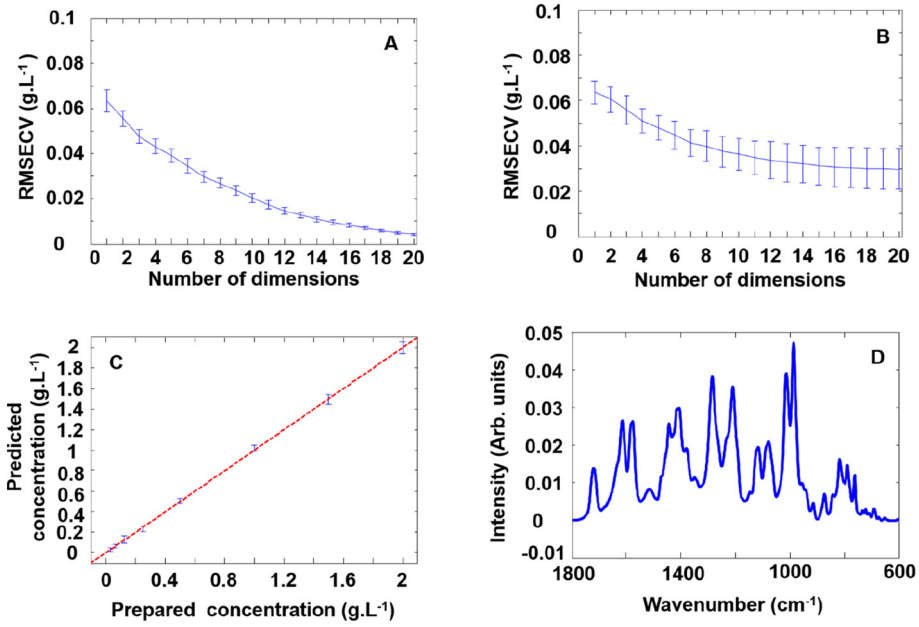


Fig. 10. PLSR analysis performed on TEVA®. A: Standard deviation error of calibration; B: Standard deviation error of validation; C: Regression fitting and D: Weighting vector. Error bars represent the standard deviation.

4. Overall discussion

Direct comparison between infrared and Raman spectroscopy has been conducted for the identification and quantification of 3 anthracyclines (TEVA®, MYLAN® and CERUBIDINE®) in solution, at clinically relevant concentrations (i.e. in the range of concentrations administered to patients). Data mining of spectral data sets with the help of multivariate analysis demonstrates that discrimination of drugs and predicting concentrations can be achieved with both techniques, although with different reliabilities. On the one hand, Raman spectroscopy displays the best precision for quantitative analysis, with RMSECV between 0.127 and 0.220 $g \cdot L^{-1}$ obtained from PLSR analysis, while on the other hand IR spectroscopy delivers higher sensitivity and specificity (above 95%) for drug identification with PCA-FDA. Both techniques behave differently due to differences in the intrinsic nature of the signal collected. Raman spectroscopy is strongly dependent on polarisability of the molecules which, in the case of TEVA®, MYLAN® and CERUBIDINE®, results in spectra clearly dominated by contributions from the conjugated ring structures. In contrast, IR is sensitive to small variations in side-chains but also to additives. Commercial chemotherapeutic solutions are formulae or mixtures with different degrees of complexity, depending on the number of ingredients present. The drug is usually the most concentrated chemical constituent of the solution, by many orders of magnitude, therefore with little or no contribution from the other constituents. However, in some cases the presence of a specific molecule at higher concentrations can change the balance and generate additional features in the spectral signatures. In CERUBIDINE®, for example, the presence of mannitol contributes significantly to the profile of the infrared spectra, which are therefore representative of mixed contributions of the drug and the sugar used as additive. This does not represent a limitation of the technique, but rather a strength of ATR-IR compared to Raman, as manifested in the significantly improved discriminative power of the technique and its higher sensitivity in classification. Some ingredient or additive signatures, once combined with the spectral bands of the drug, can play the role of spectral markers for more reliable identification of the stock solution used to prepare the diluted solution. In the present study, TEVA®, MYLAN® and CERUBIDINE® are the ones and only brands used for respectively doxorubicin, epirubicin and daunorubicin. Thus the spectral bands identified and used for discrimination will be reproducible and consistent over time. At present, quality control laboratories in hospitals typically employ flow injection analysis which is able to deliver accurate quantification for the majority of the 100+ solutions tested daily. The technique lacks the required specificity, however, when challenged with the discrimination of isomers such as TEVA®, MYLAN® and CERUBIDINE®, which display similar absorbance in the visible range, which can result in significant delays in administration of the solutions on a daily basis. As an augmentation to the current workflow, ATR-IR provides a potential solution for the rapid differentiation of the solutions. Performing the ATR analysis requires small volumes (few μL) compared to other current systems with injection of aliquots of at least 1.5 mL necessary. Considering the whole process of data analysis can be automated and completed in <1 min, the overall time to get the result does not exceed 5 min, which is comparable to systems already in use. Ultimately, ATR-IR spectroscopy is a cost effective technique with compact bench top apparatus that does not represent a huge capital investment and are increasingly user friendly, such that the data preprocessing and analysis routines can be easily incorporated into the instrument software and implemented in an automated protocol.

Table 8
PLSR results obtained from the 3 chemotherapeutic solutions tested.

Commercialized formulation	Active drug	R^2	RMSECV ($g \cdot L^{-1}$)	Dimensions
TEVA®	DOX	0.9972	0.0362	10
MYLAN®	EPI	0.9984	0.0244	10
CERUBIDINE®	DAU	0.9971	0.0349	10

5. Conclusion

Both Raman and Infrared spectroscopy are valuable analytical tools with demonstrated potential for clinical applications. Although often proposed as complementary, instrumental set up would have a strong influence of their performance to a given application. The quantitative analysis of chemotherapeutic drugs can be achieved in solution with Raman spectroscopy or following air drying with ATR-IR. In contrast, the discrimination of anthracyclines such as TEVA® (doxorubicin), MYLAN® (epirubicin) and CERUBIDINE® (daunorubicin) as part of quality control of therapeutic solutions suggests specificity of Raman

analysis is more limited than that of IR. Although air drying is required for IR, analysis results are promising and enable both identification and quantification of all 3 molecules tested. With specificity and sensitivity above 95%, ATR-IR spectrophotometry appears to be the most valuable approach to address current needs for discrimination of therapeutic solutions containing isomeric drugs and should be positioned as a highly relevant technique. Having an ATR just beside on the bench as a complementary tool to current techniques could provide an unambiguous identification in 5 min. To summarise, ATR-IR spectrophotometry remains a cost effective, rapid and user friendly method which with optimization of methods would lead to fast implantation in the hospital routine.

Acknowledgements

The authors aknowledge the french ambassy in Sudan and Campus for financial support.

References

[1] N.D. Popowicz, S.J. O'Halloran, D. Fitzgerald, Y.C.G. Lee, D.A. Joyce, A rapid, LC-MS/MS assay for quantification of piperacillin and tazobactam in human plasma and pleural fluid; application to a clinical pharmacokinetic study, J. Chromatogr. B 1081-1082 (2018) 58–66.
[2] A.J. McShane, D.R. Bunch, S. Wang, Therapeutic drug monitoring of immunosuppressants by liquid chromatography–mass spectrometry, Clin. Chim. Acta 454 (2016) 1–5.
[3] A. Delmas, J.B. Gordien, J.M. Bernadou, M. Roudaut, A. Gresser, L. Malki, M.C. Saux, D. Breilh, Quantitative and qualitative control of cytotoxic preparations by HPLC-UV in a centralized parenteral preparations unit, J. Pharm. Biomed. Anal. 49 (2009) 1213–1220.
[4] J.D. Hofer, B.A. Olsen, E.C. Rickard, Is HPLC assay for drug substance a useful quality control attribute? J. Pharm. Biomed. Anal. 44 (2007) 906–913.
[5] C. Bazin, B. Cassard, E. Caudron, P. Prognon, L. Havard, Comparative analysis of methods for real-time analytical control of chemotherapies preparations, Int. J. Pharm. 494 (2015) 329–336.
[6] C. Bazin, V. Vieillard, A. Astier, M. Paul, Implementation of real-time identification analysis and quantification of chemotherapies preparations with a Multispec® analyser, Ann. Pharm. Fr. 72 (2014) 33–40.
[7] F. Nardella, M. Beck, P. Collart-Dutilleul, G. Becker, C. Boulanger, L. Perello, A. Gairard-Dory, B. Gourieux, G. Ubeaud-Sequier, A UV-Raman spectrometry method for quality control of anticancer preparations: results after 18 months of implementation in hospital pharmacy, Int. J. Pharm. 499 (2016) 343–350.
[8] P. Bourget, A. Amin, F. Vidal, C. Merlette, F. Lagarce, Comparison of Raman spectroscopy vs. high performance liquid chromatography for quality control of complex therapeutic objects: model of elastomeric portable pumps filled with a fluorouracil solution, J. Pharm. Biomed. Anal. 91 (2014) 176–184.
[9] P. Bourget, A. Amin, F. Vidal, C. Merlette, P. Troude, A. Baillet-Guffroy, The contribution of Raman spectroscopy to the analytical quality control of cytotoxic drugs in a hospital environment: eliminating the exposure risks for staff members and their work environment, Int. J. Pharm. 470 (2014) 70–76.
[10] K. Kong, C. Kendall, N. Stone, I. Notingher, Raman spectroscopy for medical diagnostics–from in-vitro biofluid assays to in-vivo cancer detection, Adv. Drug Deliv. Rev. 89 (2015) 121–134.
[11] M.J. Baker, J. Trevisan, P. Bassan, R. Bhargava, H.J. Butler, K.M. Dorling, P.R. Fielden, S.W. Fogarty, N.J. Fullwood, K.A. Heys, C. Hughes, P. Lasch, P.L. Martin-Hirsch, B. Obinaju, G.D. Sockalingum, J. Sulé-Suso, R.J. Strong, M.J. Walsh, B.R. Wood, P. Gardner, F.L. Martin, Using Fourier transform IR spectroscopy to analyze biological materials, Nat. Protoc. 9 (2014) 1771–1791.
[12] B. Bird, M.S. Miljkovic, S. Remiszewski, A. Akalin, M. Kon, M. Diem, Infrared spectral histopathology (SHP): a novel diagnostic tool for the accurate classification of lung cancer, Lab. Investig. 92 (2012) 1358–1373.
[13] I.R. Ramos, A.D. Meade, O. Ibrahim, H.J. Byrne, M. McMenamin, M. McKenna, A. Malkin, F.M. Lyng, Raman spectroscopy for cytopathology of exfoliated cervical cells, Faraday Discuss. 187 (2016) 187–198.
[14] V. Vuiblet, M. Fere, E. Bankole, A. Wynckel, C. Gobinet, P. Birembaut, O. Piot, P. Rieu, Raman-based detection of hydroxyethyl starch in kidney allograft biopsies as a potential marker of allograft quality in kidney transplant recipients, Sci. Rep. 6 (2016), 33045.
[15] I.P. Santos, E.M. Barroso, T.C. Bakker Schut, P.J. Caspers, C.G.F. van Lanschot, D.H. Choi, M.F. van der Kamp, R.W.H. Smits, R. van Doorn, R.M. Verdijk, V. Noordhoek Hegt, J.H. von der Thusen, C.H.M. van Deurzen, L.B. Koppert, G. van Leenders, P.C. Ewing-Graham, H.C. van Doorn, C.M.F. Dirven, M.B. Busstra, J. Hardillo, A. Sewnaik, I. Ten Hove, H. Mast, D.A. Monserez, C. Meeuwis, T. Nijsten, E.B. Wolvius, R.J. Baatenburg de Jong, G.J. Puppels, S. Koljenovic, Raman spectroscopy for cancer detection and cancer surgery guidance: translation to the clinics, Analyst 142 (2017) 3025–3047.
[16] A. Jaworska, S. Fornasaro, V. Sergo, A. Bonifacio, Potential of surface enhanced Raman spectroscopy (SERS) in therapeutic drug monitoring (TDM). A critical review, Biosensors (Basel) 6 (2016).
[17] S. Wartewig, R.H. Neubert, Pharmaceutical applications of Mid-IR and Raman spectroscopy, Adv. Drug Deliv. Rev. 57 (2005) 1144–1170.
[18] F. Bonnier, H. Blasco, C. Wasselet, G. Brachet, R. Respaud, L.F. Carvalho, D. Bertrand, M.J. Baker, H.J. Byrne, I. Chourpa, Ultra-filtration of human serum for improved quantitative analysis of low molecular weight biomarkers using ATR-IR spectroscopy, Analyst 142 (2017) 1285–1298.
[19] D. Rohleder, W. Kiefer, W. Petrich, Quantitative analysis of serum and serum ultrafiltrate by means of Raman spectroscopy, Analyst 129 (2004) 906–911.
[20] Z. Farhane, F. Bonnier, H.J. Byrne, Monitoring doxorubicin cellular uptake and trafficking using in vitro Raman microspectroscopy: short and long time exposure effects on lung cancer cell lines, Anal. Bioanal. Chem. 409 (2017) 1333–1346.
[21] D. Šahnić, E. Meštrović, T. Jednačak, I. Habinovec, J. Parlov Vuković, P. Novak, Monitoring and quantification of omeprazole synthesis reaction by in-line Raman spectroscopy and characterization of the reaction components, Org. Process Res. Dev. 20 (2016) 2092–2099.
[22] L.M.M. Lê, A. Tfayli, J. Zhou, P. Prognon, A. Baillet-Guffroy, E. Caudron, Discrimination and quantification of two isomeric antineoplastic drugs by rapid and non-invasive analytical control using a handheld Raman spectrometer, Talanta 161 (2016) 320–324.
[23] A. Amin, P. Bourget, F. Vidal, F. Ader, Routine application of Raman spectroscopy in the quality control of hospital compounded ganciclovir, Int. J. Pharm. 474 (2014) 193–201.
[24] M. Kiehntopf, B. Monch, R. Salzer, M. Kupfer, M. Hartmann, Quality control of cytotoxic drug preparations by means of Raman spectroscopy, Pharmazie 67 (2012) 95–96.
[25] P. Bourget, A. Amin, A. Moriceau, B. Cassard, F. Vidal, R. Clement, La Spectroscopie Raman (SR): un nouvel outil adapté au contrôle de qualité analytique des préparations injectables en milieu de soins. Comparaison de la SR aux techniques CLHP et UV/visible-IRTF appliquée à la classe des anthracyclines en cancérologie, Pathol. Biol. 60 (2012) 369–379.
[26] T. Lan, Y. Fang, W. Xiong, C. Kong, Automatic baseline correction of infrared spectra, Chin. Opt. Lett. 5 (2007) 613–616.
[27] N.K. Afseth, A. Kohler, Extended multiplicative signal correction in vibrational spectroscopy, a tutorial, Chemom. Intell. Lab. Syst. 117 (2012) 92–99.
[28] F. Bonnier, H.J. Byrne, Understanding the molecular information contained in principal component analysis of vibrational spectra of biological systems, Analyst 137 (2012) 322–332.
[29] D. Bertrand, P. Courcoux, J.C. Autran, R. Meritan, P. Robert, Stepwise canonical discriminant analysis of continuous digitalized signals: application to chromatograms of wheat proteins, J. Chemom. 4 (1990) 413–427.
[30] S. Guo, T. Bocklitz, U. Neugebauer, J. Popp, Common mistakes in cross-validating classification models, Anal. Methods 9 (2017) 4410–4417.
[31] M.E. Keating, H. Nawaz, F. Bonnier, H.J. Byrne, Multivariate statistical methodologies applied in biomedical Raman spectroscopy: assessing the validity of partial least squares regression using simulated model datasets, Analyst 140 (2015) 2482–2492.
[32] L. Miloudi, F. Bonnier, D. Bertrand, H.J. Byrne, X. Perse, I. Chourpa, E. Munnier, Quantitative analysis of curcumin-loaded alginate nanocarriers in hydrogels using Raman and attenuated total reflection infrared spectroscopy, Anal. Bioanal. Chem. 409 (2017) 4593–4605.
[33] F. Allegrini, A.C. Olivieri, IUPAC-consistent approach to the limit of detection in partial least-squares calibration, Anal. Chem. 86 (2014) 7858–7866.
[34] S. Charak, D.K. Jangir, G. Tyagi, R. Mehrotra, Interaction studies of Epirubicin with DNA using spectroscopic techniques, J. Mol. Struct. 1000 (2011) 150–154.
[35] H. Nawaz, F. Bonnier, A.D. Meade, F.M. Lyng, H.J. Byrne, Comparison of subcellular responses for the evaluation and prediction of the chemotherapeutic response to cisplatin in lung adenocarcinoma using Raman spectroscopy, Analyst 136 (12) (2011) 2450–2463, https://doi.org/10.1039/c1an15104e.
[36] L.M.M. Lê, M. Berge, A. Tfayli, J. Zhou, P. Prognon, A. Baillet-Guffroy, E. Caudron, Rapid discrimination and quantification analysis of five antineoplastic drugs in aqueous solutions using Raman spectroscopy, Eur. J. Pharm. Sci. 111 (2018) 158–166.
[37] D. Nieciecka, A. Królikowska, I. Setiawan, P. Krysinski, G.J. Blanchard, Interactions of doxorubicin with organized interfacial assemblies. 2. Spectroscopic characterization, Langmuir 29 (2013) 14570–14579.
[38] E. Szafraniec, K. Majzner, Z. Farhane, H.J. Byrne, M. Lukawska, I. Oszczapowicz, S. Chlopicki, M. Baranska, Spectroscopic studies of anthracyclines: structural characterization and in vitro tracking, Spectrochim. Acta A Mol. Biomol. Spectrosc. 169 (2016) 152–160.
[39] N.L. Marc, G.R. Alan, Comparison of derivative preprocessing and automated polynomial baseline correction method for classification and quantification of narcotics in solid mixtures, Appl. Spectrosc. 60 (2006) 182–193.
[40] K.H. Liland, A. Kohler, N.K. Afseth, Model-based pre-processing in Raman spectroscopy of biological samples, J. Raman Spectrosc. 47 (2016) 643–650.
[41] Z. Farhane, F. Bonnier, A. Casey, A. Maguire, L. O'Neill, H.J. Byrne, Cellular discrimination using in vitro Raman micro spectroscopy: the role of the nucleolus, Analyst 140 (2015) 5908–5919.
[42] G.L. Owens, K. Gajjar, J. Trevisan, S.W. Fogarty, S.E. Taylor, B.D. Gama-Rose, P.L. Martin-Hirsch, F.L. Martin, Vibrational biospectroscopy coupled with multivariate analysis extracts potentially diagnostic features in blood plasma/serum of ovarian cancer patients, J. Biophotonics 7 (2014) 200–209.
[43] F. Bonnier, A. Mehmood, P. Knief, A.D. Meade, W. Hornebeck, H. Lambkin, K. Flynn, V. McDonagh, C. Healy, T.C. Lee, F.M. Lyng, H.J. Byrne, In vitro analysis of immersed human tissues by Raman microspectroscopy, J. Raman Spectrosc. 42 (2011) 888–896.
[44] F. Bonnier, G. Brachet, R. Duong, T. Sojinrin, R. Respaud, N. Aubrey, M.J. Baker, H.J. Byrne, I. Chourpa, Screening the low molecular weight fraction of human serum using ATR-IR spectroscopy, J. Biophotonics 9 (2016) 1085–1097.
[45] P. Bassan, H.J. Byrne, F. Bonnier, J. Lee, P. Dumas, P. Gardner, Resonant Mie scattering in infrared spectroscopy of biological materials - understanding the 'dispersion artefact, Analyst 134 (2009) 1586–1593.

PUBLICATION 2: Vibrational spectroscopy for discrimination and quantification of clinical chemotherapeutic preparations

The revised manuscript has been re-submitted to Vibrational Spectroscopy in December 1st, 2020

Alaa A. Makki [a, b], Victor Massot [c], Hugh J. Byrne [f], Renaud Respaud [d], Dominique Bertrand [e], Elhadi Mohammed [b], Igor Chourpa [a], Franck Bonnier [a,*]

[a] Université de Tours, EA 6295 Nanomédicaments et Nanosondes, 31 avenue Monge, 37200 Tours, France

[b] Faculty of Pharmacy, University of Gezira, P.O. Box 20, 21111 Wad Madani, Sudan

[c] Unité de Biopharmacie Clinique Oncologique, Pharmacie, CHU de Tours, France

[d] Université de Tours, UMR 1100, CHRU de Tours, Service de Pharmacie, F-37032 Tours, France

[e] Data_Frame, 25 rue Stendhal, 44300 Nantes, France

[f] FOCAS Research Institute, TU Dublin, City Campus, Kevin Street, Dublin 8, Ireland

Abstract

In a clinical setting, analytical quality control of the administration of chemotherapeutic preparations is required to ensure patient safety with respect to the dose and more importantly the correct anticancer drug. As such, analytical tools enabling both qualitative and quantitative verification of the composition of prepared solutions can greatly benefit the hospital workflow, reducing cost and ultimately ensuring optimum patient care and outcome. Raman and infrared spectroscopy are rapid and cost-effective techniques, delivering label free molecular characterisation of samples. A comparative study has been conducted using four commercial intravenous formulations, DOXORUBICINE TEVA®, CERUBIDINE®, HOLOXAN® and METHOTREXATE MYLAN®, respectively containing doxorubicin, daunorubicin, ifosfamide and methotrexate as active drugs. Using clinically relevant concentration ranges prepared in 0.9% NaCl or 5% glucose solutions, it is demonstrated that 100% discrimination can be achieved for all formulations using either Raman or IR spectroscopic techniques, combined with multivariate discriminant analysis. Employing a partial least square regression analysis, Raman spectroscopy performed on liquid samples delivers a better accuracy compared to infrared, based on the mean squared error of cross validation. However, it is demonstrated that,

despite the strong contribution of glucose and mannitol, an excipient found in CERUBIDINE®, infrared spectroscopy remains an equally viable option for translation into clinics.
Key words: ATR-FTIR spectroscopy, Raman spectroscopy, chemotherapeutics, Chemometrics, Partial least squares regression.

1. Introduction:

Chemotherapeutic drugs remain one of the main treatments for cancer, although they can result in serious side effects, due to the non-selective targeting of both cancer and healthy cells, and toxicity to patients is a major concern (1,2). Nowadays, individualised doses, in the form of solutions of commercial formulations, are prescribed to minimise adverse effects to patients while aiming to administer chemotherapeutic drugs within a sometimes-narrow therapeutic window. The safety for patients is strongly dependent on the precise preparation and administration of the chemotherapeutic solutions, i.e. the correct drug administered at the prescribed dose. Therefore, analytical quality control (AQC), i.e. identification and quantification of active drugs, before the solutions are released from the preparation units to the patient's bedside for administration has become a crucial step in the clinical workflow, and intravenous chemotherapeutic solutions are systematically analysed and approved to prevent discrepancies between prescription and administration. Although practices vary in different hospitals, the identification of the active pharmaceutical ingredients (APIs) should be achieved with 100% accuracy, while the tolerance for errors between targeted and estimated concentrations can be as high as 10% (3).

There is, however, no universally accepted or agreed protocol for AQC of prepared solutions and a diverse range of analytical techniques are used in the hospital setting for this purpose, including high-performance liquid chromatography (HPLC) or flow injection analysis (FIA), generally coupled to UV detection, or more elaborated techniques such as mass spectrometry (MS). HPLC remains the gold standard for quality control (4,5), while MS plays a rather crucial role during the drug discovery and development process, for chemotherapeutic characterisation (6–8) or for therapeutic drug monitoring (TDM), which requires quantification of low concentration of drugs within biological matrices such as serum (9). Considering the huge number of solutions which have to be analysed every single day, in addition to the analytical performance of the techniques, other criteria such as the need for sample preparation, time/material consumption, cost and staff requirements are considered prior to selection of an

appropriate technique. Reducing the costs and the pressure on the workflow while preserving the reliability of the analytical protocols is a challenge.

Vibrational spectroscopic techniques, Raman scattering (RS) and infrared (IR) absorption, are structure-specific methods that can provide a molecular fingerprint for both qualitative and quantitative analysis of solutions (10). They are non-destructive, label-free methods, that have gained recognition for clinical applications and quality control due to the minimal requirement for sample preparation and short analysis time (11). Vibrational spectroscopy has previously been explored in hospital settings in the context of AQC, which is performed before releasing the therapeutic prescriptions for administration (12–17). An instrument combining UV-visible and IR absorption techniques (Multispec ®, Microdom) has been proposed to perform analysis on chemotherapeutic solutions (18). However, the appropriateness of such a set up to fully exploit the coupling of those two methods is quite limited in aqueous solutions, since infrared suffers from the strong water absorbance (19). More recently, based on the fact that water is a relatively weak Raman scatter, the coupling of UV-visible absorption and Raman spectroscopy has emerged as a strong candidate for analysis of aqueous solutions (3,20).

Surprisingly, the literature reporting IR absorption and Raman spectroscopic analysis of chemotherapeutic solutions is limited (21–23). Although some relevant pharma-based publications can be found, none propose an in depth understanding of the origin of the spectra collected. A direct comparison between IR and Raman spectroscopy was performed by Makki *et al.*,(24) for the case of doxorubicin, epirubicin and daunorubicin in aqueous solutions. However, intravenous chemotherapeutic solutions are either prepared in the presence of 0.9% NaCl or 5% glucose (22,25,26), which potentially impact the signatures of the collected spectra. Therefore, the present study investigates the identification/discrimination and quantification of therapeutic solutions of four chemotherapeutic drugs (doxorubicin, daunorubicin, ifosfamide and methotrexate) by means of Attenuated Total Reflectance Infrared spectroscopy (ATR-IR) and Raman spectroscopy. In addition, to describe the vibrational characteristics of the drug molecule, the study assesses the possible matrix effect linked to either 0.9% NaCl or 5% glucose, for the drug solutions prepared at various concentrations corresponding to their respective therapeutic range.

2. Materials and Methods:

2.1 Anticancer drugs and sample preparation:

Four commercial formulations have been provided through a collaboration established with the University Hospital of Tours. More precisely, the UBCO unit (Unité de Biopharmacie Clinique

Oncologique, Tours, France) deals with the preparation of individualised chemotherapeutic doses directly on site for rapid administration to patients.

DOXORUBICINE TEVA® (doxorubicin, injectable solution, 2 $g{\cdot}L^{-1}$ with HCl and NaOH (<1%) as excipients), and CERUBIDINE® (daunorubicin, lyophilised powder, 20 % w/w in mannitol), are anthracyclines which inhibit DNA and RNA synthesis (27), and are used in the treatment of breast cancer, lymphomas and multiple myelomas, lung cancer (28,29), Hodgkin's lymphomas, bladder lymphomas, soft tissues sarcomas, lung and testicular cancers (30).

HOLOXAN® (ifosfamide, 1000 mg powder for solution) is an oxazophosphorine alkylating drug, which induces DNA cross linking (31), used in the treatment of non-Hodgkin lymphomas, bone and soft tissues sarcomas (32). For HOLOXAN®, no excipients are listed by the manufacturers.

METHOTREXATE MYLAN® (methotrexate injectable solution 100 $g{\cdot}L^{-1}$ with NaCl as excipient) is an antifolate, which inhibits folic acid synthesis and is widely used to treat osteosarcomas, lymphomas, solid tumours, psoriasis, rheumatoid arthritis (33), head and neck cancer (34), breast cancer (35), acute lymphocytic leukaemia (36) and central nervous system lymphomas (37).

Based on records for recently prepared solutions at the UBCO unit, relevant therapeutic concentration ranges were established for the study. Sets of 10 solutions of each were prepared using serial dilutions in either 0.9% sodium chloride or 5% glucose (Table 1). 3 independent sets of samples were prepared from the stock solution for a total of 30 samples per drug. All samples were prepared freshly on the day of analysis and stored at 4°C in a dark room to avoid photo-damaging prior to spectral analysis.

For clarity, throughout the manuscript, commercial formulas are identified using their brand names DOXORUBICINE TEVA®, CERUBIDINE®, HOLOXAN®, METHOTREXATE MYLAN® while doxorubicin, daunorubicin, ifosfamide and methotrexate solely refer to the active drugs themselves.

Table 1. Concentration range for the 4 drugs analysed

Brand	Drug	Concentration range analysed (n = 10)
TEVA®	Doxorubicin	0.10 $g{\cdot}L^{-1}$ - 1.45 $g{\cdot}L^{-1}$
CERUBIDINE®	Daunorubicin	1.1 $g{\cdot}L^{-1}$ - 2 $g{\cdot}L^{-1}$
HOLOXAN®	Ifosfamide	2 $g{\cdot}L^{-1}$ - 17.75 $g{\cdot}L^{-1}$
MYLAN®	Methotrexate	3 $g{\cdot}L^{-1}$ – 21 $g{\cdot}L^{-1}$

1.2.1 Raman spectroscopic analysis

Raman spectra were collected using a Labram spectrometer (Horiba Jobin-Yvon, France) equipped with a 690 nm laser source. The set up was adapted to perform macroanalysis from solutions in quartz cuvettes. A macro-cuvette holder (Horiba Jobin-Yvon, France), was attached to the turret of the microscope, redirecting the laser through the samples with a 45° incidence mirror, allowing the micro spectrometer to be operated in a similar way to a UV/Vis benchtop spectrophotometer, sliding in and out the cuvettes between measurements. Using such a set up ensures maximum reproducibility during data collection without the requirement to readjust the laser focus between measurements, while enabling analysis of a large volume of solutions. 500 µL of the solution were placed in a quartz cuvette. The spectral range was set between 150 and 3750 cm^{-1}, with a spectral resolution of ~3 cm^{-1}, achieved using a 300 lines/mm grating. Two accumulations of 20 seconds were taken for each spectrum. 9 spectra were collected from each sample, 27 per concentration, and thus 270 for each drug analysed for each matrix, i.e. 0.9% NaCl and 5% glucose.

1.2.2 Infrared spectroscopic analysis

Infrared spectra were recorded with a Frontier, Fourier Transform IR (FTIR) spectrometer (Perkin Elmer, France) equipped with a multi-reflection diamond (n = 10) ATR accessory (ConcentratIR2™, Eurolabo, France). A drop of 2 µL was deposited directly on the ATR crystal and allowed to air dry prior to analysis. A background was acquired (4 scans) and ratioed with the sample spectra by the acquisition software (Spectrum, Perkin Elmer). Each IR spectrum resulted from 4 co-averaged scans collected over the range 600 – 4000 cm^{-1} with a spectral resolution of 2 cm^{-1}. 9 spectra were collected from each sample, 27 per concentration. Thus,

270 spectra were collected for each drug analysed for each matrix, i.e. 0.9% NaCl and 5% glucose.

2.2.3 Data handling:

Raman and IR data sets have been pre-processed and analysed using MATLAB (Mathworks, USA).

a) Discriminant analysis: For the purpose of discriminative analysis, Raman and FTIR spectra were subjected to background correction by Extended Multiplicative Scattering Correction (EMSC) (38–40), in the range 300 – 3750 cm^{-1} for Raman spectra, whereas for ATR-FTIR spectra the range was 600 – 4000 cm^{-1}, followed by Lieber baseline correction (41–43) and vector normalisation (44) to minimise interferences from backgrounds (45). Pre-processed Raman and IR spectra were analysed in the fingerprint region of 600 – 1800 cm^{-1} by Partial Least Squares Discriminant Analysis (PLSDA), which is a well-established and widely used supervised classification method (22,46).While multivariate approaches such as PCA (Principal Components Analysis) provide valuable insights to the source of variance within datasets by reducing dimensionality to reveal underlying patterns, the interpretability of the analysis is directly linked to the complexity of the date set (i.e. number of samples), and it has been demonstrated the most specific analysis is obtained for pair wise system (47). Presently, the data set includes 80 groups (4 drugs, 2 matrices 0.9% NaCl and 5% glucose, of 10 systematically varied concentrations). PCA cannot readily be applied to differentiate all samples (data not shown), and moreover cannot provide a quantitative discriminative analysis. PLS-DA has been increasingly used over the last two decades to solve classification and discrimination problems of spectroscopic data (48). This supervised approach, like other discriminant analysis, requires knowledge of the class of each sample to construct a training set. Presently, PLSDA was used to discriminate between the 4 tested chemotherapeutic drugs in the 2 different matrices used for preparation of solutions. In order to avoid overoptimistic outcomes, it is recommended to perform the analysis between independent sets of data. 3 sets of 10 concentrations, Set 01, Set 02 and Set 03, have been recorded for each drug. For the discriminant analysis, the combination Set 1 and Set 2 were used as training sets (n = 40) for the construction of the model, while Set 03 was used solely as the test set (blind samples, n = 20). Therefore calibration, validation and test sets are kept independent. The optimal number of latent variables was selected with the validation set while the outcome of the PLSDA represents the classification of samples from the test set. Ultimately, the results were presented

in the form of confusion matrices, allowing calculation of the specificity and sensitivity of the discrimination achieved for the test set.

b) Quantitative analysis:

For the purpose of quantitative analysis, data were subjected to background correction by EMSC. No normalisation was applied, to maintain the linear relationship between spectral signal and concentration. Partial Least Squares Regression (PLSR) was applied to extract the quantitative information from data sets in the fingerprint region of 600 – 1800 cm^{-1}. Similar to PLSDA, Set 01 and Set 02 were used as training sets (n = 40) while Set 03 was used as the test set (n = 20). The 40 samples of the training set were further separated in the calibration and validation sets. For the purpose of quantitative analysis, 2/3 of samples were randomly selected as the calibration set and the remaining 1/3 were used as validation set. A 100-fold iteration was implemented to evaluate the robustness of the analysis with multiple random combinations of calibration/validation sets. However, the models were always tested with Set 03, used as unknown samples to be determined. The output of the PLSR analysis was evaluated using the Coefficient of Determination (R^2), and the Root Mean Square Error of Prediction (RMSEP) calculated from the test set (i.e. Set 03). The number of latent variables (LVs) was selected using the plot of Root Mean Square Error of Cross Validation (RMSECV), to preserve independency between training and test sets. The regression coefficients were also used to elucidate the spectral variables (wavenumbers) which contribute prominently to the regression models.

3. Results and discussions

3.1. Spectral characterisation of formulations

3.1.1. Raman analysis of commercial formulations

Figure 1 presents the chemical structures of doxorubicin, daunorubicin, ifosfamide and methotrexate, while Figure 2A shows the fingerprint region of corresponding Raman spectra obtained from their commercial stock solutions (DOXORUBICINE TEVA®, CERUBIDINE®, HOLOXAN® and METHOTREXATE MYLAN®, respectively). The Raman spectra recorded from distilled water and from relevant solutions of mannitol, glucose and 0.9% NaCl are displayed in Figure 2B. As expected, only 1% mannitol (spectrum a) and 5% glucose (spectrum

b) solutions show some additional bands to those of water, while NaCl in solution is dissolved into its constituent ions and thus does not exhibit any vibrations.

Doxorubicin and daunorubicin are anthracyclines composed of a tetracycline ring, the aromatic moiety being linked by a glycosidic bond to daunosamine sugar (49–51) (Figure 1). Therefore, the fingerprint region of DOXORUBICINE TEVA® and CERUBIDINE® (Figure 2Aa and 2Ab) show strong Raman spectral features around 1100 cm^{-1} (aromatic C-H bending), between 1200-1250 cm^{-1} (C-O-H and in plane C-O stretching), 1300 cm^{-1} (C-O-H bending), 1450 cm^{-1} and 1580 cm^{-1} (aromatic ring stretching) and at 1650 cm^{-1} (stretching of H-bonded C=O group) (24). The chemical composition of the commercialised drug CERUBIDINE® differs from that of DOXORUBICINE TEVA® due to the presence of quite a high concentration of mannitol as excipient. Accordingly, in the Raman spectrum of CERUBIDINE®, a band originating from mannitol can be observed at 890 cm^{-1} (Figure 2B, spectrum a). The other bands of mannitol, expected at 798 cm^{-1}, 1276 cm^{-1}, 1309 cm^{-1} and 1468 cm^{-1} (Figure 2A, spectrum b), are overlapped by stronger Raman features from the aromatic chromophore of daunorubicin.
The chemical structure of ifosfamide (Figure 1) is comprised of chloroethyl groups attached to an endocyclic nitrogen (32,52). The main spectral characteristics of HOLOXAN® (Figure 2A, spectrum c) are thus observed at 668 cm^{-1} (ring bending), 791 cm^{-1} (C-Cl stretching), 1052 cm^{-1} (C-C aliphatic chain stretching), 1295 cm^{-1} (ring stretching), 1452 cm^{-1} (N-H bending), 1484 cm^{-1} (CH_2 scissoring) and 1649 (CH_2 deformation) (53,54). METHOTREXATE MYLAN® (methotrexate) spectrum is characterised by strong features at 1209 cm^{-1}, 1352 cm^{-1} and 1554 cm^{-1} and 1606 cm^{-1} assignable respectively to CH_2 wagging, aromatic C-C stretching and C-N stretching (Figure 2Ad). Other weaker bands are observed at 673 cm^{-1} (aromatic C-C-C in plane bending), 700 cm^{-1} (C-C in plane bending), 765 cm^{-1} (C-C out of plane bending) and 1292 cm^{-1} (-CH_3 symmetric deformation) (55). For both HOLOXAN® and METHOTREXATE MYLAN®, excipients present are either HCl or NaOH, which are not expected to present spectral features contributing in the Raman spectra in this range. Therefore, the peaks observed can be specifically attributed to the active drugs in solution.

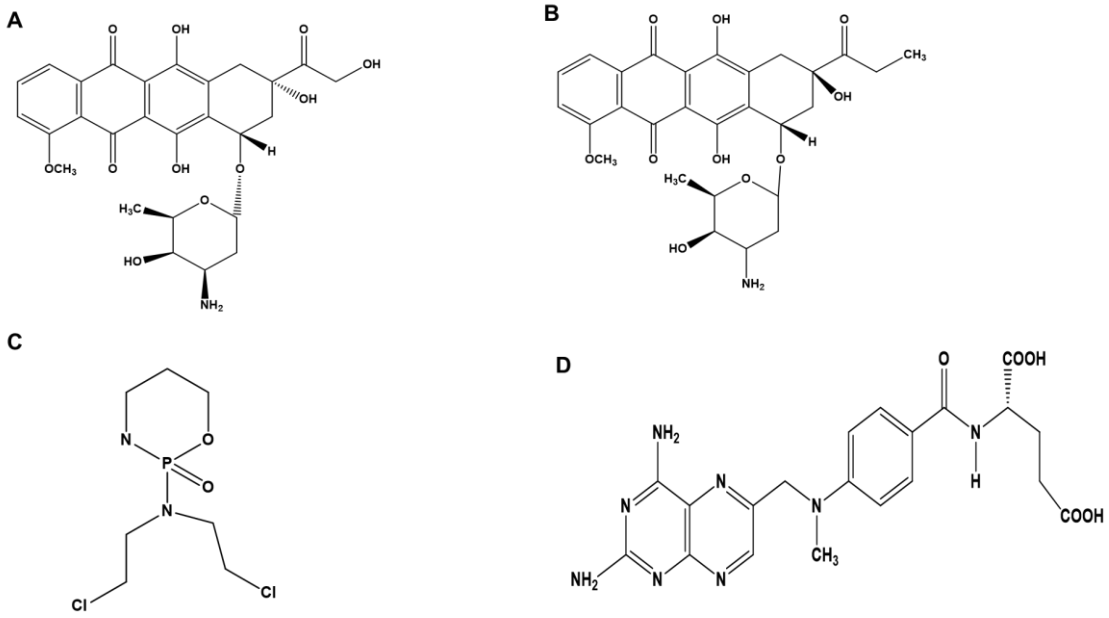
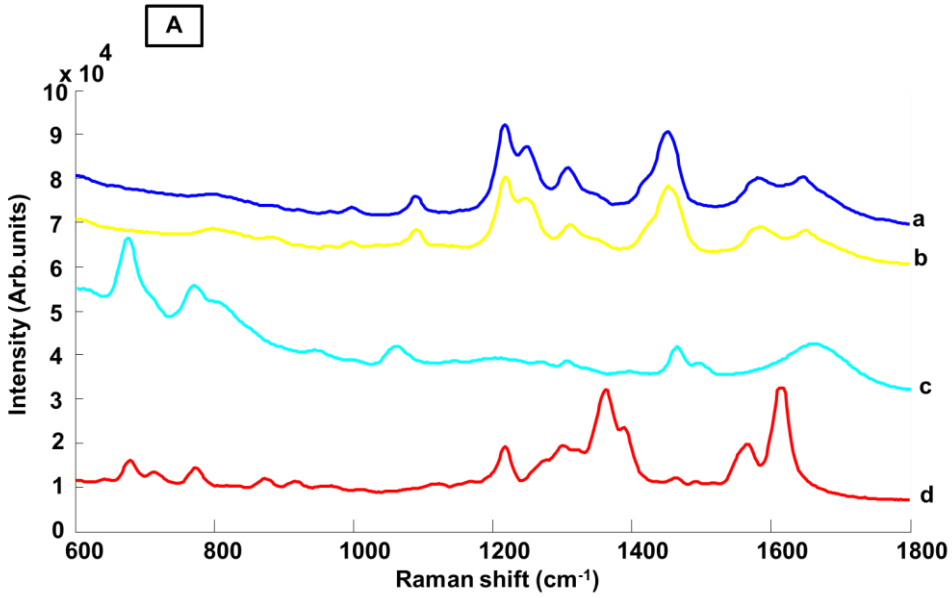


Figure 1: *chemical structures of A) Doxorubicin, B) Daunorubicin, C) Ifosfamide, D) Methotrexate.*



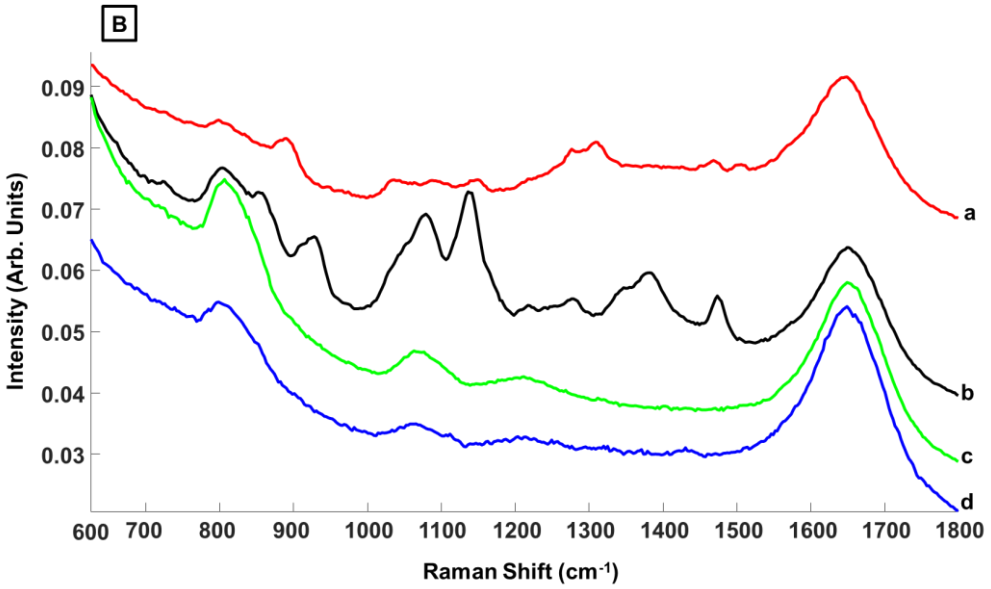


Figure 2: (A): Mean Raman spectra recorded from commercialised chemotherapeutics drug formula. DOXORUBICINE TEVA® 2 g·L^{-1} (a), CERUBIDINE® 2 g·L^{-1} (b), HOLOXAN® 40 g·L^{-1} (c) and METHOTREXATE MYLAN® 100 g·L^{-1} (d). (B): Mean Raman spectra recorded from Mannitol 1% (a), 5% glucose (b), 0.9% NaCl (c) and de-ionised water (d). Spectra are offset for clarity.

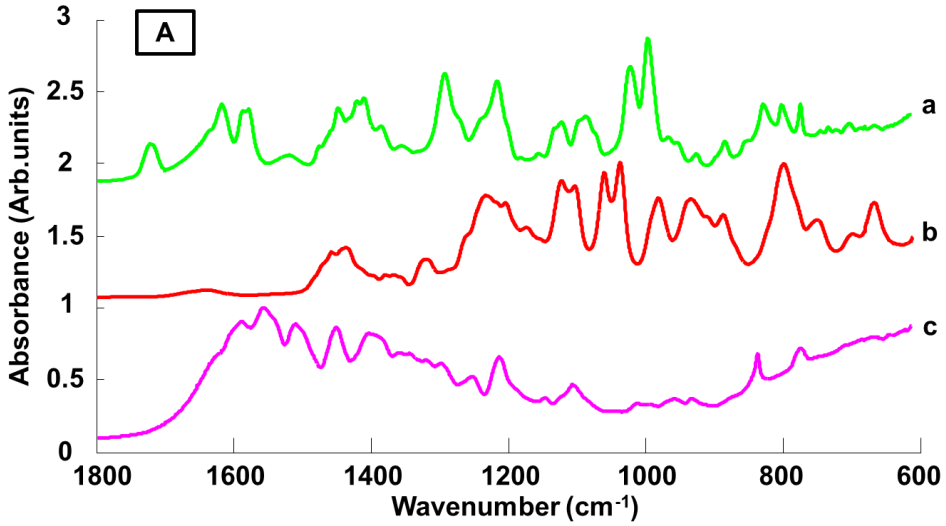
3.1.2. ATR-IR analysis of commercial formulations

In the ranges of concentrations used in this study, the strong water absorption at ~1640cm^{-1} dominates the IR spectrum of solutions, swamping characteristic features of the drugs (data not shown) and thus the only option was to record spectra from air dried drops deposited onto the ATR crystal for spectral characterisation. Figure 3A and Figure 3B presents ATR-FTIR spectra collected from the 4 drugs.

DOXORUBICINE TEVA® (Figure 3Aa) displays specific features at 1721 cm^{-1} (C=O stretching), 1616 cm^{-1} (N-H bending), 1576 cm^{-1} (ring breathing), 1444 cm^{-1} (-CH_3 bending), 1406 cm^{-1} (-CH_3 bending), 1210 cm^{-1} (C-C stretching), 1014 cm^{-1} (C-O (alcoholic) bending) and 987 cm^{-1} (C-O-H bending) (24). Mannitol presents a strong IR signature with a number of intense, sharp peaks across the 1800-600 cm^{-1} region (Figure 3Bb). As a consequence, numerous bands of the IR spectrum from CERUBIDINE® (Figure 3Ba) are attributed to features originating from this sugar. However, the strongest bands from CERUBIDINE® can be observed at 1712 cm^{-1} (C=O stretching), 1617 cm^{-1} (N-H bending), 1580 cm^{-1} (ring breathing), 1449 cm^{-1} (-CH_3 bending), 1139 cm^{-1} (ring breathing coupled with C-C=O bending), 1053 cm^{-1} (C-O (alcoholic) bending), 989 cm^{-1} (C-O-H bending), 966 cm^{-1} (-CH_3 rocking), 845 cm^{-1} (=C-H (aromatic) bending) and 818 cm^{-1} (N-H out of plane bending) (24). The combined

contribution of daunorubicin and mannitol bands implies some substantial differences between DOXORUBICINE TEVA® and CERUBIDINE®.

Considering the chemical structures of ifosfamide (Figure 1), it is not surprising that the infrared signature of HOLOXAN® greatly differs from that of the other drugs (Figure 3Ab), with strong bands at 1436 cm^{-1} (-CH_2 wagging), 1229 cm^{-1} (CH_2-Cl rocking), 1116 cm^{-1} (C-O bending), 1096 cm^{-1} (ring stretching), 1053 cm^{-1} (C-H wagging), 1030 cm^{-1} (C-C stretching), 973 cm^{-1} (ring stretching deformation), 925 cm^{-1} (C-O stretching), 876 cm^{-1} (ring stretching), 788 cm^{-1} (CH_2-Cl rocking) and 655 cm^{-1} (C-Cl stretching) (53,54). While the Raman spectrum of METHOTREXATE MYLAN® exhibits sharp, isolated intense peaks (Figure 3Ac), the ATR-IR spectrum has numerous overlapping bands resulting in broader features, notably in the range 1700-1200 cm^{-1}. However, specific peaks are found at 1587 cm^{-1} (C-C stretching), 1554 cm^{-1} (aromatic C-C stretching), 1506 cm^{-1} (C-N stretching), 1447 cm^{-1} (C-C stretching), 1398 cm^{-1} (CH_3 symmetric deformation), 1206 cm^{-1} (CH_2 wagging), 1097 cm^{-1} (CH_2 twisting) and 825 cm^{-1} (aromatic C-H out of plane bending) (55).



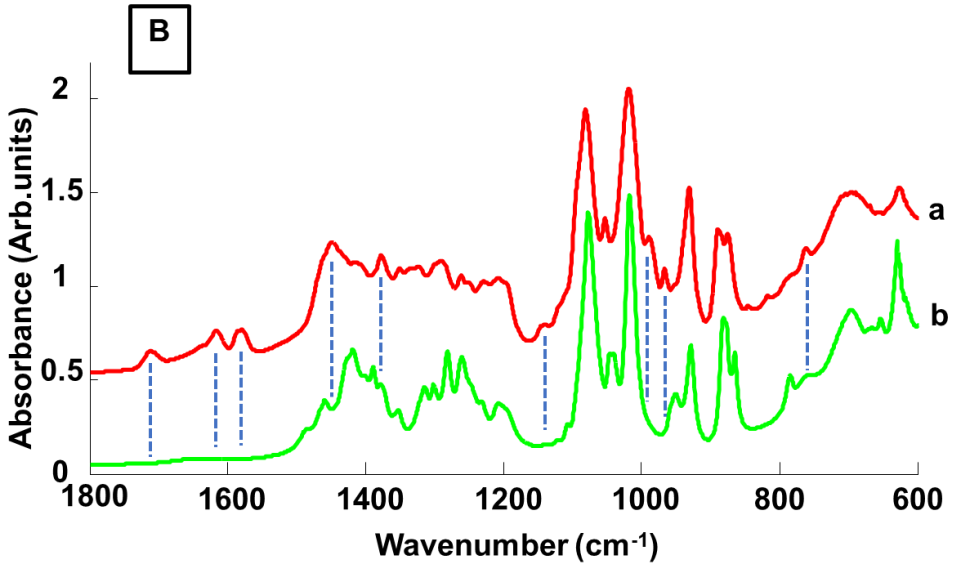


Figure 3: ***(A):*** *mean ATR-FTIR spectra recorded from commercial stock solutions. DOXORUBICINE TEVA® 2 g·L^{-1} (a), HOLOXAN® 40 g·L^{-1} (b) and METHOTREXATE MYLAN® 100 g·L^{-1} (c),* ***(B):*** *mean ATR-FTIR spectra recorded from CERUBIDINE® 2 g·L^{-1} (a) and mannitol 1% (b). Spectra are offset for clarity.*

3.2. Discriminant analysis using Raman and ATR-IR spectroscopy

Sensitivity and specificity are the main parameters used to determine the discriminative power of an analytical method. PLSDA was used to discriminate between the 4 tested chemotherapeutic drugs in the 2 different matrices used for preparation of solutions. For this purpose, samples of Set 01 and Set 02 have been used as the calibration and validation sets (n= 40) and Set 03 (n =20) was used a test set, i.e. as blind samples tested against the classification model constructed from the training sets. Therefore calibration, validation and test sets are kept independent. The optimal number of latent variables is selected with the validation set while the outcome of the PLSDA represents the classification of samples from the test set. Ultimately, the results were presented in the form of confusion matrices, allowing calculation of the specificity and sensitivity of the discrimination achieved for the test set. For Raman data, the discrimination was achieved using 5 latent variables (LVs) (as shown in Table 2). Ultimately, 100 % specificity and sensitivity were obtained.

Table 2. Specificity and sensitivity % of PLSDA calculated for the test set of Raman data using 5 LVs

Brand	0.9% NaCl		5% Glucose	
	Specificity	Sensitivity	Specificity	Sensitivity
TEVA®	100	100	100	100
CERUBIDINE®	100	100	100	100
HOLOXAN®	100	100	100	100
MYLAN®	100	100	100	100

Table 3 summarises the classification output for ATR-FTIR obtained with 11 LVs. Similar to Raman, 100% specificity and sensitivity are reached for the 4 tested chemotherapeutics drugs in either matrix. For both techniques, despite the structural similarities between doxorubicin and daunorubicin, as they belong to the anthracycline family of anticancer drugs and display structural similarities (56), PLSDA was able to differentiate between the DOXORUBICINE TEVA® and CERUBIDINE® formulations very clearly. This is in accordance with previous observations made by Makki *et al.,* (24), suggesting that the combination of structural differences and contribution of other formulation excipients provides sufficient spectral contrast to enable efficient discrimination.

Regression coefficients can be used to highlight the wavenumbers discriminating solutions prepared from the commercialised formulations. Figure 4 presents the regression coefficient resulting from the PLSDA applied to Raman spectra. The strong double bands between 1200-1250 cm^{-1} coupled to the strong feature at 1449 cm^{-1}, corresponding to DOXORUBICINE TEVA® and CERUBIDINE® are observed in the first regression coefficient (Figure 4a), whereas peaks identified in the first regression coefficient at 880 cm^{-1} and 1311 cm^{-1}, originating from mannitol, discriminate DOXORUBICINE TEVA® from CERUBIDINE®.

HOLOXAN® peaks can be identified at 680 cm^{-1} and 777 cm^{-1} in the first regression coefficient (Figure 4a). Peaks identifiable in the second regression coefficient (Figure 4b) at 673 cm^{-1}, 1216 cm^{-1}, 1360 cm^{-1}, 1561 cm^{-1} and 1607 cm^{-1} can be assigned to METHOTREXATE MYLAN®.

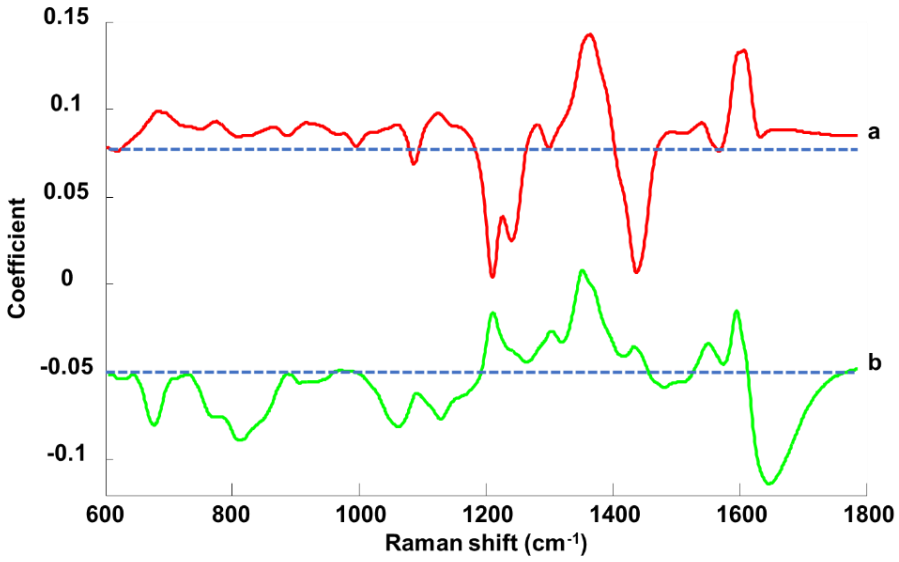


Figure 4: Regression coefficients a) 1 and b) 2 obtained from PLSDA analysis of Raman data. Offset for clarity, dot line indicates the zero.

In comparison, the contribution of glucose after air drying of samples is much more pronounced in ATR-FTIR spectra, and therefore the discrimination between solutions prepared in the two matrices can be easily achieved. This is highlighted by the first regression coefficient of PLSDA performed on IR spectra presented in Figure 5a, which displays pronounced features of glucose in the range 1000-1150 cm^{-1} (displayed in Figure 9). Moreover, as discussed in section 3.1.2, CERUBIDINE® ATR-FTIR spectra are strongly influenced by mannitol peaks, observed as the two main features between 1000-1100 cm^{1} in the 2^{nd} regression coefficient Figure 5b. Chemotherapeutic solutions also have specific additional features, as illustrated in Figure 3, and are therefore observed in both regression coefficients. For instance, the negative peaks in Figure 5a at 1587 cm^{-1}, 1554 cm^{-1}, 1506 cm^{-1}, 1447 cm^{-1}, 1206 cm^{-1}, 825 cm^{-1} correspond to specific peaks of METHOTREXATE MYLAN®, while the negative bands at 810 cm^{-1}, 788 cm^{-1}, 655 cm^{-1} and the quite specific double peaks at 1096 cm^{-1} and 1053 cm^{-1} can be assigned to HOLOXAN®.

Table 3. Specificity and sensitivity % of PLSDA calculated for the test set of ATR-FTIR data using 11 LVs

Brand	0.9% NaCl		5% Glucose	
	Specificity	Sensitivity	Specificity	Sensitivity
TEVA®	100	100	100	100
CERUBIDINE®	100	100	100	100
HOLOXAN®	100	100	100	100
MYLAN®	100	100	100	100

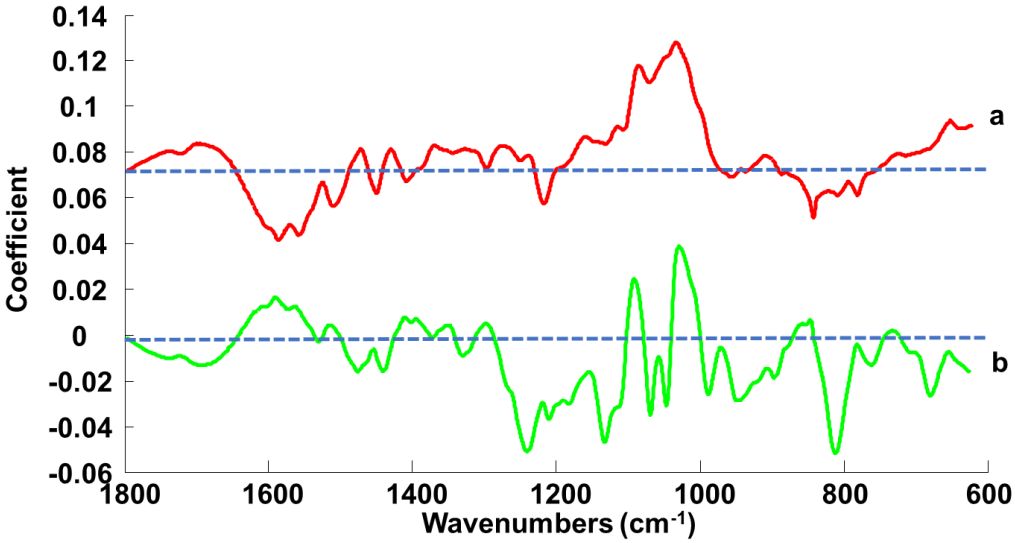


Figure 5: Regression coefficients, a) 1 and b) 2 obtained from PLSDA analysis on ATR-FTIR data. Offset for clarity, dot line indicates the zero.

3.3. Quantitative analysis of chemotherapeutics solutions

3.3.1. Raman spectroscopy

As an illustration of the quantitative potential of Raman spectroscopy, Figure 6 presents mean Raman spectra of the METHOTREXATE MYLAN® formula at different concentrations, from 21 to 3 $g{\cdot}L^{-1}$, all prepared in the presence of 5% glucose. Specific features at 1213 cm^{-1}, 1296 cm^{-1}, 1357 cm^{-1}, 1556 cm^{-1} and 1605 cm^{-1} are clearly identifiable and they naturally appear more pronounced as the drug concentration increases (Figure 6). Compared to those of the commercial sample, the band positions of the solutions prepared in glucose were only slightly affected (minor band shifts). Glucose displays only limited contributions identified at 927 cm^{-1}, 1079 cm^{-1} and 1136 cm^{-1} (Figure 2B, spectrum b).

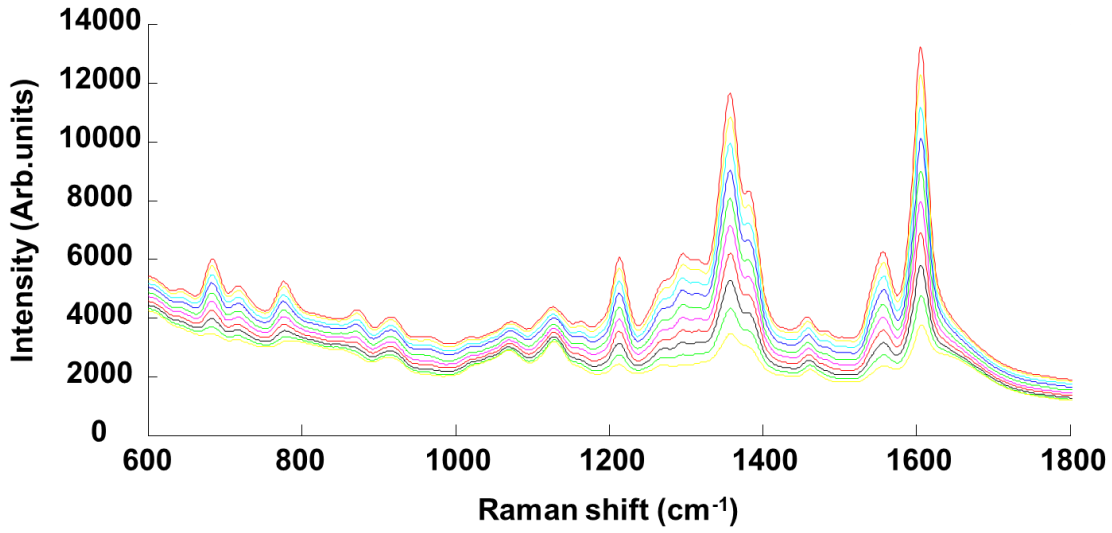


Figure 6: Mean Raman spectra of fingerprint regions of METHOTREXATE MYLAN® in 5% glucose solution following serial dilution. Spectra are organised as decreasing concentrations from the top to bottom, respectively corresponding to methotrexate concentrations of 21 g·L^{-1}, 19 g·L^{-1}, 17 g·L^{-1}, 15 g·L^{-1}, 13 g·L^{-1}, 11 g·L^{-1}, 9 g·L^{-1}, 7 g·L^{-1}, 5 g·L^{-1} and 3 g·L^{-1}.

In the present study, the approach for PLSR consisted of dividing the data into training and test sets. 2/3 of samples of the training set (n sample = 13) were identified as calibration and the remaining 1/3 (n sample = 7) were used as validation set. The samples from Set 03 were used independently and injected in the constructed quantitative model as bind samples. The RMSECV shows a marked decrease as a function of the number of LVs used in the PLSR model (Figure 7A). Above 3 LVs, there was no further statistical difference, indicating that only noise remained in the data and no further improvement in quantification could be achieved. The corresponding regression model presented in Figure 7B has been obtained from the test set. The error bars were calculated form the 100-fold iterations, indicating the reproducibility of the spectral collection using the macro set up. The R^2 value was found to be 0.9999 and the RMSEP was equal to 0.0448 g·L^{-1}, highlighting the quality of the fitting achieved and the accuracy of the predictive model. The mean standard deviation (STD) for the RMSEP was found to be 0.028 g·L^{-1}. The regression coefficient confirmed the predictive model was constructed based on METHOTREXATE MYLAN® features (Figure 7C). Notably, the presence of peaks at 1213 cm^{-1}, 1296 cm^{-1}, 1357 cm^{-1}, 1556 cm^{-1} and 1605 cm^{-1} confirmed the molecular specificity of the analysis has been preserved. Moreover, no prominent features of glucose are evident.

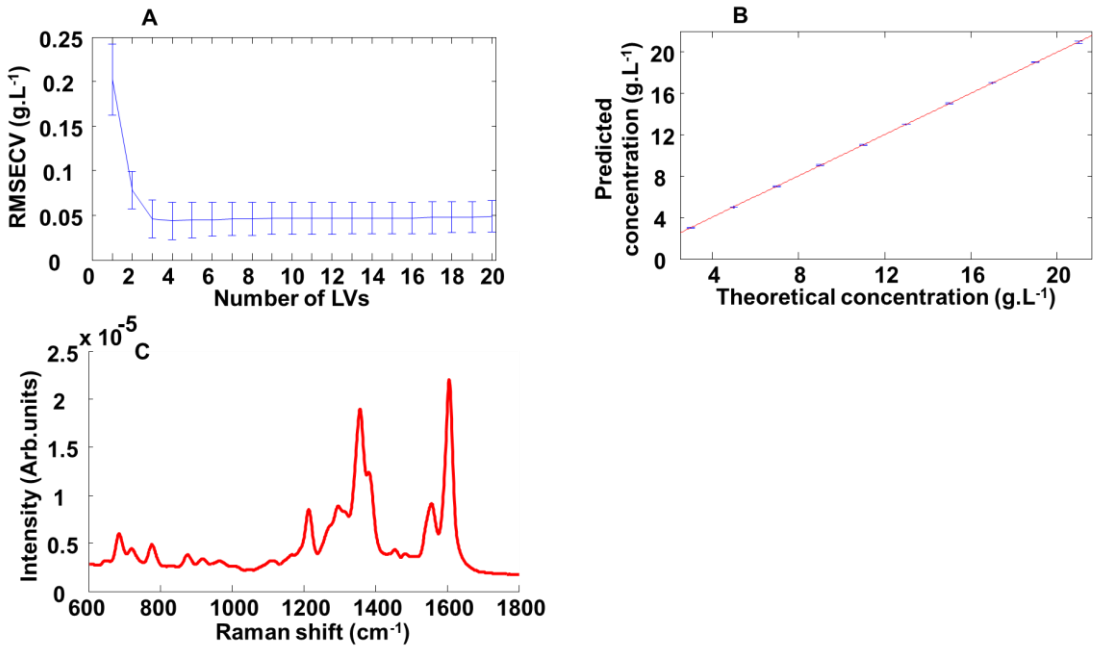


Figure 7: PLSR analysis performed on Raman spectra collected from METHOTREXATE MYLAN® solution in 5% glucose. A) RMSECV, B) Regression plot for the test set with 3 LVs and C) Regression coefficient.

Table 4 presents the PLSR results for all 4 commercial formulations, under the different conditions tested. For most of them, R^2 is close to, or equal to, 1 in both NaCl and glucose matrices. The lowest value of R^2 is found to be 0.9973 for CERUBIDINE®, in 0.9% NaCl. RMSEP values range from 0.0027 g·L^{-1} to 0.1759 g·L^{-1}, depending on the formulation and matrix used. To better appreciate the implication of the results, one could compare the RMSEP with the median concentration of the range used. For example, in the case of DOXORUBICINE TEVA® in 0.9% NaCl, the median concentration is 0.77 g·L^{-1}, and thus the RMSEP represents 0.6% of this value, suggesting the model is quite accurate. The highest RMSEP of 0.1759 g·L^{-1} is found for HOLOXAN® in 5% glucose, which only represents 1.8% of the median concentration. Therefore, it is observed that, overall, the RMSEP is relatively low compared to the range of concentrations analysed, indicating suitable sensitivity of Raman analysis for the chemotherapeutic solutions analysed, considering the clinical tolerance between the targeted concentration and the estimated concentration is 10%. As illustrated in Figure 1, the different commercial drug formulations do not have the same Raman response, and while METHOTREXATE MYLAN® has strong features, the signal collected from HOLOXAN® has much lower intensity. Figure 8 further illustrates the spectral variations in the range of concentrations analysed for HOLOXAN® in 5% glucose. One can see that the underlying contribution from water (Figure 2Bd) and glucose (Figure 2Bb) are more prominent across the

range of concentrations analysed, compared to the other solutions. Nevertheless, PLSR analysis enables accurate quantification.

Table 4. PLSR results obtained from the 4 chemotherapeutic drugs solutions tested in 2 matrices by Raman spectroscopy

Drug	Matrix	R^2	RMSEP	%RMSEP	LVs
TEVA®	0.9%NaCl	0.9999	0.0048	0.6	3
	5% glucose	1	0.0027	0.3	3
CERUBIDINE®	0.9%NaCl	0.9973	0.0152	0.9	4
	5% glucose	0.9994	0.0075	0.5	2
HOLOXAN®	0.9%NaCl	0.9995	0.1117	1.1	3
	5% glucose	0.9989	0.1759	1.8	4
MYLAN®	0.9%NaCl	1	0.0451	0.4	3
	5% glucose	0.9999	0.0448	0.4	3

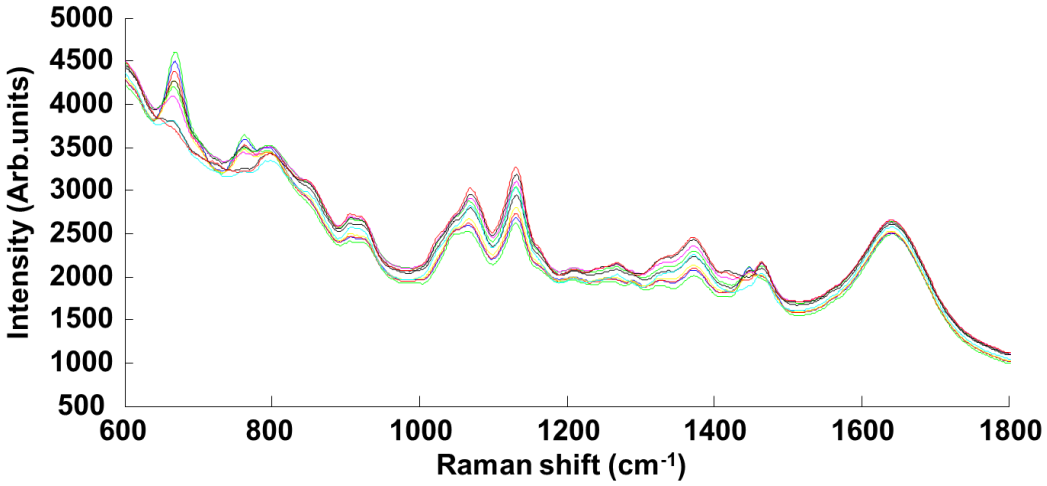


Figure 8: Mean Raman spectra of fingerprint regions of HOLOXAN® in 5% glucose solution following serial dilution. Spectra are organised as decreasing concentrations from the top to bottom, respectively corresponding to HOLOXAN® concentrations of 17.75 $g{\cdot}L^{-1}$, 16 $g{\cdot}L^{-1}$, 14.25$g{\cdot}L^{-1}$, 12.5 $g{\cdot}L^{-1}$, 10.75 $g{\cdot}L^{-1}$, 9 $g{\cdot}L^{-1}$, 7.25 $g{\cdot}L^{-1}$, 5.5 $g{\cdot}L^{-1}$, 3.75 $g{\cdot}L^{-1}$ and 2 $g{\cdot}L^{-1}$.

3.3.2. ATR-FTIR spectroscopy

Similar to Raman, the ATR-FTIR spectra have been subjected to PLSR to perform quantitative analysis. Glucose displays bands over the fingerprint range with main features found at 1420 cm^{-1}, 1358 cm^{-1}, 1315 cm^{-1}, 1258 cm^{-1}, 1145 cm^{-1}, 1100 cm^{-1}, 1071 cm^{-1}, 1020 cm^{-1}, 899 cm^{-1}, 842 cm^{-1} and 770 cm^{-1} (Figure 9A), while NaCl displays no significant spectral contribution (data not shown). Figure 9B illustrates, for the example of METHOTREXATE MYLAN®, how glucose has a strong contribution resulting in a spectral signature mixed with the drug features. The RMSECV was used to determine the optimal number of latent variables while avoiding overfitting of results, as illustrated for METHOTREXATE MYLAN® in Figure 10A. The regression plot from the samples of the test set constructed with 5 LVs delivers an R^2 value of 0.9966 and RMSEP of 0.3492 $g{\cdot}L^{-1}$ (Figure 10B). The regression coefficient presented in Figure 10C exhibits features related to METHOTREXATE MYLAN® at 1589 cm^{-1}, 1558 cm^{-1}, 1511 cm^{-1}, 1451 cm^{-1}, 1394 cm^{-1}, 1338 cm^{-1}, 1292 cm^{-1}, 1247 cm^{-1}, 1208 cm^{-1}, 1139 cm^{-1}, 825 cm^{-1} and 760 cm^{-1} consistent with those identified as characteristic in Figure 3Ac. The regression coefficient also exhibits features from the glucose that are negative, indicating they are anti-correlated with METHOTREXATE MYLAN® concentrations.

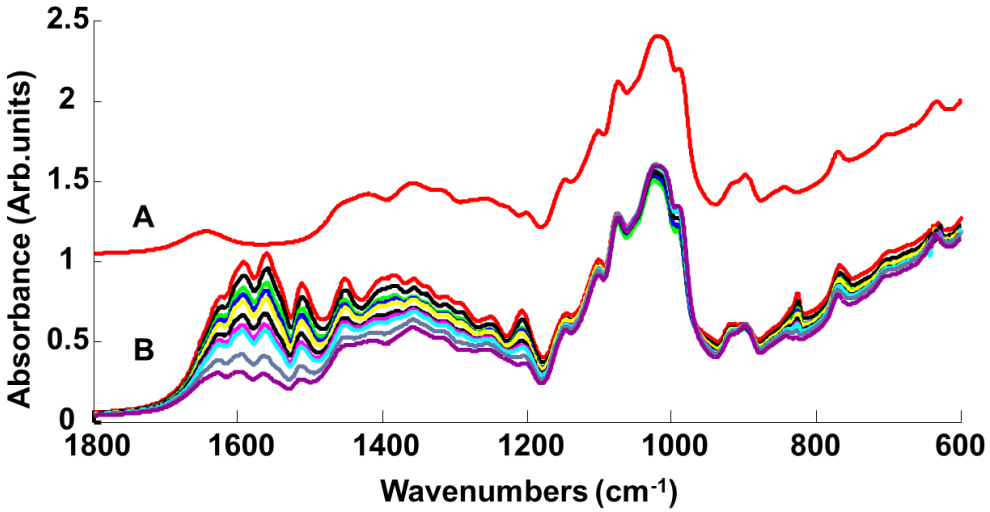


Figure 9: mean ATR-FTIR spectra of fingerprint regions of: A) 5% glucose and B) methotrexate in 5% glucose solution following serial dilution. METHOTREXATE MYLAN® spectra are organised as decreasing concentrations from the top to bottom, respectively corresponding to methotrexate concentrations of 21 $g{\cdot}L^{-1}$ (red), 19 $g{\cdot}L^{-1}$ (black), 17 $g{\cdot}L^{-1}$ (green), 15 $g{\cdot}L^{-1}$ (blue), 13 $g{\cdot}L^{-1}$ (yellow), 11 $g{\cdot}L^{-1}$ (black), 9 $g{\cdot}L^{-1}$ (magenta), 7 $g{\cdot}L^{-1}$ (cyan), 5 $g{\cdot}L^{-1}$ (grey) and 3 $g{\cdot}L^{-1}$ (purple). 5% glucose spectrum is offset for clarity.

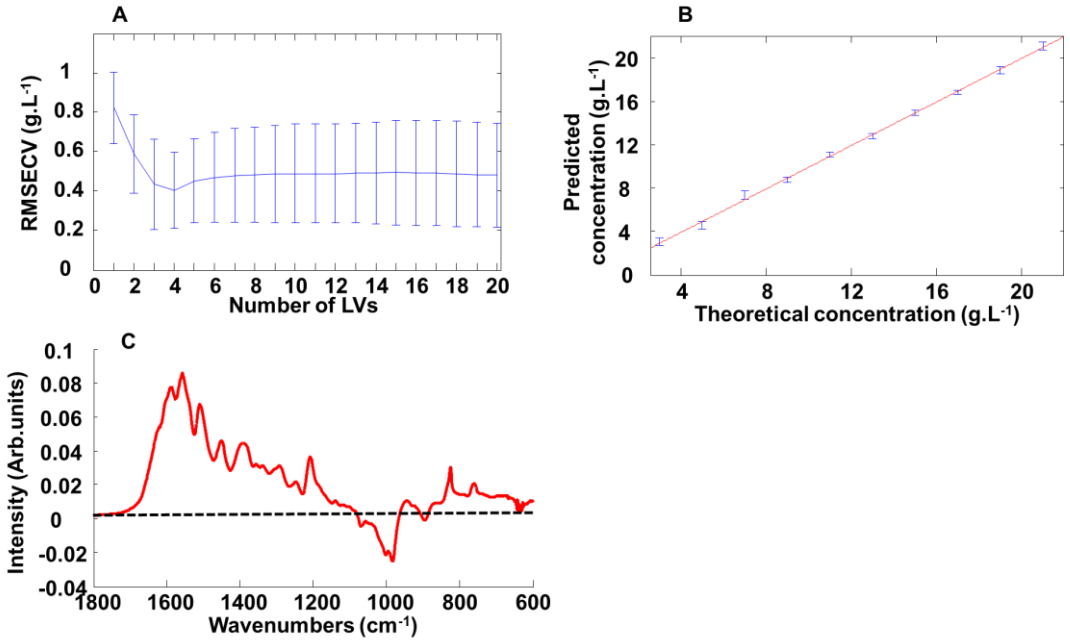


Figure 10: PLSR analysis performed on METHOTREXATE MYLAN® in 5% glucose solution tested by ATR-FTIR. A) RMSECV, B) Regression fitting for the test set obtained with 5 LVs and C) regression coefficient.

Table 5 summarises the PLSR results obtained for the four commercial drugs. Although the R^2 values are comparable to those observed with Raman analysis, the RMSEP are generally higher for ATR-FTIR, ranging from 0.018 $g{\cdot}L^{-1}$ and 0.8252 $g{\cdot}L^{-1}$. Comparing the RMSEP to the median concentration of the range analysed for CERUBIDINE® in 0.9% NaCl (the lowest), represents value of 1.2% is obtained, while for METHOTREXATE MYLAN® in 0.9% NaCl (the highest) it increases to 6.9%. As a reminder, for Raman analysis, the highest value, for HALOXAN® in 5% glucose was found to be 1.8% of the median concentration (Table 4). Undoubtedly, the precision of analysis performed with ATR-FTIR is lower than that of Raman spectroscopy, most probably explained by the extra processing step of sample drying. It has been demonstrated that the linear, Lambert-Beer like relationship between measured absorbance and solution concentration is not well preserved in ATR-FTIR measurements of dried precipitates (57), and other effects such as spot size difference, variation in drop centring on the reduced diamond crystal surface and drying behaviour between drops could also contribute to the larger error of the ATR-FTIR analysis. Nevertheless, ATR-FTIR coupled to PLSR displays exhibits excellent performance for quantitative analysis, within the accepted clinical tolerance. Although glucose is a particularly strong absorber in the infrared, within the

respective relevant ranges of each drugs, specific features can be extracted and used for reliable regression models.

Table 5. PLSR results obtained from the 4 chemotherapeutic drugs solutions tested in 2 matrices by ATR-FTIR

Drug	Matrix	R^2	RMSEP	%RMSEP	LVs
TEVA®	0.9%NaCl	0.9983	0.0180	2.3	4
	5% glucose	0.9884	0.0489	6.3	6
CERUBIDINE®	0.9%NaCl	0.9964	0.0183	1.2	5
	5% glucose	0.9959	0.0184	1.2	6
HOLOXAN®	0.9%NaCl	0.9968	0.2829	2.9	6
	5% glucose	0.9953	0.3491	3.5	5
MYLAN®	0.9%NaCl	0.9811	0.8252	6.9	3
	5% glucose	0.9966	0.3492	2.9	5

4. Discussion

Analytical quality control is used to validate the conformity of chemotherapeutic solutions before release to a patient's bedside for injection represents a substantial economic burden as well as daily workload for hospitals. While sophisticated techniques such as liquid chromatography coupled to mass spectrometry could be deployed to ensure the safety of patients, time constraints and cost of analysis are limiting factors. Rapid, cost effective techniques with minimal sample preparation could contribute to speeding up the workflow. Vibrational spectroscopy enables direct molecular fingerprinting of samples to deliver quantification and discrimination of the chemotherapeutic solutions studied.

The first observation is that both Raman and ATR-FTIR are both affected by the type of matrix used, either NaCl 0.9% or 5% glucose. Glucose presents a number of specific features found in Raman and infrared spectra collected from chemotherapeutic solutions (Figure 6 and 9). However, it is observed that the glucose contribution is greater in infrared spectra, exhibiting more intense bands compared to the commercialised drugs solutions (see Figure 9b for MYALN®). This observation was consistent for the four solutions (data not shown). The relative contribution of glucose will differ depending on the strength of the spectral response collected from chemotherapeutic drugs. While, for Raman spectroscopy, molecules with conjugated rings are well known to be strong scatters, delivering intense Raman peaks covering

the glucose features (see example of METHOTREXATE MYLAN® for methotrexate, Figure 6), other chemical structures such as ifosfamide found in HOLOXAN® are considerably less Raman active. The Raman features from the chemotherapeutic solution are weaker (Figure 8), although the range of concentrations is close to that of METHOTREXATE MYLAN®, and consequently the glucose bands appear more prominent. The second observation is that, in both Raman and infrared, the samples are analysed as complex solutions with possible spectral contribution from all ingredients (i.e. excipients). For CERUBIDINE®, mannitol is present in the formulation at a concentration 5 times higher than daunorubicin itself. Similar, to glucose, mannitol is not a strong Raman scatterer and, as a result, its spectral features are not observed prominently in the Raman spectra of the chemotherapeutic solution (Figure 2Ab). However, sugars display strong absorbance in the IR, and, as a result, the spectra are dominated by mannitol features (Figure 3Ba).

Overall, both techniques enable quantitative and discriminative analysis. Glucose having a low contribution in spectra, it is not surprising to achieve 100% discrimination between the four chemotherapeutic solutions, although it is interesting to note that, for IR, the specificity of the analysis is preserved thanks to bands assigned to the drugs and/or excipients.

In terms of quantitative analysis, Raman is found to be slightly more accurate than IR, based on the values of RMSEP (Table 4 and Table 5). For DOXORUBICINE TEVA® in 5% glucose and METHOTREXATE MYLAN® in 0.9% NaCl, the RMSEP obtained was more than 5% of the median concentration of the range analysed by IR spectroscopy, while for Raman the highest was 1.8%.

The observations of the study lead directly to a discussion about the adaptivity of vibrational techniques. Raman microspectroscopy has benefitted from significant technological evolutions in recent decades (58–61). The systems are confocal thus potentially enabling analysis through packaging (62), and, notably, Spatially Offset Raman Spectroscopy is now being introduced in airport security screening to analyse suspicious items without opening containers (https://www.agilent.com/en/technology/spatially-offset-raman-spectroscopy). This is relevant for the safety of staff members performing AQC, as the ability to analyse the prescription without the requirement of extracting it from the infusion bag could reduce exposure to toxic compounds. Although early studies have investigated such applications of confocal Raman spectroscopy with inverted microscope setups or transportable devices (12,15), in recent years, few documented studies have supported the translation into clinics of non-invasive analysis. Considering the strength of spectral features and the concentrations used in treatments, it could be expected that exploitable data could be collected directly through plastic layers, although

extended investigations are required to confirm the accuracy and specificity. Secondly, manufacturers have devoted considerable efforts towards miniaturisation of the Raman spectroscopic systems, ranging from transportable (benchtop) apparatus equipped with deported probes to handheld systems. Recently Lee *et al.*, have reported demonstration of analytical performance of handheld systems to control anthracyclines (21) and taxanes (22). However, the experimental design used solutions contained in glass vials during the analysis, and therefore the results hardly demonstrate the feasibility to work directly in plastic bags. The exact analytical performance of non-invasive Raman has therefore yet to be established and validated.

In comparison, the main handicap for infrared spectroscopy in this context is the strong absorption of water. Although protocols for analysis of, for example protein secondary structure in the native aqueous environment have been described (63), optically thin cells, (of order <10 μm), with IR transparent windows are required, and relatively high concentration solutions (>3 mg/mL) are recommended, rendering the technique not so conducive to routine clinical analysis. The requirement for drying of samples prior to analysis ultimately means a fraction of the sample needs to be taken from the bags, although volumes as low as 2 μL suffice, reducing considerably the risk of exposure for personnel. Although Fourier transform infrared instruments are highly robust and reliable in terms of alignment and calibration, requiring minimal maintenance, the technique mainly suffers from the lack of dedicated design for clinical transfer. Nevertheless, recent advancements in the field of ATR-FTIR spectroscopy could help to strengthen the potential of and interest in the technique. For instance, high throughput ATR plates reader (Pike technologies) have been developed to increase the workflow, but also to enable preparation of samples remote from the system. This is of great interest for example to perform sample deposition inside a fume hood and then manipulation of dry samples with reduced hazard. Moreover, a new generation of 3D printed disposable ATR substrates have been developed for single use (64), which could be also adapted for toxic samples. Commercialised by ClinSpec Dx (https://www.clinspecdx.com/), such innovations in the concept of ATR-FTIR spectroscopy could strengthen its position for applications in AQC of chemotherapeutic solutions in clinical settings. Moreover, the brighter light sources of quantum cascade lasers (QCL) could provide increased sensitivity for the emerging alternative of QCL- IR spectroscopy (65). In the near future, infrared spectroscopy could therefore potentially compete with Raman for liquid samples analysis.

5. Conclusion

Analytical quality control of intravenous chemotherapeutic solutions is a critical checkpoint in the process of patient treatment. While chromatography-based gold standards are well established, there is a need to evolve towards rapid and cost-effective methods. Raman and infrared spectroscopy provide label free molecular characterisation of samples in spectral signatures encompassing both quantitative and qualitative information. Despite the contribution from the matrix used to prepare the solutions (either NaCl 0.9% or glucose 5%) or excipients found in the commercial formulas, both techniques deliver accurate identification of the active, and quantification of its concentration. While ultimately Raman spectroscopy could be applied non-invasively, directly into infusion bags, infrared spectroscopy remains a robust and reliable analytical tool for pharmaceuticals characterisation, including chemotherapeutic solutions. Optimisation of methods could lead to user friendly tools supporting fast implantation in the hospital routine.

Acknowledgement

We acknowledge ministry of higher education in Sudan and Campus France for financial support and administrative arrangement of Alaa A. Makki's PhD in cotutelle between the university of Gezira and university of Tours.

References:

1. Nussbaumer S, Bonnabry P, Veuthey JL, Fleury-Souverain S. Analysis of anticancer drugs: A review. Talanta. 2011;85(5):2265–89.
2. Aga QAAK, Bataineh YA, Sbaih HM. Therapeutic drug monitoring of cytotoxic drugs. Int J Drug Deliv Technol [Internet]. 2020;10(2):284–91. Available from: http://ovidsp.ovid.com/ovidweb.cgi?T=JS%7B&%7DPAGE=reference%7B&%7DD=emed5%7B&%7DNEWS=N%7B&%7DAN=2001313284
3. Nardella F, Beck M, Collart-Dutilleul P, Becker G, Boulanger C, Perello L, et al. A UV-Raman spectrometry method for quality control of anticancer preparations: Results after 18 months of implementation in hospital pharmacy. Int J Pharm [Internet]. 2016;499(1–2):343–50. Available from: http://dx.doi.org/10.1016/j.ijpharm.2016.01.002
4. Delmas A, Gordien JB, Bernadou JM, Roudaut M, Gresser A, Malki L, et al. Quantitative and qualitative control of cytotoxic preparations by HPLC-UV in a centralized parenteral preparations unit. J Pharm Biomed Anal. 2009;49(5):1213–20.
5. Castagne V, Habert H, Abbara C, Rudant E, Bonhomme-Faivre L. Cytotoxics

compounded sterile preparation control by HPLC during a 16-month assessment in a French university hospital: Importance of the mixing bags step. J Oncol Pharm Pract. 2011;17(3):191–6.

6. Bondarenko P V., Second TP, Zabrouskov V, Makarov AA, Zhang Z. Mass Measurement and Top-Down HPLC/MS Analysis of Intact Monoclonal Antibodies on a Hybrid Linear Quadrupole Ion Trap-Orbitrap Mass Spectrometer. J Am Soc Mass Spectrom. 2009;20(8):1415–24.
7. Prideaux B, Stoeckli M. Mass spectrometry imaging for drug distribution studies. J Proteomics [Internet]. 2012;75(16):4999–5013. Available from: http://dx.doi.org/10.1016/j.jprot.2012.07.028
8. Osawa T, Naito T, Suzuki N, Imai K, Nakanishi K, Kawakami J. Validated method using liquid chromatography-electrospray ionization tandem mass spectrometry for the determination of contamination of the exterior surface of vials containing platinum anticancer drugs. Talanta. 2011;85(3):1614–20.
9. Kort A, Hillebrand MJX, Cirkel GA, Voest EE, Schinkel AH, Rosing H, et al. Quantification of cabazitaxel, its metabolite docetaxel and the determination of the demethylated metabolites RPR112698 and RPR123142 as docetaxel equivalents in human plasma by liquid chromatography-tandem mass spectrometry. J Chromatogr B Anal Technol Biomed Life Sci [Internet]. 2013;925:117–23. Available from: http://dx.doi.org/10.1016/j.jchromb.2013.02.034
10. Balan V, Mihai CT, Cojocaru FD, Uritu CM, Dodi G, Botezat D, et al. Vibrational spectroscopy fingerprinting in medicine: From molecular to clinical practice. Materials (Basel). 2019;12(18):1–40.
11. Pudlas M, Koch S, Bolwien C, Walles H. Raman spectroscopy as a tool for quality and sterility analysis for tissue engineering applications like cartilage transplants. Int J Artif Organs. 2010;33(4):228–37.
12. Amin A, Bourget P, Vidal F, Ader F. Routine application of Raman spectroscopy in the quality control of hospital compounded ganciclovir. Int J Pharm [Internet]. 2014;474(1–2):193–201. Available from: http://dx.doi.org/10.1016/j.ijpharm.2014.08.028
13. Bourget P, Amin A, Vidal F, Merlette C, Troude P, Baillet-Guffroy A. The contribution of Raman spectroscopy to the analytical quality control of cytotoxic drugs in a hospital environment: Eliminating the exposure risks for staff members and their work environment. Int J Pharm [Internet]. 2014;470(1–2):70–6. Available from:

http://dx.doi.org/10.1016/j.ijpharm.2014.04.064

14. Bourget P, Amin A, Vidal F, Merlette C, Lagarce F. Comparison of Raman spectroscopy vs. high performance liquid chromatography for quality control of complex therapeutic objects: Model of elastomeric portable pumps filled with a fluorouracil solution. J Pharm Biomed Anal [Internet]. 2014;91:176–84. Available from: http://dx.doi.org/10.1016/j.jpba.2013.12.030
15. Lê L, Berge M, Tfayli A, Baillet Guffroy A, Prognon P, Dowek A, et al. Quantification of gemcitabine intravenous drugs by direct measurement in chemotherapy plastic bags using a handheld Raman spectrometer. Talanta. 2019;196:376–80.
16. Solís-Gómez A, Sato-Berrú RY, Mata-Zamora ME, Saniger JM, Guirado-López RA. Characterizing the properties of anticancer silibinin and silybin B complexes with UV–Vis, FT-IR, and Raman spectroscopies: A combined experimental and theoretical study. J Mol Struct. 2019;1182:109–18.
17. Bazin C, Cassard B, Caudron E, Prognon P, Havard L. Comparative analysis of methods for real-time analytical control of chemotherapies preparations. Int J Pharm [Internet]. 2015;494(1):329–36. Available from: http://dx.doi.org/10.1016/j.ijpharm.2015.08.041
18. Bazin C, Vieillard V, Astier A, Paul M. Implementation of real-time identification analysis and quantification of chemotherapies preparations with a Multispec® analyser. Ann Pharm Fr [Internet]. 2014;72(1):33–40. Available from: http://dx.doi.org/10.1016/j.pharma.2013.09.006
19. Bellisola G, Sorio C. Infrared spectroscopy and microscopy in cancer research and diagnosis. Am J Cancer Res. 2012;2(1):1–21.
20. Dziopa F, Galy G, Bauler S, Vincent B, Crochon S, Tall ML, et al. A quantitative and qualitative method to control chemotherapeutic preparations by Fourier transform infrared-ultraviolet spectrophotometry. J Oncol Pharm Pract. 2013;19(2):121–9.
21. Lê LMM, Tfayli A, Zhou J, Prognon P, Baillet-Guffroy A, Caudron E. Discrimination and quantification of two isomeric antineoplastic drugs by rapid and non-invasive analytical control using a handheld Raman spectrometer. Talanta. 2016;161:320–4.
22. Lê L, Berge M, Tfayli A, Prognon P, Caudron E. Discriminative and Quantitative Analysis of Antineoplastic Taxane Drugs Using a Handheld Raman Spectrometer. Biomed Res Int. 2018;2018:12–5.
23. Lê LMM, Berge M, Tfayli A, Zhou J, Prognon P, Baillet-Guffroy A, et al. Rapid discrimination and quantification analysis of five antineoplastic drugs in aqueous

solutions using Raman spectroscopy. Eur J Pharm Sci [Internet]. 2018;111:158–66. Available from: http://dx.doi.org/10.1016/j.ejps.2017.09.046

24. Makki AA, Bonnier F, Respaud R, Chtara F, Tfayli A, Tauber C, et al. Qualitative and quantitative analysis of therapeutic solutions using Raman and infrared spectroscopy. Spectrochim Acta - Part A Mol Biomol Spectrosc. 2019;218:97–108.
25. Bourget P, Amin A, Vidal F, Merlette C, Lagarce F. Comparison of Raman spectroscopy vs. high performance liquid chromatography for quality control of complex therapeutic objects: Model of elastomeric portable pumps filled with a fluorouracil solution. J Pharm Biomed Anal. 2014;91:176–84.
26. Lê LMM, Caudron E, Baillet-Guffroy A, Eveleigh L. Non-invasive quantification of 5 fluorouracil and gemcitabine in aqueous matrix by direct measurement through glass vials using near-infrared spectroscopy. Talanta [Internet]. 2014;119:361–6. Available from: http://dx.doi.org/10.1016/j.talanta.2013.10.060
27. Szuławska A, Czyz M. Molekularne mechanizmy działania antracyklin. Postepy Hig Med Dosw. 2006;60:78–100.
28. Wall R, McMahon G, Crown J, Clynes M, O'Connor R. Rapid and sensitive liquid chromatography-tandem mass spectrometry for the quantitation of epirubicin and identification of metabolites in biological samples. Talanta. 2007;72(1):145–54.
29. Barker IK, Crawford SM, Fell AF. Determination of plasma concentrations of epirubicin and its metabolites by high-performance liquid chromatography during a 96-h infusion in cancer chemotherapy. J Chromatogr B Biomed Appl. 1996;681(2):323–9.
30. Lachâtre F, Marquet P, Ragot S, Gaulier JM, Cardot P, Dupuy JL. Simultaneous determination of four anthracyclines and three metabolites in human serum by liquid chromatography-electrospray mass spectrometry. J Chromatogr B Biomed Sci Appl. 2000;738(2):281–91.
31. Česen M, Kosjek T, Busetti F, Kompare B, Heath E. Human metabolites and transformation products of cyclophosphamide and ifosfamide: analysis, occurrence and formation during abiotic treatments. Environ Sci Pollut Res. 2016;23(11):11209–23.
32. Whelan J, Khan A, Sharma A, Rothermundt C, Dileo P, Michelagnoli M, et al. Interval compressed vincristine, doxorubicin, cyclophosphamide alternating with ifosfamide, etoposide in patients with advanced Ewing's and other Small Round Cell Sarcomas. Clin Sarcoma Res [Internet]. 2012;2(1):12. Available from: http://www.ncbi.nlm.nih.gov/pubmed/22998944
33. Hagner N, Joerger M. Cancer chemotherapy: Targeting folic acid synthesis. Cancer

Manag Res [Internet]. 2010;2(1):293–301. Available from: www.dovepress.com
34. Guardiola E, Peyrade F, Chaigneau L, Cupissol D, Tchiknavorian X, Bompas E, et al. Results of a randomised phase II study comparing docetaxel with methotrexate in patients with recurrent head and neck cancer. Eur J Cancer. 2004;40(14):2071–6.
35. Society MM. , m.d., p. 1995;332(14):1–6.
36. Kantarjian H, Thomas D, O'Brien S, Cortes J, Giles F, Jeha S, et al. Long-term follow-up results of hyperfractionated cyclophosphamide, vincristine, doxorubicin, and dexamethasone (Hyper-CVAD), a dose-intensive regimen, in adult acute lymphocytic leukemia. Cancer. 2004;101(12):2788–801.
37. Ferreri AJM, Reni M, Dell'Oro S, Ciceri F, Bernardi M, Camba L, et al. Combined treatment with high-dose methotrexate, vincristine and procarbazine, without intrathecal chemotherapy, followed by consolidation radiotherapy for primary central nervous system lymphoma in immunocompetent patients. Oncology. 2001;60(2):134–40.
38. Santos Panero P dos, Santos Panero F dos, Santos Panero J dos, Bezerra da Silva HE. Application of Extended Multiplicative Signal Correction to Short-Wavelength near Infrared Spectra of Moisture in Marzipan. J Data Anal Inf Process. 2013;01(03):30–4.
39. Li Q, Gao Q, Zhang G. Improved extended multiplicative scatter correction algorithm applied in blood glucose noninvasive measurement with FT-IR spectroscopy. J Spectrosc. 2013;1(1).
40. Parachalil DR, Bruno C, Bonnier F, Blasco H, Chourpa I, McIntyre J, et al. Raman spectroscopic screening of high and low molecular weight fractions of human serum. Analyst. 2019;144(14):4295–311.
41. Schulze HG, Rangan S, Piret JM, Blades MW, Turner RFB. Developing Fully Automated Quality Control Methods for Preprocessing Raman Spectra of Biomedical and Biological Samples. Appl Spectrosc. 2018;72(9):1322–40.
42. Leger MN, Ryder AG. Comparison of derivative preprocessing and automated polynomial baseline correction method for classification and quantification of narcotics in solid mixtures. Appl Spectrosc. 2006;60(2):182–93.
43. Liland KH, Almøy T, Mevik BH. Optimal choice of baseline correction for multivariate calibration of spectra. Appl Spectrosc. 2010;64(9):1007–16.
44. Vergote GJ, Vervaet C, Remon JP, Haemers T, Verpoort F. Near-infrared FT-Raman spectroscopy as a rapid analytical tool for the determination of diltiazem hydrochloride in tablets. Eur J Pharm Sci. 2002;16(1–2):63–7.

45. Afseth NK, Kohler A. Extended multiplicative signal correction in vibrational spectroscopy, a tutorial. Chemom Intell Lab Syst [Internet]. 2012;117:92–9. Available from: http://dx.doi.org/10.1016/j.chemolab.2012.03.004
46. Chevallier S, Bertrand D, Kohler A, Courcoux P. Application of PLS-DA in multivariate image analysis. J Chemom. 2006;20(5):221–9.
47. Bonnier F, Byrne HJ. Understanding the molecular information contained in principal component analysis of vibrational spectra of biological systems. Analyst. 2012;137(2):322–32.
48. Lee LC, Liong CY, Jemain AA. Partial least squares-discriminant analysis (PLS-DA) for classification of high-dimensional (HD) data: A review of contemporary practice strategies and knowledge gaps. Analyst. 2018;143(15):3526–39.
49. Szafraniec E, Majzner K, Farhane Z, Byrne HJ, Lukawska M, Oszczapowicz I, et al. Spectroscopic studies of anthracyclines: Structural characterization and in vitro tracking. Spectrochim Acta - Part A Mol Biomol Spectrosc [Internet]. 2016;169:152–60. Available from: http://dx.doi.org/10.1016/j.saa.2016.06.035
50. Sottani C, Tranfo G, Bettinelli M, Faranda P, Spagnoli M, Minoia C. Trace determination of anthracyclines in urine: A new high-performance liquid chromatography/tandem mass spectrometry method for assessing exposure of hospital personnel. Rapid Commun Mass Spectrom. 2004;18(20):2426–36.
51. Ricciarello R, Pichini S, Pacifici R, Altieri I, Pellegrini M, Fattorossi A, et al. Simultaneous determination of epirubicin, doxorubicin and their principal metabolites in human plasma by high-performance liquid chromatography and electrochemical detection. J Chromatogr B Biomed Appl. 1998;707(1–2):219–25.
52. Martins I, Souza JO, Sanson AL, Vieira EP, Giusti-Paiva A. Simultaneous determination of cyclophosphamide and ifosfamide in plasma using SPEHPLC-UV method. Lat Am J Pharm. 2009;28(1):41–6.
53. Lê LMM, Berge M, Tfayli A, Zhou J, Prognon P, Baillet-Guffroy A, et al. Rapid discrimination and quantification analysis of five antineoplastic drugs in aqueous solutions using Raman spectroscopy. Eur J Pharm Sci. 2018;111:158–66.
54. Badawi HM, Förner W. DFT and MP2 study of the molecular structure and vibrational spectra of the anticancer agent cyclophosphamide. Zeitschrift fur Naturforsch - Sect B J Chem Sci. 2012;67(12):1305–13.
55. Ayyappan S, Sundaraganesan N, Aroulmoji V, Murano E, Sebastian S. Molecular structure, vibrational spectra and DFT molecular orbital calculations (TD-DFT and

NMR) of the antiproliferative drug Methotrexate. Spectrochim Acta - Part A Mol Biomol Spectrosc. 2010;77(1):264–75.

56. Mourant JR, Johnson TM, Los G, Bigio IJ. Non-invasive measurement of chemotherapy drug concentrations in tissue: Preliminary demonstrations of in vivo measurements. Phys Med Biol. 1999;44(5):1397–417.
57. Bonnier F, Brachet G, Duong R, Sojinrin T, Respaud R, Aubrey N, et al. Screening the low molecular weight fraction of human serum using ATR-IR spectroscopy. J Biophotonics. 2016;9(10):1085–97.
58. Matousek P. Deep non-invasive Raman spectroscopy of living tissue and powders. Chem Soc Rev. 2007;36(8):1292–304.
59. Movasaghi Z, Rehman S, Rehman IU. Raman spectroscopy of biological tissues. Appl Spectrosc Rev. 2007;42(5):493–541.
60. Paudel A, Raijada D, Rantanen J. Raman spectroscopy in pharmaceutical product design. Adv Drug Deliv Rev [Internet]. 2015;89:3–20. Available from: http://dx.doi.org/10.1016/j.addr.2015.04.003
61. Ellis DI, Cowcher DP, Ashton L, O'Hagan S, Goodacre R. Illuminating disease and enlightening biomedicine: Raman spectroscopy as a diagnostic tool. Analyst. 2013;138(14):3871–84.
62. Eliasson C, Matousek P. Noninvasive authentication of pharmaceutical products through packaging using spatially offset Raman spectroscopy. Anal Chem. 2007;79(4):1696–701.
63. Yang H, Yang S, Kong J, Dong A, Yu S. Obtaining information about protein secondary structures in aqueous solution using Fourier transform IR spectroscopy. Nat Protoc. 2015;10(3):382–96.
64. Butler HJ, Brennan PM, Cameron JM, Finlayson D, Hegarty MG, Jenkinson MD, et al. Development of high-throughput ATR-FTIR technology for rapid triage of brain cancer. Nat Commun [Internet]. 2019;10(1):1–9. Available from: http://dx.doi.org/10.1038/s41467-019-12527-5
65. Sala A, Spalding KE, Ashton KM, Board R, Butler HJ, Dawson TP, et al. Rapid analysis of disease state in liquid human serum combining infrared spectroscopy and "digital drying." J Biophotonics. 2020;13(9):1–10.

3.2 Discussion and perspectives

The first study has demonstrated the strength of IR and Raman for discriminant and quantitative analysis of chemotherapeutic molecules in water. Although Raman has delivered good quantification results of solutions and small lower limit of detection (LOD), the discrimination results have been obtained with low sensitivity and specificity. Formulations used in this study contains HCl, NaOH (TEVA® and MYLAN®) and mannitol (CERUBIDINE®). Very weak bands for mannitol are observed in Raman despite its high concentration compared to daunorubicin. Other excipients have no signature but might have added effect on the background thereby collectively can affect the discrimination obtained. Quantification by ATR-FTIR delivered larger LOD than that obtained by Raman, but the discrimination has been obtained with high sensitivity and specificity. ATR-FTIR is highly sensitive for excipients presents in formulation as well as the minor structural difference between the tested isomers. Discrimination has been mainly obtained due to spectral contribution of the drugs themselves plus some features observed for mannitol.

The promising results obtained in the first study has given motivation to go further and investigate the spectral effect of matrices used for dilution of chemotherapeutic formulations.

In the second study, 4 drug molecules of different chemical structure (not isomers) were studied. The strength of IR and Raman spectroscopy for identification and quantification of chemotherapeutic drugs in their solubilisation matrices and excipients has been evaluated. No effect in drug signature has been observed when 0.9% NaCl matrix is used as this molecule didn't had characteristic Raman or IR features while contribution of 5% glucose solutions in Raman and IR has been observed. In Raman analysis, glucose exhibits few weak bands at the range 1000 - 1200 cm^{-1} that didn't affected the drugs signature while in IR it has very strong features which dominate the spectra due to air drying before analysis. However, the IR spectra results from both glucose contribution in the spectral range and weaker bands from the drugs. Ultimately, discrimination and quantification have been obtained with high specificity to the drug features.

During the PhD the 2 notions of analysing isomeric drugs and working in injectable matrices were treated separately in a step by step approach. However, it would indeed of interest to further explore the limit of specificity of VS for current analytical challenges encountered in centralised units during AQC. Discrimination of isomeric drugs such as doxorubicin (DOX), epirubicin (EPI) and daunorubicin (DAU) in 5% glucose by IR could be difficult due the domination of IR spectra by very strong glucose features, as can be seen in Figure 27 that have

been recorded for the highest concentration of clinical range. Very weak bands can be observed for the 3 molecules approximately at 1073 cm^{-1}, 988 cm^{-1}, 896 cm^{-1}, 788 cm^{-1} and 769 cm^{-1}, also very weak bands can be observed for DAU at 1713 cm^{-1}, 1619 cm^{-1} and 1579 cm^{-1}. The very few weak bands observed compared to the strong signature of glucose in IR can make discrimination between those isomers difficult.

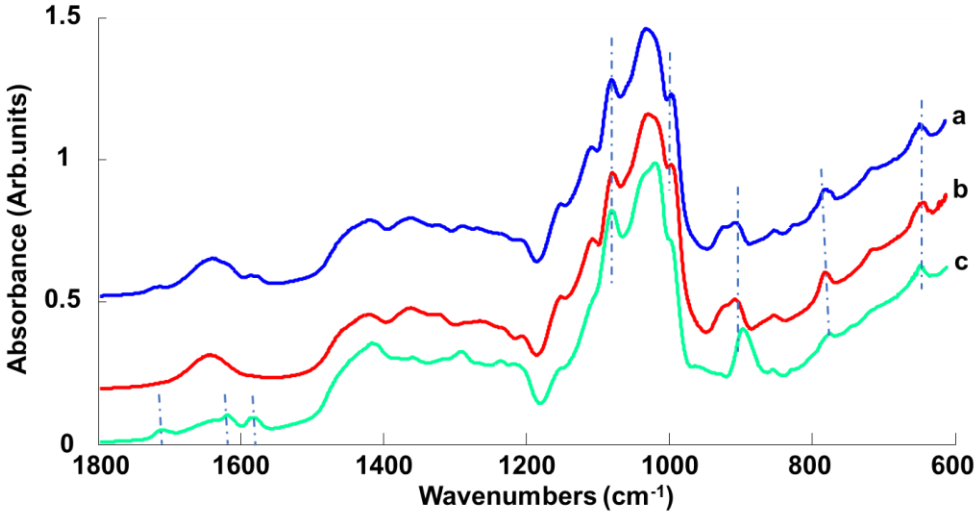


Figure 27. Mean ATR-FTIR spectra of: a) DOX (1.2 $g{\cdot}L^{-1}$), b) EPI (0.65 $g{\cdot}L^{-1}$) and c) DAU (2 $g{\cdot}L^{-1}$) in 5% glucose. Spectra are offset for clarity.

Raman spectra obtained for DOX, EPI and DAU at the highest concentration (Figure 28) used clinically have shown no characteristic spectral differences between them can be observed, also glucose contribution was very weak near 1170 cm^{-1} and 1129 cm^{-1} and not affected the specific spectral region for those molecules.

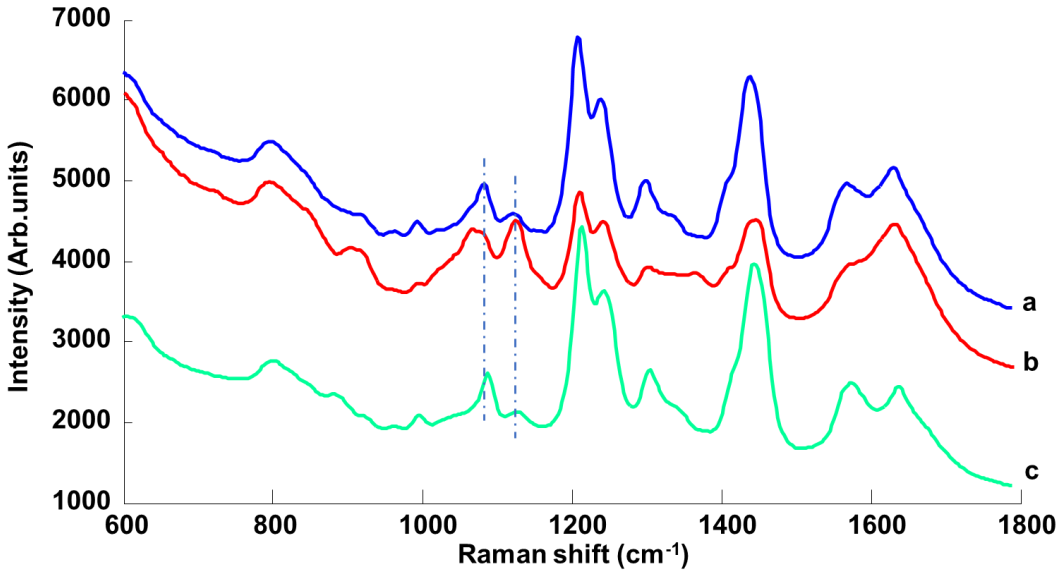


Figure 28. Mean Raman spectra of: a) DOX (1.2 $g \cdot L^{-1}$), b) EPI (0.65 $g \cdot L^{-1}$) and c) DAU (2 $g \cdot L^{-1}$) in 5% glucose. Spectra are offset for clarity.

Cyclophosphamide (CYA) and Ifosfamide (IFA) are another type of positional isomers that differ only in the attachment of the side chain (chloroethyl group) either to exocyclic group in CYA or endocyclic nitrogen atom in IFA structures. Raman response is not always strong for all molecules, it depends on the chemical structure. CYA and IFA have weak Raman spectra (Figure 29), but they display higher spectral similarities characteristic bands can be seen at approximately 667 cm^{-1}, 761 cm^{-1}, 1371 cm^{-1} and 1448 cm^{-1} which can make their discrimination somehow difficult.

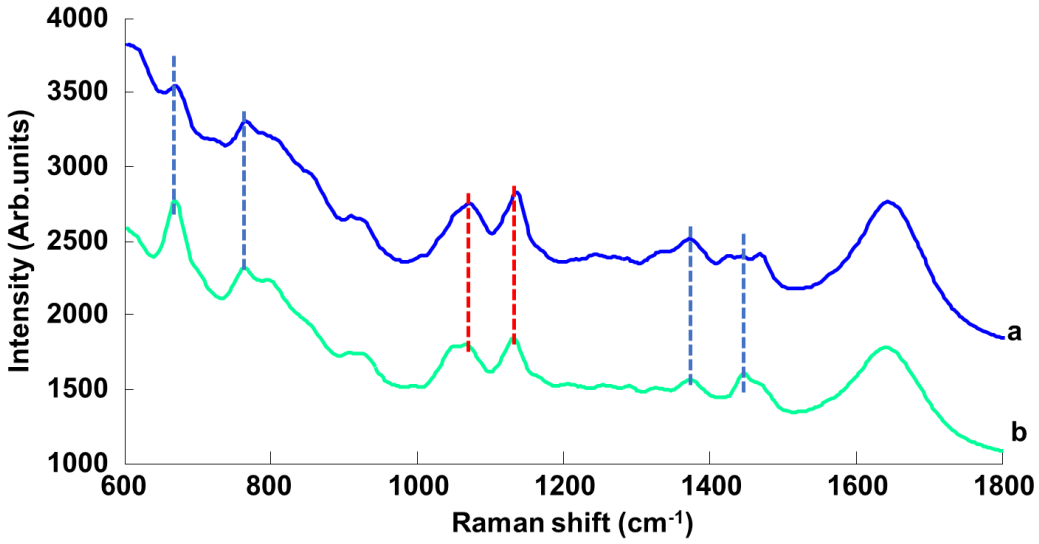


Figure 29. Mean Raman spectra of: a) CYA (7.75 $g \cdot L^{-1}$) and b) IFA (17.75 $g \cdot L^{-1}$) in 5% glucose solution. Spectra are offset for clarity.

The obtained preliminary spectral results from those isomers need to be further studied and investigated in term of their discrimination for AQC purpose. Some of the currently used chemotherapeutic drugs belong to the same family and hence can have higher structural similarities such as taxanes, vinca alkaloids and platins anticancer drugs which need to be studied in the future work by VS. In literature few studies have been conducted for discrimination between isomeric drugs by Raman spectroscopy but not all information of the spectral differences have been stated [78,79].

4. UNDERSTANDING THE DISCRIMINATION AND QUANTIFICATION OF MONOCLONAL ANTIBODIES PREPARATIONS USING VIBRATIONAL SPECTROSCOPY

4.1 Context and motivation:

The massive progress in research and development has been oriented toward production of biopharmaceutical therapeutic agents such as monoclonal antibodies (mAbs) for clinical uses. They are used since the 90s for treatment of cancer, inflammatory diseases, infectious diseases and cardiovascular diseases [123]. In cancer therapy, they attracted great interest due to their specificity of targeting antigens and high efficacy. They act via immune-mediated cell killing mechanism [71]. The great challenge in AQC of mAbs is to find specific and comprehensive method for their characterisation since mAbs are subjected to different conditions during the long bio-production process, i.e. pH, temperature, glycosylation process and shear stress, all these conditions can result in micro-heterogenicities between mAbs. Separation techniques using liquid chromatography and capillary zone electrophoresis (CZE) as well as mass spectrometry (MS) have been increasingly used for characterisation of mAbs and assessment of their homogeneity by providing information about amino acid sequences and degradation products resulting from the different steps of production [124]. Although those techniques are considered as standard tools for analysis of mAbs; AQC in centralised units requires simple and fast methods. VS is commonly used to investigate modification of the structure of mAbs under different stress and aggregation conditions [125,126]. In contrary, ATR-FTIR has delivered good information on studying mAbs aggregates at different conditions (pH, heating and agitation) from air dried drops [125].

Raman analysis of small chemotherapeutic molecules solutions has shown promising results, in that the spectral signature of chemotherapeutic molecule has overcome the weak water contribution and thereby, the fingerprint region is representative of the drug features [127]. In the literature, the weak Raman response of mAbs (humanised mAbs and murine types) has however been documented [128]. To date, there is only one study published by Lê et al. about AQC of mAbs using Raman spectroscopy coupled to complex chemometric prediction methods (machine learning approach) [71]. Using selected mAbs molecules (infliximab, bevacizumab,

rituximab and ramucirumab), it is demonstrated that discrimination and quantification can be achieved. However, in their study no data is provided to appreciate the quality of Raman spectra collected from mAbs therapeutic solutions but also to clarify the spectral origin for the discrimination between the 4 antibodies. mAbs have limited differences in their amino acids sequence according to the origin of their production which is either humanised or chimeric, therefore their classification can be expected to be difficult solely based on minor variations in protein composition and/or conformation.

In this chapter Raman and IR spectroscopy have been used for discrimination and quantification of 4 mAbs used in cancer therapy (cetuximab, rituximab, trastuzumab and bevacizumab) corresponding to the respective commercial formulations ERBITUX®, TRUXIMA®, ONTRUZANT® and AVASTIN®. A range of concentrations corresponding to the therapeutic range has been prepared in 0.9% NaCl solution.

Firstly, the chapter provides a study using Raman spectroscopy ”Understanding the Discrimination and Quantification of Monoclonal Antibodies preparations using Raman Spectroscopy” (*Paper has been accepted in journal of pharmaceutical and biomedical analysis in October 26th, 2020*). Commercial mAbs formulations contain several types of excipients (amino acids, sugars and buffers) added for example to maintain the stability of mAbs molecules their selves during the shelf life and prevent aggregation, thereby maintain the therapeutic efficacy. Those excipients might have strong Raman signatures, and the exact role in the discrimination and quantification has been evaluated. To understand the origin of spectral features observed in commercial mAbs and solutions prepared from intravenous injection an approach using centrifugal ultrafiltration has been proposed.

Secondly, ATR-FTIR analysis have also been performed on the same samples. Although not included in the submitted paper, the results will be presented and discussed.

4.2 Ultrafiltration approach

30K (Kilo-Daltons) cut-off centrifugal ultrafiltration devices have been used. These filters enable passage of small molecules like excipients (in the filtrate) while retaining proteins (in the concentrate). Figure 30 is an illustration of the filtration process with centrifugal device. At the first step, the filtration device has been filled with mAbs solution to the mark, here the maximum volume capacity of Amicon® Ultra is 500 µL. Then the centrifugal device has been fitted in a fixed angle centrifuge (Sigma Laboratory centrifuge 3-30 K) and spun at 14000 g at 4 °C for 10 minutes. After each cycle the filtrate is collected. For the next centrifugation cycle,

the concentrate reside in the filtration device has been topped up with Milli Q water for the next spin. Similarly, to dialysis, the small molecules can be eliminated from the concentrate containing the molecules with the highest molecular weight, for instance the mAbs.

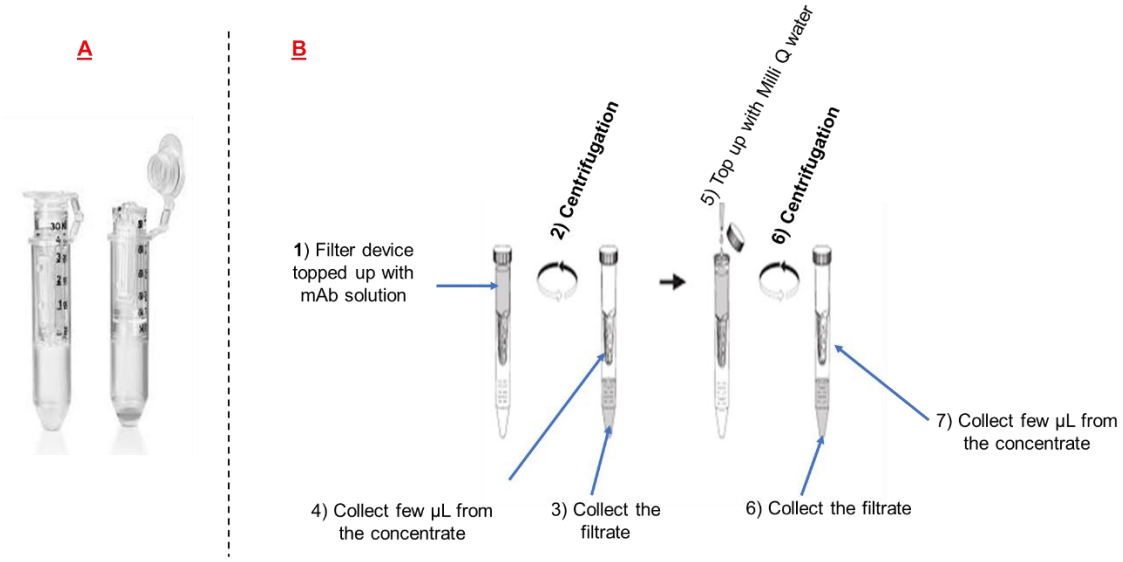


Figure 30. A) Ultra-filtration device Amicon® and B) ultrafiltration protocol

The monitoring of the filtration process has been performed by ATR-FTIR after each cycle by recording spectra from the filtrate and the concentrate and compared to the spectra collected from the commercial stock solutions.

Figure 31 illustrates ATR-FTIR spectra recorded from the filtrate and concentrate after each cycle of the ultrafiltration for ONTRUZANT®. In Figure 31A it is observed that protein signature became more pronounced as excipients are washed away. On contrary, Figure 31B presents strong excipients features in the first 3 cycles of ultrafiltration but the intensity of the bands quickly decreases to disappear in subsequent steps. It suggests, the excipients are completely washed out.

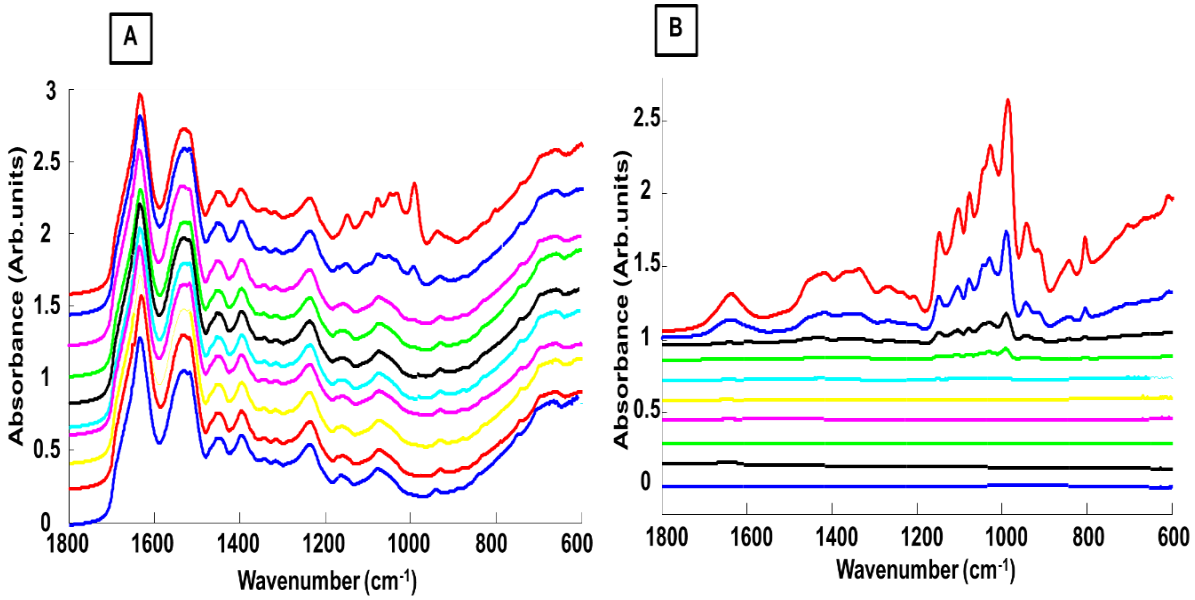


Figure 31. ATR-FTIR spectra recorded form concentrate (A) and filtrate (B) for ONTRUZANT® during ultrafiltration cycles. Spectra are organised from the top to the bottom from cycle 1 to cycle 10. Spectra are offset for clarity

Figure 32 presents the pure mAbs spectra recorded after 10 filtration cycles. The 4 test mAbs shows high spectral similarities with more of less difference in intensity of some band, those band are: amide I band (1633-1638 cm^{-1}), amide II band (1533 cm^{-1}), CH_2 deformation at (1448-1452 cm^{-1}), CH_2 and CH_3 stretching of alanine (1317- 1398 cm^{-1}), amide III band (1236-1240 cm^{-1}), C=O stretching (1072- 1159 cm^{-1}), C-C stretching at (930 cm^{-1}) and COOH deformation at (830 – 876 cm^{-1}).

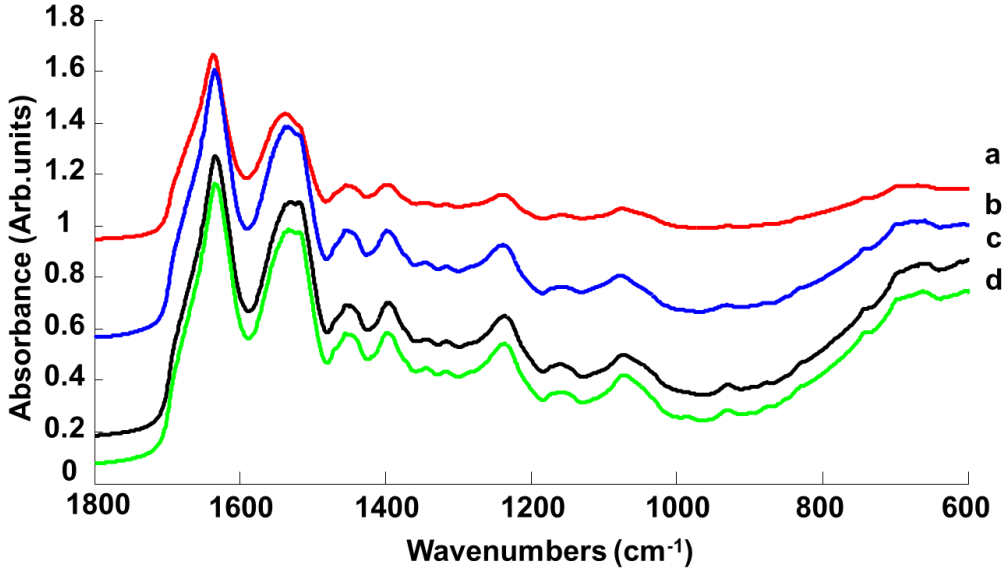


Figure 32. ATR-FTIR spectra recorded from the concentrate after cycle 10 of commercial stock solutions of: ERBITUX® (a), TRUXIMA® (b), ONTRUZANT® (c) and AVASTIN® (d). Spectra are offset for clarity

Ultrafiltration presents a new approach to help understanding the origin of spectral variations, in case of AQC could help interpreting results according to APIs or excipients.

4.3 PUBLICATION 3: Understanding the Discrimination and Quantification of Monoclonal Antibodies preparations using Raman Spectroscopy

Journal of Pharmaceutical and Biomedical Analysis xxx (xxxx) xxx

Contents lists available at ScienceDirect

Journal of Pharmaceutical and Biomedical Analysis

journal homepage: www.elsevier.com/locate/jpba

Understanding the discrimination and quantification of monoclonal antibodies preparations using Raman spectroscopy

Alaa A. Makki[a,b], Victor Massot[c], Hugh J. Byrne[d], Renaud Respaud[e], Dominique Bertrand[f], Elhadi Mohammed[b], Igor Chourpa[a], Franck Bonnier[a,*]

[a] Université de Tours, EA 6295 Nanomédicaments et Nanosondes, 31 avenue Monge, 37200 Tours, France
[b] Faculty of Pharmacy, University of Gezira, P.O. Box 20, 21111 Wad Madani, Sudan
[c] Unité de Biopharmacie Clinique Oncologique, Pharmacie, CHU de Tours, France
[d] FOCAS Research Institute, Technological University Dublin, City Campus, Kevin Street, Dublin 8, Ireland
[e] Université de Tours, UMR 1100, CHRU de Tours, Service de Pharmacie, F-37032 Tours, France
[f] Data_Frame, 25 rue Stendhal, 44300 Nantes, France

ARTICLE INFO

Article history:
Received 18 August 2020
Received in revised form 22 October 2020
Accepted 26 October 2020
Available online xxx

Keywords:
Raman spectroscopy
Monoclonal antibodies
Excipients
Intravenous solutions
Quantification
Discrimination
Human health

ABSTRACT

The use of Raman spectroscopy for analytical quality control of anticancer drug preparations in clinical pharmaceutical dispensing units is increasing in popularity, notably supported by commercially available, purpose designed instruments. Although not legislatively compulsory, analytical methods are frequently used post-preparation to verify the accuracy of a preparation in terms of identity and quantity of the drug in solution. However, while the rapid, cost effective and label free analysis achieved with Raman spectroscopy is appealing, it is important to understand the molecular origin of the spectral contributions collected from the solution of actives and excipients, to evaluate the strength and limitation for the technique, which can be used to identify and quantify either the prescribed commercial formulation, and/or the active drug itself, in personalised solutions. In the current study, four commercial formulations, Erbitux®, Truxima®, Ontruzant® and Avastin® of monoclonal antibodies (mAbs), corresponding respectively to cetuximab, rituximab, trastuzumab and bevacizumab have been used to highlight the key role of excipients in discrimination and quantification of the formulations. It is demonstrated that protein based anticancer drugs such as mAbs have a relatively weak Raman response, while excipients such as glycine, trehalose or histidine contribute significantly to the spectra. Multivariate analysis (partial least square regression and partial least square discriminant analysis) further demonstrates that the signatures of the mAbs themselves are not prominent in mathematical models and that those of the excipients are solely responsible for the differentiation of formulation and accurate determination of concentrations. While Raman spectroscopy can successfully validate the conformity of mAbs intravenous infusion solutions, the basis for the analysis should be considered, and special caution should be given to excipient compositions in commercial formulations to ensure reliability and reproducibility of the analysis.
© 2020 Elsevier B.V. All rights reserved.

1. Introduction

The analytical quality control (AQC) of anticancer drug solutions represents a significant daily workload for technicians and pharmacists in healthcare establishments. Commercial formulations of drugs are prescribed and may be diluted to a patient specific concentration in aqueous solutions, before delivery to the bedside. To ensure administration of the correct medication to patients, the injectable solutions are frequently analysed prior to being released from the preparation units. The two key parameters are (i) identification of the drug and (ii) validation of the concentration, to prevent either therapeutic failure or more importantly protect patients from adverse effects.

Monoclonal antibodies (mAbs) are biopharmaceutics produced by bioengineering technology; they are used as targeted therapy in cancer treatment and are associated with fewer and less severe side effects compared to other chemotherapeutics [1]. In addition to their valuable role in cancer therapy, they are used in preventing or modulating viral diseases [2], for multiple sclerosis [3] and some autoimmune diseases [4]. mAbs are glycoproteins of molecular weight ~150 KDa; their structure consists of two heavy chains,

* Corresponding author at: Université de Tours, Faculté de pharmacie, EA 6295 NanoMédicaments et NanoSondes (NMNS), 31 avenue Monge, 37200 Tours, France.
E-mail address: franck.bonnier@univ-tours.fr (F. Bonnier).

https://doi.org/10.1016/j.jpba.2020.113734
0731-7085/© 2020 Elsevier B.V. All rights reserved.

Please cite this article as: A.A. Makki, V. Massot, H.J. Byrne et al., Understanding the discrimination and quantification of monoclonal antibodies preparations using Raman spectroscopy, J. Pharm. Biomed. Anal., https://doi.org/10.1016/j.jpba.2020.113734

each of which contains 447 amino acids linked by 4 disulphide bonds, and two light chains, each containing 215 amino acids, linked by 2 disulphide bonds [5]. Typically, the different types of mAbs (chimeric, humanised and fully humanised types) [6], only differ in their sequences of amino acids, respectively 240 amino acids for chimeric mAbs and only 65–70 amino acids for the humanised mAbs [1]. As a consequence, approaches for AQC need to be adapted. Reversed phase high performance liquid chromatography (RP-HPLC) coupled to mass spectrometry is the main method for characterisation of proteins and intact mAbs molecules, although the extensive pre-column sample preparation and after-column ionisation steps for mass fragmentation and analysis make the technique costly and time consuming [7]. Furthermore, HPLC with different separation modes, including reversed phase, size exclusion chromatography, weak cation exchange chromatography and strong anion exchange chromatography, are used to identify and quantify mAbs with different precision profiles [8]. Capillary electrophoresis, coupled to electrospray ionisation-mass spectrometry, is used for the comprehensive study of mAbs structures as well as detection of dimer formation, despite the requirement for high separative affinity and mass detection sensitivity which involve cleaving mAbs into different levels of fragments [9]. The main drawback of capillary size electrophoresis is the adsorption of proteins in silica walls, resulting in a loss of precision in determining their migration time [10].

Reversed phase liquid chromatography with diode detectors is used for quantification of mAbs in their intact status, but long term stability of mAbs during the pre-column and column step at high temperature (60–90 °C) is not assured [11]. Immunoassay methods such as enzyme linked immunoassay (ELISA) can be used to check the stability of mAbs in infusion bags, as well as bioavailability in biological matrices (plasma, serum) [12].

Although a number of methods are available, their complexity, need for highly trained personnel and time-consuming protocols suggest that, in the context of daily AQC of large cohorts of samples, a simple, direct and rapid quantitative screening tool could greatly reduce the workflow and accelerate safe administration of mAbs to patients.

Vibrational spectroscopy, namely Raman and infrared spectroscopy, are label free and non-destructive methods. They have been demonstrated to be relevant tools to investigate the effect of stress conditions on the secondary and tertiary structure of mAbs aggregates and unfolded species during the manufacturing and formulation [13,14].

Vibrational spectroscopy have also been well described in literature for QC of injectable small molecule chemotherapeutic drugs such as taxanes [15] or anthracyclines [16]. Raman spectroscopy has been implemented for real time AQC of chemotherapeutic preparations in hospitals [17,18]. Recently, commercialised flow injection instrumentation QCPrep+® (Icônes Services, France), combining Raman with UV detection, has been reported for QC of chemotherapeutic preparations into healthcare establishment [19]. Moreover, miniaturisation of instruments and commercialisation of so-called handheld Raman open further perspectives for performing non-invasive measurements directly in plastic infusion bags, consequently reducing potentially hazardous exposure to solutions of staff members [20].

However, reports of application of vibrational spectroscopy for QC of mAbs are few. Bazin et al., [21] reported a study using a Multispec® analyser (Microdom, Taverny, France) which, coupling UV/vis to IR absorption, has been applied for QC of small molecule chemotherapeutic drugs and mAbs (cetuximab, rituximab, trastuzumab and bevacizumab). The true classification, respectively, was 97 % and 99.95 % for molecules and solvents, but there were difficulties in discriminating structurally related molecules such as anthracyclines (doxorubicin, epirubicin and daunorubicin) and oxazophosphorines (cyclophosphamide and ifosfamide) as well as mAbs. More recently, classification of selected mAbs (bevacizumab, rituximab, infliximab and ramucirumab) in their commercialised form by Raman micro-spectroscopy coupled to advanced machine learning data mining approaches has been documented [22]. Although the results are promising in the context of classification of formulations in terms of their characteristic spectra, the spectral origin of the analysis outcome is not elucidated, while instrumental interferences or spectral artefacts can bias advanced supervised data mining methods [21,22]. Moreover, the sensitivity of Raman spectroscopy to detect and quantify features originating from the therapeutic antibodies within the complex, multicomponent injectable mixtures is not discussed. This highlights that, presently, the extent of information encompassed in Raman spectra collected from mAbs formulations is still not fully understood or explored in the context of applications to clinical AQC. Misconceptions about the true potential of the spectroscopic technique could lead to its misuse and misinterpretation of results. Therefore, the present study aims to provide further insights into the analysis of commercial mAbs formulations in the context of clinical administration AQC, by analysing 4 commonly administered formulations (Erbitux®, Truxima®, Ontruzant® and Avastin®) of anticancer drugs (cetuximab, rituximab, trastuzumab and bevacizumab). The quantification and discrimination will be illustrated and discussed on the basis of the spectral features observed in the context of their respective chemical compositions.

Table 1
Excipients list present in the tested mAbs.

Brand	mAb	Excipients
ERBITUX®	CTX	Sodium chloride, Glycine, Polysorbate 80, Citric acid monohydrate Sodium hydroxide and Water for injections.
TRUXIMA®	RTX	Sodium chloride, Tri-sodium citrate dihydrate, Polysorbate 80 and Water for injections.
ONTRUZANT®	TRS	L-histidine hydrochloride monohydrate, L-histidine, α,α-trehalose dihydrate, polysorbate 20.
AVASTIN®	BEV	Trehalose dihydrate, Sodium phosphate, Polysorbate 20 and Water for injections.

2. Materials and methods

2.1. Monoclonal antibodies and sample preparation

The study has been conducted in collaboration with the Unité de Biopharmacie Clinique Oncologique (UBCO) of the University Hospital of Tours (CHU Tours, France). UBCO manages the daily preparation of systemic therapeutic solutions, and it provided samples of the 4 most frequently clinically prescribed mAbs formulations: ERBITUX®, (Merck - cetuximab 5 $g{\cdot}L^{-1}$), TRUXIMA®, (Healthcare Celltrion - rituximab 10 $g{\cdot}L^{-1}$), ONTRUZANT®, (Samsung Bioepis - trastuzumab 150 mg powder for injection) and AVASTIN® (Roche - bevacizumab 25 $g{\cdot}L^{-1}$). Commercial formulations of mAbs contain several excipients, listed in Table 1. Throughout the paper for clarity, ERBITUX®, TRUXIMA®, ONTRUZANT® and AVASTIN® will refer to the commercial mAbs formulations while the respective antibodies themselves will be designated as CTX (cetuximab), RTX (rituximab), TRS (trastuzumab) and BEV (bevacizumab).

Based on recent administration records of solutions prepared at UBCO, relevant therapeutic ranges were defined. Ultimately 5 different concentrations were prepared for each commercial mAb as follows: AVASTIN®: 2 $g{\cdot}L^{-1}$, 4 $g{\cdot}L^{-1}$, 8 $g{\cdot}L^{-1}$, 12 $g{\cdot}L^{-1}$ and 15 $g{\cdot}L^{-1}$; ERBITUX®, TRUXIMA® and ONTRUZANT®: 0.5 $g{\cdot}L^{-1}$, 1 $g{\cdot}L^{-1}$, 2 $g{\cdot}L^{-1}$, 3 $g{\cdot}L^{-1}$ and 4 $g{\cdot}L^{-1}$.

The different concentrations were prepared from the stock formulations using serial dilutions in 0.9 % normal saline (matrix used at the hospital for injection) and analysed directly with Raman spectroscopy. All samples were prepared freshly on the day of analysis.

2.2. Ultrafiltration of mAbs

Amicron® Ultra-0.5 mL (Merck, Germany) with cut-off points at 30 K (Kilo-Daltons) were used for centrifugal dialysis of mAbs solutions. For the purpose of the study, 0.5 mL of ERBITUX® 4 g·L^{-1}, TRUXIMA® 4 g·L^{-1}, ONTRUZANT® 4 g·L^{-1} and AVASTIN® 4 g·L^{-1} were subjected to ultrafiltration. Filters were placed in a fixed angle centrifuge (Sigma Laboratory centrifuge 3–30 K) and spun at 14,000 *g* at 4 °C for 10 min. At the end of a spinning cycle, solutions were separated in 2 fractions: the concentrate (retained in the filter) and the filtrate (passed through the membrane). Having high molecular weight, mAbs were retained in the filter, while excipients were found in the filtrate. Filters containing concentrated mAbs were topped up with 0.5 mL Milli Q water and subjected to another spinning cycle. To ensure efficient dialysis, 10 cycles were applied to each mAb solution.

For Raman measurement, the washing procedure is important to avoid molecular contamination with glycerine residue on the membrane of filters [23]. Therefore, prior to filtering mAbs, 3 cycles of washings with 0.1 M NaOH solution followed by 3 cycles of rinsing with Milli Q water were undertaken (10 min., 14,000 g).

2.3. Raman spectroscopic analysis

Raman spectra were collected using a Labram spectrometer (Horiba Jobin-Yvon, France) equipped with a 690 nm laser source delivering ~10 mW at the sample. Spectra were collected over the 150 and 3750 cm^{-1} range with a 300 lines/mm grating, resulting in spectral resolution of ~ 3 cm^{-1}. 2 instrumentals set up were used. 1) *Macro set up:* A macro sampling cuvette holder (Horiba Jobin-Yvon, France) attached to the turret of the microscope has been used for recording using 500 μL in quartz cuvette, thereby recording from a large sample volume and ensuring very high reproducibility in recording, without the need to refocus the laser each time, as well as reduced risk of photothermal damage to the sample by the laser. From each prepared concentration; 15 spectra have been recorded using 2 accumulations of 20 s, giving a total of 75 spectra recorded for each mAb in 0.9 % NaCl. 2) *Microscope set up:* A x100 objective (Olympus, NA = 0.9) has been used to record Raman spectra from air dried drops on a CaF_2 slide before and after the centrifugation cycle. The laser spot size was roughly 1 μm. Spectra resulted from 2 accumulations of 60 s, recorded from 5 different sites within the drop.

2.4. Data handling

Raman data sets have been pre-processed and analysed using MATLAB® (Mathworks, USA).

a) Quantitative analysis:

Firstly, data were EMSC corrected (Extended Multiplicative Scattering Correction) in the range 300 – 3750 cm^{-1}) [24]. Secondly, Partial Least Squares Regression (PLSR) analysis has been applied to the fingerprint region of corrected spectra (600 – 1800 cm^{-1}). A 100-fold Leave K Out Cross Validation (LKOCV) has been applied, in which 2/3 of the data set were selected randomly for calibration and the remaining 1/3 for validation. The process was run automatically in a random way, with no repetition of data in each set. The output from PLSR was evaluated using the linearity of the regression model (R^2), the Root Mean Square Error of Cross Validation (RMSECV) as well as the regression coefficients, highlighting the variables (spectral features) used to construct the regression models.

b) Discriminant analysis:

Partial Least Squares Discriminant Analysis (PLSDA) is a well-established supervised classification method and was employed in this study to demonstrate the discriminative potential of the analytical techniques. Prior to analysis, data were subjected to pre-processing with EMSC in the range 300 – 3750 cm^{-1} followed by baseline correction (Lieber correction) and vector normalisation in order to remove the background interference. To perform the analysis, Raman spectra were cut to the fingerprint region (600 –1800 cm^{-1}), in which the most relevant spectral features are observed. 2/3 of the data was used for calibration and the remaining 1/3 for classification. The output of PLSDA is presented under confusion matrix allowing calculation of specificity and sensitivity of the discrimination [25].

3. Results and discussion

3.1. Spectral characterisation of commercial mAbs solutions studied

a) Air dried stock formulations

To elucidate the spectral features and aid interpretation of the quantitative analysis, the following section uses Raman spectra collected from air dried drops of stock commercial mAbs formulations, the spectra of which are presented in Fig. 1. mAbs are proteins and therefore the main features are observed at ~640 cm^{-1} (tyrosine), 755 cm^{-1} (tryptophan), 954 cm^{-1} (C–H stretching of α-helix structure), 1001 cm^{-1} (phenylalanine), 1237 cm^{-1} (amide III), 1335 cm^{-1} and 1445 cm^{-1} (CH_2 deformation), 1551 cm^{-1} (amide II) and 1668 cm^{-1} (amide I) [26,27]. Notably, however, while Raman spectra can reflect modifications in chemical compositions of samples, it is not expected that modifications in small sequences in amino acids compared to the overall size of mAbs can lead to the large spectral variations observed in Fig. 1 (highlighted regions). Table 1 provides a list of excipients found in commercialised mAbs solutions that can possibly contribute significantly to the spectra collected. Excipients are, however, relatively small molecular entities compared to antibodies (≈ 150 kD), and thus they can be separated for independent spectral characterisation using ultrafiltration.

b) Air dried filtrates: excipients

Although the excipients list is provided for each product and they can be purchased individually, the concentration of each one of these ingredients in the formula is not disclosed. Therefore, for the purpose of this study, it was deemed preferable to consider the fraction of product corresponding to excipients as a whole to clearly differentiate the spectral contributions of mAbs and the combination of all other ingredients. Using a centrifugal filter with a 30 K (Kilo-Daltons) cut-off, the excipients can be separated from the mAbs. The filtrate, fraction passing through the membrane, can be analysed following air drying. Fig. 2 presents the spectra of the filtrates collected from the 4 mAbs commercial formulations. Clearly, the fractions collected significantly differ between mAbs.

The spectrum collected from ERBITUX® filtrate (Fig. 2a) is dominated by glycine [28]. Characteristic bands of the amino acid can be observed at 895 cm^{-1} (COOH deformation), 1330 cm^{-1} (CH_2 wag-

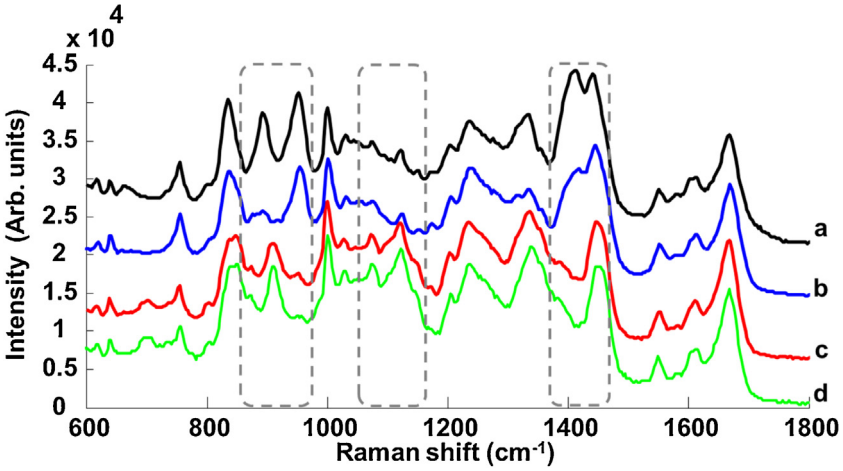


Fig. 1. Mean Raman spectra recorded from air dried drops of the commercial stock solutions: ERBITUX® 5 g·L^{-1} (a), TRUXIMA® 10 g·L^{-1} (b), ONTRUZANT® 21 g·L^{-1} (c) and AVASTIN® 25 g·L^{-1} (d). Spectra are offset for clarity.

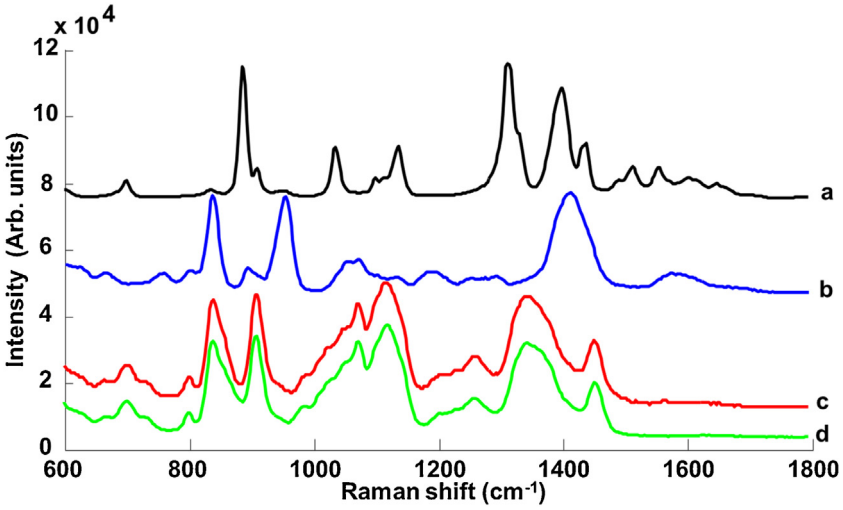


Fig. 2. Raman spectra from filtrates ERBITUX® (a), TRUXIMA® (b), ONTRUZANT® (c) and AVASTIN® (d). Spectra are offset for clarity.

ging), 1411 cm^{-1} (CH_2 and CH_3 stretching) and 1444 cm^{-1} (CH_2 deformation).

For TRUXIMA® (Fig. 2b), strong features can be observed at 838 cm^{-1} (CH_2 rocking), 957 cm^{-1} (CH_2 rocking) and 1417 cm^{-1} (C–H bending) correspond to specific features of polysorbate 80 [29].

ONTRUZANT® and AVASTIN® (Fig. 2c and 2d) both exhibit strong contributions from trehalose and histidine [30]. The features observed at 841 cm^{-1} (COC skeletal structure and CC—— stretching), 911 cm^{-1} and 1122 cm^{-1} C-C stretching of saccharides (trehalose), while band at 1076 cm^{-1} (=C-N deformation), 1349 cm^{-1} (ring (C—N) deformation) and 1457 cm^{-1} (N—H bending) are specific peaks of histidine added to mAbs formulations [31].

c) Air dried concentrates: mAbs

An advantage of performing dialysis of excipients using centrifugal ultrafiltration is the isolation of the mAbs, hence enabling unambiguous identification of its characteristic Raman spectroscopic signature. Unlike the filtrates, the spectra of the concentrates of the ultrafiltration process, the pure mAbs, exhibit a much higher degree of similarity (Fig. 3). It is therefore clearly demonstrated that the excipients strongly contribute to the spectral signatures collected from stock formulations.

Table 2
PLSR results obtained for the 4 mAbs.

Brand	mAb	R^2	RMSECV (g·L^{-1})	LVs
ERBITUX®	CTX	0.9995	0.0275	5
TRUXIMA®	RTX	0.9984	0.0516	5
ONTRUZANT®	TRS	0.9951	0.0843	5
AVASTIN®	BEV	0.9950	0.3599	6

3.2. Quantitative analysis by Raman spectroscopy

Quantitative analysis is better conducted in the native aqueous environment. Notably, however, although water is commonly described as a weak scatterer, enabling Raman analysis of aqueous liquid samples [16], within the range of concentrations, the relatively intense OH bending vibration at 1638 cm^{-1} compared to the mAbs signal results in a strong underlying background (Fig. 4).

Fig. 5 presents an example of PLSR analysis using ERBITUX® in 0.9 % NaCl solutions. It can be observed in Fig. 5a that the RMSECV decreases as a function of the number of latent variables (LVs) included in the regression models. Errors bars represent the standard deviation and they suggest that, above 5 LVs, no significant improvement is achieved. Moreover, overfitting of data should be avoided by limiting as much as possible the number of LVs, thus

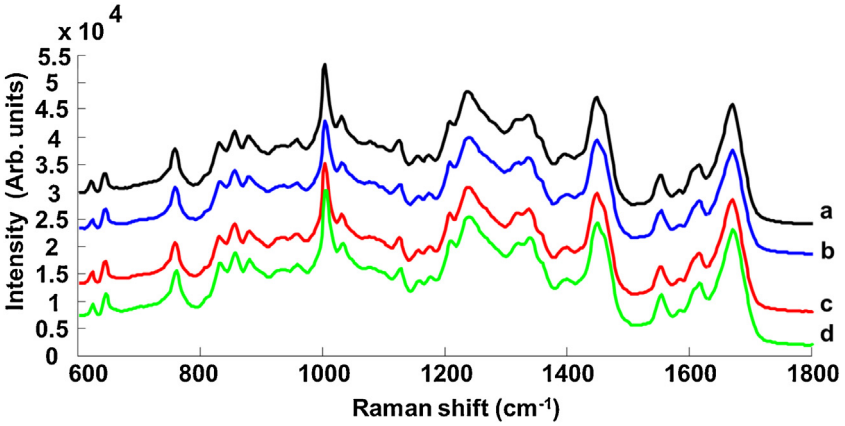


Fig. 3. Raman spectra concentrates after cycle 10 of ultrafiltration ERBITUX® (a), TRUXIMA® (b), ONTRUZANT® (c) and AVASTIN® (d). Spectra are offset for clarity.

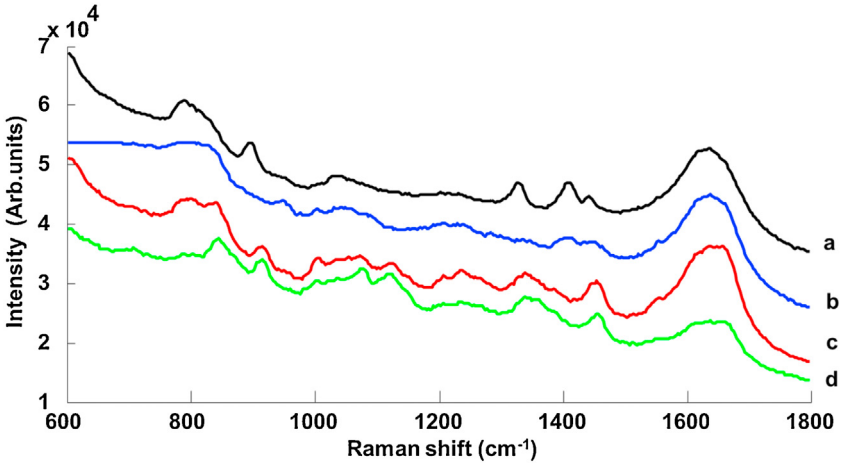


Fig. 4. Raman spectra recorded from commercial stock solutions: a) ERBITUX® 5 g·L^{-1}, b) TRUXIMA® 10 g·L^{-1}, c) ONTRUZANT® 21 g·L^{-1} and d) AVASTIN® 25 g·L^{-1}. Spectra are offset for clarity.

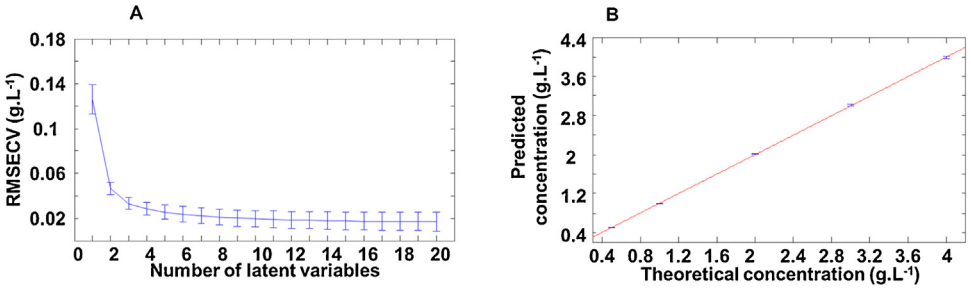


Fig. 5. PLSR analysis performed on Raman spectra collected from ERBITUX® in 0.9 % NaCl. A) RMSECV and B) Regression plot with 5 LVs.

results presented correspond to n = 5. Fig. 5b presents the regression plot with an R^2 value equal to 0.9996 and RMSECV of 0.0253 g·L^{-1}. These criteria support the quality of the fitting achieved and the performance of Raman spectroscopy to deliver quantitative analysis for ERBITUX®.

Table 2 summarises the PLSR results obtained for the 4 mAbs formulations studied. R^2 is consistently greater than 0.99, indicating acceptable regression can be achieved for all. AVASTIN® displays, however, a significantly higher RMSECV compared to other mAbs, with a value of 0.3599 g·L^{-1}. This can be explained by the clinical concentration range extending from 2 g·L^{-1} to 15 g·L^{-1}, while for others the highest concentration does not exceed 4 g·L^{-1}. For the purpose of comparison, the RMSECV can be expressed as a percentage of the mean concentration of the range tested, in which case, a value of 4.4 % is found for AVASTIN®, while for ERBITUX®, TRUXIMA® and ONTRUZANT®, respective values of 1.2 %, 2.4 % and 4 % are obtained. Thus, depending on the mAb formulation considered, the outcome of the analysis differs, but PLSR of AVASTIN® and ONTRUZANT® deliver a similar outcome once the range used is considered. While dialysis of excipients by means of ultrafiltration enables separation and collection of the mAbs from commercial products, the process also modifies the concentrations of the constituent fractions. The mAbs fraction is retained, but significantly concentrated within the filter of the centrifugal device, and therefore its concentration does not reflect the composition of the stock solution. As a consequence, no attempt to perform PLSR on the

Table 3
Specificity and sensitivity % of PLSDA of Raman using 6 LVs, data pre-processed with EMSC, Lieber correction and vector normalisation.

Brand	mAb	Specificity%	Sensitivity%
ERBITUX®	CTX	100	100
TRUXIMA®	RTX	96.7	98.9
ONTRUZANT®	TRS	100	100
AVASTIN®	BEV	100	100

concentrate has been performed, due to poor correlation with the concentration in the commercial product.

Regression coefficients in Fig. 6 provide information about the spectral features used during PLSR. For ERBITUX® (Fig. 6a), dominants peaks at 895 cm^{-1}, 1330 cm^{-1}, 1411 cm^{-1} and 1444 cm^{-1} correspond to features previously observed in the filtrate and are thus associated with the formulation excipients (Fig. 2). Similarly, for AVASTIN® (Fig. 6d) the main bands are found at 846 cm^{-1}, 911 cm^{-1}, 1001 cm^{-1}, 1076 cm^{-1}, 1117 cm^{-1}, 1341 cm^{-1} and 1457 cm^{-1}, suggesting contributions predominantly from excipients. Although a small feature is observable at 1668 cm^{-1} that can be attributed to the amide I band of proteins, the model remains dominated by other constituents of the formulation. For TRUXIMA® (Fig. 6b) and ONTRUZANT® (Fig. 6c), the regression coefficients exhibit lower signal to noise ratio. The spectrum collected from the stock solution of TRUXIMA® 10 $g{\cdot}L^{-1}$ (Fig. 4b) already displays weak features while the range tested is between 0.5 $g{\cdot}L^{-1}$ and 4 $g{\cdot}L^{-1}$. While analysis of the filtrate for ONTRUZANT® and AVASTIN® demonstrated that trehalose was the main excipient contributing to the spectra, the 2 mAbs are not prescribed in the same range of concentrations. For instance, AVASTIN® was tested between 2 $g{\cdot}L^{-1}$ and 15 $g{\cdot}L^{-1}$ compared to 0.5 $g{\cdot}L^{-1}$ to 4 $g{\cdot}L^{-1}$ for ONTRUZANT®. As a result, all constituents are more diluted in solution. Although all PLSR deliver relatively good RMSECV, it appears the analysis strongly depends on the ability to detect spectral variations not specifically attributed to the active mAbs.

3.3. Discriminant analysis using PLSDA

PLSDA has been used to discriminate between 0.9 % NaCl mAbs solutions prepared within the clinical range using the 4 mAbs commercial formulations (Table 3). Specificity and sensitivity have been calculated from the confusion matrix using 6 LVs. All mAbs delivered 100 % sensitivity and specificity, except for solutions prepared from TRUXIMA®, for which the values were determined to be 98.9 % and 96.7 %, respectively. Misclassification observed between mAbs solutions has been attributed to their weak Raman signal (Fig. 3) For instance, misclassifications observed are TRUXIMA® solutions recognised as ONTRUZANT® due to some shared bands between them. One can see that the spectral signature for the stock solution of TRUXIMA® at 10 $g{\cdot}L^{-1}$ presents broad and weak bands (Fig. 4). Therefore, at lower concentrations, it can be expected that the specificity of the analysis is lost, leading to false identifications.

Fig. 7a and b displays first and second regression coefficients from PLSDA. Regression coefficient enables to highlight the wavenumbers, hence the chemical species, used for the discrimination of the 4 mAbs solutions (Table 3). It is clearly demonstrated that there is a strong correspondence between the regression coefficient and the spectral features observed in filtrates. Negative features of the first regression coefficient (Fig. 7a) at 841 cm^{-1}, 911 cm^{-1}, 1076 cm^{-1}, 1120 cm^{-1}, 1349 cm^{-1} and 1454 cm^{-1} match the main spectral features found in spectra collected from filtrates of AVASTIN® (Fig. 2d) and ONTRUZANT® (Fig. 2c). Bands at 895 cm^{-1}, 1330 cm^{-1} and 1411 cm^{-1} correspond, however, to peaks found in ERBITUX® (Fig. 2a). Unambiguously, analysis of the PLSDA regression coefficients demonstrates that the identification of mAbs solutions cannot be achieved based on the spectral signatures of the antibodies themselves but rather on the spectral signatures of the unique combination of excipients of the commercial mAbs.

3.4. Perspectives and caution

Raman spectroscopy holds numerous promises for applications in the clinical environment. The technology is evolving at great pace, incorporating automation, miniaturisation and hyphenated instruments such as UV coupled to Raman spectroscopy. In addition, chemometrics helps to push the limits of the technique [32], facilitating implementation of translational research. In principle, Raman spectroscopy is a powerful tool delivering a specific molecular fingerprint of a sample for characterisation or even quantification of compounds. However, one should bear in mind that all molecules do not have equal Raman response. It has been well documented that most of chemotherapeutic agents such as small molecules like doxorubicin, daunorubicin and epirubicin exhibit strong and sharp features within the clinical range [16]. Numerous drugs have conjugated rings in their chemical structures which are particularly active in Raman spectroscopy. Therefore, their detection, identification and quantification can even be easily achieved [33]. Furthermore, the strength of the signal for those drugs have open encouraging perspective for direct analysis into containers (infusion bags, syringe) [15,20]. In contrast, mAbs do not deliver particularly intense Raman signals in solutions, especially diluted. As a consequence, other constituents of the formulation can dominate the spectra collected.

In the analysis of the aqueous formulations, firstly, it can be observed that, although the water is a relatively weak scatterer, as the primary constituent of the formulation, its contribution to the spectra collected is quite noticeable (Fig. 4), further highlighting the limited Raman response from proteins bands. Secondly, other compounds used as excipients can also be observed. Unambiguously, when it comes to quantification and discrimination, excipients play a major role in the analysis outcome.

There is no specific legislation governing analytical quality control of chemotherapeutic solutions. However, for drugs with narrow therapeutic windows, centralized units for preparation of chemotherapy inside hospital have established systematic prevention strategies such as double visual check coupled to an additional method to detect preparation errors. Gravimetric [34] or video assisted control protocols are currently employed in process production methods [35]. In addition, numerous units also implement analytical methods to control and validate the final product [35]. There is, however, no general consensus on optimum protocols, and techniques currently used include conventional high-performance liquid chromatography, thin-layer chromatographic, high-performance liquid chromatography, flow injection analysis, but also increasingly more popular and accepted spectroscopy techniques (near infrared, mid-infrared and Raman spectroscopy). While separation techniques have the advantage of specificity, spectroscopy approaches remain attractive for low cost and speed of analysis. There are no international guidelines which specifically address ACQ of personalised chemotherapeutic solutions. For instance, the French Good Preparation Practices controls of chemotherapeutics solutions, established by the ANSM (National Agency for Drug Safety and Products for Health), are part of good practice to guarantee that necessary and appropriate analyses have been applied to ensure the quality of raw material, product packaging and therapeutic preparations before release. In the context of AQC, results of analysis of anticancer drugs in solutions are acceptable, as long as the method employed is experimentally validated and appropriate to ensure the conformity of the solutions prepared for administration to the prescribed therapy. Clearly, for the case of intravenous solutions prepared from commercial for-

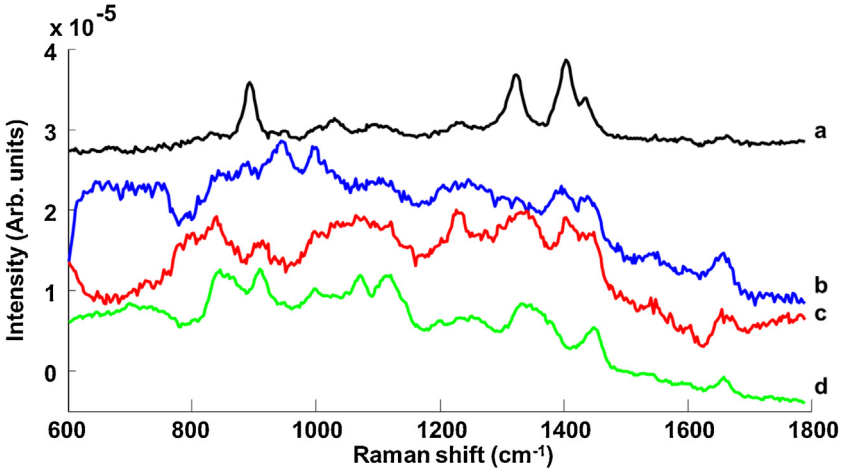


Fig. 6. Regression coefficients of the PLSR. a) ERBITUX®, b) TRUXIMA®, c) ONTRUZANT® and d) AVASTIN®. Spectra are offset for clarity.

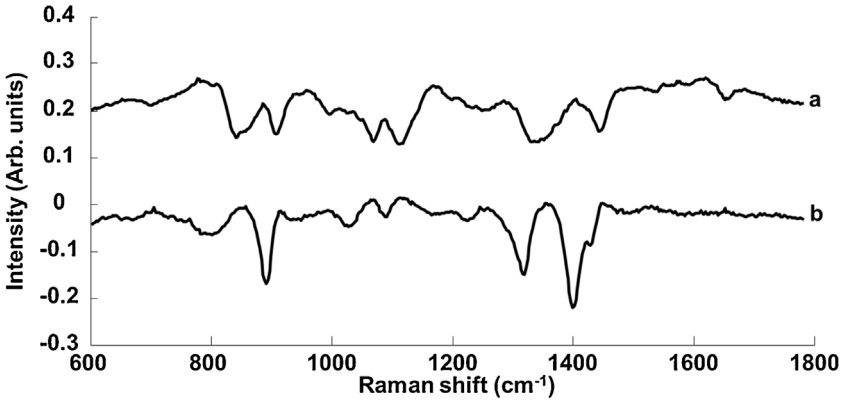


Fig. 7. First (a) and second (b) regression coefficients of the PLSDA. Spectra are offset for clarity.

mulations of mAbs, the excipients are the majority components and dominate the Raman spectra of the solutions. This observation raises a number of concerns, in the absence of clear guidelines or legislation available for this particular situation. On one hand, the sensitivity of Raman analysis to identify intravenous solutions based on their specific spectral signatures can be used to verify the current commercial mAbs formulations and the concentrations used in the preparation of the solution. Raman has indeed a strong potential for AQC for rapid control of solutions for release. On the other hand, the discrimination and quantification of solutions are based on the excipients not the spectral contribution from mAbs themselves. Experimentally, some of the ingredients found in commercial products act as internal standard, enabling indirect analysis of mAbs in solutions. While from the analytical point of view this is not an aberrant application of the technique, there is nevertheless a higher risk of errors in the identification process. The approach relies only on the specificity of the composition of excipients in commercial products. However, it can be seen in Table 3 that polysorbate 80, polysorbate 20 or trehalose are found in multiple mAbs formulations. Raman analysis is presently based on signal originating from a mixture of molecules rather than a single ingredient specifically attributed to a specific mAb. Although the number of commercially available mAbs is currently increasing, the selection of excipients used by the pharmaceutical industry is well established and tends to remain consistent. As a result, there is a high degree of duplication of ingredients found in mAbs formulations which could significantly compromise the robustness of the models established for AQC with Raman spectroscopy. If two or more commercial products have the same, or similar, excipient compositions, they will display Raman signatures with a high degree of similarity of feature positions and intensities, which could compromise the identification of mAbs in solutions. Indeed, the study included only four examples of mAbs used in clinics and further investigation is required to cover a broader range of commercial products and fully address the issue of the role of excipients in the Raman based AQC protocols.

4. Conclusion

Raman spectroscopy is a powerful tool for AQC. It presents a number of advantages, such as label free, rapid and cost-effective molecular characterisation of samples. There is no doubt that the technique can address needs for clinical or industrial applications, for instance for therapeutic solutions analysis. It is, however, crucial to recognise that Raman spectroscopy delivers a global analysis of a sample. On one hand, quantitative analysis can be performed high degree of accuracy and discrimination of solutions can be achieved with high classification rate. On the other hand, all the outcomes of the multivariate analysis are based on excipients not the mAbs itself. It is crucial to raise awareness among the clinical community that the origin of the signature collected needs to be understood to avoid misuse of the technique. Presently, it is clearly demonstrated that, in the case of mAbs, the response to Raman spectroscopy for proteins in solutions of clinically relevant concentrations is limited, and therefore other compounds dominate the analysis. It is crucial to proceed carefully as all models presently validated on instruments used in research or dedicated to QC of anticancer solutions can become obsolete if the formula is modified by manufacturers.

Indeed, the present study remains a preliminary demonstration and further investigation including additional mAbs and more importantly formula sharing excipients in their composition could bring further insight in the real potential of Raman spectroscopy for this specific application.

Declaration of Competing Interest

The authors declare that they have no known competing financial interests or personal relationships that could have appeared to influence the work reported in this paper.

Acknowledgements

Campus France, ministry of higher education and University of Gezira in Sudan for financial support for PhD in cotutelle between University of Gezira and University of Tours.

References

[1] E. Jaccoulet, J. Boccard, M. Taverna, A.S. Azevedos, S. Rudaz, C. Smadja, High-throughput identification of monoclonal antibodies after compounding by UV spectroscopy coupled to chemometrics analysis, Anal. Bioanal. Chem. 408 (2016) 5915–5924, http://dx.doi.org/10.1007/s00216-016-9708-4.
[2] L. Both, A.C. Banyard, C. Van Dolleweerd, E. Wright, J.K.C. Ma, A.R. Fooks, Monoclonal antibodies for prophylactic and therapeutic use against viral infections, Vaccine 31 (2013) 1553–1559, http://dx.doi.org/10.1016/j.vaccine.2013.01.025.
[3] X. Xu, S. Chi, Q. Wang, C. Li, B. Xu, J. Zhang, X. Chen, Efficacy and safety of monoclonal antibody therapies for relapsing remitting multiple sclerosis: a network meta-analysis, Mult. Scler. Relat. Disord. 25 (2018) 322–328, http://dx.doi.org/10.1016/j.msard.2018.08.026.
[4] R. Pérez-Robles, L. Cuadros-Rodríguez, A. Salmerón-García, N. Navas, Development and validation of a (RP)UHPLC-UV-(HESI/Orbitrap)MS method for the identification and quantification of mixtures of intact therapeutical monoclonal antibodies using a monolithic column, J. Pharm. Biomed. Anal. 159 (2018) 437–448, http://dx.doi.org/10.1016/j.jpba.2018.07.013.
[5] R.F. Perobelli, B. Xavier, A.R. da Silveira, G.L. Remuzzi, L.G.J. Motta, S.L. Dalmora, Quantitation of the monoclonal antibody Denosumab by bioassay and validated LC methods, Int. J. Biol. Macromol. 119 (2018) 96–104, http://dx.doi.org/10.1016/j.ijbiomac.2018.07.120.
[6] D. Psimadas, P. Georgoulias, V. Valotassiou, G. Loudos, Molecular nanomedicine towards cancer, J. Pharm. Sci. 101 (2012) 2271–2280, http://dx.doi.org/10.1002/jps.
[7] P.V. Bondarenko, T.P. Second, V. Zabrouskov, A.A. Makarov, Z. Zhang, Mass measurement and top-down HPLC/MS analysis of intact monoclonal antibodies on a hybrid linear quadrupole ion trap-orbitrap mass spectrometer, J. Am. Soc. Mass Spectrom. 20 (2009) 1415–1424, http://dx.doi.org/10.1016/j.jasms.2009.03.020.
[8] S. Grotefend, L. Kaminski, S. Wroblewitz, S. El Deeb, N. Kühn, S. Reichl, M. Limberger, S. Watt, H. Wätzig, Protein quantitation using various modes of high performance liquid chromatography, J. Pharm. Biomed. Anal. 71 (2012) 127–138, http://dx.doi.org/10.1016/j.jpba.2012.08.024.
[9] J. Giorgetti, A. Beck, E. Leize-Wagner, Y.N. François, Combination of intact, middle-up and bottom-up levels to characterize 7 therapeutic monoclonal antibodies by capillary electrophoresis – mass spectrometry, J. Pharm. Biomed. Anal. 182 (2020), http://dx.doi.org/10.1016/j.jpba.2020.113107.
[10] E. Jaccoulet, C. Smadja, P. Prognon, M. Taverna, Capillary electrophoresis for rapid identification of monoclonal antibodies for routine application in hospital, Electrophoresis 36 (2015) 2050–2056, http://dx.doi.org/10.1002/elps.201400603.
[11] A. Martínez-Ortega, A. Herrera, A. Salmerón-García, J. Cabeza, L. Cuadros-Rodríguez, N. Navas, Study and ICH validation of a reverse-phase liquid chromatographic method for the quantification of the intact monoclonal antibody cetuximab, J. Pharm. Anal. 6 (2016) 117–124, http://dx.doi.org/10.1016/j.jpha.2015.11.007.
[12] I. Suárez, A. Salmerón-García, J. Cabeza, L.F. Capitán-Vallvey, N. Navas, Development and use of specific ELISA methods for quantifying the biological activity of bevacizumab, cetuximab and trastuzumab in stability studies, J. Chromatogr. B Anal. Technol. Biomed. Life Sci. 1032 (2016) 155–164, http://dx.doi.org/10.1016/j.jchromb.2016.05.045.
[13] I. Ettah, L. Ashton, Engaging with Raman spectroscopy to investigate antibody aggregation, Antibodies 7 (2018) 24, http://dx.doi.org/10.3390/antib7030024.
[14] B.S. McAvan, L.A. Bowsher, T. Powell, J.F. O'Hara, M. Spitali, R. Goodacre, A.J. Doig, Raman spectroscopy to monitor post-translational modifications and degradation in monoclonal antibody therapeutics, Anal. Chem. 92 (2020) 10381–10389, http://dx.doi.org/10.1021/acs.analchem.0c00627.
[15] L. Lê, M. Berge, A. Tfayli, P. Prognon, E. Caudron, Discriminative and quantitative analysis of antineoplastic taxane drugs using a handheld Raman spectrometer, Biomed Res. Int. 2018 (2018) 12–15, http://dx.doi.org/10.1155/2018/8746729.
[16] A.A. Makki, F. Bonnier, R. Respaud, F. Chtara, A. Tfayli, C. Tauber, D. Bertrand, H.J. Byrne, E. Mohammed, I. Chourpa, Qualitative and quantitative analysis of therapeutic solutions using Raman and infrared spectroscopy, Spectrochim. Acta - Part A Mol. Biomol. Spectrosc. 218 (2019) 97–108, http://dx.doi.org/10.1016/j.saa.2019.03.056.
[17] C. Bazin, B. Cassard, E. Caudron, P. Prognon, L. Havard, Comparative analysis of methods for real-time analytical control of chemotherapies preparations, Int. J. Pharm. 494 (2015) 329–336, http://dx.doi.org/10.1016/j.ijpharm.2015.08.041.
[18] P. Bourget, A. Amin, F. Vidal, C. Merlette, P. Troude, A. Baillet-Guffroy, The contribution of Raman spectroscopy to the analytical quality control of cytotoxic drugs in a hospital environment: eliminating the exposure risks for staff members and their work environment, Int. J. Pharm. 470 (2014) 70–76, http://dx.doi.org/10.1016/j.ijpharm.2014.04.064.
[19] T. Chouquet, G. Benoit, K. Morand, Analytical control of pediatric chemotherapy preparations with a UV-raman automaton: results after 18 months of implementation and development of a suitable method for low volume preparations, Pharm. Technol. Hosp. Pharm. 2 (2017) 117–129, http://dx.doi.org/10.1515/pthp-2017-0021.
[20] L. Lê, M. Berge, A. Tfayli, A. Baillet Guffroy, P. Prognon, A. Dowek, E. Caudron, Quantification of gemcitabine intravenous drugs by direct measurement in chemotherapy plastic bags using a handheld Raman spectrometer, Talanta 196 (2019) 376–380, http://dx.doi.org/10.1016/j.talanta.2018.11.062.
[21] C. Bazin, V. Vieillard, A. Astier, M. Paul, Implementation of real-time identification analysis and quantification of chemotherapies preparations with a Multispec® analyser, Ann. Pharm. Fr. 72 (2014) 33–40, http://dx.doi.org/10.1016/j.pharma.2013.09.006.
[22] L.M.M. Le, B. Kégl, A. Gramfort, C. Marini, D. Nguyen, M. Cherti, S. Tfaili, A. Tfayli, A. Baillet-Guffroy, P. Prognon, P. Chaminade, E. Caudron, Optimization of classification and regression analysis of four monoclonal antibodies from Raman spectra using collaborative machine learning approach, Talanta 184 (2018) 260–265, http://dx.doi.org/10.1016/j.talanta.2018.02.109.
[23] F. Bonnier, H. Blasco, C. Wasselet, G. Brachet, R. Respaud, L.F.C.S. Carvalho, D. Bertrand, M.J. Baker, H.J. Byrne, I. Chourpa, Ultra-filtration of human serum for improved quantitative analysis of low molecular weight biomarkers using ATR-IR spectroscopy, Analyst 142 (2017) 1285–1298, http://dx.doi.org/10.1039/c6an01888b.
[24] K.H. Liland, A. Kohler, N.K. Afseth, Model-based pre-processing in Raman spectroscopy of biological samples, J. Raman Spectrosc. 47 (2016) 643–650, http://dx.doi.org/10.1002/jrs.4886.
[25] L.C. Lee, C.Y. Liong, A.A. Jemain, Partial least squares-discriminant analysis (PLS-DA) for classification of high-dimensional (HD) data: a review of contemporary practice strategies and knowledge gaps, Analyst 143 (2018) 3526–3539, http://dx.doi.org/10.1039/c8an00599k.
[26] Z. Farhane, F. Bonnier, H.J. Byrne, Monitoring doxorubicin cellular uptake and trafficking using in vitro Raman microspectroscopy: short and long time exposure effects on lung cancer cell lines, Anal. Bioanal. Chem. 409 (2017) 1333–1346, http://dx.doi.org/10.1007/s00216-016-0065-0.
[27] S.K. Paidi, S. Siddhanta, R. Strouse, J.B. McGivney, C. Larkin, I. Barman, Rapid identification of biotherapeutics with label-free Raman spectroscopy, Anal. Chem. 88 (2016) 4361–4368, http://dx.doi.org/10.1021/acs.analchem.5b04794.
[28] M.T. Rosado, M.L.T.S. Duarte, R. Fausto, Vibrational spectra of acid and alkaline glycine salts, Vib. Spectrosc. 16 (1998) 35–54, http://dx.doi.org/10.1016/S0924-2031(97)00050-7.
[29] M. Saggu, J. Liu, A. Patel, Identification of subvisible particles in biopharmaceutical formulations using Raman spectroscopy provides insight into polysorbate 20 degradation pathway, Pharm. Res. 32 (2015) 2877–2888, http://dx.doi.org/10.1007/s11095-015-1670-x.
[30] J.A. Seo, A. Hédoux, Y. Guinet, L. Paccou, F. Affouard, A. Lerbret, M. Descamps, Thermal denaturation of beta-lactoglobulin and stabilization mechanism by trehalose analyzed from Raman spectroscopy investigations, J. Phys. Chem. B 114 (2010) 6675–6684, http://dx.doi.org/10.1021/jp1006022.
[31] J.K. Lim, Y. Kim, S.Y. Lee, S.W. Joo, Spectroscopic analysis of l-histidine adsorbed on gold and silver nanoparticle surfaces investigated by surface-enhanced Raman scattering, Spectrochim. Acta - Part A Mol. Biomol. Spectrosc. 69 (2008) 286–289, http://dx.doi.org/10.1016/j.saa.2007.05.007.
[32] H.J. Byrne, P. Knief, M.E. Keating, F. Bonnier, Spectral pre and post processing for infrared and Raman spectroscopy of biological tissues and cells, Chem. Soc. Rev. 45 (2016) 1865–1878, http://dx.doi.org/10.1039/c5cs00440c.
[33] L.M.M. Lê, M. Berge, A. Tfayli, J. Zhou, P. Prognon, A. Baillet-Guffroy, E. Caudron, Rapid discrimination and quantification analysis of five antineoplastic drugs in aqueous solutions using Raman spectroscopy, Eur. J. Pharm. Sci. 111 (2018) 158–166, http://dx.doi.org/10.1016/j.ejps.2017.09.046.
[34] L. Carrez, L. Bouchoud, S. Fleury-Souverain, C. Combescure, L. Falaschi, F. Sadeghipour, P. Bonnabry, Reliability of chemotherapy preparation processes: evaluating independent double-checking and computer-assisted gravimetric control, J. Oncol. Pharm. Pract. 23 (2017) 83–92, http://dx.doi.org/10.1177/1078155215620001.
[35] M. Savelli, M. Roche, C. Curti, C. Bornet, P. Rathelot, M. Montana, P. Vanelle, Methods to control anticancer chemotherapy preparations ranked by risk analysis, Pharmazie 73 (2018) 251–259, http://dx.doi.org/10.1691/ph.2018.7205.

4.4 Evaluating Silicon Internal Reflection Element (Si IRE) disposable ATR slides for quantification and discrimination of mAbs compared to standard ATR-FTIR

4.4.1 Context and motivation

This study was performed simultaneously to the investigation of Raman spectroscopy for analysis of mAbs therapeutic solutions.

It has been clearly demonstrated that mAbs in solution weakly contribute to spectra and therefore AQC is solely performed based on excipients contributions. ATR-FTIR was also applied to AQC of mAbs from air dried drops using mAbs preparations in the therapeutically used concentration range:

Firstly, the analysis has been performed with standard ATR multireflection diamond crystal.

Secondly, micro-fabricated disposable Silicon internal reflection element (Si IRE) slides were evaluated. Si IRE initially developed for analysis of human serum for diagnosis purposes [129], they can also be used for other liquid samples. It has been designed to contain four samples area; one to record the background spectrum and the remaining three area to allow triplicate measurement of samples as seen in Figure 33.

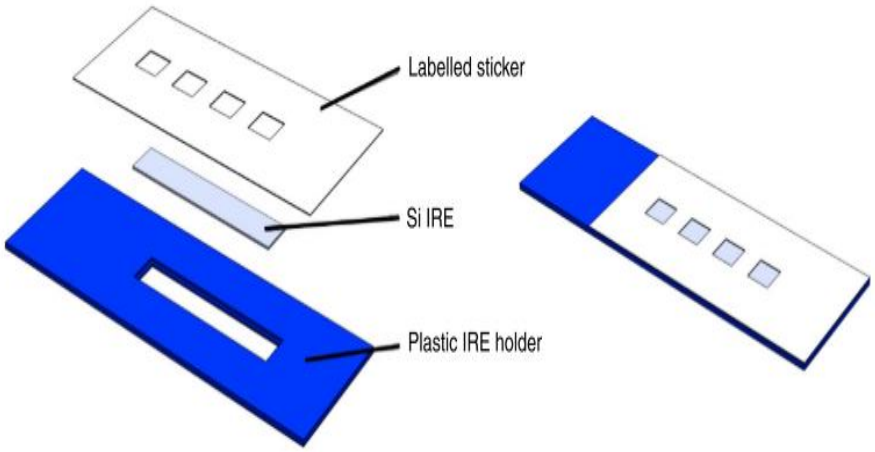


Figure 33. Silicon internal reflection element (Si IRE) are sandwiched between a 3D printed plastic holder and a medical grade labelled sticker [129].

Si IRE enables rapid preparation of many samples at one time and then these slides can be fitted on the IR instrument, thereby enables high throughput analysis.

4.4.2 Materials and Methods

The commercial formulations of mAbs and the concentration ranges used are the same as the Rama study.

4.4.2.1 ATR-FTIR analysis

IR spectra have been obtained using Frontier spectrometer (PerkinElmer, France) over the range 400 – 4000 cm^{-1} with a spectral resolution of 2 cm^{-1} using the two set ups. A background was acquired (4 scans) and ratioed with the sample spectra by the software (Spectrum, Perkin Elmer):

a) A multi-reflection (n = 10) Attenuated Total Reflectance (ATR) diamond accessory (Eurolabo, France). 2 µL drops were deposited directly on the diamond crystal and allowed to air dry prior analysis. For mAbs prepared in 0.9% NaCl at 5 different concentrations, 5 drops have been measured for each concentration tested, 3 spectra recorded each time for a total of 75 spectra recorded for each antibody.

b) Si IRE slides have been placed in ATR accessary by taking out the diamond compartment. 3 drops have measured for each concentration, 5 spectra have been recorded for each drop giving a total of 75 spectra for each molecule.

4.4.2.2 Data handling

At first data has been subjected to EMSC then quantitative analysis has been obtained using 100-fold LKOCV model of PLSR at the fingerprint region 600 - 1800 cm^{-1}. 2/3 of the data set has been used for calibration and 1/3 for validation. The out of PLSR is evaluated using linear regression (R^2), RMSECV and regression coefficient.

The discriminant analysis performed using PLSDA on data subjected to EMSC followed by Lieber correction and vector normalisation. The out-put of PLSDA is in the form of a confusion matrix that enables calculation of specificity and sensitivity of classification. Regression coefficient of PLSDA gives informations about the variables on which discrimination was based on.

4.4.3 Results

4.4.3.1 Spectral characterisation by ATR-FTIR and Si IRE-ATR

Figure 34 presents ATR-FTIR spectra recorded from the concentrated stock solutions after air drying. The four commercial formulations (ERBITUX®, TRUXIMA®, ONTRUZANT® and AVASTIN®) contain excipients added during the manufacturing process for different purposes. IR spectra results from combined contributions of the proteins characteristic bands and excipients bands. Proteins bands can be observed at approximately: 1635 cm^{-1} (amide I), 1539 cm^{-1} (amide II), 1451 cm^{-1} (CH_2 deformation), 1391-1410 cm^{-1} (CH_2 and CH_3 stretching of glycine or alanine), 1340 cm^{-1} (CH_2 wagging of glycine or alanine), 1235 – 1255 cm^{-1} (amide III), 1144 cm^{-1} (NH_3 rocking), 941 cm^{-1} and 988 cm^{-1} (C-C stretching) and 660 cm^{-1} (tyrosine) [126].

Glycine is the excipient presents in ERBITUX® formula has characteristic bands at 895 cm^{-1} (C-C stretching), 1033 cm^{-1} (C-N stretching), 1117 cm^{-1} (NH_3 rocking), 1330 cm^{-1} (CH_2 wagging), 1410 cm^{-1} (CH_2 and CH_3 stretching, O=C-O stretching) and 1443 cm^{-1} (CH_2 deformation) [130]. Polysorbate that found in ERBITUX®, ONTRUZANT® and AVASTIN® has characteristic peaks shown at 838 cm^{-1} and 941 cm^{-1} due to CH_2 rocking and OH deformation, respectively [131]. Histidine and trehalose are presents in ONTRUZANT® and AVASTIN® formulations have characteristic bands at 841 cm^{-1} (C-C stretching), 912 cm^{-1} (C-C stretching), 1078 cm^{-1} (C-O stretching), 1451 cm^{-1} (CH_2 wagging) [132].

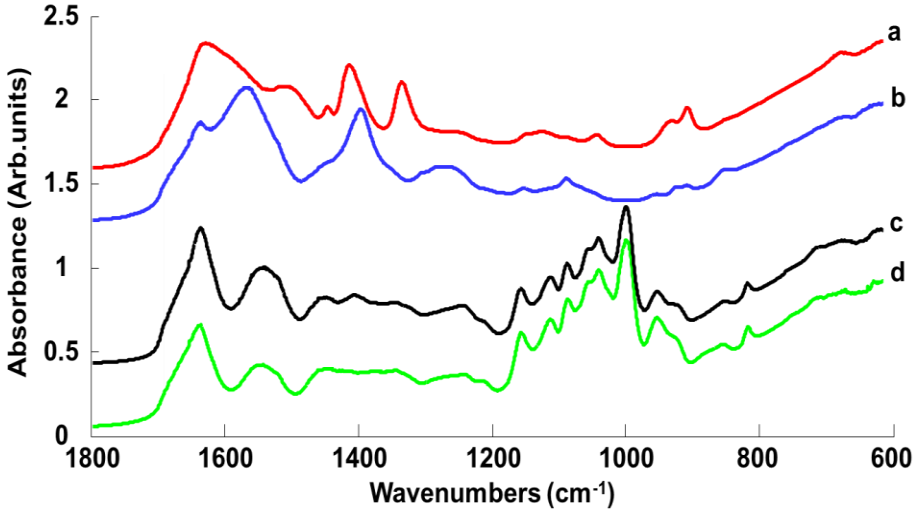


Figure 34. Mean ATR-FTIR spectra recorded from commercial stock solutions of: ERBITUX® 5 $g{\cdot}L^{-1}$ (a), TRUXIMA® 10 $g{\cdot}L^{-1}$ (b), ONTRUZANT® 21 $g{\cdot}L^{-1}$ (c) and AVASTIN® 25 $g{\cdot}L^{-1}$ (d). Spectra are offset for clarity

Figure 35 presents mean IR spectra obtained by Si IRE of the highest concentration recorded for each formulation. The spectra show high similarity in spectral features with those obtained by multireflection diamond in Figure 34, but weaker bands intensities have been observed with Si IRE-ATR.

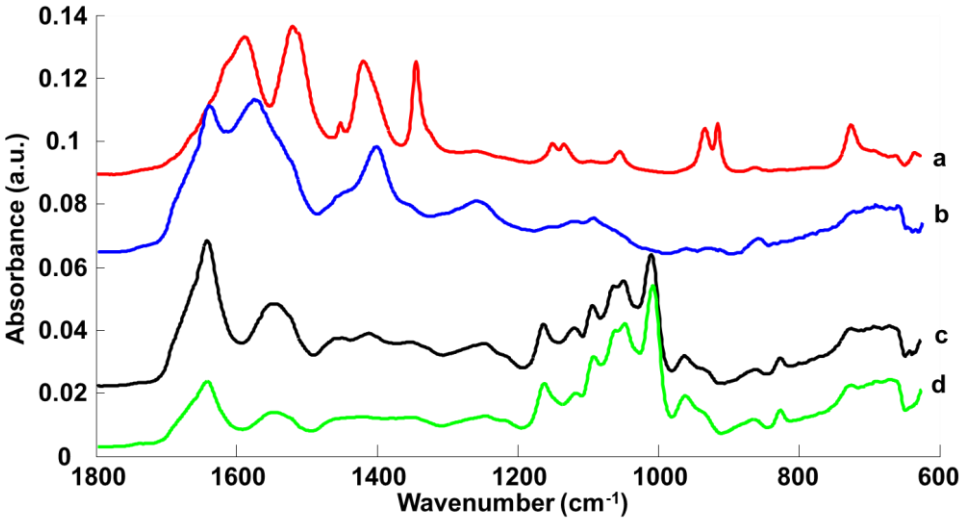


Figure 35. Mean ATR-FTIR spectra obtained by Si IRE recorded from solutions prepared in 0.9% NaCl solution: ERBITUX® 4 g·L^{-1} (a), TRUXIMA® 4 g·L^{-1} (b), ONTRUZANT® 4 g·L^{-1} (c) and AVASTIN® 15 g·L^{-1} (d). Spectra are offset for clarity

4.4.3.2 Quantification of mAbs by ATR-FTIR and Si IRE-ATR

Figure 36 illustrates the quantitative potential of ATR-FTIR for mAbs using the two set ups (Figure 36A and 36B). The example presented here is mean IR spectra of ONTRUZANT® at 4 g·L^{-1}, 3 g·L^{-1}, 2 g·L^{-1}, 1 g·L^{-1} and 0.5 g·L^{-1} prepared in 0.9% NaCl solution. The decrease in peak's intensity is directly proportional to the decrease in concentration making quantification possible with ATR for those proteins.

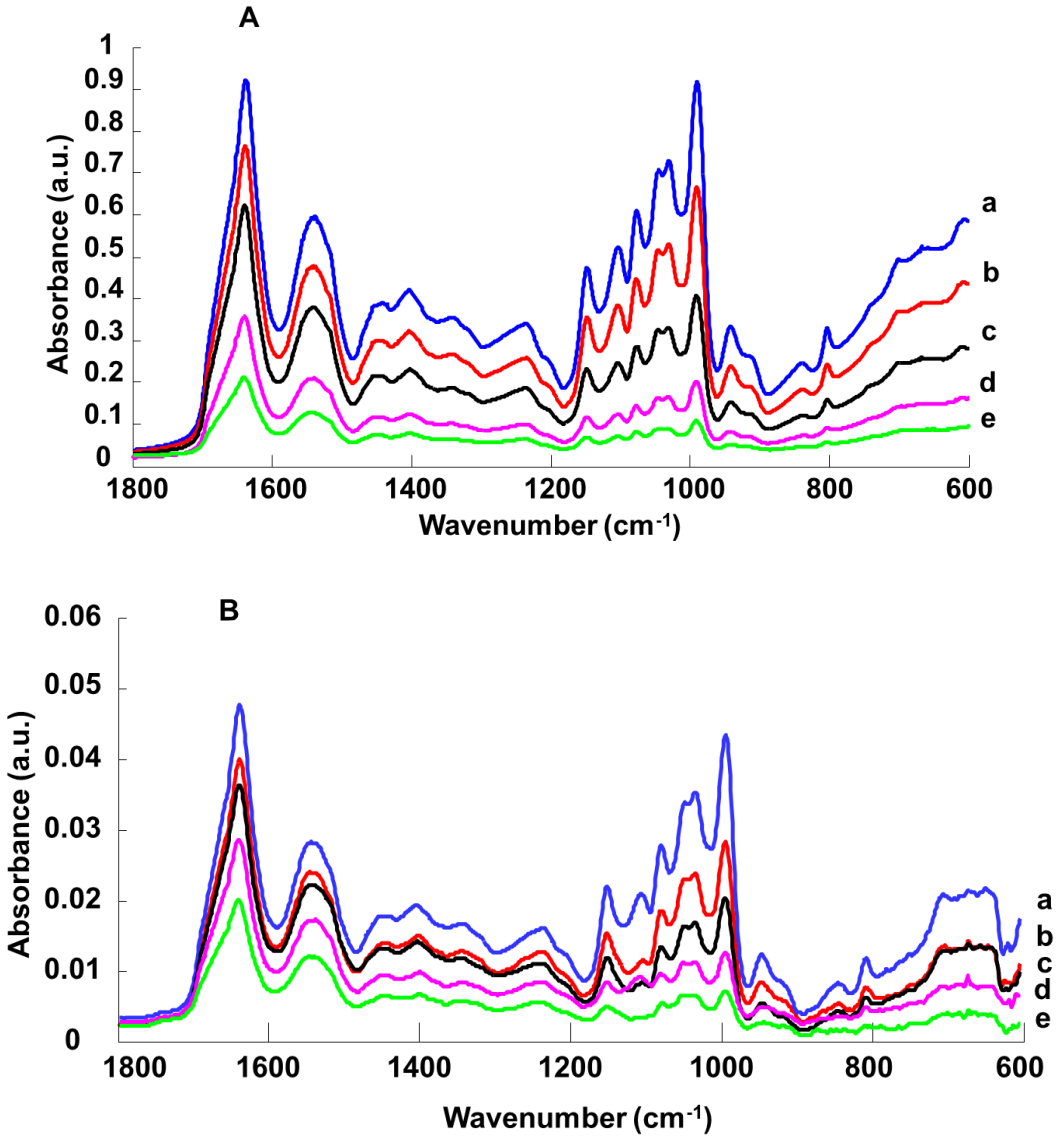


Figure 36. Mean IR spectra in the fingerprint region of ONTRUZANT® in 0.9% NaCl following serial dilution using: A) ATR-FTIR and B) Si IRE-ATR. Spectra ordered from top to the bottom corresponding to 4 $g{\cdot}L^{-1}$, 3 $g{\cdot}L^{-1}$, 2 $g{\cdot}L^{-1}$, 1 $g{\cdot}L^{-1}$ and 0.5 $g{\cdot}L^{-1}$

The quantitative approach has been evaluated using PLSR on ATR data obtained from the two set ups. Figure 37I presents PLSR results obtained for ONTRUZANT® in 0.9% NaCl using ATR-FTIR. Figure 37Ia presents a decrease in RMSECV as a function number of LVs where after 4 LVs there is no marked change is observed. Therefore, the linear regression is obtained using 4 LVs to avoid overfitting of the quantitative model. Figure 37Ib presents the linear regression obtained with R^2 =1 and RMSECV of 0.0013 $g{\cdot}L^{-1}$. Figure 37II presents PLSR

obtained for Si IRE-ATR data. From Figure 37IIa, 5 LVs were enough to construct the regression model which resulted in R^2 = 0.9926 (Figure 37IIb) and RMSECV = 0.1062 g·L^{-1}.

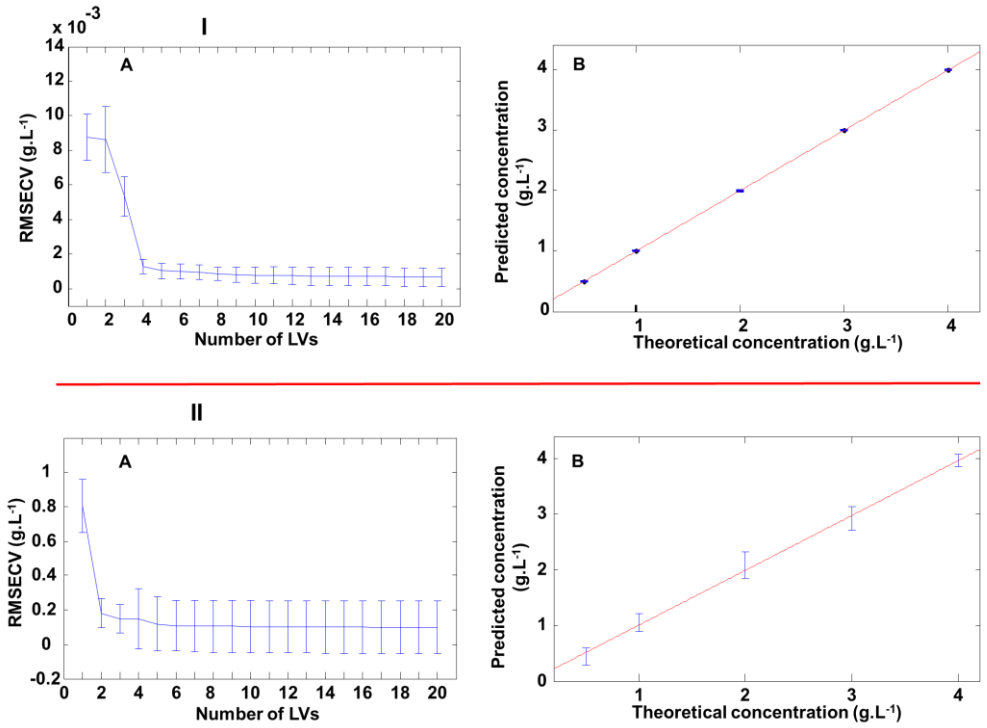


Figure 37. PLSR analysis performed on ATR-FTIR spectra collected from ONTRUZANT® in 0.9% NaCl using standard multireflection diamond crystal (I) and Si IRE (II). A) RMSECV and B) Regression plot

Figure 38 presents the regression coefficients of PLSR obtained for the 4 tested mAbs formulations with both set ups used. It represents the spectral features used in the quantitative model. Regression coefficients in Figure 38A and 38B display strong similarities with the spectra collected from stock solutions (Figure 34) or highest concentration analysed for Si IRE (Figure 35) with a mixed contribution from antibodies and excipients.

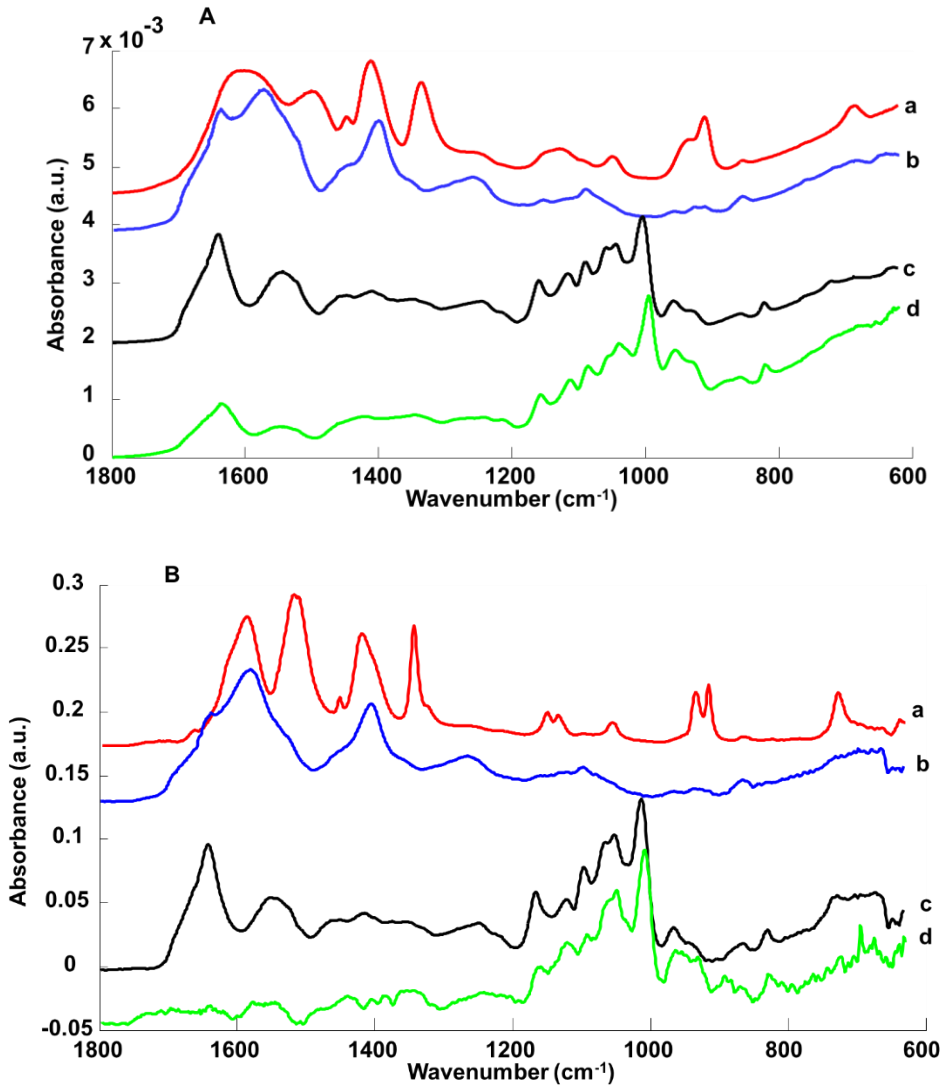


Figure 38. Regression coefficients of PLSR of ATR-FTIR (I) and (II) Si IRE-ATR for: a) ERBITUX®, b) TRUXIMA®, c) ONTRUZANT® and d) AVASTIN®. Spectra are offset for clarity

Table 4 presents a summary of PLSR results for the 4 tested mAbs formulations obtained by the two tested setups:

- For standard multireflection diamond crystal ATR, the obtained R^2 is greater than 0.99 which is a gauge for the goodness of the regression model. ONTRUZANT® formula delivered the lowest RMSECV value while AVASTIN® has the highest value of 0.3202 $g{\cdot}L^{-1}$.

- For Si IRE ATR; the quantification by PLSR delivered acceptable results with R^2 is greater than 0.88 and large %error. The lowest error obtained by Si IRE is 1.3 times more than the highest percentage obtained by diamond for ONTRUZANT®.

For all tested mAbs formulations, ATR-FTIR delivered quantification results with relatively small number of LVs. The highest error observed with Si IRE can be attributed to non-reproducible positioning between measurements.

Table 4. PLSR results obtained for the 4 mAbs formulations by ATR-FTIR and Si IRE-ATR

Brand	mAb	Standard diamond ATR				Si IRE ATR			
		LVs	R^2	RMSECV ($g \cdot L^{-1}$)	%RMSECV	LVs	R^2	RMSECV ($g \cdot L^{-1}$)	%RMSECV
ERBITUX®	CTX	5	0.9981	0.0463	2.2	4	0.9668	0.1843	8.8
TRUXIMA®	RTX	4	0.9996	0.0176	0.84	4	0.9661	0.2148	10.2
ONTRUZANT®	TRS	4	1	0.0013	0.06	5	0.9924	0.1062	5
AVASTIN®	BEV	4	0.9953	0.3202	3.9	6	0.8859	1.9290	23.5

4.4.3.3 Discrimination of mAbs formulations

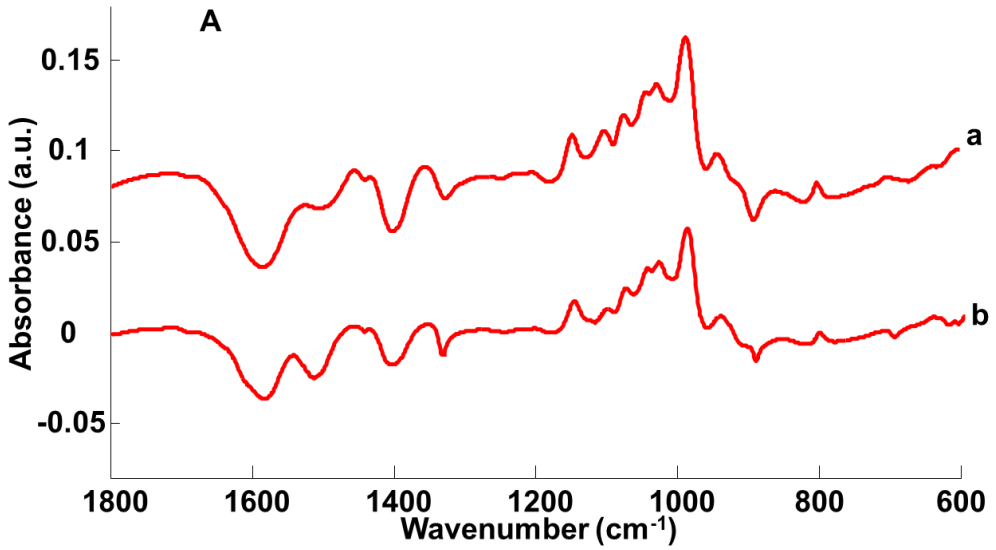
PLSDA has been performed on ATR-FTIR data of mAbs formulations in 0.9% NaCl solutions recorded by the two set ups. Specificity and sensitivity have been calculated from confusion matrix obtained using 3 and 5 LVs for ATR-FTIR and Si IRE-ATR. PLSDA has delivered 100% specificity and sensitivity on discrimination between the 4 mAbs formulations (Table 5).

Table 5. Specificity and sensitivity % obtained by PLSDA for IR data pre-processed with EMSC, Lieber correction and vector normalization

Brand	mAbs	Standard ATR (LVs =3)		Si IRE-ATR (LVs =5)	
		Specificity %	Sensitivity %	Specificity %	Sensitivity %
ERBITUX®	CTX	100	100	100	100
TRUXIMA®	RTX	100	100	100	100
ONTRUZANT®	TRS	100	100	100	100
AVASTIN®	BEV	100	100	100	100

Regression coefficients presented in Figure 39 highlight the spectral features used for discrimination between the 4 tested mAbs formulations. The first regression coefficient (Figure 39Aa and 39Ba) displays spectral regions at 988 cm^{-1} and 1149 cm^{-1} are identified for proteins while bands at 923 cm^{-1}, 977 cm^{-1}, 1029 cm^{-1} and 1075 cm^{-1} are due to trehalose in ONTRUZANT® and AVASTIN® formulations.

Bands at 896 cm^{-1}, 1104 cm^{-1}, 1329 cm^{-1},1412 cm^{-1} in the in Figure 39Ab and 39Bb are identified for glycine in ERBITUX® whereas slightly shifted bands at 665 cm^{-1}, 1490 cm^{-1} and 1605 cm^{-1} are being identified for proteins. According to the assigned bands in the regression coefficients; the discrimination between mAbs has been based on both spectral bands from mAbs and excipients.



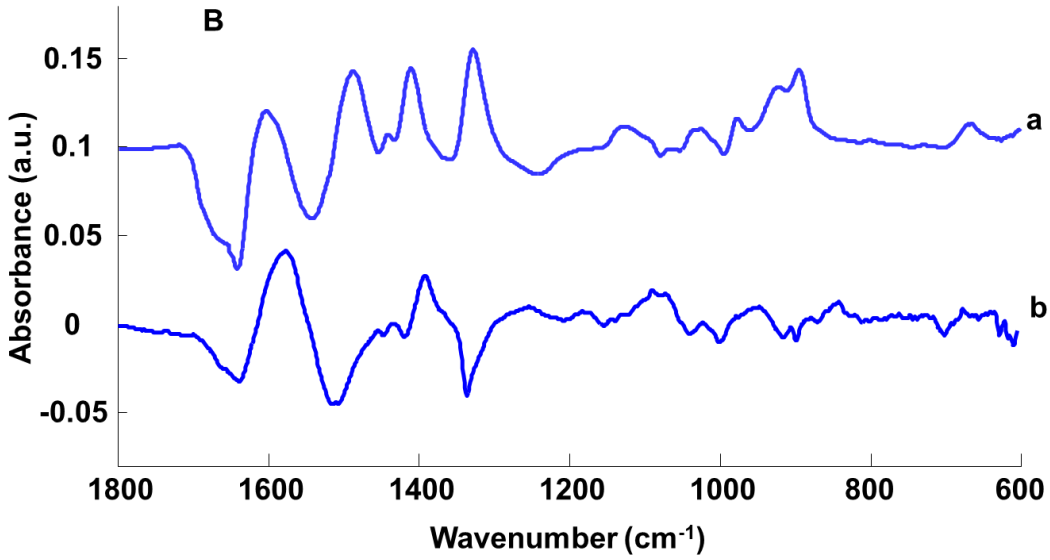


Figure 39. Regression coefficients of the PLSDA. A) the first regression coefficient obtained by a) standard diamond ATR and b) Si IRE-ATR. B) the second regression coefficient obtained by a) standard diamond ATR and b) Si IRE-ATR. Spectra are offset for clarity

4.4.4 Discussion and perspectives

In this study, mAbs are formulated with different excipients of different nature which are sugars (trehalose), amino acids (glycine and histidine), lipids (polysorbate 20 and 80) and surfactant (citric acid). Each type of those molecules has its strong IR spectral characteristics that can be identified in the formulated mAbs solutions (Figure 34 and 35).

ATR-FTIR analysis of mAbs in this study is based both on proteins features and excipients while Raman is based only excipients. Although, one can consider that mAbs are peptides in nature and being produced from different sources (chimeric or humanised) but at the end the peptide nature is consisting of the same amino acids. The difference in spectral features of the therapeutic peptides might resides in very small part in their large chemical structure which is presented during the manufacturing process for example at the glycosylation step which is done for stability purposes and to retain their therapeutic efficacy. The IR spectra recorded from the concentrate have exerted minor variations in the spectral features between the tested mAbs molecules (Figure 32) which might be attributed to different orientation and geometry of functional groups in amino acids sequences.

ATR-FTIR enabled performing analysis based on data recorded after air drying. Before each drop the crystal should be cleaned which at hospital might be an extra task to do. Although collaboration with university of Glasgow has provided Si IRE slides for ATR recording, those slides have been tested for diagnosis of brain cancer. No cleaning is needed when using Si IRE and the slides are designed for single use, therefor enhance the speed of analysis.

The two ATR setups used here delivered good quantification and discrimination of mAbs, but Si IRE-ATR is associated with larger RMSECV than standard diamond ATR-FTIR. Si IRE slides are a promising approach for large scale analysis but still at the development stage. Few parameters need to be characterised concerning the hydrophobicity of the Si IRE surface and its effect on the drop size and the spreading. Therefore, further improved based on those preliminary studies, the approach might provide good alternative tool when Raman analysis in solution is not possible.

4.4.5 Conclusion

Application of ATR-FTIR spectroscopy in the area of AQC can play very strong role in identification of highly similar molecules as the technique is very sensitive to minor change in the chemical structure. Excipients present in mAbs formulations has played as a strong internal standard for identification, but the case will be different, and the risk of analysis will increase when the same types of excipients are present in formulations. Although, ONTRUZANT® and AVASTIN® contain trehalose as excipient in their formulations, the discrimination can be obtained because of ratio between proteins / excipients plus other excipients present in each formulation. The case of IR and Raman for discrimination might be different if mAbs formulations contain the same concentration of excipients which is a point to validate for future work.

5. DIRECT CONFOCAL RAMAN ANALYSIS IN INFUSION BAGS FOR INCREASED SAFETY OF PERSONNEL

5.1 Context and motivation

Although not mandatory, AQC is implemented in most of the hospitals inside centralised preparation units. Everyday 100s of solutions are analysed for validation before release for administration. All the current protocols require to withdraw a fraction of the solutions from the infusion bags for analysis which can pose cytotoxic risk to the working staff as well as the working environment. Two types of instruments are used in centralised units either separation techniques such as HPLC coupled to different detectors systems (UV-vis) or FIA which can enhance the speed of analysis [60,133]. Moreover, FIA instruments using VS, UV-IR or UV-Raman [134] are used in few preparation units.

Although, UV/vis is a powerful technique for quantification with high precision, Raman can provide discrimination of structurally similar molecules. In literature, some of the published work on UV-Raman, results are discussed considering the system as one compartments and no detailed informations concerning the sensitivity of Raman for delivering quantification and discrimination [73,74] while in other work it is mentioned that electronic library is used to match spectra of solvent and drugs but still the studies lack of discussion in spectral details [75]. While IR and Raman are generally accepted for AQC but still not used at full potential. Notably the confocality during Raman analysis is not yet considered.

Direct AQC of chemotherapeutic preparations in their infusion bags can help to avoid such toxicities to the working staff. Few studies have been done with inverted Raman system for analysis through glass vials or using Raman with optical fibre probes for analysis of chemotherapeutic solutions contained in elastomeric infusion pumps. Handheld Raman for analysis through glass vials and plastic infusion bags is also found. However, in literature limited studies for investigation of the potential of Raman spectroscopy for direct AQC in infusion bags are found. More specifically no study has been published using confocal Raman micro-spectroscopy (CRM).

This chapter presents a study conducted with CRM for direct analysis of chemotherapeutic drugs in infusion bags. In brief the general protocol used can be presented as:

a) Drugs

Raman confocal microscopy is used for AQC of methotrexate (MTX), 5-fluorouracil (5-FU) and gemcitabine (GEM) have been prepared in 5% glucose bag at the clinically used therapeutic concentrations. The three drugs are chosen according to the frequency of prescribing and preparation in UBCO unit. They are belonging to two different families of anticancer drugs; folic acid analogue (MTX), pyrimidine analogues drugs (5-FU and GEM), their chemical structures are presented in Figure 40.

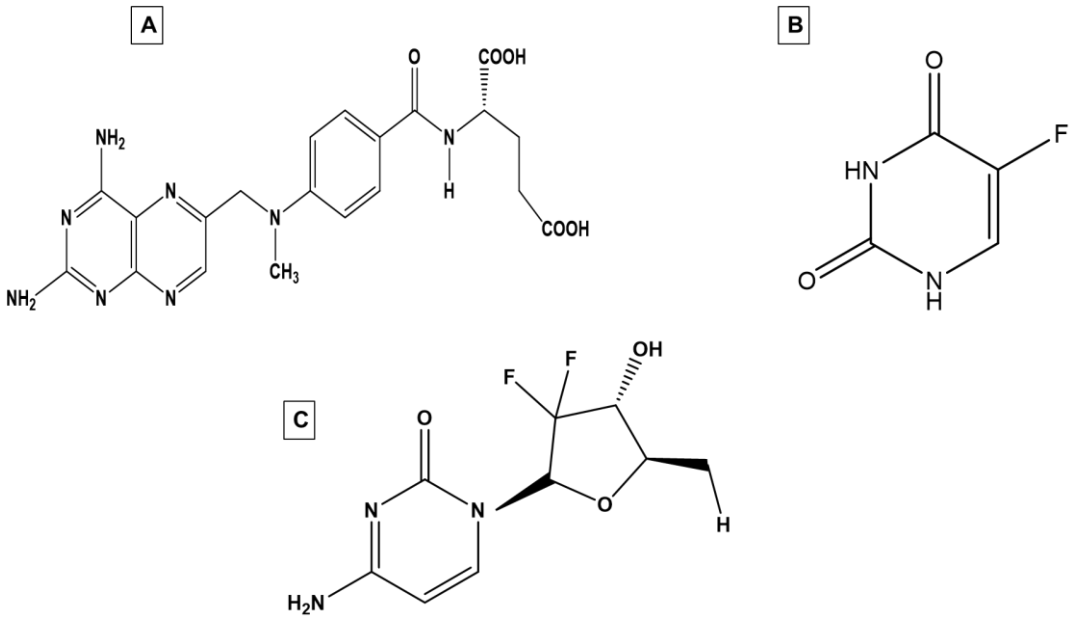


Figure 40. Chemical structures of: A) MTX, B) 5-FU and C) GEM

b) Experimental design

The main limitation of working with infusion bags is the inaccuracy of the stated volume in the bag, so that the final concentration of the commercial drug formulation inside the bag can't be assured thus possibly biasing the application of multivariate analysis such as PLSR. Therefore, reliable concentration usable as reference values have been collected using UV/vis spectrometry. The tested drugs have specific absorbance; for MTX, 5-FU and GEM, the absorbance readings have been taken at 303 nm, 266 nm and 269 nm (Figure 41) and can have robust linear model for calibration curve (Figure 42). The calibration curves have been prepared absorbance reading obtained from triplicate preparations for each concentration in the range used for its construction.

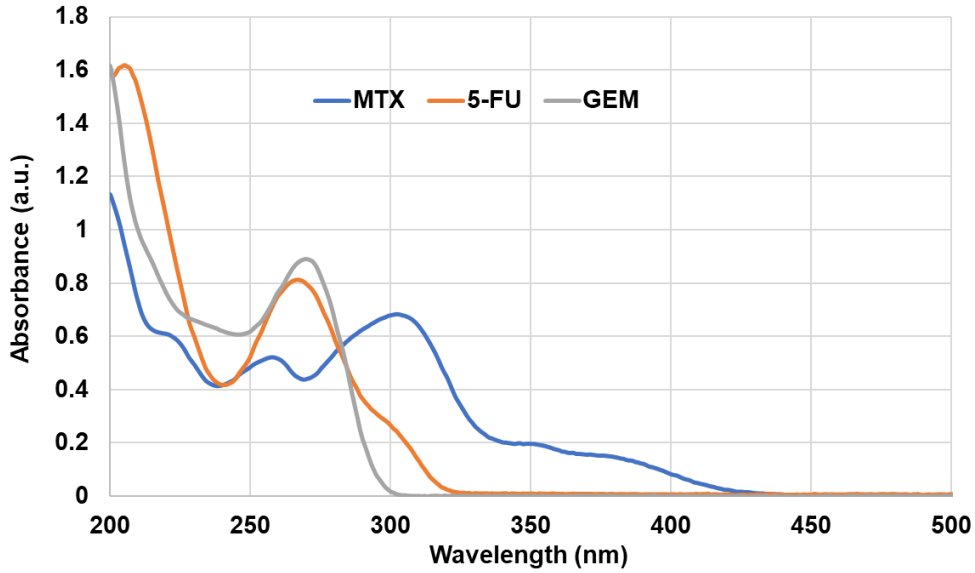


Figure 41. Absorbance spectra for: A) MTX, B) 5-FU and C) GEM

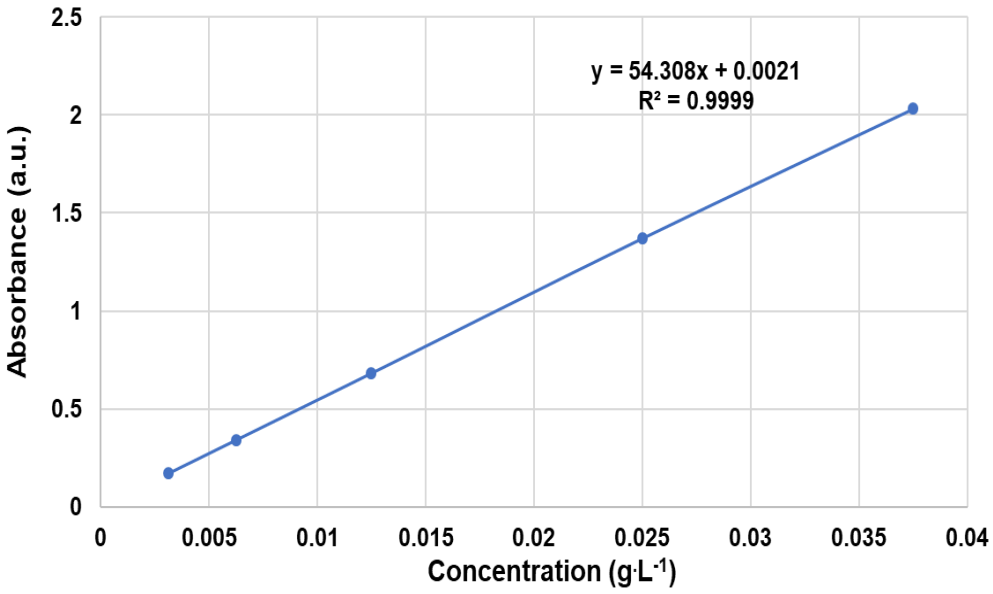


Figure 42. Calibration curve of MTX on the concentration range

Figure 43 illustrates the protocol used. Preparation of the tested drugs inside the bag has been started from the highest concentration and subsequent lower concentrations by serial dilution with 5% glucose. After each preparation inside the bag: 1) small volume (~100 µL) has been withdrawn and suitable dilution made for absorbance reading by UV/vis and then concentration is calculated from the calibration curve for each drug. 2) the bag is fitted on the stage of CRM for recording of spectra.

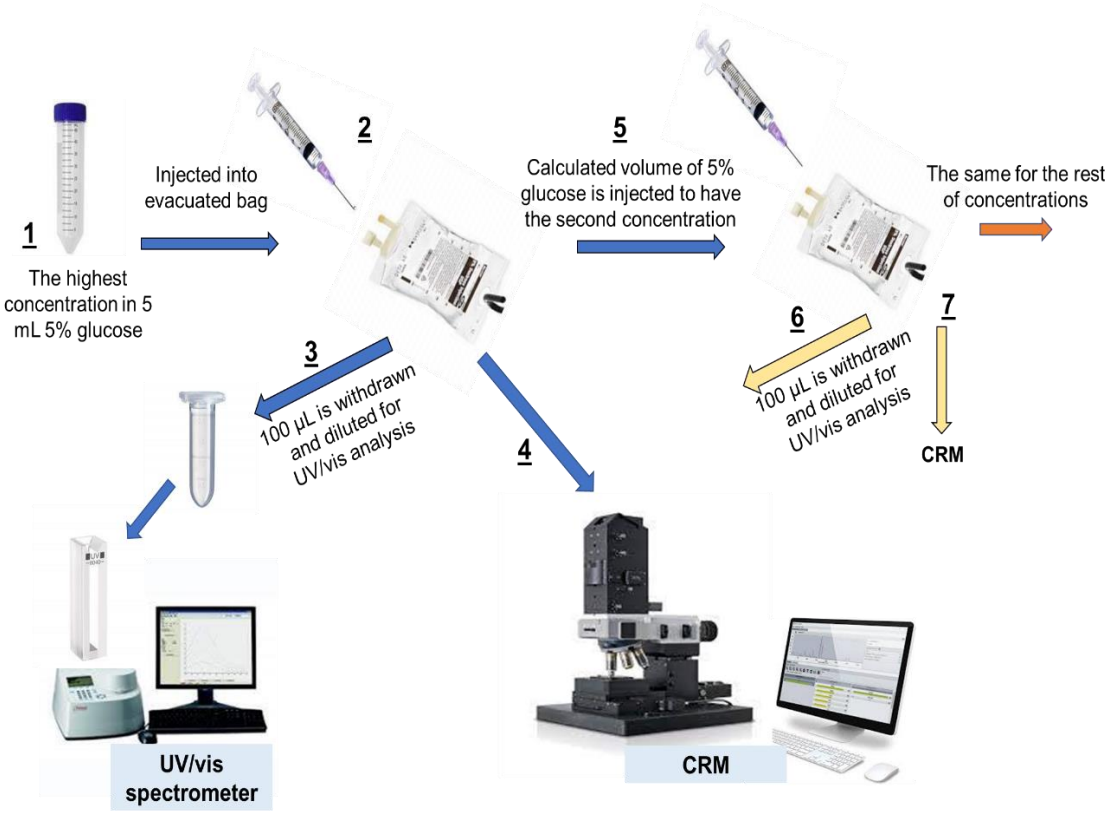


Figure 43. Illustrates the protocol used for preparation of chemotherapeutic drugs inside the bag and analysis by UV/vis spectrometry and CRM

c) Raman data collection

The automatic advantage of the confocal Raman microscope of Alpha300R micro-spectrometer (WITec, Germany) providing Z profiling at different depths and Z line scan using a finite number of µm selected to collect spectra.

The microscope has been focused on the surface and the position has set to zero and automatically set to record spectra every 200 µm using Z line scan, thereby spectra have been obtained at -300 µm, -500 µm, -700 µm and -900 µm. The collected spectra enable to know the optimum depth that can be used for analysis without or the least contribution from the bag material. This chapter contains two parts of work done with 2 laser lines:

- The first part in the paper (*In situ Analytical Quality Control of chemotherapeutic solutions in infusion bags by Raman spectroscopy, submitted to Talanta in October 2020*) has been performed using 532 nm excitation laser with 20 mW energy on the sample and grating 300 lines/mm.
- The second part presents results and discussion of results obtained by 633 nm laser with energy of the sample of about 20 mW and grating 600 lines/mm.

5.2 PUBLICATION 4: In situ Analytical Quality Control of chemotherapeutic solutions in infusion bags by Raman spectroscopy

Alaa A. Makki[a, b], Suha Elderderi[a, b], Victor Massot[c], Renaud Respaud[d], Hugh. J. Byrne[e], Clovis Tauber[f], Dominique Bertrand[g], Elhadi Mohammed[h], Igor Chourpa[a], Franck Bonnier [a,*]

[a] Université de Tours, EA 6295 Nanomédicaments et Nanosondes, 31 avenue Monge, 37200 Tours, France

[b] University of Gezira, Faculty of Pharmacy, Department of Pharmaceutical Chemistry, P.O. Box 20, 21111 Wad Madani, Sudan

[c] CHU de Tours, Unité de Biopharmacie Clinique Oncologique, Pharmacie, France.

[d] Université de Tours, UMR 1100, CHRU de Tours, Service de Pharmacie, F-37032 Tours, France

[e] FOCAS Research Institute, TU Dublin, City Campus, Kevin Street, Dublin 8, Ireland

[f] Université de Tours, INSERM UMR 1253 iBrain, 37000 Tours, France.

[g] Data_Frame, 25 rue Stendhal, 44300 Nantes, France

[h] University of Gezira, Faculty of Pharmacy, Medicinal and Aromatic Plants Research Center (MAPRC), P.O. Box 20, 21111 Wad Madani, Sudan

Corresponding author:

Dr. Franck Bonnier

University of Tours, faculty of pharmacy

EA 6295 NMNS

31 Avenue Monge

37200 Tours, France

Key words:

Raman Confocal micro-spectroscopy, Chemotherapeutics, non-invasive analysis, analytical quality control

Abstracts

Analytical Quality Control (AQC) in centralised preparation units is a common procedure relying on the identification and quantification of the prepared chemotherapeutic solutions for safe administration to patients. The use of Raman spectroscopy for AQC has gained much interest however it remains coupled to flow injection analyser (FIA) requiring withdrawal of the solution for analysis. In addition to current needs for faster and more cost-effective analysis, the risk of exposure to the toxic molecules manipulated daily for staff is a serious concern to address. Raman instruments, for instance Confocal Raman microscope (CRM), could enable direct analysis (non-invasive) for AQC directly in infusion bags. In this study, 3 anticancer drugs, methotrexate (MTX), 5-fluorouracil (5-FU) and gemcitabine (GEM) have been selected to highlight the potential of CRM for withdrawal free analysis. Solutions corresponding to clinical range of each drug were prepared in 5% glucose and data collected from infusion bags placed under the Raman microscope. Firstly, 100% discrimination has been obtained by Partial Least Square Discriminant Analysis (PLS-DA) validating the identification of drugs can be performed. Secondly, using Partial Least Square Regression (PLSR) quantitative analysis was performed with mean % error of predicted concentrations of respectively 3.31%, 5.54% and 8.60% for MTX, 5-FU and GEM. These results are in accordance with the 15% acceptance criteria used for the current clinical standard technique, FIA, and the Limits of Detection for all drugs were determined to be substantially lower than the administered range, thus putting emphasis on the relevancy to further investigate the potential of confocal Raman spectroscopy for direct analysis of chemotherapeutic solutions.

1. Introduction

Increasingly, preparation of chemotherapeutic drugs is centralised in dedicated units in hospitals, to reduce cost and waste generated during reconstitution of individualised doses, but also to increase the security in the process from the receipt of commercial stock products (highly concentrated liquid or powder) to their release to patient bedsides [1]. Meanwhile, in recent years, concepts of personalised medicine have considerably increased the complexity and precision of prescriptions for, for example, complex anticancer treatment protocols.

The control of chemotherapy is compulsory with at least double visual inspection (non-analytical control) but there is no consensus on the methods to be applied [2]. Analytical Quality Control (AQC) is one of the potential methodological frameworks and is widely used in large oncology centers for chemotherapeutic preparations because it enables both the qualitative (identification) and quantitative analysis of the solutions assayed [3].

Among the AQC techniques used, chromatographic methods such as high-performance liquid chromatography (HPLC) remains the gold standard for quality control of chemotherapeutic preparations for qualitative and quantitative analysis [3–6]. AQC can be a very time consuming and costly control method (consumables, solvents), although it is expected the analysis is reliable and rapid, allowing prompt release of the treatment without impacting patient planning. Therefore, alternative approaches using vibrational spectroscopic techniques have been developed in recent years to propose cost effective and rapid alternatives to identify and quantify the anticancer drug within their solubilisation matrices [7].

Vibrational spectroscopic techniques, namely infrared (IR) and Raman spectroscopy, are structure specific techniques delivering molecular fingerprints. The techniques are label free, non-invasive and non-destructive, require no separation of chemical species prior to analysis, no sample preparation and as a result they are less demanding, consumables wise (solvent, column, etc.). IR and Raman spectroscopy have several applications in medical, biomedical and biopharmaceutical sciences as well as in forensic medicine [8–17]. In the context of AQC of chemotherapeutic solutions, it has been demonstrated that coupling vibrational techniques with multivariate analysis enables qualitative (identification of drug) and quantitative analysis [18,19].

Originally, the first dedicated instruments commercialised for qualitative and quantitative analysis of chemotherapeutic preparations were performed using a system coupling Fourier transform infrared spectroscopy (FTIR) to UV/vis spectrometry (Multispec® analyser, Microdom, Taverny, France) [20–23]. Despite the well-known limitation due to water

absorbance in the mid-IR region, this flow injection system was used for analysis of liquid samples by Bazin et al. [24] using the most prescribed drugs (n = 35) over 24 months. Although, the technique enabled 97% true recognition of molecules and 99.95% recognition of solvents, difficulties have been encountered in the discrimination of structurally related molecules: anthracyclines (doxorubicin, epirubicin and daunorubicin), oxazophosporines (cyclophosphamide and ifosfamide) as well as monoclonal antibodies (cetuximab, rituximab, trastuzumab and bevacizumab).

More recently, the focus shifted to Raman spectroscopy, considered more suited for liquid samples analysis [25]. A new generation of dedicated system for AQC which combines UV/vis spectrometry with Raman spectroscopy has been commercialised (QCPrep+®, Icônes Service, France). The instrument is also a flow injection analyser, progressively implemented in hospitals for AQC of small volume chemotherapeutic preparations. The method has been validated according to International Conference on Harmonisation (ICH) and resulted in a good quantification as well as identification of tested drugs [26]. Notably, a study conducted over 18 months at the University Hospital of Strasbourg (France) using a QCPrep+® analyser for AQC of 14 molecule-solvent combinations (ifosfamide, cyclophosphamide, doxorubicin, carboplatin, cisplatin, dacarbazine, docetaxel, etoposide, gemcitabine, oxaliplatin, paclitaxel, pemetrexed, vinorelbine) resulted in 99% identification of drugs and solvents while for quantitative analysis 1.52% of the preparations did not match the acceptance criteria, set to be ±15% [27].

Although Raman has great potential to ease the workload of AQC for preparation of chemotherapeutic solutions, one of the rising concerns is the safety of staff members manipulating molecules with carcinogenicity, mutagenicity and teratogenicity [28,29]. Therefore, non-invasive control directly into containers, i.e. without withdrawal and injection into a flow injection analyser, remains a current concern to be addressed.

The literature remains limited on the topic of AQC of chemotherapeutic solutions with Raman spectroscopy with a number of study performed in glass vials [18,30–32]. Glass vials are useful models in research to demonstrate the potential of Raman spectroscopy, but have limited relevancy to support transfer of the technique into clinics, firstly because such glassware is never used to prepare individualised intravenous anticancer solutions, and secondly because transparent glass delivers a considerably different spectral signature to that of polymer or plastic based materials used in hospital infusion bags.

However, In 2014, Bourget et al. [7] documented a study about direct analysis of 5-fluorouracil prepared in elastomeric portable infusion pumps (1.5 - 50 $g{\cdot}L^{-1}$) using a RXN-1 Raman system (Kaiser Optical Systems, Ann Arbor, USA) in which the laser source (785nm) is connected via an optic fibre to the Raman illumination chamber (RIC). More recently, in 2019, a follow up study from Lê et al. reported the AQC of gemcitabine directly in plastic bags using a handheld Raman instrument, in the range of concentrations from 1 – 20 $g{\cdot}L^{-1}$ [33]. These 2 publications clearly highlight the analytical potential of Raman analysis with (trans-) portable devices for transfer to the clinical environment for AQC of chemotherapeutic solutions. However, the literature remains scarce and there is a sparsity of investigations using non-invasive Raman analysis, and notably no reports of application of Confocal Raman Microspectroscopy (CRM), i.e. a Raman microscope, for this purpose, despite it being potentially the instrumental set up delivering the best performance in terms of spectral quality and sensitivity of analysis.

The present study reports the investigation of CRM performed directly in infusion bags for AQC (discriminant and quantitative analysis) of three anticancer drugs (methotrexate, 5-fluorouracil and gemcitabine). Notably the prospects to develop a sensitive, reproducible and automated analytical method will be discussed.

2. Materials and Methods

2.1 Anticancer drugs and samples preparation

5% glucose infusion bags (Baxter, VIAFLO containers 50 mL, USA) and the 3 chemotherapeutic drugs used in this study have been provided through a collaboration with the UBCO unit (Unité de Biopharmacie Clinique Oncologique, Tours, France) that deals with the preparation of individualised chemotherapeutic doses at the University Hospital of Tours (CHU Tours, France).

Methotrexate (Mylan®, 100 $g{\cdot}L^{-1}$) is an antimetabolite that inhibits folic acid synthesis, hence inhibiting DNA synthesis and cell division [34–36]. It is used for the treatment of leukaemias, lymphomas, solid tumours, choriocarcinomas and rheumatoid arthritis [37,38].

5-fluorouracil (Accord®, 50 $g{\cdot}L^{-1}$) is a pyrimidine analogue that leads to DNA and RNA chain termination, and is used for treatment of gastrointestinal cancer, head, neck, pancreatic, colorectal and breast cancers [4,39,40]. Structurally, 5-fluorouracil is similar to uracil but one hydrogen atom is replaced by fluorine atom at carbon number 5 [41].

Gemcitabine (Sandoz®, 40 $g \cdot L^{-1}$) is a pyrimidine analogue used mainly for treatment of pancreatic adenocarcinomas as well as head, neck, breast ovarian and bladder cancers [42–45]. Based on track records of recently prepared solutions at UBCO, therapeutic ranges have been prepared for each drug. Sets of 8 concentrations have been prepared in 5% glucose directly into infusion bags using serial dilution (Table 1)

The highest concentration was prepared in the infusion bag, then 5% glucose was added to dilute the solutions to reach the next targeted concentration. Ultimately, 6 bags were prepared for each drug to enable Raman analysis (see Table 1 for more details). Throughout the study, samples are identified based on the drug contained in infusion bags as MTX (methotrexate), 5-FU (5-fluorouracil) and GEM (gemcitabine).

Table 1: Concentration range analysed

Drug	**Concentration range analysed (n = 6)**
MTX	3 $g \cdot L^{-1}$ – 21 $g \cdot L^{-1}$
5-FU	1 $g \cdot L^{-1}$ – 45 $g \cdot L^{-1}$
GEM	4 $g \cdot L^{-1}$ – 11 $g \cdot L^{-1}$

2.2 UV/vis spectrometric analysis

For each concentration prepared, a small volume has been withdrawn from the infusion bag and analysed with a Genesys 10S UV–vis spectrophotometer (Thermo Scientific, France) to obtain the exact concentration of the solution. For each drug, a calibration curve was constructed at their respective maximum absorbance found at 303 nm (MTX), 266 nm (5-FU) and 269 nm (GEM). The concentrations determined using UV absorbance was later used for the datamining of Raman spectra and to construct the quantitative models (see section 2.4 Data handling).

2.3 Raman spectroscopy analysis

Raman spectra were recorded using an Alpha300R Raman micro-spectrometer (WITec, Germany) equipped with a 532 nm diode laser set up to deliver 20 mW at the sample. The grating with 300 lines/mm was selected. Spectra were collected over the range 300-1800 cm^{-1} thanks to a back illuminated deep depletion charged coupled device (CCD) detector. Every day,

a calibration of the instrument for each laser line has been performed using the silica peak at 521 cm^{-1} prior to data collection.

1) Macro set up: A macro sampling cuvette holder (Horiba Jobin-Yvon, France) attached to the turret of the microscope has been used for recording using 500 µL of commercial stock solutions in quartz cuvette. Acquisition time was set to 2 accumulations of 30 seconds. *2) Microscope set up (confocal measurements):* Spectra have been collected using a x10 objective (Zeiss EC Epiplan-Neofluar Dic, NA=0.25 and 9.3 mm working distance). Additionally, the backscattered light is collected through a 10 µm diameter optical fibre, ensuring the high confocality of the measurements performed. Spectra resulted from 2 accumulations of 60 seconds and were collected in triplicates from 3 different infusion bags (for each drug). For each bag and each concentration, recording was made from 10 different positions on the bag, for total of 180 acquisition for each drug. For each position, the laser was focussed at the surface of the infusion bags and the position was set as 0 µm. Then, a Z scan was performed to automatically record spectra at 4 different depths, -300 µm, -500 µm, -700 µm and -900 µm.

2.4 Data handling

Raman and IR data sets have been pre-processed and analysed using MATLAB® (Mathworks, USA).

a) Qualitative analysis:

Partial Least Squares Discriminant Analysis (PLSDA) is a well-established unsupervised method. Data were subjected to EMSC and rubber band corrected, and then 2/3 of the data has been used for calibration and 1/3 for validation. The output of the model is a confusion matrix that enables calculation of specificity and sensitivity of the discrimination.

b) Quantitative analysis:

Data has been subjected Extended Multiplicative Signal Correction (EMSC-toolbox) [46] followed by a baseline correction method with the rubber band correction [10]. Partial Least Squares Regression (PLSR) has been applied in the fingerprint region (300 – 1800 cm^{-1}) to extract the relevant quantitative information concerning intensity to concentration relationship. Leave K Out Cross Validation (LKOCV) has been applied, which randomly selects 2/3 of the samples for calibration and 1/3 for validation. The output of this model gives information to evaluate PLSR using the linearity of the regression (R^2), Root Mean Square Error of Cross Validation (RMSECV) and the regression coefficient which represents the variables

(wavenumbers) used to create the regression model. Additionally, the lower Limit Of Detection (lower LOD) has been estimated based on the methodology of Allegrini et al. which established a mathematical model using the outcome of PLSR analysis [47].

3. Results

3.1 Spectral characterisation of infusion bags

Spectra from chemotherapeutics solutions in infusion bags have been collected using a confocal Raman micro-spectrometer using a x10 objective. The confocality of the Raman microscope enables to collect at defined focal depth, presently -300 µm, -500 µm, -700 µm and -900 µm. The depth of focus for the x10 objective lens is estimated to be ~140 µm, taking into account the wavelength of the laser (532 nm) and the numerical aperture (NA = 0.25) (*https://www.olympusims.com/en/microscope/terms/focal_depth/#:~:text=The%20focal%20depth%20refers%20to,the%20specimen%20plane%20by%20microscope*). Therefore, the aim is to find a position with the laser focus sufficiently inside the infusion bag where the spectral contribution from the materials of the bag is negligible compared to the signal originating from the solution. According to manufacturer specifications, infusion bags used in this study are composed of polyolefin/polyamide co-extruded plastic; therefore a strong contribution can be expected in the Raman spectra collected. This is confirmed with Figure 1a, which presents a typical mean Raman spectrum collected at depth -300µm. The spectrum exhibits strong contributions at 400 cm^{-1} (CH_2 wagging), 811 cm^{-1} (C-CH_3 stretching), 846 cm^{-1} (C-C backbone stretching), 1065 cm^{-1} (C-C backbone stretching), 1132 cm^{-1} (C-H twisting), 1174 cm^{-1} (C-H bending), 1298 cm^{-1} (CH_2 twisting), 1372 cm^{-1} (CH_3 symmetric bending), 1420 cm^{-1} (CH_3 asymmetric stretching), 1444 cm^{-1} (CH_2 bending), 1465 cm^{-1} (CH_2 asymmetric bending) and 1640 cm^{-1} (C=O stretching of amide) all assigned to infusion bags materials [48,49]. However, Figure 1b, 1c and 1d highlights these features decrease significantly when recording is performed from respectively -500 µm, -700 µm, -900 µm. Clearly, it is possible to reduce the residual contribution from the infusion bag to reveal the features of the contents, in this case the OH bending of water, at 1640 cm^{-1}. Therefore, for subsequent analysis of chemotherapeutic solutions the depth – 900 µm has been preferred.

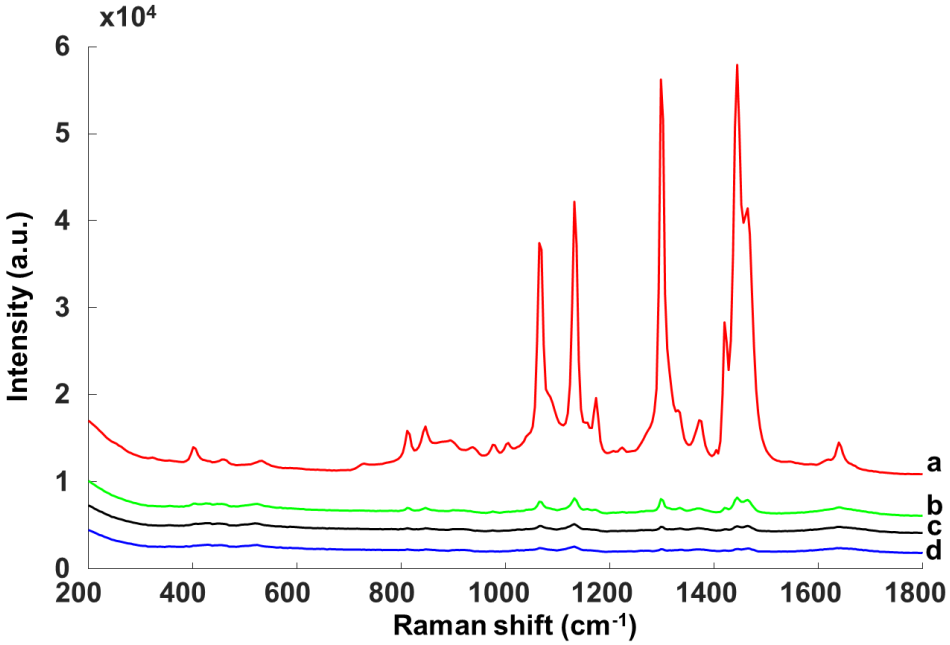


Figure 1: Mean Raman spectra of 5% glucose recorded through infusion bag at: a) 300 µm (red), b) 500 µm (green), c) 700 µm (black) and d) 900 µm (blue) depth by 532 nm. Spectra are offset for clarity.

3.2 Spectral characterisation of anticancer drugs analysed

Figure 2 presents the mean spectra obtained from commercial solutions of the 3 chemotherapeutic drugs analysed using the macro set up in quartz cuvettes (See 2. Materials and Methods). Figure 2a shows the mean spectrum of MTX, with characteristic bands at 679 cm^{-1} (aromatic C-C-C in plane bending), 715 cm^{-1} (C-C in plane bending), 772 cm^{-1} (C-C out of plane bending), 1215 cm^{-1} (CH_2 wagging), 1294 cm^{-1} (-CH_3 symmetric deformation), 1359 cm^{-1} (aromatic C-C stretching), 1384 cm^{-1}(-CH_3 symmetric deformation), 1457 cm^{-1} (C-N stretching), 1561 cm^{-1} (aromatic C-C stretching) and 1608 cm^{-1} (C-N stretching) [50]. Figure 2b shows the mean spectrum of 5-FU with features found at 364 cm^{-1} (out of plane ring bending), 487 cm^{-1} (in plane ring bending), 573 cm^{-1} (out of plane ring and C=O bending), 648 cm^{-1} (in plane ring bending), 772 cm^{-1} (pyrimidine ring breathing), 820 cm^{-1} (trigonal ring and C-F bending), 1014 cm^{-1} (C-H and N-H wagging), 1186 cm^{-1} (N-H in plane bending), 1232 cm^{-1} (ring and C-F bending), 1290 cm^{-1} (ring stretching), 1355 cm^{-1} (C-H wagging), 1616 cm^{-1} (trigonal ring mode) and 1679 cm^{-1} (symmetric C=O stretching) [51]. Finally, Figure 2c presents the mean spectrum of GEM with bands at 789 cm^{-1} (pyrimidine ring breathing), 824

cm^{-1} (C-F bending), 1261 cm^{-1} (ring stretching), 1457 cm^{-1} (CH_2 and CH_3 scissoring), 1545 cm^{-1} (C=C stretching) and 1659 cm^{-1} (hydrogen bonded C=O stretching) [18].
Unambiguously the 3 drugs display different Raman signatures with specific features enabling rapid identification.

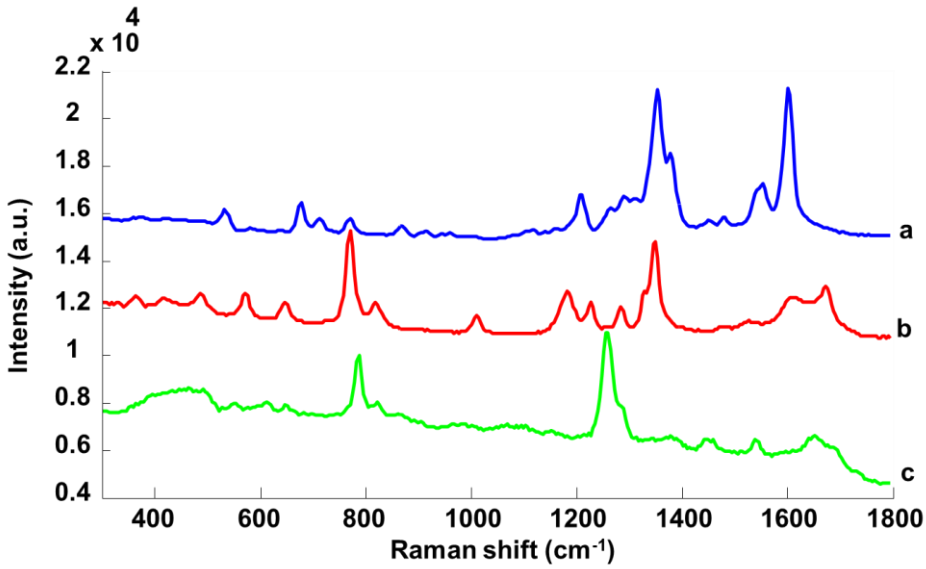


Figure 2: Mean Raman spectra recorded from concentrated stock solutions of: a) MTX 100 $g{\cdot}L^{-1}$, b) 5-FU 50 $g{\cdot}L^{-1}$ and c) GEM 40 $g{\cdot}L^{-1}$ by 532 nm. Spectra are offset for clarity.

3.3 Discriminant analysis

PLSDA has been applied to data subjected to pre-processing, including a vector normalisation. Specificity and sensitivity of 100% were achieved (Table 2). The pure spectra collected from the 3 commercial drug solutions display distinct characteristic spectral signatures, (Figure 2), and therefore such an outcome can be expected.

Table 2: Specificity and sensitivity % obtained by PLSDA using 3 Latent variables

Drug	Specificity	Sensitivity
MTX	100	100
5-FU	100	100
GEM	100	100

Figure 3 presents the regression coefficient obtained from PLSDA. The regression coefficient in Figure 6a presents negative features at 532, 680, 716, 772, 1216, 1360, 1384, 1560 and 1608

cm^{-1} which are identical to MTX spectrum collected from stock solution (Figure 2a). The regression coefficient in Figure 3b presents negative features at 364, 492, 572, 652, 772, 824, 1016, 1188, 1232, 1292, 1684 cm^{-1} which are identical to 5-FU (Figure 2b). The regression coefficient in Figure 3c isn't directly comparable to spectrum of GEM (Figure 2c) however the 2 strong positive peaks at 789 cm^{-1} and 1261 cm^{-1} in addition to the weaker bands at 1545 cm^{-1} can be specifically assigned to the drug.

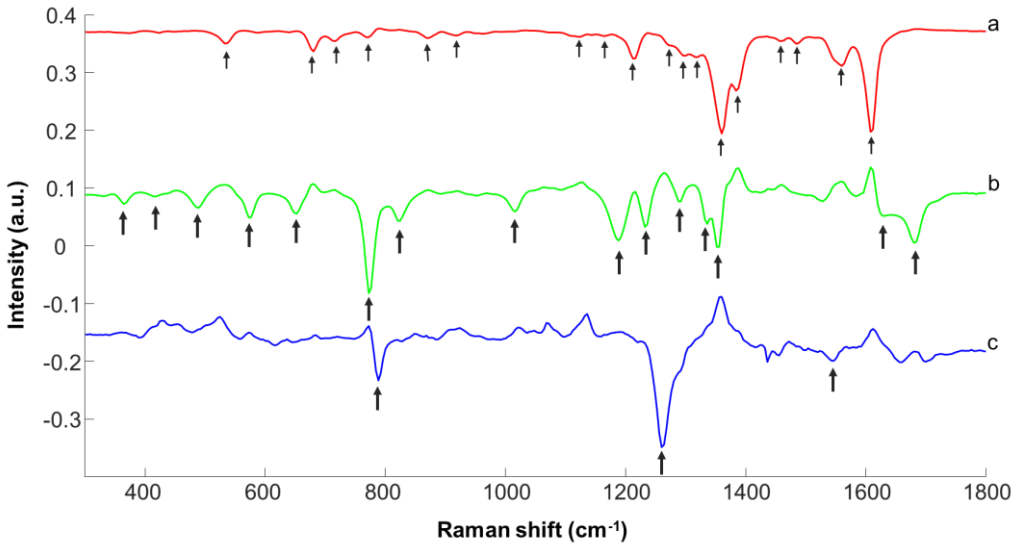


Figure 3: Regression coefficients of PLSDA performed using 3 LVs.

3.3 Direct quantitative analysis in infusion bags

Figure 4 presents the mean Raman spectra collected for the 6 concentrations for MTX solutions inside infusion bags at the depth -900 µm. It is observed that spectral features of the drug proportionally decrease with the concentration of solutions. The data used for illustration in figure 3 are from the first infusion bag analysed for MTX, while the concentrations indicated, 20.1 $g{\cdot}L^{-1}$, 14.3 $g.L^{-1}$, 9.5 $g.L^{-1}$, 4.98 $g.L^{-1}$, 3.8 $g.L^{-1}$ and 3.2 $g.L^{-1}$, correspond to the quantification performed using UV-Vis absorbance (see 2. Materials and Methods). These values can be used as reference concentrations (true concentrations) for PLSR analysis.

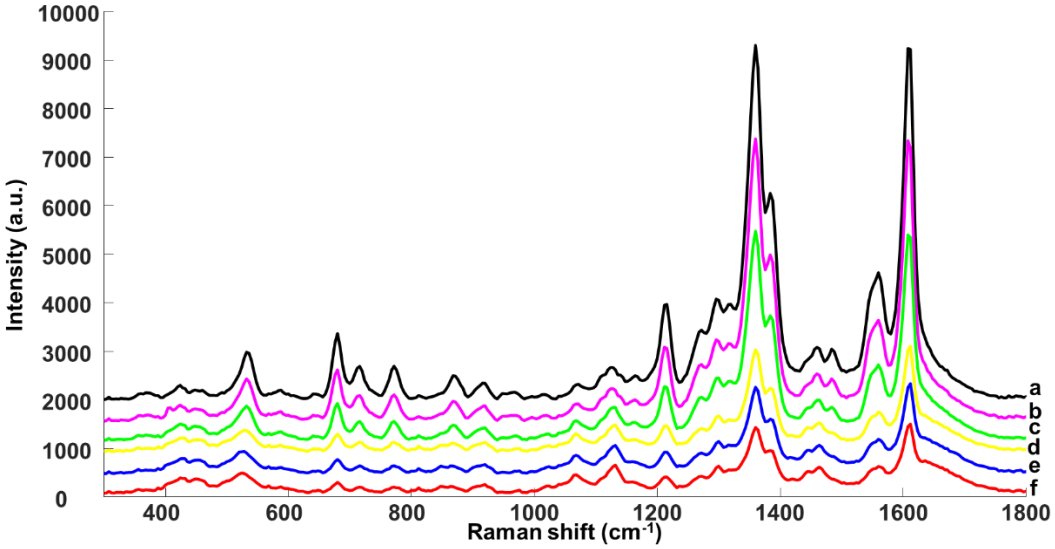


Figure 4: Mean Raman spectra of MTX in 5% glucose bag following at 900 µm for respective concentrations of: a) 20.1 g.L^{-1}, b) 14.3 g.L^{-1}, c) 9.5 g.L^{-1}, d) 4.98 g.L^{-1}, e) 3.8 g.L^{-1} and f) 3.2 g.L^{-1}. Spectra are offset for clarity.

Figure 5 presents the results from PLSR of MTX performed using LKOCV. The RMSECV (Figure 5A) displays a slight decrease as a function of latent variables (LVs). It is observed that, above 4 LVs, no improvement of the precision can be reached. The plot of predicted concentration against prepared concentration (measured with UV) in Figure 5B confirms the quality of the regression model. With a R^2 equal to 0.9936, the linear regression is acceptable and is characterised by a RMSECV of 0.5696 g.L^{-1}. Table 3 summarises the PLSR results for the 3 drugs with RMSECV for 5-FU and GEM higher compared to MTX, respectively 1.5661 g.L^{-1} and 0.6116 g.L^{-1}. However, the higher values of RMSECV can reflect the differences in the range of concentration analysed (Table 1). The results can also be represented as the RMSECV expressed as percentage of the median concentration of the range tested. In this way, values of 6.7%, 11.8% and 9.5% for MTX, 5-FU and GEM are determined, respectively. It confirms the best accuracy is obtained for MTX followed by 5-FU and GEM. Additionally, the lower limit of detection (LOD) calculated from the PLSR analysis indicates that Raman directly in infusion bags enables determination of concentrations as low as 0.6469 g.L^{-1}, 0.6962 g.L^{-1} and 0.2895 g.L^{-1}, respectively for 5-FU, GEM and MTX. All 3 LOD are substantially lower than the lowest clinical concentration used in this study for these drugs (See table 1). While for 5-FU the LOD remains close to the lowest dose administered to patients for MTX it is nevertheless 10 times lower.

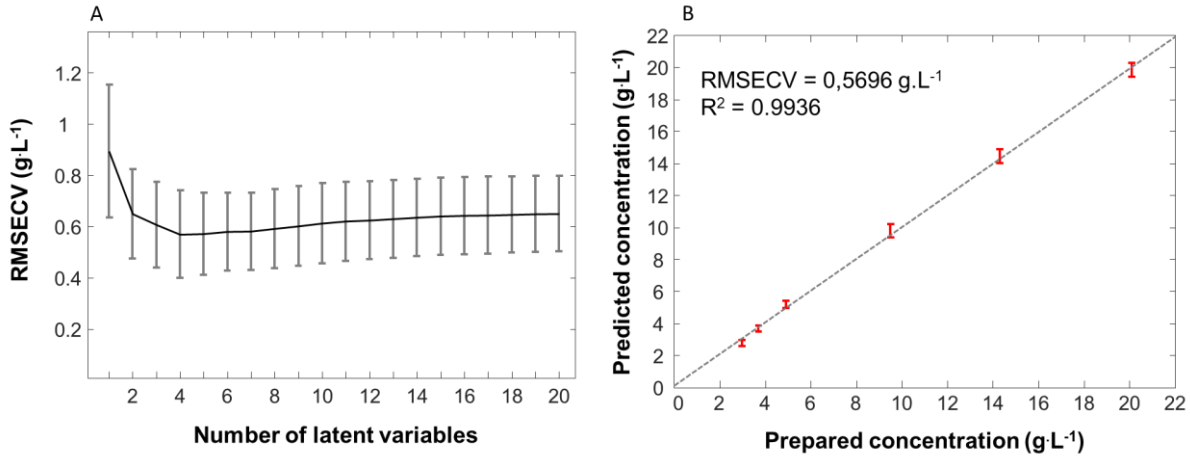


Figure 5: PLSR analysis performed on Raman data of MTX in 5% glucose bag recorded by 532 nm laser at -900 µm*: A) RMSECV and B) regression plot with 4 LVs.*

Table 3: Summary of PLSR results at depth 900 µm:

Drug	**LVs**	***R²***	**RMSECV (g·L⁻¹)**	**% RMSECV**
MTX	4	0.9936	0.5696	4.7
5-FU	2	0.9879	1.5661	6.8
GEM	4	0.9409	0.6116	8.2

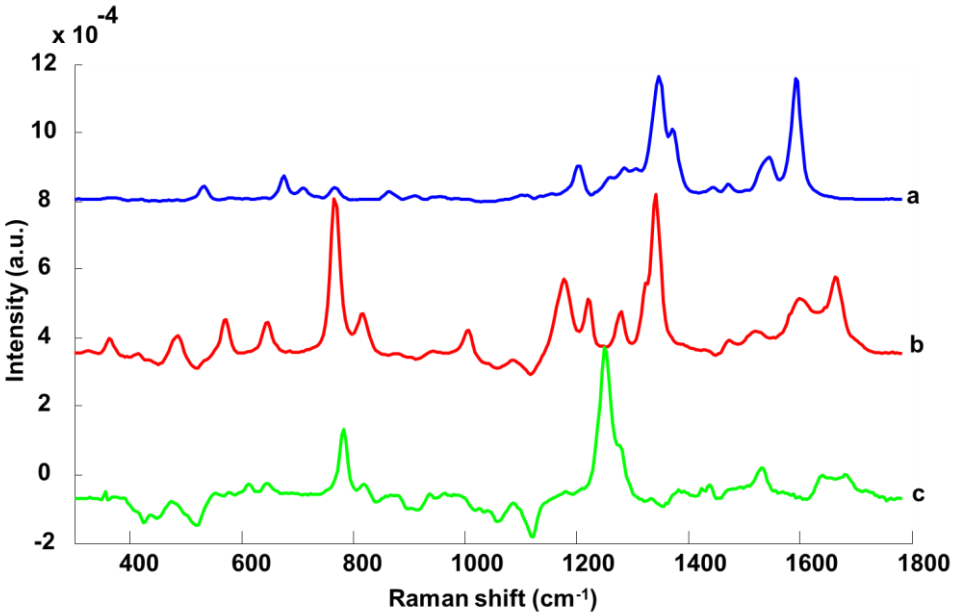


Figure 6: First regression coefficients of PLSR: a) MTX, b) 5-FU and c) GEM. Spectra are offset for clarity.

Regression coefficients (Figure 6) highlight the spectral features used in the quantitative models constructed with PLSR. For MTX (Figure 6a), bands at 536 cm^{-1}, 680 cm^{-1}, 716 cm^{-1}, 772 cm^{-1}, 1216 cm^{-1}, 1360 cm^{-1}, 1384 cm^{-1}, 1456 cm^{-1}, 1484 cm^{-1}, 1560 cm^{-1} and 1608 cm^{-1} are characteristic of MTX and resemble those observed in Figure 2a. This illustrates the specificity of quantification which is performed on MTX bands. Similarly, Figure 6b presents characteristic bands of 5-FU at 364 cm^{-1}, 488 cm^{-1}, 576 cm^{-1}, 652 cm^{-1}, 772 cm^{-1}, 824 cm^{-1}, 1016 cm^{-1}, 1188 cm^{-1}, 1232 cm^{-1}, 1292 cm^{-1}, 1356 cm^{-1}, 1616 cm^{-1} and 1680 cm^{-1} which coincide with that obtained in Figure 2b. Finally Figure 5c, presents peaks of GEM at 780 cm^{-1}, 816 cm^{-1}, 1252 cm^{-1}, 1444 cm^{-1}, 1536 cm^{-1} and 1648 cm^{-1} which are the characteristic features observed in Figure 2c.

Unambiguously, Raman analysis in infusion bags coupled to PLSR analysis enables correlation of spectral variations with concentrations of chemotherapeutic solutions. In addition to quality of the fitting model constructed by PLSR, the estimated concentrations can be extracted to evaluate accuracy of prediction. Table 4 summarises the errors (expressed as percentage) in the estimated concentrations with Raman spectroscopy compared to the reference concentrations obtained with UV-Vis spectroscopy. C1 refers to the lowest concentration of the target range while C6 is the highest. Notably, there is no clear legislation regarding the acceptance criteria for individualised chemotherapeutic solutions. As an example, the centralised unit at the

University Hospital of Tours has a 10% tolerance in the quantification of drugs in final solutions. However, in the literature, some studies report acceptance criteria up to 15% [27]. In the current study, it is observed that MTX and 5-FU display errors in predicted concentrations significantly below the 10% threshold, the highest error found to be 5.7% For GEM, errors between 7% and 17% are found for the 3 lower concentrations, while for the 3 highest, the % error greatly decreases to, respectively, 5%, 5.78% and 2.48% for C4, C5 and C6.

Table 4: Summary of %error in predicted concentrations (Raman spectroscopy) compared to reference concentrations (UV-Vis absorbance).

Concentration	MTX	5-FU	GEM
C1	5.58%	3.35%	7.47%
C2	3.45%	3.65%	17.14%
C3	4.28%	5.7%	13.72%
C4	3.25%	1.19%	5.00%
C5	1.14%	1.54%	5.79%
C6	2.16%	5.54%	2.48%

4. General Discussion

Confocality of Raman microspectroscopic analysis, when performed with suitable instruments, is a well-established a valuable strength of the technique used in numerous applications in the biomedical and pharmaceutical fields [8,52,53]. Over the last decade, the development of compact benchtop Raman spectrometer equipped with remote confocal probes connected with optical fibres have greatly contributed to increasing the attractiveness of Raman spectroscopy for direct analysis of solutions or powders contained within glassware or other containers [54,55]. It is particularly suited for quality control of raw materials or solvents in the pharmaceutical industry [14]. Nowadays, miniaturisation and compaction of analytical devices is a strong marketing trend, the range of portable systems now including handheld Raman devices [32]. However, transfer of these technologies to the clinical environment is a slow process. Although, custom designed commercial systems, such as the QCPrep+®, are available, the literature describing Raman spectroscopy for AQC of chemotherapeutic solutions remains scarce. For instance, only 3 studies are referenced in the literature for this system, despite the strong interest to of combining UV and Raman detections into a flow injection system

[26,27,56]. Since the initial works published by Bourget et al. [4,57], who were first to highlight the potential of Raman spectroscopy for analysis of anticancer solutions, there has been no significant development to further validate the technique for non-invasive analysis. It is only recently, in 2018, that Le et al. reported a study about quantification of gemcitabine, directly in infusion bags, using a handheld Raman device [33]. Indeed, performing analysis without the requirement for withdrawal of the solution is highly relevant to ensure safety of staff working in centralised units in hospitals. However, to date, no benchmarking has been set to clearly demonstrate the instrumental set up delivering the optimal analytical output for quantification and discrimination of chemotherapeutic solutions, also considering other parameters such as cost of purchase, maintenance or ergonomic design.

In terms of analytical performances, the RMSECV of 0.6116 $g{\cdot}L^{-1}$ found presently for GEM with CRM is comparable to the output of the previous study published by Le et al., who reported an RMSECV of 0.44 $g{\cdot}L^{1}$ for analysis in glass vials. The slight difference can be explained by differences in the range of concentrations analysed, respectively 4 -11 $g{\cdot}L^{-1}$ and 1 -20 $g{\cdot}L^{-1}$. The recent study from Le et al. using handheld Raman reported a RMSECV of 0.42 $g{\cdot}L^{-1}$ for analysis directly in infusion bags. However, it is important to mention that the commercial gemcitabine solution used was from Mylan®, which is prepared in ethanol, while the brand used in the present study is Sandoz®, without ethanol. Ethanol is a relatively strong Raman scatterer, which contributes strongly to the data collected [33], therefore improving the PLSR fitting. The lack of consistency between experimental designs can give rise to diversity in the outcomes and, notably, the influence of the laser power and the wavelength used on the signal to noise ratio make direct comparison difficult. For 5-FU, the RMSECV of 1.5561 $g{\cdot}L^{-1}$ found with CRM appears superior to the value of 0.482 $g{\cdot}L^{-1}$ reported by Bourget et al. in elastomeric infusion pumps [4] or the 0.9 $g{\cdot}L^{-1}$ of the study of Le at al. in a glass vial [18]. Although the type of containers can be a crucial parameter influencing the quality of the fitting achieved, there is no evidence that differences are related to the instrumental set up, the collection efficiency (sample presentation), range of concentration selected or number of samples in the calibration / validation sets. Despite the differences in RMSECV, the errors in predicted concentrations measured here are below 5.7% for 5-FU, and therefore significantly lower than the 10-15% acceptance criteria commonly defined in studies. Therefore, the results presently collected with CRM are encouraging and highlight the reliability of analysis performed. However, the investigation remains preliminary and a more extended panel of molecules should be included to provide an in-depth investigation of direct, non-invasive, analysis in infusion bags.

In terms of applicability, the performance of both systems with remote probes and handheld devices will be dependent of the manual positioning at the surface of the bags during analysis. Therefore, the variability between days and staff performing the analysis could have an impact on the robustness of the results (repeatability and reproducibility). The motorised stage associated with CRM enables standardised movements in the Z direction with high precision. Moreover, commercialised Raman microscopes commonly include functionalities for autofocus that can be used to repeatedly set the 0 position at the surface of the bags. Therefore, a software protocol to automatically increment a pre-defined movement to focus the laser inside the infusion bag is readily achievable. Moreover, CRM can be purchased with an inverted set up (objective lens pointing toward the ceiling) that can be used for liquid samples analysis [58,59]. It implies pharmacists or technicians would have to simply place the bag on top of the motorised stage then the process of data collection would be automated thus significantly faster and reproducible. A dedicated inverted Raman microscope with a simplified configuration would be competitive cost wise with other benchtop systems and handhelds devices that remain relatively expensive technologies.

Ultimately, a number of parameters should be considered and compared to fully address the suitability of each instrument for AQC. The present preliminary study clearly demonstrates the feasibility to quantify and discriminate 3 common drugs, gemcitabine, 5-fluorouracile and methotrexate, directly inside infusion bags. Developing CRM for AQC of chemotherapeutic solution should therefore be considered as one of suitable options.

5. Conclusion:

Raman spectroscopy is a powerful tool for non-invasive AQC of chemotherapeutic drugs in infusion bags. Performing analysis without withdrawal of solutions it a major step forward to ensure safety of staff members of the preparation units. Moreover, the analysis performed on MTX, 5-FU and GEM also highlights that analytical performances of Raman spectroscopy for anticancer drugs correspond to current requirements for accuracy in quantification and specificity for discrimination. Although the free, rapid and cost-effective molecular characterisation of samples are undeniable advantages, the investigation remains to date preliminary and broader sets of molecules are required. While the literature remains scarce on the topic of non-invasive analysis, there is no doubt that CRM has the potential to be used as routine protocol for AQC, at least for a selected number of molecules with strong spectral response.

Acknowledgement

Campus France and French embassy in Sudan for financial support for PhD in cotutelle between University of Gezira and University of Tours.

Bibliography

[1] A. Shkoza, M. Likmeta, E. Balla, L. Malaj, Therapeutic and economic benefits of a centralized unit for cytotoxic drugs processing, Int. J. Pharm. Sci. Res. 7 (2016) 1039–1042. https://doi.org/10.13040/IJPSR.0975-8232.7(3).1039-42.

[2] M. Savelli, M. Roche, C. Curti, C. Bornet, P. Rathelot, M. Montana, P. Vanelle, Methods to control anticancer chemotherapy preparations ranked by risk analysis, Pharmazie. 73 (2018) 251–259. https://doi.org/10.1691/ph.2018.7205.

[3] A. Delmas, J.B. Gordien, J.M. Bernadou, M. Roudaut, A. Gresser, L. Malki, M.C. Saux, D. Breilh, Quantitative and qualitative control of cytotoxic preparations by HPLC-UV in a centralized parenteral preparations unit, J. Pharm. Biomed. Anal. 49 (2009) 1213–1220. https://doi.org/10.1016/j.jpba.2009.03.007.

[4] P. Bourget, A. Amin, F. Vidal, C. Merlette, F. Lagarce, Comparison of Raman spectroscopy vs. high performance liquid chromatography for quality control of complex therapeutic objects: Model of elastomeric portable pumps filled with a fluorouracil solution, J. Pharm. Biomed. Anal. 91 (2014) 176–184. https://doi.org/10.1016/j.jpba.2013.12.030.

[5] I. Badea, L. Lazăr, D. Moja, D. Nicolescu, A. Tudose, A HPLC method for the simultaneous determination of seven anthracyclines, J. Pharm. Biomed. Anal. 39 (2005) 305–309. https://doi.org/10.1016/j.jpba.2005.03.039.

[6] E. Gravel, P. Bourget, L. Mercier, A. Paci, Fluorescence detection combined with either HPLC or HPTLC for pharmaceutical quality control in a hospital chemotherapy production unit: Application to camptothecin derivatives, J. Pharm. Biomed. Anal. 39 (2005) 581–586. https://doi.org/10.1016/j.jpba.2005.05.010.

[7] P. Bourget, A. Amin, F. Vidal, C. Merlette, F. Lagarce, Comparison of Raman spectroscopy vs. high performance liquid chromatography for quality control of complex therapeutic objects: Model of elastomeric portable pumps filled with a fluorouracil solution, J. Pharm. Biomed. Anal. 91 (2014) 176–184. https://doi.org/10.1016/j.jpba.2013.12.030.

[8] L.M. Moreira, L. Silveira, F. V. Santos, J.P. Lyon, R. Rocha, R.A. Zângaro, A.B.

Villaverde, M.T.T. Pacheco, Raman spectroscopy: A powerful technique for biochemical analysis and diagnosis, Spectroscopy. 22 (2008) 1–19. https://doi.org/10.3233/SPE-2008-0326.

[9] L. Miloudi, F. Bonnier, A. Tfayli, F. Yvergnaux, H.J. Byrne, I. Chourpa, E. Munnier, Confocal Raman spectroscopic imaging for in vitro monitoring of active ingredient penetration and distribution in reconstructed human epidermis model, J. Biophotonics. 11 (2018) 1–17. https://doi.org/10.1002/jbio.201700221.

[10] F. Bonnier, G. Brachet, R. Duong, T. Sojinrin, R. Respaud, N. Aubrey, M.J. Baker, H.J. Byrne, I. Chourpa, Screening the low molecular weight fraction of human serum using ATR-IR spectroscopy, J. Biophotonics. 9 (2016) 1085–1097. https://doi.org/10.1002/jbio.201600015.

[11] B. Van Eerdenbrugh, L.S. Taylor, Application of mid-IR spectroscopy for the characterization of pharmaceutical systems, Int. J. Pharm. 417 (2011) 3–16. https://doi.org/10.1016/j.ijpharm.2010.12.011.

[12] R. Gasper, J. Dewelle, R. Kiss, T. Mijatovic, E. Goormaghtigh, IR spectroscopy as a new tool for evidencing antitumor drug signatures, Biochim. Biophys. Acta - Biomembr. 1788 (2009) 1263–1270. https://doi.org/10.1016/j.bbamem.2009.02.016.

[13] K. Kong, C. Kendall, N. Stone, I. Notingher, Raman spectroscopy for medical diagnostics - From in-vitro biofluid assays to in-vivo cancer detection, Adv. Drug Deliv. Rev. 89 (2015) 121–134. https://doi.org/10.1016/j.addr.2015.03.009.

[14] R.S. Das, Y.K. Agrawal, Raman spectroscopy: Recent advancements, techniques and applications, Vib. Spectrosc. 57 (2011) 163–176. https://doi.org/10.1016/j.vibspec.2011.08.003.

[15] L.P. Choo-Smith, H.G.M. Edwards, H.P. Endtz, J.M. Kros, F. Heule, H. Barr, J.S. Robinson, H.A. Bruining, G.J. Puppels, Medical applications of Raman spectroscopy: From proof of principle to clinical implementation, Biopolym. - Biospectroscopy Sect. 67 (2002) 1–9. https://doi.org/10.1002/bip.10064.

[16] D.I. Ellis, D.P. Cowcher, L. Ashton, S. O'Hagan, R. Goodacre, Illuminating disease and enlightening biomedicine: Raman spectroscopy as a diagnostic tool, Analyst. 138 (2013) 3871–3884. https://doi.org/10.1039/c3an00698k.

[17] Z. Movasaghi, S. Rehman, I.U. Rehman, Raman spectroscopy of biological tissues, Appl. Spectrosc. Rev. 42 (2007) 493–541. https://doi.org/10.1080/05704920701551530.

[18] L.M.M. Lê, M. Berge, A. Tfayli, J. Zhou, P. Prognon, A. Baillet-Guffroy, E. Caudron, Rapid discrimination and quantification analysis of five antineoplastic drugs in aqueous

solutions using Raman spectroscopy, Eur. J. Pharm. Sci. 111 (2018) 158–166. https://doi.org/10.1016/j.ejps.2017.09.046.

[19] V. Balan, C.T. Mihai, F.D. Cojocaru, C.M. Uritu, G. Dodi, D. Botezat, I. Gardikiotis, Vibrational spectroscopy fingerprinting in medicine: From molecular to clinical practice, Materials (Basel). 12 (2019) 1–40. https://doi.org/10.3390/ma12182884.

[20] F. Dziopa, G. Galy, S. Bauler, B. Vincent, S. Crochon, M.L. Tall, F. Pirot, C. Pivot, A quantitative and qualitative method to control chemotherapeutic preparations by Fourier transform infrared-ultraviolet spectrophotometry, J. Oncol. Pharm. Pract. 19 (2013) 121–129. https://doi.org/10.1177/1078155212457963.

[21] C. Bazin, V. Vieillard, A. Astier, M. Paul, Implementation of real-time identification analysis and quantification of chemotherapies preparations with a Multispec® analyser, Ann. Pharm. Fr. 72 (2014) 33–40. https://doi.org/10.1016/j.pharma.2013.09.006.

[22] P. Bourget, A. Amin, F. Vidal, C. Merlette, P. Troude, A. Baillet-Guffroy, The contribution of Raman spectroscopy to the analytical quality control of cytotoxic drugs in a hospital environment: Eliminating the exposure risks for staff members and their work environment, Int. J. Pharm. 470 (2014) 70–76. https://doi.org/10.1016/j.ijpharm.2014.04.064.

[23] P. Bourget, A. Amin, A. Moriceau, B. Cassard, F. Vidal, R. Clement, La Spectroscopie Raman (SR): Un nouvel outil adapté au contrôle de qualité analytique des préparations injectables en milieu de soins. Comparaison de la SR aux techniques CLHP et UV/visible-IRTF appliquée à la classe des anthracyclines en canct, Pathol. Biol. 60 (2012) 369–379. https://doi.org/10.1016/j.patbio.2011.10.010.

[24] C. Bazin, V. Vieillard, A. Astier, M. Paul, Implementation of real-time identification analysis and quantification of chemotherapies preparations with a Multispec® analyser, Ann. Pharm. Fr. 72 (2014) 33–40. https://doi.org/10.1016/j.pharma.2013.09.006.

[25] A.A. Makki, F. Bonnier, R. Respaud, F. Chtara, A. Tfayli, C. Tauber, D. Bertrand, H.J. Byrne, E. Mohammed, I. Chourpa, Qualitative and quantitative analysis of therapeutic solutions using Raman and infrared spectroscopy, Spectrochim. Acta - Part A Mol. Biomol. Spectrosc. 218 (2019) 97–108. https://doi.org/10.1016/j.saa.2019.03.056.

[26] T. Chouquet, G. Benoit, K. Morand, Implementation of Analytical Control of Low Volume Pediatric Cytotoxic Drugs Preparations using a UV/Raman Spectrophotometer, Pharm. Technol. Hosp. Pharm. 1 (2016) 151–162. https://doi.org/10.1515/pthp-2016-0013.

[27] F. Nardella, M. Beck, P. Collart-Dutilleul, G. Becker, C. Boulanger, L. Perello, A.

Gairard-Dory, B. Gourieux, G. Ubeaud-Séquier, A UV-Raman spectrometry method for quality control of anticancer preparations: Results after 18 months of implementation in hospital pharmacy, Int. J. Pharm. 499 (2016) 343–350. https://doi.org/10.1016/j.ijpharm.2016.01.002.

[28] C.B.P. da Silva, I.P. Julio, G.E. Donadel, I. Martins, UPLC-MS/MS method for simultaneous determination of cyclophosphamide, docetaxel, doxorubicin and 5-fluorouracil in surface samples, J. Pharmacol. Toxicol. Methods. 82 (2016) 68–73. https://doi.org/10.1016/j.vascn.2016.08.004.

[29] C. Rioufol, F. Ranchon, V. Schwiertz, N. Vantard, E. Joue, C. Gourc, N. Gauthier, M.G. Guedat, G. Salles, P.J. Souquet, B. Favier, L. Gilles, G. Freyer, B. You, V. Trillet-Lenoir, J. Guitton, Administration of anticancer drugs: Exposure in hospital nurses, Clin. Ther. 36 (2014) 401–407. https://doi.org/10.1016/j.clinthera.2014.01.016.

[30] A. Amin, P. Bourget, F. Vidal, F. Ader, Routine application of Raman spectroscopy in the quality control of hospital compounded ganciclovir, Int. J. Pharm. 474 (2014) 193–201. https://doi.org/10.1016/j.ijpharm.2014.08.028.

[31] L.M.M. Lê, A. Tfayli, J. Zhou, P. Prognon, A. Baillet-Guffroy, E. Caudron, Discrimination and quantification of two isomeric antineoplastic drugs by rapid and non-invasive analytical control using a handheld Raman spectrometer, Talanta. 161 (2016) 320–324. https://doi.org/10.1016/j.talanta.2016.07.025.

[32] L. Lê, M. Berge, A. Tfayli, P. Prognon, E. Caudron, Discriminative and Quantitative Analysis of Antineoplastic Taxane Drugs Using a Handheld Raman Spectrometer, Biomed Res. Int. (2018) 12–15. https://doi.org/10.1155/2018/8746729.

[33] L. Lê, M. Berge, A. Tfayli, A. Baillet Guffroy, P. Prognon, A. Dowek, E. Caudron, Quantification of gemcitabine intravenous drugs by direct measurement in chemotherapy plastic bags using a handheld Raman spectrometer, Talanta. 196 (2019) 376–380. https://doi.org/10.1016/j.talanta.2018.11.062.

[34] I. Rodin, A. Braun, A. Stavrianidi, O. Shpigun, A validated LC-MS/MS method for rapid determination of methotrexate in human saliva and its application to an excretion evaluation study, J. Chromatogr. B Anal. Technol. Biomed. Life Sci. 937 (2013) 1–6. https://doi.org/10.1016/j.jchromb.2013.07.026.

[35] S. Nussbaumer, P. Bonnabry, J.L. Veuthey, S. Fleury-Souverain, Analysis of anticancer drugs: A review, Talanta. 85 (2011) 2265–2289. https://doi.org/10.1016/j.talanta.2011.08.034.

[36] E. Dickens, S. Ahmed, Principles of cancer treatment by chemotherapy, Surg. (United

Kingdom). 36 (2018) 134–138. https://doi.org/10.1016/j.mpsur.2017.12.002.

[37] D.M. Bach, J.A. Straseski, W. Clarke, Therapeutic drug monitoring in cancer chemotherapy, Bioanalysis. 2 (2010) 863–879. https://doi.org/10.4155/bio.10.48.

[38] S. Nussbaumer, P. Bonnabry, J.L. Veuthey, S. Fleury-Souverain, Analysis of anticancer drugs: A review, Talanta. 85 (2011) 2265–2289. https://doi.org/10.1016/j.talanta.2011.08.034.

[39] A.A. Thoppil, S. Choudhary, N. Kishore, Competitive binding of anticancer drugs 5-fluorouracil and cyclophosphamide with serum albumin: Calorimetric insights, Biochim. Biophys. Acta - Gen. Subj. 1860 (2016) 917–929. https://doi.org/10.1016/j.bbagen.2016.01.026.

[40] E.J.B. Derissen, M.J.X. Hillebrand, H. Rosing, J.H.M. Schellens, J.H. Beijnen, Development of an LC-MS/MS assay for the quantitative determination of the intracellular 5-fluorouracil nucleotides responsible for the anticancer effect of 5-fluorouracil, J. Pharm. Biomed. Anal. 110 (2015) 58–66. https://doi.org/10.1016/j.jpba.2015.02.051.

[41] H.K. Risinggård, S. Cooil, F. Mazzola, D. Hu, M. Kjærvik, E.R. Østli, N. Patil, A. Preobrajenski, D. Andrew Evans, D.W. Breiby, T.T. Trinh, J.W. Wells, Degradation of the chemotherapy drug 5-fluorouracil on medical-grade silver surfaces, Appl. Surf. Sci. 435 (2018) 1213–1219. https://doi.org/10.1016/j.apsusc.2017.11.221.

[42] J. Ciccolini, C. Serdjebi, G.J. Peters, E. Giovannetti, Pharmacokinetics and pharmacogenetics of Gemcitabine as a mainstay in adult and pediatric oncology: an EORTC-PAMM perspective, Cancer Chemother. Pharmacol. 78 (2016) 1–12. https://doi.org/10.1007/s00280-016-3003-0.

[43] C.M. Li, L. Zhang, Y.H. Hou, N. Li, M.H. Che, Targeted delivery of gemcitabine to pancreatic adenocarcinoma using anti-EGFR antibody as a targeting agent, World Chinese J. Dig. 23 (2015) 1890–1896. https://doi.org/10.11569/wcjd.v23.i12.1890.

[44] O. Caffo, S. Fallani, E. Marangon, S. Nobili, M.I. Cassetta, V. Murgia, F. Sala, A. Novelli, E. Mini, M. Zucchetti, E. Galligioni, Pharmacokinetic study of gemcitabine, given as prolonged infusion at fixed dose rate, In combination with cisplatin In patients with advanced non-small-cell lung cancer, Cancer Chemother. Pharmacol. 65 (2010) 1197–1202. https://doi.org/10.1007/s00280-010-1255-7.

[45] K.Y. Hsu, W.H. Hao, J.J. Wang, S.P. Hsueh, P.J. Hsu, L.C. Chang, C.S. Hsu, In vitro and in vivo studies of pharmacokinetics and antitumor efficacy of D07001-F4, an oral gemcitabine formulation, Cancer Chemother. Pharmacol. 71 (2013) 379–388.

https://doi.org/10.1007/s00280-012-2017-5.

[46] L.E. Jamieson, H.J. Byrne, Vibrational spectroscopy as a tool for studying drug-cell interaction: Could high throughput vibrational spectroscopic screening improve drug development?, Vib. Spectrosc. 91 (2017) 16–30. https://doi.org/10.1016/j.vibspec.2016.09.003.

[47] F. Allegrini, A.C. Olivieri, IUPAC-consistent approach to the limit of detection in partial least-squares calibration, Anal. Chem. 86 (2014) 7858–7866. https://doi.org/10.1021/ac501786u.

[48] G.S.K. Donald L. Pavia, Gary M. Lampman, J.R. Vyvyan, Introduction to spectroscopy, 2013. https://doi.org/10.1887/0750303468/b293c1.

[49] E. Andreassen, Infrared and Raman spectroscopy of polypropylene, (1999) 320–328. https://doi.org/10.1007/978-94-011-4421-6_46.

[50] S. Ayyappan, N. Sundaraganesan, V. Aroulmoji, E. Murano, S. Sebastian, Molecular structure, vibrational spectra and DFT molecular orbital calculations (TD-DFT and NMR) of the antiproliferative drug Methotrexate, Spectrochim. Acta - Part A Mol. Biomol. Spectrosc. 77 (2010) 264–275. https://doi.org/10.1016/j.saa.2010.05.021.

[51] S. Farquharson, A. Gift, C. Shende, F. Inscore, B. Ordway, C. Farquharson, J. Murren, Surface-enhanced Raman spectral measurements of 5-fluorouracil in saliva, Molecules. 13 (2008) 2608–2627. https://doi.org/10.3390/molecules13102608.

[52] H.J. Butler, L. Ashton, B. Bird, G. Cinque, K. Curtis, J. Dorney, K. Esmonde-White, N.J. Fullwood, B. Gardner, P.L. Martin-Hirsch, M.J. Walsh, M.R. McAinsh, N. Stone, F.L. Martin, Using Raman spectroscopy to characterize biological materials, Nat. Protoc. 11 (2016) 664–687. https://doi.org/10.1038/nprot.2016.036.

[53] K.A. Esmonde-White, M. Cuellar, C. Uerpmann, B. Lenain, I.R. Lewis, Raman spectroscopy as a process analytical technology for pharmaceutical manufacturing and bioprocessing, Anal. Bioanal. Chem. 409 (2017) 637–649. https://doi.org/10.1007/s00216-016-9824-1.

[54] A. Paudel, D. Raijada, J. Rantanen, Raman spectroscopy in pharmaceutical product design, Adv. Drug Deliv. Rev. 89 (2015) 3–20. https://doi.org/10.1016/j.addr.2015.04.003.

[55] B. Gotter, W. Faubel, R.H.H. Neubert, FTIR microscopy and confocal Raman microscopy for studying lateral drug diffusion from a semisolid formulation, Eur. J. Pharm. Biopharm. 74 (2010) 14–20. https://doi.org/10.1016/j.ejpb.2009.07.006.

[56] T. Chouquet, G. Benoit, K. Morand, Analytical Control of Pediatric Chemotherapy

Preparations with a UV-Raman Automaton: Results After 18 Months of Implementation and Development of A Suitable Method for Low Volume Preparations, Pharm. Technol. Hosp. Pharm. 2 (2017) 117–129. https://doi.org/10.1515/pthp-2017-0021.

[57] P. Bourget, A. Amin, F. Vidal, C. Merlette, P. Troude, A. Baillet-Guffroy, The contribution of Raman spectroscopy to the analytical quality control of cytotoxic drugs in a hospital environment: Eliminating the exposure risks for staff members and their work environment, Int. J. Pharm. 470 (2014) 70–76. https://doi.org/10.1016/j.ijpharm.2014.04.064.

[58] D.R. Parachalil, C. Bruno, F. Bonnier, H. Blasco, I. Chourpa, J. McIntyre, H.J. Byrne, Raman spectroscopic screening of high and low molecular weight fractions of human serum, Analyst. 144 (2019) 4295–4311. https://doi.org/10.1039/c9an00599d.

[59] F. Bonnier, F. Petitjean, M.J. Baker, H.J. Byrne, Improved protocols for vibrational spectroscopic analysis of body fluids, J. Biophotonics. 7 (2014) 167–179. https://doi.org/10.1002/jbio.201300130.

5.2.1 Discussion on experimental conditions

In the paper, the presented results have shown good quantification and discrimination in the fingerprint region with 532 nm laser. Although, full range can be investigated to have more insight about quantification. Also, 633 nm results can be used to compare in the context of quantification and discrimination.

1) Role of spectral range

The quantification build on the fingerprint region is based on the proportional change in drug intensity versus concentration. Although, the quantification model can be also build using the full range. In this approach, quantification can be based on the ratio between the decrease in drug's band intensity with increase in intensity of the water band near 3500 cm^{-1} which should increase with dilution of the drug.

Table 6 summarise PLSR results obtained using the full range spectra using 532 nm laser. The results are comparable to those obtained using the fingerprint region. However, the explained % RMSECV for MTX and 5-FU which is 6.5% and 8.3% is larger than that obtained for the fingerprint of 4.7% and 6.8%. GEM showed better %RMSECV on the full range of 7.3% compared to 8.2% obtained in the fingerprint. Although one can imagine that full range can provide much better quantification, but it seems that the quantification is prone to more errors and the best to quantify based on the fingerprint signature of a molecule. It appears the decrease in water intensity is not always following the dilution factor but is also influenced by other interferences (Figure 44). Confocality and depth of analysis are highly depending of wavelength and it has not been demonstrated that both the fingerprint and high wavenumber regions follow similar pattern, therefore using the full spectral range for PLSR can lead to reduce precision in concentration estimated.

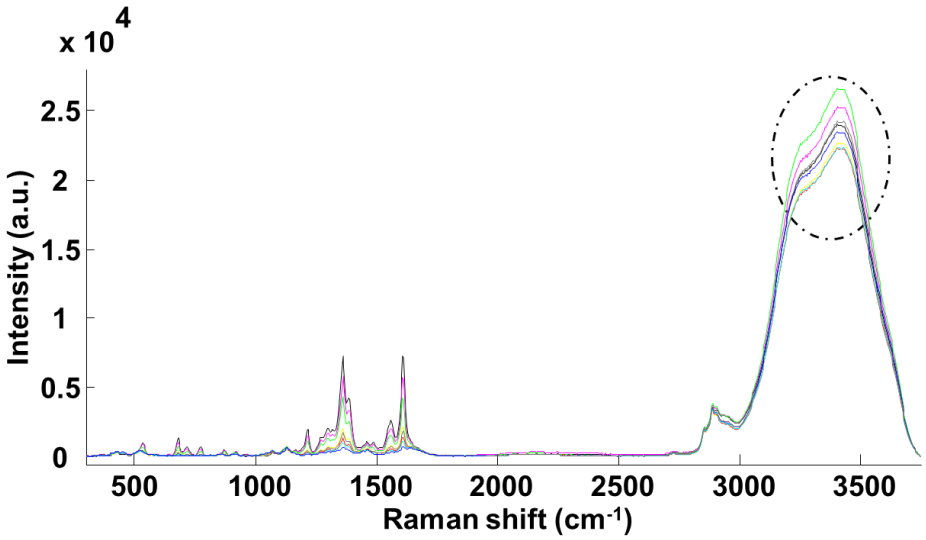


Figure 44. Mean Raman spectra of MTX in 5% glucose bag following at 900 µm for respective concentrations of: a) 20.1 g·L^{-1}, b) 14.3 g·L^{-1}, c) 9.5 g·L^{-1}, d) 4.98 g·L^{-1}, e) 3.8 g·L^{-1} and f) 3.2 g·L^{-1}

Table 6. Summary of PLSR results at depth 900 µm using 532 nm laser for full range spectra

Drug	LVs	R^2	RMSECV (g·L^{-1})	% RMSECV
MTX	4	0.9907	0.6121	6.5
5-FU	3	0.9876	1.3786	8.3
GEM	6	0.9730	0.5592	7.3

2) Influence of laser wavelength

On the system used, it was possible to perform analysis with 2 lasers. The results obtained by 633 nm will be presented. Figure 45 illustrates Raman analysis of 5-FU g·L^{-1} in 5% glucose infusion bag at different depths. The same is observed as before with 532nm laser where the intensity of spectral contribution of the plastic bag goes down with going deeper and the drug's spectral intensity become stronger. Figure 45a presents spectrum obtained at -300 µm predominant by strong feature from the bag packaging at 1132 cm^{-1}, 1174 cm^{-1}, 1298 cm^{-1}, 1444 cm^{-1} and 1420 cm^{-1} with very weak contribution of 5-FU bands at 364 cm^{-1}, 574 cm^{-1}, 648 cm^{-1}, 772 cm^{-1}, 820 cm^{-1} and 1232 cm^{-1}. While at -500 µm (Figure 45b), -700 µm (Figure 45c)

and -900 µm (Figure 45d), 5-FU bands form are predominant in the spectra which are at 364 cm^{-1}, 488 cm^{-1}, 574 cm^{-1}, 648 cm^{-1}, 772 cm^{-1}, 820 cm^{-1}, 1026 cm^{-1}, 1188 cm^{-1}, 1232 cm^{-1}, 1292 cm^{-1}, 1356 cm^{-1}, 1616 cm^{-1} and 1680 cm^{-1}. Spectrum of 5-FU 50 $g{\cdot}L^{-1}$ in Figure 45e is used as a comparison to identify 5-FU regions in the bag.

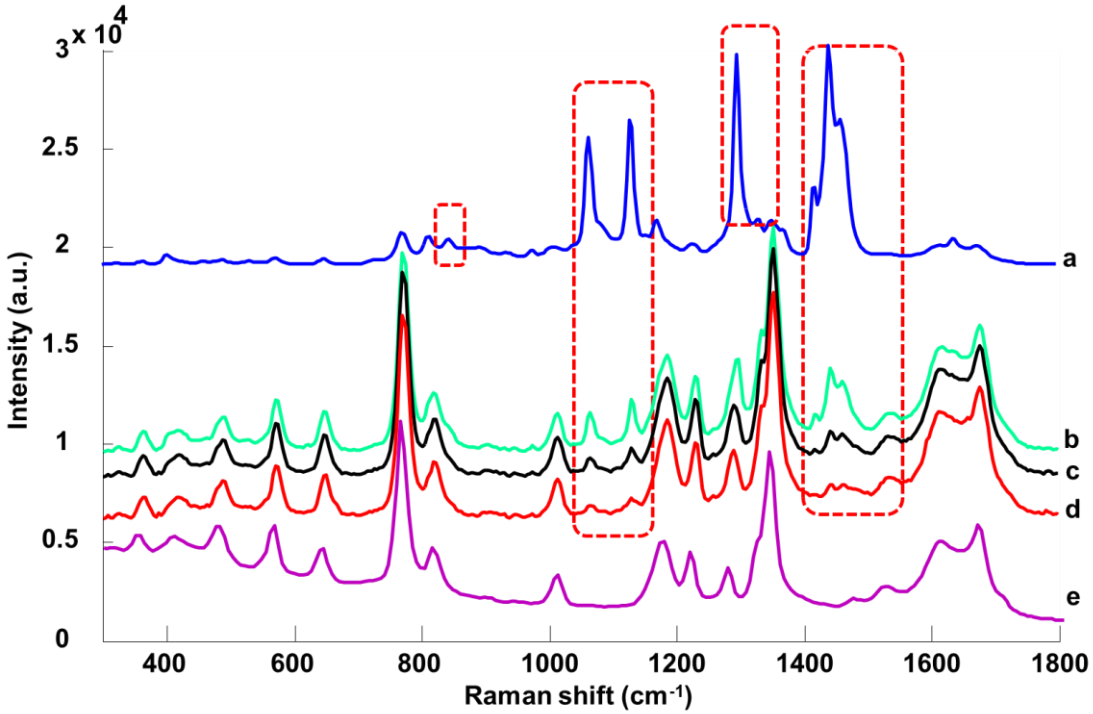


Figure 45. Mean Raman spectra of 5-FU 40 $g{\cdot}L^{-1}$ in 5% glucose bag using 633 nm laser at: a) -300 µm, b) -500 µm, c) -700 µm and d) -900 µm compared to a spectrum of the commercial solution 5-FU (50 $g{\cdot}L^{-1}$) recorded using a quartz cuvette. Spectra are offset for clarity

- Quantification by 633 nm

Figure 46 presents mean Raman spectra recorded at 900µm. A proportional decrease in intensity can be observed with the decrease in concentration and strong 5-FU dominated the spectra. Although, for the lowest concentration (1.3 $g{\cdot}L^{-1}$, Figure 46e) bag features at 1068 cm^{-1}, 1232 cm^{-1}, 1448 cm^{-1} and 1464 cm^{-1} are become more pronounced as the drug features become very weak.

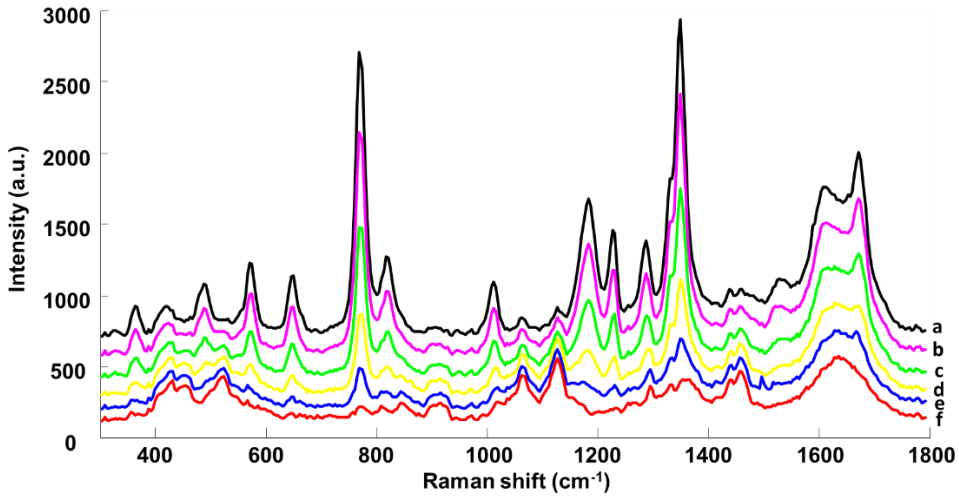


Figure 46. Mean Raman spectra of 5-FU in 5% glucose bag using 633 nm laser at 900 µm. Concentrations are arranged from the top to the bottom according to decrease in intensity. a) 40 $g{\cdot}L^{-1}$, b) 30.6 $g{\cdot}L^{-1}$, c) 20.7 $g{\cdot}L^{-1}$, d) 10.9 $g{\cdot}L^{-1}$, e) 5.4 $g{\cdot}L^{-1}$ and f) 1.3 $g{\cdot}L^{-1}$

The quantification of chemotherapeutic solutions by 633 nm has also shown optimistic results at the fingerprint region (Table 7) as those obtained with 532 nm at the same depth. The specificity of the PLSR is illustrated in Figure 47 for 5-FU with the regression coefficient.

Table 7. Summary of PLSR results of data recorded using 633 nm laser at 900µm using 4 LVs

Drug	**LVs**	R^2	**RMSECV ($g{\cdot}L^{-1}$)**
MTX	3	0.9889	0.6818
5-FU	4	0.9884	1.4655
GEM	5	0.9458	0.571

Figure 47 presents the regression coefficients of PLSR at 900µm. Negative features of the packing are presented at 1132 cm^{-1}, 1174 cm^{-1} and 1444 cm^{-1} and the rest of peaks are characteristic features of 5-FU that have been observed in Figure 45.

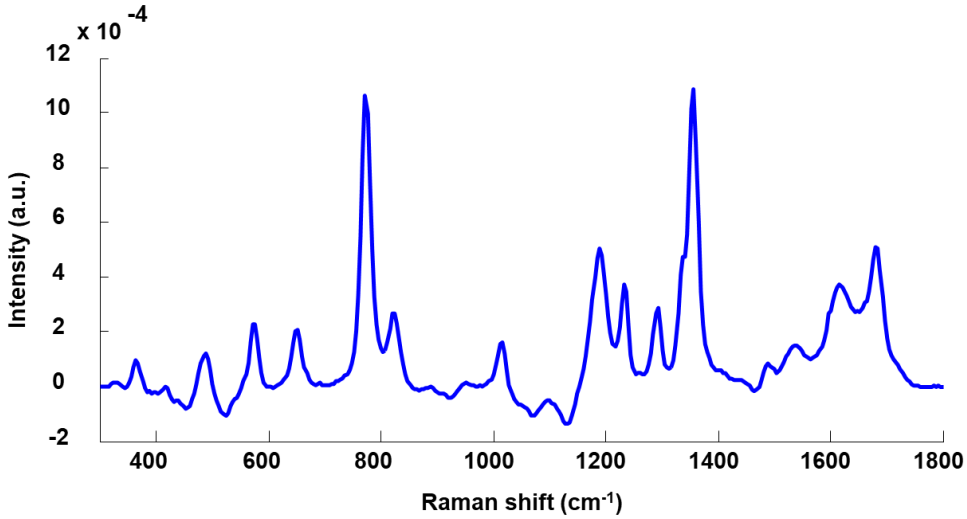


Figure 47. Regression coefficients of PLSR at -900 µm for 5-FU by 633 nm laser

- Discrimination by 633 nm

Table 8 presents specificity and sensitivity calculated from PLSDA confusion matrix at 900 µm which presented 100% of classification for the 3 tested drugs.

Table 8. Specificity and sensitivity% obtained by PLSDA at 900 µm by 633 nm laser

Drug	Specificity	Sensitivity
MTX	100	100
5-FU	100	100
GEM	100	100

Figure 48 presents regression coefficients of PLSDA using 633 nm laser which are presenting similar features observed before with 532 nm laser. Figure 48a presents bands at 520 cm^{-1}, 668 cm^{-1}, 1200 cm^{-1}, 1348 cm^{-1}, 1572 cm^{-1}, 1548 cm^{-1} and 1596 cm^{-1} are characteristic of MTX while bands observed in the second regression coefficient (Figure 48b) at 572 cm^{-1}, 652 cm^{-1}, 772 cm^{-1}, 824 cm^{-1}, 1188 cm^{-1}, 1336 cm^{-1} , 1356 cm^{-1} and 1680 cm^{-1} are due to 5-FU. However, GEM features are presented in the third regression coefficient (Figure 48c) at 780 cm^{-1} and 1252 cm^{-1}.

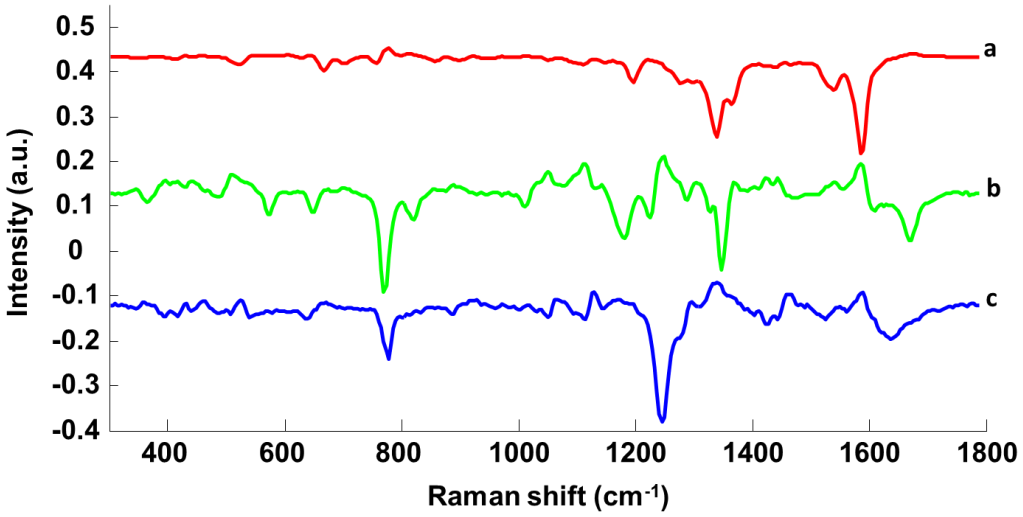


Figure 48. Regression coefficients of PLSDA; a) the first, b) the second and c) the third. Spectra are offset for clarity

5.2.2 Perspectives and future work with CRM

Direct analysis of chemotherapeutic preparations through infusion bags remains a hot topic to be further investigated. This study has demonstrated the potential of CRM for a limited number of drugs (n = 3) but highlighted the potential of Raman spectroscopy. Although, other Raman instruments can be used, inverted microscope, remote optical fibres probes and handheld devices, no thorough benchmarking has been performed to date. Ideally a standardised protocol should be used to propose a direct comparison of performances and correlate analytical performances to a number of parameters such as selection of laser lines, concentration range and sample presentation.

The results presented in **Section 5** remains preliminary however they demonstrate that the 2 lasers deliver similar results for the molecules selected. No noticeable difference in Raman spectra were observed. MTX, 5-FU and GEM absorb in the UV range (Figure 41) hence, with the 532 nm laser source no interference from fluorescence or other background was observed. In comparison anthracyclines drugs used in **Section 3** (i.e. DOX, EPI and DAU) have maximum absorbance in the visible range at 480 nm. However, the Raman analysis has been performed using a 691 nm excitation laser hence possible fluorescence wasn't a limitation. It would be relevant to extend the direct analysis for such molecules to demonstrate the importance of laser source used, notably for the case of green lasers.

Ultimately, the confocality and automated nature of the Raman system has enabled investigation of the spectral characters at different depths. It can be anticipated that with optimised protocol the microscope could be set to directly perform the analysis at a defined depth (for example 900 µm). As a result, the acquisition time could be significantly reduced to match requirement for AQC in the preparation units.

To evaluate the performance of analytical method, it is important to develop model for the estimation and evaluation of the quality of measurement. Limit of detection (LOD) and limit of quantification (LOQ) are figures of merit frequently used. Although, chemotherapeutic drugs are used at high concentration range delivering strong Raman signature, the spectral response depends on the structural characteristic of the drug molecule. LOD and LOQ estimation depends on the spectral features present for a molecule. At the university hospital of Tours, UBCO, about 40 different chemotherapeutic molecules are used. It is most likely that each one of them is characterised by a different Raman response. Ideally, validation of Raman spectroscopy for direct analysis in infusion bags should include an investigation of the detection and quantification limits for each anticancer drug.

The LOD is a critical criterion to establish the applicability of the analytical technique. PCA performed on the spectra recorded from solutions at lower concentrations than the clinical range highlight that the 3 drugs won't have the same LOD (Figure 49). Here, the spectra collected from the solutions containing the drugs have been compared to the blank solution (5% glucose). The three drugs are at roughly the same concentration (MTX tested at 0.75 $g{\cdot}L^{-1}$ and 2 $g{\cdot}L^{-1}$; 5-FU at 0.5 $g{\cdot}L^{-1}$ and 0.75 $g{\cdot}L^{-1}$ and GEM at 1 $g{\cdot}L^{-1}$ and 2 $g{\cdot}L^{-1}$).

For MTX the scatter plot (Figure 49A) the blank containing glucose is discriminated from the solutions along PC1 therefore the LOD is below the clinical range. The loading spectra (Figure 49Da) presents negative bands at 667 cm^{-1}, 1204 cm^{-1}, 1349 cm^{-1}, 1547 cm^{-1} and 1597 cm^{-1} which are characteristic of MTX. Similarly, for GEM a clear identification has been obtained for GEM 1 $g{\cdot}L^{-1}$ and 2 $g{\cdot}L^{-1}$ from the blank glucose solution as seen in scatter plot (Figure 49B). The loading plot in Figure 49Db has shown positive bands at 780 cm^{-1} and 1250 cm^{-1} which are due to GEM and other 2 negative bands at 1049 cm^{-1} and 1115 cm^{-1} for the 5% glucose or the bag material. Hence the LOD for GEM seems to be less than 1 $g{\cdot}L^{-1}$.

However, for 5-FU for concentrations at 0.5 $g{\cdot}L^{-1}$ and 0.75 $g{\cdot}L^{-1}$ no clear separation from the glucose solution is seen (Figure 49C). Moreover, the loading spectra (Figure 49Dc) showed bands at 1285 cm^{-1} and 1434 cm^{-1} which are due the bag material. LOD of 5-FU is greater than 0.5 $g{\cdot}L^{-1}$.

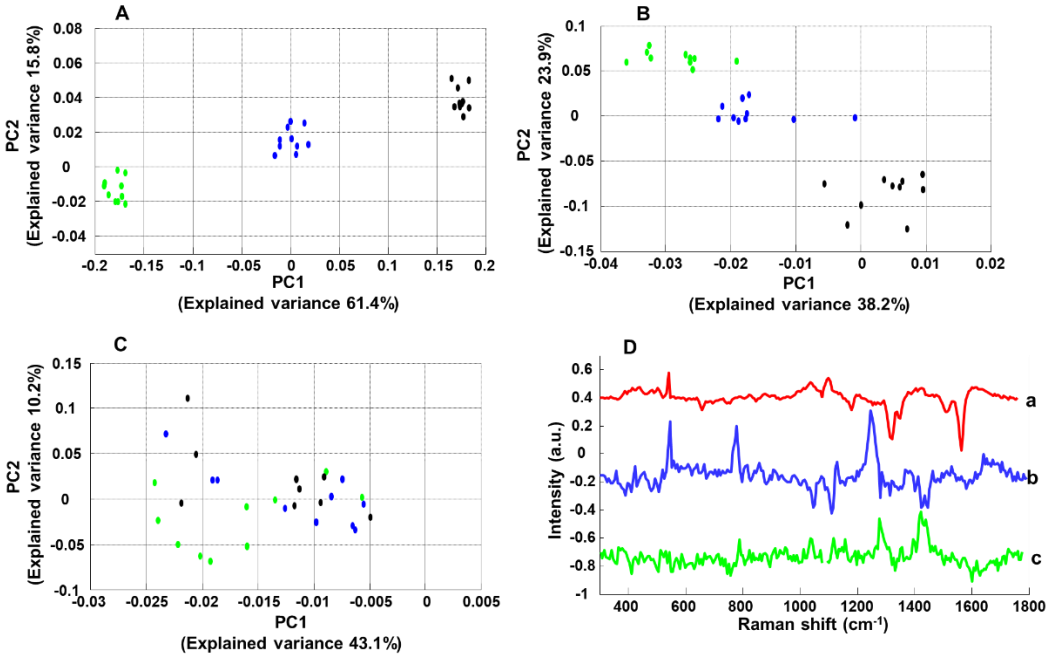


Figure 49. PCA performed for MTX, GEM and 5-FU presenting the scatter plot of: A), MTX B), GEM and C) 5-FU. D plot presents the loading spectrum of a) MTX, b) GEM and c) 5-FU. Spectra are offset for clarity

6. PERSPECTIVES AND FUTURE WORK

1) The UBCO unit has purchased a QCPrep+® analyser for AQC of chemotherapeutic preparations. It would be interesting to set up benchmarking of this system with CRM. The UV-Vis detection could be used to provide the reference concentrations while the performance of the Raman analysis would be compared for both set ups.

2) The Raman response differs significantly between small molecules and mAbs. Actually, it has been demonstrated that quantification and discrimination is achieved thanks to excipients in formulations that play the role of internal standard. There is still little literature about application of VS on those therapeutic proteins. Firstly, it would be of interest to gather a list of all mAbs currently prescribed at the UBCO and seek for commercial solutions with identical compositions. An extended investigation on a larger panel of mAbs is necessary to highlight evaluate the potential of Raman spectroscopy for discrimination of this class of anticancer agents. Secondly, the study reported in publication 3 could be easily transposed to direct analysis into infusion bags for direct analysis with CRM.

7. REFERENCES:

[1] S.R. Khandasammy, M.A. Fikiet, E. Mistek, Y. Ahmed, L. Halámková, J. Bueno, I.K. Lednev, Bloodstains, paintings, and drugs: Raman spectroscopy applications in forensic science, Forensic Chem. 8 (2018) 111–133. https://doi.org/10.1016/j.forc.2018.02.002.

[2] N.A. Macleod, P. Matousek, Emerging non-invasive raman methods in process control and forensic applications, Pharm. Res. 25 (2008) 2205–2215. https://doi.org/10.1007/s11095-008-9587-2.

[3] K.C. Doty, I.K. Lednev, Raman spectroscopy for forensic purposes: Recent applications for serology and gunshot residue analysis, TrAC - Trends Anal. Chem. 103 (2018) 215–222. https://doi.org/10.1016/j.trac.2017.12.003.

[4] B. Kann, H.L. Offerhaus, M. Windbergs, C. Otto, Raman microscopy for cellular investigations - From single cell imaging to drug carrier uptake visualization, Adv. Drug Deliv. Rev. 89 (2015) 71–90. https://doi.org/10.1016/j.addr.2015.02.006.

[5] K. Chrabaszcz, A. Jasztal, M. Smęda, B. Zieliński, A. Blat, M. Diem, S. Chlopicki, K. Malek, K.M. Marzec, Label-free FTIR spectroscopy detects and visualizes the early stage of pulmonary micrometastasis seeded from breast carcinoma, Biochim. Biophys. Acta - Mol. Basis Dis. 1864 (2018) 3574–3584. https://doi.org/10.1016/j.bbadis.2018.08.022.

[6] G. Bellisola, C. Sorio, Infrared spectroscopy and microscopy in cancer research and diagnosis, Am. J. Cancer Res. 2 (2012) 1–21.

[7] L.M. Moreira, L. Silveira, F. V. Santos, J.P. Lyon, R. Rocha, R.A. Zângaro, A.B. Villaverde, M.T.T. Pacheco, Raman spectroscopy: A powerful technique for biochemical analysis and diagnosis, Spectroscopy. 22 (2008) 1–19. https://doi.org/10.3233/SPE-2008-0326.

[8] M. Kyriakidou, J. Anastassopoulou, A. Tsakiris, M. Koui, T. Theophanides, FT-IR spectroscopy study in early diagnosis of skin cancer, In Vivo (Brooklyn). 31 (2017) 1131–1137. https://doi.org/10.21873/invivo.11179.

[9] L. Franzen, M. Windbergs, Applications of Raman spectroscopy in skin research - From skin physiology and diagnosis up to risk assessment and dermal drug delivery, Adv. Drug Deliv. Rev. 89 (2015) 91–104. https://doi.org/10.1016/j.addr.2015.04.002.

[10] L.P. Choo-Smith, H.G.M. Edwards, H.P. Endtz, J.M. Kros, F. Heule, H. Barr, J.S. Robinson, H.A. Bruining, G.J. Puppels, Medical applications of Raman spectroscopy: From proof of principle to clinical implementation, Biopolym. - Biospectroscopy Sect. 67 (2002) 1–9. https://doi.org/10.1002/bip.10064.

[11] Z. Farhane, F. Bonnier, A. Casey, H.J. Byrne, Raman micro spectroscopy for in vitro drug screening: Subcellular localisation and interactions of doxorubicin, Analyst. 140 (2015) 4212–4223. https://doi.org/10.1039/c5an00256g.

[12] Z. Farhane, H. Nawaz, F. Bonnier, H.J. Byrne, In vitro label-free screening of chemotherapeutic drugs using Raman microspectroscopy: Towards a new paradigm of spectralomics, J. Biophotonics. 11 (2018). https://doi.org/10.1002/jbio.201700258.

[13] Z. Farhane, F. Bonnier, M.A. Maher, J. Bryant, A. Casey, H.J. Byrne, Differentiating responses of lung cancer cell lines to Doxorubicin exposure: in vitro Raman micro spectroscopy, oxidative stress and bcl-2 protein expression, J. Biophotonics. 10 (2017) 151–165. https://doi.org/10.1002/jbio.201600019.

[14] G. Zhang, D.J. Moore, K.B. Sloan, C.R. Flach, R. Mendelsohn, Imaging the prodrug-to-drug transformation of a 5-fluorouracil derivative in skin by confocal Raman microscopy, J. Invest. Dermatol. 127 (2007) 1205–1209. https://doi.org/10.1038/sj.jid.5700690.

[15] L. Miloudi, F. Bonnier, A. Tfayli, F. Yvergnaux, H.J. Byrne, I. Chourpa, E. Munnier,

Confocal Raman spectroscopic imaging for in vitro monitoring of active ingredient penetration and distribution in reconstructed human epidermis model, J. Biophotonics. 11 (2018) 1–17. https://doi.org/10.1002/jbio.201700221.
[16] G.L. Owens, K. Gajjar, J. Trevisan, S.W. Fogarty, S.E. Taylor, B. Da Gama-Rose, P.L. Martin-Hirsch, F.L. Martin, Vibrational biospectroscopy coupled with multivariate analysis extracts potentially diagnostic features in blood plasma/serum of ovarian cancer patients, J. Biophotonics. 7 (2014) 200–209. https://doi.org/10.1002/jbio.201300157.
[17] H.J. Byrne, F. Bonnier, J. McIntyre, D.R. Parachalil, Quantitative analysis of human blood serum using vibrational spectroscopy, Clin. Spectrosc. 2 (2020) 100004. https://doi.org/10.1016/j.clispe.2020.100004.
[18] D.R. Parachalil, J. McIntyre, H.J. Byrne, Potential of Raman spectroscopy for the analysis of plasma/serum in the liquid state: recent advances, Anal. Bioanal. Chem. 412 (2020) 1993–2007. https://doi.org/10.1007/s00216-019-02349-1.
[19] K.A. Esmonde-White, M. Cuellar, C. Uerpmann, B. Lenain, I.R. Lewis, Raman spectroscopy as a process analytical technology for pharmaceutical manufacturing and bioprocessing, Anal. Bioanal. Chem. 409 (2017) 637–649. https://doi.org/10.1007/s00216-016-9824-1.
[20] A. Paudel, D. Raijada, J. Rantanen, Raman spectroscopy in pharmaceutical product design, Adv. Drug Deliv. Rev. 89 (2015) 3–20. https://doi.org/10.1016/j.addr.2015.04.003.
[21] G.N. Kalinkova, Infrared spectroscopy in pharmacy, Vib. Spectrosc. 19 (1999) 307–320. https://doi.org/10.1016/S0924-2031(99)00017-X.
[22] A. Rohman, Application of Fourier Transform Infrared Spectroscopy for Quality Control of Pharmaceutical Products: a Review, Indones. J. Pharm. 23 (2013) 1–8. http://indonesianjpharm.com/index.php/jurnal/article/view/57%5Cnhttp://indonesianjpharm.com/index.php/jurnal/article/download/57/57.
[23] A.A. Bunaciu, H.Y. Aboul-Enein, V.D. Hoang, Vibrational spectroscopy used in polymorphic analysis, TrAC - Trends Anal. Chem. 69 (2015) 14–22. https://doi.org/10.1016/j.trac.2015.02.006.
[24] M.C. Hennigan, A.G. Ryder, Quantitative polymorph contaminant analysis in tablets using Raman and near infra-red spectroscopies, J. Pharm. Biomed. Anal. 72 (2013) 163–171. https://doi.org/10.1016/j.jpba.2012.10.002.
[25] G. Lawson, J. Ogwu, S. Tanna, Quantitative screening of the pharmaceutical ingredient for the rapid identification of substandard and falsified medicines using reflectance infrared spectroscopy, PLoS One. 13 (2018) 1–17. https://doi.org/10.1371/journal.pone.0202059.
[26] S. Wartewig, R.H.H. Neubert, Pharmaceutical applications of Mid-IR and Raman spectroscopy, Adv. Drug Deliv. Rev. 57 (2005) 1144–1170. https://doi.org/10.1016/j.addr.2005.01.022.
[27] T.S. Renuga Devi, S. Gayathri, FTIR And FT-Raman spectral analysis of Paclitaxel drugs, Int. J. Pharm. Sci. Rev. Res. 2 (2010) 106–110.
[28] A.A. Nuhu, Recent analytical approaches to counterfeit drug detection, J. Appl. Pharm. Sci. 1 (2011) 06–13.
[29] G. Lawson, Counterfeit Tablet Investigations: Can ATR FT/IR Provide Rapid Targeted Quantitative Analyses?, J. Anal. Bioanal. Tech. 5 (2014). https://doi.org/10.4172/2155-9872.1000214.
[30] F. Lu, X. Weng, Y. Chai, Y. Yang, Y. Yu, G. Duan, A novel identification system for counterfeit drugs based on portable Raman spectroscopy, Chemom. Intell. Lab. Syst. 127 (2013) 63–69. https://doi.org/10.1016/j.chemolab.2013.06.001.
[31] L. Miloudi, F. Bonnier, D. Bertrand, H.J. Byrne, X. Perse, I. Chourpa, E. Munnier,

Quantitative analysis of curcumin-loaded alginate nanocarriers in hydrogels using Raman and attenuated total reflection infrared spectroscopy, Anal. Bioanal. Chem. 409 (2017) 4593–4605. https://doi.org/10.1007/s00216-017-0402-y.
[32] T. Rajalahti, O.M. Kvalheim, Multivariate data analysis in pharmaceutics: A tutorial review, Int. J. Pharm. 417 (2011) 280–290. https://doi.org/10.1016/j.ijpharm.2011.02.019.
[33] H.J. Byrne, P. Knief, M.E. Keating, F. Bonnier, Spectral pre and post processing for infrared and Raman spectroscopy of biological tissues and cells, Chem. Soc. Rev. 45 (2016) 1865–1878. https://doi.org/10.1039/c5cs00440c.
[34] F. Bonnier, H.J. Byrne, Understanding the molecular information contained in principal component analysis of vibrational spectra of biological systems, Analyst. 137 (2012) 322–332. https://doi.org/10.1039/c1an15821j.
[35] S.J. Mazivila, A.C. Olivieri, Chemometrics coupled to vibrational spectroscopy and spectroscopic imaging for the analysis of solid-phase pharmaceutical products: A brief review on non-destructive analytical methods, TrAC - Trends Anal. Chem. 108 (2018) 74–87. https://doi.org/10.1016/j.trac.2018.08.013.
[36] L.C. Lee, C.Y. Liong, A.A. Jemain, Partial least squares-discriminant analysis (PLS-DA) for classification of high-dimensional (HD) data: A review of contemporary practice strategies and knowledge gaps, Analyst. 143 (2018) 3526–3539. https://doi.org/10.1039/c8an00599k.
[37] M. Febrero-Bande, P. Galeano, W. González-Manteiga, Functional Principal Component Regression and Functional Partial Least-squares Regression: An Overview and a Comparative Study, Int. Stat. Rev. 85 (2017) 61–83. https://doi.org/10.1111/insr.12116.
[38] S. Guo, T. Bocklitz, U. Neugebauer, J. Popp, Common mistakes in cross-validating classification models, Anal. Methods. 9 (2017) 4410–4417. https://doi.org/10.1039/c7ay01363a.
[39] M. Najafi, M.R. Hooshangi Shayesteh, K. Mortezaee, B. Farhood, H. Haghi-Aminjan, The role of melatonin on doxorubicin-induced cardiotoxicity: A systematic review, Life Sci. 241 (2020). https://doi.org/10.1016/j.lfs.2019.117173.
[40] K. Yu, M. Liu, H. Dai, X. Huang, Targeted drug delivery systems for bladder cancer therapy, J. Drug Deliv. Sci. Technol. 56 (2020) 101535. https://doi.org/10.1016/j.jddst.2020.101535.
[41] C. Rojas, Y. Casablanca, Chemotherapy, Biologic, and Immunotherapy Breakthroughs in Cancer Care, Obstet. Gynecol. Clin. North Am. 46 (2019) 137–154. https://doi.org/10.1016/j.ogc.2018.09.009.
[42] M. Norouzi, M. Amerian, M. Amerian, F. Atyabi, Clinical applications of nanomedicine in cancer therapy, Drug Discov. Today. 25 (2020) 107–125. https://doi.org/10.1016/j.drudis.2019.09.017.
[43] P.S. Hegde, D.S. Chen, Top 10 Challenges in Cancer Immunotherapy, Immunity. 52 (2020) 17–35. https://doi.org/10.1016/j.immuni.2019.12.011.
[44] E. Dickens, S. Ahmed, Principles of cancer treatment by chemotherapy, Surg. (United Kingdom). 36 (2018) 134–138. https://doi.org/10.1016/j.mpsur.2017.12.002.
[45] C.D. Phung, H.T. Nguyen, T.H. Tran, H.G. Choi, C.S. Yong, J.O. Kim, Rational combination immunotherapeutic approaches for effective cancer treatment, J. Control. Release. 294 (2019) 114–130. https://doi.org/10.1016/j.jconrel.2018.12.020.
[46] B. V. Patel, J.M. Hotaling, Impact of chemotherapy on subsequent generations, Urol. Oncol. Semin. Orig. Investig. 38 (2020) 10–13. https://doi.org/10.1016/j.urolonc.2019.02.011.
[47] G. Bregni, T. Akin Telli, S. Camera, A. Deleporte, L. Moretti, A.M. Bali, G. Liberale,

S. Holbrechts, A. Hendlisz, F. Sclafani, Adjuvant chemotherapy for rectal cancer: Current evidence and recommendations for clinical practice, Cancer Treat. Rev. 83 (2020) 101948. https://doi.org/10.1016/j.ctrv.2019.101948.
[48] J.I. Griffiths, A.L. Cohen, V. Jones, R. Salgia, J.T. Chang, A.H. Bild, Opportunities for improving cancer treatment using systems biology, Curr. Opin. Syst. Biol. 17 (2019) 41–50. https://doi.org/10.1016/j.coisb.2019.10.018.
[49] H. Abdel-Razeq, Current frontline endocrine treatment options for women with hormone receptor-positive, Human Epidermal Growth Factor Receptor 2 (HER2)-negative advanced-stage breast cancer, Hematol. Oncol. Stem Cell Ther. 12 (2019) 1–9. https://doi.org/10.1016/j.hemonc.2018.04.002.
[50] H.L. McLeod, Therapeutic drug monitoring opportunities in cancer therapy, Pharmacol. Ther. 74 (1997) 39–54. https://doi.org/10.1016/S0163-7258(96)00201-X.
[51] C. Monneret, Recent developments in the field of antitumour anthracyclines, Eur. J. Med. Chem. 36 (2001) 483–493. https://doi.org/10.1016/S0223-5234(01)01244-2.
[52] R.K. Singh, S. Kumar, D.N. Prasad, T.R. Bhardwaj, Therapeutic journery of nitrogen mustard as alkylating anticancer agents: Historic to future perspectives, Eur. J. Med. Chem. 151 (2018) 401–433. https://doi.org/10.1016/j.ejmech.2018.04.001.
[53] N. Brock, Ideas and reality in the development of cancer chemotherapeutic agents, with particular reference to oxazaphosphorine cytostatics, J. Cancer Res. Clin. Oncol. 111 (1986) 1–12. https://doi.org/10.1007/BF00402768.
[54] S. Smith, S. Prewett, Principles of chemotherapy and radiotherapy, Obstet. Gynaecol. Reprod. Med. 30 (2020) 72–78. https://doi.org/10.1016/j.ogrm.2019.12.004.
[55] S. Nussbaumer, P. Bonnabry, J.L. Veuthey, S. Fleury-Souverain, Analysis of anticancer drugs: A review, Talanta. 85 (2011) 2265–2289. https://doi.org/10.1016/j.talanta.2011.08.034.
[56] K. Singh, M. Bhori, Y.A. Kasu, G. Bhat, T. Marar, Antioxidants as precision weapons in war against cancer chemotherapy induced toxicity – Exploring the armoury of obscurity, Saudi Pharm. J. 26 (2018) 177–190. https://doi.org/10.1016/j.jsps.2017.12.013.
[57] M. Savelli, M. Roche, C. Curti, C. Bornet, P. Rathelot, M. Montana, P. Vanelle, Methods to control anticancer chemotherapy preparations ranked by risk analysis, Pharmazie. 73 (2018) 251–259. https://doi.org/10.1691/ph.2018.7205.
[58] F. Dziopa, G. Galy, S. Bauler, B. Vincent, S. Crochon, M.L. Tall, F. Pirot, C. Pivot, A quantitative and qualitative method to control chemotherapeutic preparations by Fourier transform infrared-ultraviolet spectrophotometry, J. Oncol. Pharm. Pract. 19 (2013) 121–129. https://doi.org/10.1177/1078155212457963.
[59] C. Bazin, B. Cassard, E. Caudron, P. Prognon, L. Havard, Comparative analysis of methods for real-time analytical control of chemotherapies preparations, Int. J. Pharm. 494 (2015) 329–336. https://doi.org/10.1016/j.ijpharm.2015.08.041.
[60] A. Delmas, J.B. Gordien, J.M. Bernadou, M. Roudaut, A. Gresser, L. Malki, M.C. Saux, D. Breilh, Quantitative and qualitative control of cytotoxic preparations by HPLC-UV in a centralized parenteral preparations unit, J. Pharm. Biomed. Anal. 49 (2009) 1213–1220. https://doi.org/10.1016/j.jpba.2009.03.007.
[61] I. Badea, L. Lazăr, D. Moja, D. Nicolescu, A. Tudose, A HPLC method for the simultaneous determination of seven anthracyclines, J. Pharm. Biomed. Anal. 39 (2005) 305–309. https://doi.org/10.1016/j.jpba.2005.03.039.
[62] N. Navas, A. Herrera, A. Martínez-Ortega, A. Salmerón-García, J. Cabeza, L. Cuadros-Rodríguez, Quantification of an intact monoclonal antibody, rituximab, by (RP)HPLC/DAD in compliance with ICH guidelines, Anal. Bioanal. Chem. 405 (2013) 9351–9363. https://doi.org/10.1007/s00216-013-7368-1.

[63] V. Castagne, H. Habert, C. Abbara, E. Rudant, L. Bonhomme-Faivre, Cytotoxics compounded sterile preparation control by HPLC during a 16-month assessment in a French university hospital: Importance of the mixing bags step, J. Oncol. Pharm. Pract. 17 (2011) 191–196. https://doi.org/10.1177/1078155210376846.
[64] A.S. Rodrigues, A.R. Lopes, A. Leão, A. Couceiro, A.B.S. Ribeiro, F. Ramos, M.I.N. Da Silveira, C.R. De Oliveira, Development of an analytical methodology for simultaneous determination of vincristine and doxorubicin in pharmaceutical preparations for oncology by HPLC-UV, J. Chromatogr. Sci. 47 (2009) 387–391. https://doi.org/10.1093/chromsci/47.5.387.
[65] E. Gravel, P. Bourget, L. Mercier, A. Paci, Fluorescence detection combined with either HPLC or HPTLC for pharmaceutical quality control in a hospital chemotherapy production unit: Application to camptothecin derivatives, J. Pharm. Biomed. Anal. 39 (2005) 581–586. https://doi.org/10.1016/j.jpba.2005.05.010.
[66] J. Bouligand, T. Storme, I. Laville, L. Mercier, O. Oberlin, G. Vassal, P. Bourget, A. Paci, Quality control and stability study using HPTLC: Applications to cyclophosphamide in various pharmaceutical products, J. Pharm. Biomed. Anal. 38 (2005) 180–185. https://doi.org/10.1016/j.jpba.2004.12.001.
[67] C. Bazin, V. Vieillard, A. Astier, M. Paul, Implementation of real-time identification analysis and quantification of chemotherapies preparations with a Multispec® analyser, Ann. Pharm. Fr. 72 (2014) 33–40. https://doi.org/10.1016/j.pharma.2013.09.006.
[68] P. Bourget, A. Amin, F. Vidal, C. Merlette, P. Troude, A. Baillet-Guffroy, The contribution of Raman spectroscopy to the analytical quality control of cytotoxic drugs in a hospital environment: Eliminating the exposure risks for staff members and their work environment, Int. J. Pharm. 470 (2014) 70–76. https://doi.org/10.1016/j.ijpharm.2014.04.064.
[69] P. Bourget, A. Amin, F. Vidal, C. Merlette, F. Lagarce, Comparison of Raman spectroscopy vs. high performance liquid chromatography for quality control of complex therapeutic objects: Model of elastomeric portable pumps filled with a fluorouracil solution, J. Pharm. Biomed. Anal. 91 (2014) 176–184. https://doi.org/10.1016/j.jpba.2013.12.030.
[70] L.M.M. Lê, M. Berge, A. Tfayli, J. Zhou, P. Prognon, A. Baillet-Guffroy, E. Caudron, Rapid discrimination and quantification analysis of five antineoplastic drugs in aqueous solutions using Raman spectroscopy, Eur. J. Pharm. Sci. 111 (2018) 158–166. https://doi.org/10.1016/j.ejps.2017.09.046.
[71] L.M.M. Le, B. Kégl, A. Gramfort, C. Marini, D. Nguyen, M. Cherti, S. Tfaili, A. Tfayli, A. Baillet-Guffroy, P. Prognon, P. Chaminade, E. Caudron, Optimization of classification and regression analysis of four monoclonal antibodies from Raman spectra using collaborative machine learning approach, Talanta. 184 (2018) 260–265. https://doi.org/10.1016/j.talanta.2018.02.109.
[72] M. Kiehntopf, B. Mönch, R. Salzer, M. Kupfer, M. Hartmann, Quality control of cytotoxic drug preparations by means of Raman Spectroscopy, Pharmazie. 67 (2012) 95–96. https://doi.org/10.1691/ph.2012.1091.
[73] T. Chouquet, G. Benoit, K. Morand, Implementation of Analytical Control of Low Volume Pediatric Cytotoxic Drugs Preparations using a UV/Raman Spectrophotometer, Pharm. Technol. Hosp. Pharm. 1 (2016) 151–162. https://doi.org/10.1515/pthp-2016-0013.
[74] T. Chouquet, G. Benoit, K. Morand, Analytical Control of Pediatric Chemotherapy Preparations with a UV-Raman Automaton: Results After 18 Months of Implementation and Development of A Suitable Method for Low Volume Preparations, Pharm. Technol. Hosp. Pharm. 2 (2017) 117–129. https://doi.org/10.1515/pthp-2017-0021.

[75] F. Nardella, M. Beck, P. Collart-Dutilleul, G. Becker, C. Boulanger, L. Perello, A. Gairard-Dory, B. Gourieux, G. Ubeaud-Séquier, A UV-Raman spectrometry method for quality control of anticancer preparations: Results after 18 months of implementation in hospital pharmacy, Int. J. Pharm. 499 (2016) 343–350. https://doi.org/10.1016/j.ijpharm.2016.01.002.
[76] P. Bourget, A. Amin, F. Vidal, C. Merlette, F. Lagarce, Comparison of Raman spectroscopy vs. high performance liquid chromatography for quality control of complex therapeutic objects: Model of elastomeric portable pumps filled with a fluorouracil solution, J. Pharm. Biomed. Anal. 91 (2014) 176–184. https://doi.org/10.1016/j.jpba.2013.12.030.
[77] A. Amin, P. Bourget, F. Vidal, F. Ader, Routine application of Raman spectroscopy in the quality control of hospital compounded ganciclovir, Int. J. Pharm. 474 (2014) 193–201. https://doi.org/10.1016/j.ijpharm.2014.08.028.
[78] L.M.M. Lê, A. Tfayli, J. Zhou, P. Prognon, A. Baillet-Guffroy, E. Caudron, Discrimination and quantification of two isomeric antineoplastic drugs by rapid and non-invasive analytical control using a handheld Raman spectrometer, Talanta. 161 (2016) 320–324. https://doi.org/10.1016/j.talanta.2016.07.025.
[79] L. Lê, M. Berge, A. Tfayli, P. Prognon, E. Caudron, Discriminative and Quantitative Analysis of Antineoplastic Taxane Drugs Using a Handheld Raman Spectrometer, Biomed Res. Int. 2018 (2018) 12–15. https://doi.org/10.1155/2018/8746729.
[80] L. Lê, M. Berge, A. Tfayli, A. Baillet Guffroy, P. Prognon, A. Dowek, E. Caudron, Quantification of gemcitabine intravenous drugs by direct measurement in chemotherapy plastic bags using a handheld Raman spectrometer, Talanta. 196 (2019) 376–380. https://doi.org/10.1016/j.talanta.2018.11.062.
[81] C. Bazin, V. Vieillard, A. Astier, M. Paul, Implementation of real-time identification analysis and quantification of chemotherapies preparations with a Multispec® analyser, Ann. Pharm. Fr. 72 (2014) 33–40. https://doi.org/10.1016/j.pharma.2013.09.006.
[82] G.S. Bumbrah, R.M. Sharma, Raman spectroscopy – Basic principle, instrumentation and selected applications for the characterization of drugs of abuse, Egypt. J. Forensic Sci. 6 (2016) 209–215. https://doi.org/10.1016/j.ejfs.2015.06.001.
[83] J.R. Ferraro, K. Nakamoto, C.W. Brown, Introductory Raman Spectroscopy: Second Edition, 2003. https://doi.org/10.1016/B978-0-12-254105-6.X5000-8.
[84] G. Ramer, B. Lendl, Attenuated Total Reflection Fourier Transform Infrared Spectroscopy, Encycl. Anal. Chem. (2013) 1–27. https://doi.org/10.1002/9780470027318.a9287.
[85] D.G. Watson, R. Edrada-Ebel, Pharmaceutical Analysis: A Textbook for Pharmacy Students and Pharmaceutical Chemists, 2012.
[86] D.L. Pavia, G.M. Lampman, G.S. Kriz, J.R. Vyvyan, Introduction to spectroscopy, 2013. https://doi.org/10.1887/0750303468/b293c1.
[87] E. Smith, G. Dent, Introduction, Basic Theory and Principles, Mod. Raman Spectrosc. 5 (2019) 1–20. https://doi.org/10.1002/9781119440598.ch1.
[88] M. Stomp, J. Huisman, L.J. Stal, H.C.P. Matthijs, Colorful niches of phototrophic microorganisms shaped by vibrations of the water molecule, ISME J. 1 (2007) 271–282. https://doi.org/10.1038/ismej.2007.59.
[89] P.J. Larkin, IR and Raman Spectroscopy: Principles and Spectral Interpretation, 2011. https://doi.org/10.3390/rel9100297.
[90] V. Balan, C.T. Mihai, F.D. Cojocaru, C.M. Uritu, G. Dodi, D. Botezat, I. Gardikiotis, Vibrational spectroscopy fingerprinting in medicine: From molecular to clinical practice, Materials (Basel). 12 (2019) 1–40. https://doi.org/10.3390/ma12182884.
[91] E. Gandolpho Tótoli, H. Regina Nunes Salgado, Development and Validation of the

Quantitative Analysis of Ampicillin Sodium in Powder for Injection by Fourier-transform Infrared Spectroscopy (FT-IR), Phys. Chem. 2 (2013) 103–108. https://doi.org/10.5923/j.pc.20120206.04.
[92] S.T. Hassib, G.S. Hassan, A.A. El-Zaher, M.A. Fouad, E.A. Taha, Quantitative analysis of anti-inflammatory drugs using FTIR-ATR spectrometry, Spectrochim. Acta - Part A Mol. Biomol. Spectrosc. 186 (2017) 59–65. https://doi.org/10.1016/j.saa.2017.06.002.
[93] C. Huck, Infrared Spectroscopic Technologies for the Quality Control of Herbal Medicines, Elsevier Inc., 2015. https://doi.org/10.1016/B978-0-12-800874-4.00022-2.
[94] F.A. Settle, Handbook of Instrumental Techniques for Analytical Chemistry, (1997) 261–289.
[95] A.A. Bunaciu, H.Y. Aboul-Enein, S. Fleschin, Application of fourier transform infrared spectrophotometry in pharmaceutical drugs analysis, Appl. Spectrosc. Rev. 45 (2010) 206–219. https://doi.org/10.1080/00387011003601044.
[96] T.W. Bocklitz, S. Guo, O. Ryabchykov, N. Vogler, J. Popp, Raman Based Molecular Imaging and Analytics: A Magic Bullet for Biomedical Applications!?, Anal. Chem. 88 (2016) 133–151. https://doi.org/10.1021/acs.analchem.5b04665.
[97] J. Marzi, E. Brauchle, D.A. Carvajal Berrio, S. Lee Layland, K. Schenke-Layland, 3.7 Raman spectroscopy, Compr. Biomater. II. 3 (2017) 108–127. https://doi.org/10.1016/B978-0-12-803581-8.09323-1.
[98] S. Garrigues, M. de la Guardia, Vibrational spectroscopy, 2016. https://doi.org/10.1002/9781118654316.ch15.
[99] H.J. Butler, L. Ashton, B. Bird, G. Cinque, K. Curtis, J. Dorney, K. Esmonde-White, N.J. Fullwood, B. Gardner, P.L. Martin-Hirsch, M.J. Walsh, M.R. McAinsh, N. Stone, F.L. Martin, Using Raman spectroscopy to characterize biological materials, Nat. Protoc. 11 (2016) 664–687. https://doi.org/10.1038/nprot.2016.036.
[100] X. Zhu, T. Xu, Q. Lin, Y. Duan, Technical development of raman spectroscopy: From instrumental to advanced combined technologies, Appl. Spectrosc. Rev. 49 (2014) 64–82. https://doi.org/10.1080/05704928.2013.798801.
[101] R.S. Das, Y.K. Agrawal, Raman spectroscopy: Recent advancements, techniques and applications, Vib. Spectrosc. 57 (2011) 163–176. https://doi.org/10.1016/j.vibspec.2011.08.003.
[102] H. Sato, H. Shinzawa, Y. Komachi, Fiber-Optic Raman Probes for Biomedical and Pharmaceutical Applications, (2010) 25–45. https://doi.org/10.1007/978-3-642-02649-2_2.
[103] L. Ohannesian, A. J.Streeter, Handbook of pharmaceutical analysis, 2002. https://doi.org/10.16309/j.cnki.issn.1007-1776.2003.03.004.
[104] J.-J. Aaron, S. Trajkovska, Fluorescence Studies of Anti-Cancer Drugs - Analytical and Biomedical Applications, Curr. Drug Targets. 7 (2006) 1067–1081. https://doi.org/10.2174/138945006778226633.
[105] L.E. Jamieson, H.J. Byrne, Vibrational spectroscopy as a tool for studying drug-cell interaction: Could high throughput vibrational spectroscopic screening improve drug development?, Vib. Spectrosc. 91 (2017) 16–30. https://doi.org/10.1016/j.vibspec.2016.09.003.
[106] N.K. Afseth, A. Kohler, Extended multiplicative signal correction in vibrational spectroscopy, a tutorial, Chemom. Intell. Lab. Syst. 117 (2012) 92–99. https://doi.org/10.1016/j.chemolab.2012.03.004.
[107] K.H. Liland, A. Kohler, N.K. Afseth, Model-based pre-processing in Raman spectroscopy of biological samples, J. Raman Spectrosc. 47 (2016) 643–650. https://doi.org/10.1002/jrs.4886.
[108] P. Bassan, A. Kohler, H. Martens, J. Lee, H.J. Byrne, P. Dumas, E. Gazi, M. Brown, N.

Clarke, P. Gardner, Resonant Mie Scattering (RMieS) correction of infrared spectra from highly scattering biological samples, Analyst. 135 (2010) 268–277. https://doi.org/10.1039/b921056c.
[109] Q. Li, Q. Gao, G. Zhang, Improved extended multiplicative scatter correction algorithm applied in blood glucose noninvasive measurement with FT-IR spectroscopy, J. Spectrosc. (2013) 1–6. https://doi.org/10.1155/2013/916351.
[110] K.H. Liland, T. Almøy, B.H. Mevik, Optimal choice of baseline correction for multivariate calibration of spectra, Appl. Spectrosc. 64 (2010) 1007–1016. https://doi.org/10.1366/000370210792434350.
[111] M.J. German, A. Hammiche, N. Ragavan, M.J. Tobin, L.J. Cooper, S.S. Matanhelia, A.C. Hindley, C.M. Nicholson, N.J. Fullwood, H.M. Pollock, F.L. Martin, Infrared spectroscopy with multivariate analysis potentially facilitates the segregation of different types of prostate cell, Biophys. J. 90 (2006) 3783–3795. https://doi.org/10.1529/biophysj.105.077255.
[112] R. Bro, A.K. Smilde, Principal component analysis, Anal. Methods. 6 (2014) 2812–2831. https://doi.org/10.1039/c3ay41907j.
[113] N.L. Calvo, T.S. Kaufman, R.M. Maggio, A PCA-based chemometrics-assisted ATR-FTIR approach for the classification of polymorphs of cimetidine: Application to physical mixtures and tablets, J. Pharm. Biomed. Anal. 107 (2015) 419–425. https://doi.org/10.1016/j.jpba.2015.01.016.
[114] A. Biancolillo, F. Marini, Chemometric methods for spectroscopy-based pharmaceutical analysis, Front. Chem. 6 (2018) 1–14. https://doi.org/10.3389/fchem.2018.00576.
[115] B.R. Andjelkovic Cirkovic, Machine learning approach for breast cancer prognosis prediction, Comput. Model. Bioeng. Bioinforma. (2020) 41–68. https://doi.org/10.1016/b978-0-12-819583-3.00002-3.
[116] S. Wold, M. Sjöström, L. Eriksson, PLS-regression: A basic tool of chemometrics, Chemom. Intell. Lab. Syst. 58 (2001) 109–130. https://doi.org/10.1016/S0169-7439(01)00155-1.
[117] M.E. Keating, H. Nawaz, F. Bonnier, H.J. Byrne, Multivariate statistical methodologies applied in biomedical Raman spectroscopy: Assessing the validity of partial least squares regression using simulated model datasets, Analyst. 140 (2015) 2482–2492. https://doi.org/10.1039/c4an02167c.
[118] S. Arlot, A. Celisse, A survey of cross-validation procedures for model selection, Stat. Surv. 4 (2010) 40–79. https://doi.org/10.1214/09-SS054.
[119] D.B. Hibbert, Vocabulary of concepts and terms in chemometrics (IUPAC Recommendations 2016), Pure Appl. Chem. 88 (2016) 407–443. https://doi.org/10.1515/pac-2015-0605.
[120] M.N. Leger, A.G. Ryder, Comparison of derivative preprocessing and automated polynomial baseline correction method for classification and quantification of narcotics in solid mixtures, Appl. Spectrosc. 60 (2006) 182–193. https://doi.org/10.1366/000370206776023304.
[121] K.E. Hevener, T.A. Verstak, K.E. Lutat, D.L. Riggsbee, J.W. Mooney, Recent developments in topoisomerase-targeted cancer chemotherapy, Acta Pharm. Sin. B. 8 (2018) 844–861. https://doi.org/10.1016/j.apsb.2018.07.008.
[122] B. Ongnok, N. Chattipakorn, S.C. Chattipakorn, Doxorubicin and cisplatin induced cognitive impairment: The possible mechanisms and interventions, Exp. Neurol. 324 (2020) 113118. https://doi.org/10.1016/j.expneurol.2019.113118.
[123] C.G. Pereira, J.R. Lavoie, E. Garces, F. Basso, M. Dabić, G.S. Porto, T. Daim, Forecasting of emerging therapeutic monoclonal antibodies patents based on a decision model, Technol. Forecast. Soc. Change. 139 (2019) 185–199.

https://doi.org/10.1016/j.techfore.2018.11.002.
[124] R. Gahoual, A. Beck, E. Leize-Wagner, Y.N. François, Cutting-edge capillary electrophoresis characterization of monoclonal antibodies and related products, J. Chromatogr. B Anal. Technol. Biomed. Life Sci. 1032 (2016) 61–78. https://doi.org/10.1016/j.jchromb.2016.05.028.
[125] C. Li, T. Li, Application of Vibrational Spectroscopy to the Structural Characterization of Monoclonal Antibody and its Aggregate, Curr. Pharm. Biotechnol. 10 (2009) 391–399. https://doi.org/10.2174/138920109788488950.
[126] M. Boulet-Audet, S.G. Kazarian, B. Byrne, In-column ATR-FTIR spectroscopy to monitor affinity chromatography purification of monoclonal antibodies, Sci. Rep. 6 (2016) 1–13. https://doi.org/10.1038/srep30526.
[127] A.A. Makki, F. Bonnier, R. Respaud, F. Chtara, A. Tfayli, C. Tauber, D. Bertrand, H.J. Byrne, E. Mohammed, I. Chourpa, Qualitative and quantitative analysis of therapeutic solutions using Raman and infrared spectroscopy, Spectrochim. Acta - Part A Mol. Biomol. Spectrosc. 218 (2019) 97–108. https://doi.org/10.1016/j.saa.2019.03.056.
[128] S.K. Paidi, S. Siddhanta, R. Strouse, J.B. McGivney, C. Larkin, I. Barman, Rapid Identification of Biotherapeutics with Label-Free Raman Spectroscopy, Anal. Chem. 88 (2016) 4361–4368. https://doi.org/10.1021/acs.analchem.5b04794.
[129] H.J. Butler, P.M. Brennan, J.M. Cameron, D. Finlayson, M.G. Hegarty, M.D. Jenkinson, D.S. Palmer, B.R. Smith, M.J. Baker, Development of high-throughput ATR-FTIR technology for rapid triage of brain cancer, Nat. Commun. 10 (2019) 1–9. https://doi.org/10.1038/s41467-019-12527-5.
[130] M.T. Rosado, M.L.T.S. Duarte, R. Fausto, Vibrational spectra of acid and alkaline glycine salts, Vib. Spectrosc. 16 (1998) 35–54. https://doi.org/10.1016/S0924-2031(97)00050-7.
[131] X. Cao, R.M. Fesinmeyer, C.J. Pierini, C.C. Siska, J.R. Litowski, S. Brych, Z.Q. Wen, G.R. Kleemann, Free fatty acid particles in protein formulations, Part 1: Microspectroscopic identification, J. Pharm. Sci. 104 (2015) 433–446. https://doi.org/10.1002/jps.24126.
[132] M.J. Márquez, D. Romani, S.B. Díaz, S.A. Brandán, Structural and vibrational characterization of anhydrous and dihydrated species of trehalose based on the FTIR and FTRaman spectra and DFT calculations, J. King Saud Univ. - Sci. 30 (2018) 229–249. https://doi.org/10.1016/j.jksus.2017.01.009.
[133] E. Jaccoulet, C. Boughanem, L. Auduteau, P. Prognon, E. Caudron, UV spectroscopy and least square matching for high throughput discrimination of taxanes in commercial formulations and compounded bags, Eur. J. Pharm. Sci. 123 (2018) 143–152. https://doi.org/10.1016/j.ejps.2018.07.047.
[134] S. Armenta, S. Garrigues, M. de la Guardia, Recent developments in flow-analysis vibrational spectroscopy, TrAC - Trends Anal. Chem. 26 (2007) 775–787. https://doi.org/10.1016/j.trac.2007.06.003.